UNIVERSITÉ DE PROVENCE, AIX-MARSEILLE I

THÈSE

pour obtenir le grade de

DOCTEUR DE L'UNIVERSITÉ DE PROVENCE

Discipline: **Mathématiques appliquées**

École doctorale de mathématiques et informatique de Marseille

présentée et soutenue publiquement par

Nicolas Seguin

le 22 novembre 2002

Modélisation et simulation numérique des écoulements diphasiques

---

Directeur de thèse: **M. Jean-Marc Hérard**

Rapporteurs:

M. Alain-Yves LeRoux	Professeur, Université Bordeaux I
M. Sebastian Noelle	Professeur, Université d'Aachen

Jury:

M. Frédéric Coquel	Chargé de Recherche CNRS, Université Pierre et Marie Curie
M. Thierry Gallouët	Professeur, Université de Provence
M. Sergey Gavrilyuk	Professeur, Université Aix-Marseille III (président du jury)
Mme. Edwige Godlewski	Maître de Conférence, Université Pierre et Marie Curie
M. Jean-Marc Hérard	Directeur de Recherche CNRS associé, Université de Provence
M. Alain-Yves LeRoux	Professeur, Université Bordeaux I

Remerciements

Ce travail a été réalisé au Département mécanique des fluides et transferts thermiques de la Division recherche et développement d'EDF, en collaboration avec le Laboratoire d'analyse, topologie et probabilités de l'Université de Provence.

Je tiens tout d'abord à remercier très chaleureusement Jean-Marc Hérard. Durant ces trois années, il m'a fait partager toute sa compétence, son savoir et ses nombreuses idées, avec confiance. Cette confiance, associée à son soutien et à sa gentillesse a été un enrichissement incroyable, et pas seulement scientifique. Ce travail a donc été un réel plaisir grâce à lui ainsi qu'aux magnifiques dessins du mercredi de Fanny, Ariane et Louise !

J'ai eu la chance lors de cette thèse de pouvoir venir régulièrement à Marseille. Ces déplacements m'ont permis de rencontrer Thierry Gallouët. Intimidé au départ, j'ai vite été mis à l'aise par son enthousiasme et par sa véritable disponibilité. C'est pourquoi je tiens à le remercier de tout ce qu'il m'a appris, expliqué et fait partagé dans cette petite salle info du CMI.

J'en arrive maintenant à Alain-Yves LeRoux. Il m'a fait confiance il y a quatre ans. Je lui dois de m'avoir donné le goût de l'analyse numérique lors du DEA et de m'avoir recommandé auprès des gens cités au-dessus pour cette thèse. Je suis heureux qu'il ait accepté d'être rapporteur sur mon travail, que cela me permette de le remercier vivement une nouvelle fois.

L'autre rapporteur est Sebastian Noelle. Je ne l'ai connu pendant ces trois ans que par articles interposés. J'ai eu la chance et l'honneur de faire sa connaissance il y a peu et j'ai pu apprécier ses grandes compétences ainsi que son immense gentillesse. Je tiens donc à le remercier une nouvelle fois d'avoir rapporté sur cette thèse.

J'ai eu l'occasion de discuter plusieurs fois avec Frédéric Coquel pendant ces trois années et chacune de ces rencontres a été très intructive et sympathique. Il est certainement une des personnes les plus compétentes sur les thèmes abordés dans cette thèse et je le remercie de m'avoir fait l'honneur d'accepter d'être membre de ce jury.

Je remercie maintenant Sergey Gavrilyuk. Je suis très honoré qu'il soit présent dans ce jury et qu'il ait accepté de le présider. De même, je tiens à remercier Edwige Godlewski qui a accepté d'être membre de mon jury. Sa présence est justifiée bien sûr par ses grandes conpétences dans les domaines qu'abordent cette thèse, mais aussi par le nombre d'heures que j'aurai passé à lire son livre !

Je désire associer à ces remerciements trois personnes qui auront eu sur moi une influence primordiale. Tout d'abord, Henri Pucheu, qui m'aura transmis le goût d'apprendre. Ensuite, Denise Haugazeau, qui m'aura fait m'accrocher aux mathématiques. Enfin, Marc Dechelotte, à qui ce que je dois n'est vraiment pas descriptible en quelques lignes ...

Durant ces trois années, j'ai pu rencontrer plusieurs thésards au CMI et à EDF, que je désire remercier d'avoir contribué, chacun à sa manière, à la bonne humeur qui a accompagné le déroulement de cette thèse. Le premier est Julien, pour son accueil lors de mes venues à Marseille, sa sympathie et pour nos discussions diverses (des conditions aux limites pour les lois de conservation scalaires aux

chefs d'œuvre de Vladimir Nabokov !). J'en arrive aux thésards d'EDF, dans le désordre : Nathalie, Olga, Jean-Michel, Nicolas et Pierre-Antoine. Merci pour les pauses café, les soirées, les blagues et tout le reste (je ne rentrerai pas plus dans le détail, histoire de ne compromettre personne !). Et merci aussi à tous les stagiaires, qui ont eux aussi apporté leur pierre à la bonne ambiance des pauses cafés.

Ensuite viennent les ami(e)s/copines/copains (au choix), Nathalie, Pilou, tous les *Relis* de Paris et de Bordeaux, avec une mention spéciale pour Alesque (une petite pensée pour *Flyette*) et pour Jim (une autre petite pensée pour toutes les huîtres sauvages du monde entier). Merci beaucoup beaucoup, vivement la poursuite des réjouissances à Marseille ! Et encore merci à toutes et à tous pour le super super cadeau.

J'en viens maintenant à mes parents. Je les remercie très profondément pour leur soutien durant toutes mes études, et pour tout le reste aussi. Un petit coucou à ce cher Joris, en espérant qu'il réussisse lui aussi dans la voie qu'il s'est choisi, courage courage ! J'associe également à ces remerciements tous les autres membres de ma famille, paternelle, maternelle, de France, du Viêt-Nam et d'ailleurs et toute la famille de Gaëlle ...

Enfin, me voila arrivé à Gaëlle. Un très très grand merci, merci pour tout, merci d'être là, tout simplement, avec moi. Tout ça, c'est pour Toi.

Table des matières

Introduction générale

Cette thèse a pour objet la modélisation et l'approximation numérique à l'aide de méthodes Volumes Finis des écoulements diphasiques eau-vapeur. Les applications visées correspondent à la simulation d'écoulements en configuration indutrielle de type Réacteur à Eau Pressurisée (REP), notamment pour représenter des phénomènes d'Accidents de Perte de Réfrigérant Primaire (APRP), d'assèchement ou de formation de films.

À l'heure actuelle, il n'existe pas de consensus sur la modélisation des écoulements diphasiques par approche eulérienne. Les phénomènes complexes à modéliser (échanges entre phases, réactions chimiques, forces interfaciales, ...) et les nombreuses configurations d'écoulement différentes en sont les principales raisons. Tous les modèles utilisant l'approche eulérienne correspondent à une simplification de la *formulation locale instantanée*. Cette formulation décrit les écoulements diphasiques comme un ensemble de domaines monophasiques à frontières mobiles (ces frontières correspondent aux interfaces entre chaque phase). Les régions monophasiques sont décrites par les équations de Navier-Stokes et les interfaces sont modélisées par des lois algébriques et d'évolution. Il faut noter que cette formulation suppose la position des interfaces comme inconnue. Cette formulation n'est pas exploitable pour l'approximation des écoulements diphasiques car, pour des applications comme les écoulements à bulles par exemple, le nombre d'interfaces est bien souvent rédhibitoire et l'échelle caractéristique des bulles s'avère trop petite pour les méthodes d'approximation actuelles. Deux voies simplifiant la formulation locale instantanée permettent de rendre la simulation des écoulements diphasiques accessible aux techniques numériques actuelles : la première consiste à n'utiliser que les équations modélisant le mélange des deux fluides (*modèles monofluides*) et la seconde utilise des opérateurs de moyenne sur les équations de Navier-Stokes initiales pour obtenir des quantités phasiques pondérées par la fraction volumique de chacun des fluides (*modèles bifluides*).

Le travail principal de cette thèse est axé sur l'étude et l'approximation d'un modèle bifluide original utilisant l'approche à deux pressions. Plusieurs contributions utilisant cette approche existent, notamment celles de M.R. Baer et J.W. Nunziato [BN86], A.K. Kapila *et al.* [KSB$^+$97], J. Glimm *et al.* [GSS99], R. Saurel et R. Abgrall [SA99], S. Gavrilyuk et R. Saurel [GS02] ... En une dimension d'espace, le modèle considéré ici est décrit par un système non linéaire de sept équations aux dérivées partielles et par des lois algébriques, comme les lois d'état décrivant le comportement thermodynamique de chaque fluide. Ce système peut s'écrire

$$(Id + D(W))\frac{\partial W}{\partial t} + \frac{\partial F(W)}{\partial x} + C(W)\frac{\partial W}{\partial x} = S(W) + \frac{\partial}{\partial x}\left(E(W)\frac{\partial (W)}{\partial x}\right), \qquad (1)$$

où W est la fonction inconnue dépendant du temps t et de l'espace x,

$$\begin{aligned} W \,:\, \mathbb{R}_+ \times \mathbb{R} &\longmapsto \Omega \\ (t,x) &\longmapsto W(t,x), \end{aligned}$$

avec Ω l'espace des états admissibles, qui est inclus dans $\mathbb{R}^7$. La fonction $F : \Omega \longmapsto \mathbb{R}^7$ est la fonction *flux* (appelée également *flux physique*, par opposition au flux numérique). Les fonctions D, C et E vont de Ω dans $\mathcal{M}_{7,7}(\mathbb{R})$ (qui est l'espace vectoriel sur $\mathbb{R}$ des matrices carrées de dimension 7) et Id correspond à la matrice identité de $\mathcal{M}_{7,7}(\mathbb{R})$. Le terme $C(W)\partial_x W$ est appelé *terme non conservatif*, la fonction $S : \Omega \longmapsto \mathbb{R}^7$ correspond au *terme source* et $E(W)$ est la *matrice de diffusion*.

On peut noter que l'écriture sous la forme $\partial_x F(W) + C(W)\partial_x W$ n'est *a priori* pas unique. En effet, en utilisant la matrice jacobienne du flux $\mathrm{D}F(W)$, on a

$$\partial_x F(W) + C(W)\partial_x W = (\mathrm{D}F(W) + C(W))\partial_x W$$

On pourrait alors redéfinir le flux comme $\alpha F(W)$, $\alpha \in \mathbb{R}$, et la matrice du terme non conservatif comme $(1-\alpha)\mathrm{D}F(W)+C(W)$. Néanmoins, sous certaines hypothèses simplificatrices, le terme non conservatif disparaît et les termes différentiels d'ordre un s'écrivent alors sous la forme unique $\partial_t W + \partial_x F(W)$, dite *forme conservative*. C'est effectivement le cas si on suppose qu'on est en présence d'un seul des deux fluides, la fraction volumique du fluide restant est égale à 1 uniformément en temps et en espace et les produits $D(W)\partial_t W$ et $C(W)\partial_x W$ sont alors nuls. On verra par la suite que la forme du flux F est cruciale lors de la définition des solutions non régulières.

Lorsqu'on se focalise sur les solutions régulières du problème de Cauchy associé au système (1), la définition du flux physique et des termes non conservatifs n'a pas d'importance. Seule la connaissance de la forme des matrices $Id + D(W)$ et $\mathrm{D}F(W) + C(W)$ est utile, en particulier pour l'étude de l'*hyperbolicité* du système (1). Dans le cas du système étudié ici, on peut montrer que la matrice $(Id + D(W))^{-1}(\mathrm{D}F(W) + C(W))$ admet 7 valeurs propres réelles et 7 vecteurs propres à droite linéairement indépendants (ce qui est la définition d'un système hyperbolique [Daf99]). Cette propriété n'est en général pas vérifiée par les modèles bifluides classiques qui suppose l'égalité des pressions de chaque fluide, ce qui rend d'autant plus complexes leur analyse et leur approximation numérique.

Nous avons choisi aussi bien pour l'analyse que pour l'approximation du système (1) d'utiliser la technique de *splitting d'opérateur*, c'est-à-dire que le terme source et le terme de diffusion sont découplés de la partie différentielle d'ordre un (on renvoie à l'ouvrage de R. Dautray et J.L. Lions [DL85]). Cela signifie que le système (1) se compose successivement des trois problèmes suivants :

$$(Id + D(W))\frac{\partial W}{\partial t} + \frac{\partial F(W)}{\partial x} + C(W)\frac{\partial W}{\partial x} = 0\,, \tag{2}$$

$$(Id + D(W))\frac{\partial W}{\partial t} = S(W) \tag{3}$$

$$\text{et} \quad (Id + D(W))\frac{\partial W}{\partial t} = \frac{\partial}{\partial x}\left(E(W)\frac{\partial(W)}{\partial x}\right)\,. \tag{4}$$

Il faut noter que l'étude du système (4) n'est pas abordée dans ce travail (on réfère aux travaux de R. Eymard, T. Gallouët et R. Herbin [EGH00]).

Concernant l'analyse du système (2), nous avons étudié la solution du *problème de Riemann* associé à ce système. Ce type de problème correspond à un problème de Cauchy ayant une donnée initiale du type

$$W(t=0,x) = \begin{cases} W_L & \text{si } x < 0, \\ W_R & \text{si } x > 0, \end{cases} \tag{5}$$

avec W_L et W_R dans Ω. On se restreint à la classe des solutions auto-similaires, c'est-à-dire qu'on peut exprimer la solution W sous la forme d'une fonction dépendant uniquement du rapport x/t et des conditions initiales W_L et W_R. On suppose en plus que cette solution est composée d'états constants séparés par des ondes. Une *k-onde* correspond à un profil se déplaçant à la *vitesse caractéristique* $\lambda_k(W)$, $\lambda_k(W)$ étant la k-ième valeur propre de la matrice $(Id+D(W))^{-1}(\mathrm{D}F(W)+C(W))$. Si on note $r_k(W)$ le k-ième vecteur propre à droite de $(Id+D(W))^{-1}(\mathrm{D}F(W)+C(W))$, on dit que le k-ième *champ caractéristique* est *linéairement dégéré* si

$$\mathrm{D}\lambda_k(W).r_k(W) = 0, \quad \text{pour tout } W \in \Omega,$$

et on dit que le k-ième *champ caractéristique* est *vraiment non linéaire* si

$$\mathrm{D}\lambda_k(W).r_k(W) \neq 0, \quad \text{pour tout } W \in \Omega.$$

Les champs caractéristiques du système (2) sont soit linéairement dégérés, soit vraiment non linéaires. On peut montrer que les ondes associées à ces champs caractéristiques comportent des points singuliers lorsqu'on étudie un problème de Riemann. Le problème de Riemann n'admettant donc pas de solution classique en général, il devient donc nécessaire de définir la notion de solution faible de (2). On appelle *solution faible* du système (2) sur l'intervalle de temps $[0,T)$, $T>0$, une fonction U mesurable bornée définie sur $[0,T)\times\mathbb{R}$ à valeurs dans Ω qui vérifie (2) au sens des distributions. Il découle de cette définition une caractérisation des discontinuités de la solution. Plus précisément, pour un système conservatif $\partial_t V + \partial_x G(V) = 0$, une discontinuité de vitesse s séparant l'état V_- à gauche de l'état V_+ à droite vérifie la relation

$$-s(V_+ - V_-) + (G(V_+) - G(V_-)) = 0,$$

appelée *relation de saut de Rankine-Hugoniot*. Il est maintenant clair que la forme du flux physique influe directement sur la caractérisation des discontinuités des solutions de (2). On rappelle que le système (2) est non conservatif, car il n'existe pas de fonction flux dont la matrice jacobienne serait $(Id+D(W))^{-1}(\mathrm{D}F(W)+C(W))$, ce qui est profondément handicapant pour définir les solutions faibles de notre système et les relations de saut associées (excepté dans quelques cas simples où le système (2) dégénère sous la forme conservative $\partial_t W + \partial_x F(W) = 0$, comme on l'a évoqué plus haut). Tout ceci est étroitement lié au produit $C(W)\partial_x W$ qui n'est *a priori* pas défini lorsque W admet une discontinuité. Les premiers auteurs ayant proposé une définition de ce produit sont P.G. LeFloch [LeF88] et J.F. Colombeau [Col92] ; vient ensuite le travail de G. Dal Maso, P.G. LeFloch et F. Murat [DLM95]. Le produit $C(W)\partial_x W$ est alors défini au sens des mesures boréliennes à l'aide d'une famille de chemins localement lipschitziens $\varphi(\,.\,;W_-,W_+)$ allant de $[0,1]$ dans Ω, W_- et W_+ étant les états de part et d'autre de la discontinuité. Moyennant quelques propriétés sur φ, la notion de solution faible est alors généralisée, au sens des mesures boréliennes bornées sur $[0,T)\times\mathbb{R}$. Il est important de préciser que la relation de saut associée à ce produit est dépendante du chemin φ choisi. En clair, des informations supplémentaires sont

requises pour pouvoir sélectionner le chemin *ad hoc*. Divers auteurs, dont L. Sainsaulieu [Sai96], ont alors proposé d'utiliser la forme de la matrice de diffusion (ici notée $E(W)$) du système non conservatif. On verra pourtant que le système (2) ne nécessite pas l'utilisation de ce formalisme. Décrivons brièvement suivant la nature du champ caractérisque les relations de Rankine-Hugoniot qu'on associe au système (2). Si le champ caractérisque est vraiment non linéaire, alors on peut montrer que le système (2) devient localement le système conservatif

$$\frac{\partial W}{\partial t} + \frac{\partial F(W)}{\partial x} = 0$$

et dans ce cas, la définition des relations de Rankine-Hugoniot est unique. Si par contre le champ caractérisque est linérairement dégénéré, deux cas peuvent se présenter. Le premier est identique au cas vraiment non linéaire, c'est-à-dire que les termes non conservatifs disparaissent. Dans l'autre cas, on peut montrer, comme c'est rappelé dans l'annexe 4.C du chapitre 4, que la caractérisation par les relations de Rankine-Hugoniot est équivalente à celle fournie par les invariants de Riemann associés à ce champ. On rappelle qu'un *invariant de Riemann* associé au k-ième champ caractéristique est une fonction régulière I^k de Ω dans $\mathbb{R}$ qui vérifie

$$\mathrm{D}I^k(W).r_k(W) = 0, \quad \text{pour tout } W \in \Omega.$$

On utilise alors les invariants de Riemann pour caractériser la discontinuité de la solution.

Il reste malheureusement un obstacle majeur à la résolution du problème de Riemann (2)-(5) : le système (2) est *résonnant*, c'est-à-dire que pour certaines valeurs de W, deux valeurs propres λ_k et $\lambda_{k'}$ peuvent s'identifier et la matrice $(Id + D(W))^{-1}(\mathrm{D}F(W) + C(W))$ n'est alors plus diagonalisable dans $\mathbb{R}$. Plusieurs auteurs se sont intéressés à ce type de problème, notamment E. Isaacson et B. Temple [IT90], A.J. De Souza et D. Marchesin [SM98] et A.Y. LeRoux [LeR98] dans le cadre des systèmes. Concernant l'étude des lois de conservation scalaires incluant le phénomène de résonnance, on renvoie au chapitre 2 et aux références qui y sont citées. Différentes pathologies sont associées à ce phénomène. Tout d'abord, les valeurs propres ne sont pas ordonnées, donc l'ordre des ondes n'est pas connu *a priori*. De plus, lorsque deux valeurs propres s'identifient, la caractérisation à travers les deux ondes superposées n'est clairement pas évidente. Pour illustrer cette complexité, on peut regarder par exemple la résolution du problème de Riemann associé à l'équation scalaire résonnante du chapitre 2, présentée dans l'annexe 2.A, qui est largement plus ardue que dans le cas non résonnant.

Malgré ces difficultés, un résultat important a pu être obtenu concernant la solution de (2)-(5) : en supposant que cette solution n'est pas résonnante, c'est-à dire que les ondes sont isolées les unes des autres, alors l'étude des différents champs caractéristiques assure que cette solution est dans Ω pour tout $t > 0$ et $x \in \mathbb{R}$.

Concernant le système non linéaire d'équations différentielles (3), seuls les *termes sources de relaxation* ont été étudiés. Ces termes modélisent des déséquilibres entre les fluides. Le déséquilibre cinématique s'exprime par le quotient de la vitesse relative entre les deux fluides sur un temps de relaxation. Simplement, plus le temps de relaxation est petit, plus vite la vitesse relative de la solution de (3) tendra vers 0. Il en est de même pour le terme source associé au déséquilibre thermodynamique, qui est le quotient de la pression relative entre les deux fluides sur un autre temps de relaxation. On montre que la solution de (3) vérifie bien ce phénomène et que pour tout $t > 0$, elle appartient à Ω sous réserve que la donnée initiale est bien dans Ω.

On peut ajouter un petit commentaire sur le travail effectué dans cette thèse à propos des phénomènes de relaxation. Comme cela a été précisé plus haut, l'approche par splitting d'opérateur a été privilégiée ici, pour découpler les phénomènes convectifs (système (2)) des phénomènes de relaxation (système (3)). On peut citer l'analyse effectuée par A. Forestier dans [For02] qui détaille la relation entre certaines fermetures algébriques et la variation de l'entropie de chacun des fluides en présence lors du sous-pas de relaxation (3). Il faut signaler qu'il existe toutefois un formalisme dû à T.P. Liu [Liu88] et à G.Q. Chen, D. Levermore et T.P. Liu [CLL94], permettant l'étude de stabilité des solutions du système

$$(Id + D(W))\frac{\partial W}{\partial t} + \frac{\partial F(W)}{\partial x} + C(W)\frac{\partial W}{\partial x} = S(W)$$

lors du passage à la limite quand le temps de relaxation tend vers 0. Cela a d'ailleurs été effectué par P. Bagnerini *et al.* dans [BCG$^+$02] pour un sous-système de (1).

On vient donc de voir que la solution W des systèmes (2) et (3) est en accord avec les principes de positivité classiques, c'est-à-dire que $W(t,x)$ est dans Ω pour tout (t,x) dans $\mathbb{R}_+ \times \mathbb{R}$. Ce système semble donc un bon candidat pour la simulation des écoulements diphasiques compressibles. Pour l'approximation numérique du système (2), on utilise ici des *méthodes Volumes Finis* (la présentation qui suit ne prétend pas être exhaustive et on renvoie aux ouvrages de R. Eymard, T. Gallouët et R. Herbin [EGH00] et et de E. Godlewski et P.A. Raviart [GR96]). Ces méthodes sont particulièrement bien adaptées pour l'approximation des systèmes hyperboliques, aussi bien en une dimension d'espace qu'en deux ou trois dimensions. D'ailleurs, bien que tous les tests numériques dans cette thèse soient unidimensionnels, l'extension au cadre multidimensionnel des méthodes présentées est classique. Le principe des méthodes Volumes Finis pour les systèmes hyperboliques est le suivant. On s'intéresse à l'approximation de W, fonction de $(0,T) \times \mathbb{R}^d$ dans Ω, solution du système conservatif

$$\frac{\partial W}{\partial t}(t,x) + \mathrm{div} F(W)(t,x) = 0, \quad t \in (0,T), x \in \mathbb{R}^d, \tag{6}$$

où div est l'opérateur divergence spatiale. On associe à ce système une donnée de Cauchy W_0 qui est une fonction de $\mathbb{R}^d$ dans Ω, ce qui signifie que la solution W doit vérifier

$$W(t = 0,x) = W_0(x), \quad \forall x \in \mathbb{R}^d. \tag{7}$$

Le domaine spatial $\mathbb{R}^d$ est partitionné pour former un *maillage* en ouverts convexes disjoints (appelés *mailles*), qui sont des intervalles si $d = 1$, des polygones si $d = 2$ ou des polyèdres si $d = 3$. La fonction $W(T,.)$ est alors approchée par une fonction constante sur chaque maille et chaque constante est calculée par itérations (temporelles) successives. Plus précisément, supposons qu'on veuille calculer l'approximation de la solution W au temps $T > 0$ sur la maille M_i, $i \in \mathbb{Z}$, on définit $N + 1$ temps successifs t^n, $n = 0,...,N$ tels que $t^0 = 0 < t^1 < ... < t^{N-1} < t^N = T$. En intégrant le système (6) sur le volume $(t^n; t^{n+1}) \times M_i$, $n \in [0,N-1]$ et en appliquant la formule de Green, on obtient directement

$$\int_{M_i} (W(t^{n+1},x) - W(t^n,x))\, dx + \int_{t^n}^{t^{n+1}} \int_{\partial M_i} F(W(t,x)).\nu_i(x)\, d\gamma(x)\, dt = 0 \tag{8}$$

où ν_i est la normale unitaire sortante à ∂M_i la frontière de la maille M_i, et où $d\gamma$ est la mesure de Lebesgue sur ∂M_i. On note

$$W_i^0 = \frac{1}{|M_i|} \int_{M_i} W_0(x)\, dx. \tag{9}$$

De plus, on définit pour tout n dans [1,N] l'approximation de la solution sur la maille M_i :

$$W_i^n \approx \frac{1}{|M_i|}\int_{M_i} W(t^n,x)\,dx$$

avec $|M_i|$ la mesure (de Lebesgue dans $\mathbb{R}^d$) de la maille M_i. Notons maintenant

$$p(i) = \text{card}\{j \in \mathbb{Z}\setminus\{i\} \text{ tel que } \overline{M_i}\cap\overline{M_j} \neq \emptyset \text{ and } \dim(\overline{M_i}\cap\overline{M_j}) = d-1\}.$$

Par exemple, en supposant que $d = 2$ et que le maillage est une triangulation, alors $p(i) = 3$ pour tout i de $\mathbb{Z}$. On définit en outre σ_{ik} et ν_{ik}, $k = 1,..,p(i)$, la k-ième face de la maille M_i et la normale unitaire sortante correspondante. Si $v(i,k)$ correspond à l'indice de la maille séparée de M_i par la face σ_{ik}, on peut écrire le schéma Volumes Finis explicite suivant :

$$|M_i|(W_i^{n+1}-W_i^n) + (t^{n+1}-t^n)\sum_{k=1}^{3}|\sigma_{ik}|\varphi(W_i^n,W_{v(i,k)}^n;\nu_{ik}) = 0 \tag{10}$$

où $|\sigma_{ik}|$ est la mesure (de Lebesgue dans $\mathbb{R}^{d-1}$) de la face σ_{ik} et où la fonction φ, allant $\Omega\times\Omega\times\mathbb{R}^d$ dans Ω, doit être *consistante*, *i.e.*

$$\varphi(W,W;\nu) = F(W).\nu, \quad \forall W\in\Omega, \forall\nu\in\mathbb{R}^d$$

et vérifier la propriété de *conservation*

$$\varphi(W_a,W_b;\nu) = \varphi(W_b,W_a;-\nu), \quad \forall W_a,W_b\in\Omega, \forall\nu\in\mathbb{R}^d.$$

La fonction φ est appelée *flux numérique*. À ces deux propriétés il faut ajouter une condition de type CFL (Courant Friedrichs Levy), qui limite les pas de temps $t^{n+1}-t^n$ suivant

$$t^{n+1}-t^n \leq \frac{h}{\lambda}N_{CFL}, \quad \forall n\in[0,N-1]$$

où $N_{CFL}\in(0,1]$, $h = \sup\{\text{diam}(M_i), i\in\mathbb{Z}\}$ et λ est le maximum du module des valeurs propres de la matrice jacobienne du flux DF (voir [EGH00] ou [GR96] pour plus de précisions). Cette condition permet d'assurer la stabilité du schéma, tout au moins pour les lois de conservation scalaires. En supposant de plus que le flux numérique est consistant et conservatif, on peut montrer que le schéma (10) converge vers une solution faible du problème (6)-(7) si Ω est un ouvert de $\mathbb{R}$ (voir [EGH00] et les références citées).

On peut maintenant calculer l'approximation de la solution W au temps T sur la maille M_i à l'aide du schéma numérique (10) et de l'approximation de la donnée initiale (9). Clairement, la définition du schéma est étroitement liée au choix de la fonction φ. Il existe à l'heure actuelle une très grande variété de méthodes Volumes Finis. On trouvera dans l'ouvrage de E. Godlewski et P.A. Raviart [GR96] une présentation précise de plusieurs méthodes, ainsi que dans celui de E.F. Toro [Tor97]. Dans cette thèse, les méthodes utilisées sont essentiellement le schéma de Rusanov et le schéma nommé VFRoe-ncv.

Le schéma de Rusanov [Rus61] peut être assimilé à une méthode aux différences finies en une dimension d'espace. Il peut d'ailleurs être compris comme une version modifiée du schéma Lax-Friedrichs. Dans le cadre des équations d'Euler par exemple, il permet de plus d'assurer la positivité

de la densité discrète, même si $d > 1$ et si le maillage est non structuré (sous réserve que la densité discrète initiale est positive). Cette propriété est illustrée par plusieurs résultats numériques dans le chapitre 1, qui atteste du bon comportement du schéma pour les équations d'Euler en présence de zones à faible densité. De plus le système bifluide (2) étudié au chapitre 4 peut être vu comme deux systèmes d'Euler couplés par les termes non conservatifs. Ce schéma semble donc un très bon candidat pour la simulation des écoulements diphasiques où les phénomènes de disparition de phases posent en général de gros problèmes numériques.

Le schéma VFRoe-ncv a été introduit dans [BGH00]. Il constitue une extension du schéma VFRoe proposé par T. Gallouët dans [GM96]. Pour le schéma VFRoe, le flux numérique est basé sur une linéarisation de la matrice jacobienne du flux (on renvoie au chapitre 1 pour plus de précisions). La linéarisation du schéma VFRoe-ncv s'effectue quant à elle sur une matrice semblable à la matrice jacobienne du flux obtenue par un changement de variable non linéaire. Le choix de ce changement de variable est motivé par certaines propriétés de la solution du problème de Riemann unidimensionnel associé au système (6). On présente un comparatif de plusieurs changements de variable dans le cadre des équations d'Euler au chapitre 1 et dans le cadre des équations de Saint-Venant avec gradient de fond au chapitre 3. Les différents résultats numériques obtenus avec le schéma VFRoe-ncv attestent d'une plus grande précision que le schéma de Rusanov, notamment lorsque la solution comporte des discontinuités de contact (qui sont les ondes associées aux champs linéairement dégénérés). On voit par exemple sur la figure 1.23 du chapitre 1 (page 62) que le profil de l'approximation de la discontinuité de contact par le schéma de Rusanov est bien moins précise que celle obtenue par les schémas VFRoe et VFRoe-ncv. Néanmoins, la vitesse de convergence en norme L^1 quand h tend vers 0 de toutes ces méthodes est très proche (voir entre autres les vitesses de convergence répertoriées page 64).

On vient donc de présenter les méthodes Volumes Finis appliquées au systèmes hyperboliques conservatifs. Le système bifluide (2) étant non conservatif, la formule de Green ne peut plus être appliquée. Une adaptation non conservative des schémas doit être proposée, mais X. Hou et P.G. LeFloch [HL94] ont montré sur des cas pourtant simples qu'assurer la convergence du schéma vers la solution du problème non conservatif est très difficile. Pourtant, le système (2) ne rentre pas dans le cadre de X. Hou et P.G. LeFloch, il serait donc intéressant d'étudier, au moins numériquement, la convergence des schémas présentés dans le chapitre 4 vers des solutions analytiques non triviales, comme celle présentée figure 4.2, page 186.

Il est clair que l'analyse et l'approximation du modèle (1) est difficile, c'est pourquoi on a choisi dans les trois premiers chapitres d'étudier des modèles plus simples, mais qui en conservent certaines pathologies. Cette approche a ainsi permis une étude plus aboutie et une compréhension plus précise de différentes caractéristiques du système bifluide, tout en apportant une contribution dans le cadre de chaque problème abordé. Il faut noter que des aspects comme la prise en compte des effets de diffusion moléculaire ou de turbulence ne sont pas abordés dans cette thèse.

Comme on l'a dit précédemment, le modèle bifluide peut être interprété comme un système composé des équations d'Euler pour chaque fluide avec des termes non conservatifs couplant les deux fluides. Proposer des méthodes numériques pertinentes pour ce modèle présuppose évidemment *a minima* d'être capable d'effectuer des simulations des équations d'Euler pour toute équation d'état. Ainsi, dans le premier chapitre, on compare différents schémas Volumes Finis récents ou peu connus pour l'approximation des équations d'Euler auxquelles on associe successivement la loi des gaz parfaits, la loi de Tammann et la loi de Van der Waals. Ce système possède la même structure que les

modèles HEM (modèle homogène équilibré) ou HRM (modèle homogène relaxé). Les problèmes numériques abordés dans ce chapitre sont principalement la précision des algorithmes lorsque le « vide » est présent dans la solution au temps final ou dans la donnée initiale, et leur robustesse. Les différents tests de robustesse permettent notamment d'avoir un aperçu du comportement des schémas pour des configurations d'écoulements à obstacle (*bluff body*) dans le cadre monophasique ou pour des phénomènes d'apparition ou de disparition de phase dans le contexte diphasique. La précision des schémas est quantifiée par la mesure de l'erreur en norme L^1 entre la solution exacte et l'approximation fournie par les schémas. On a ainsi accès aux vitesses de convergence des schémas lorsque le maillage est raffiné avec un « nombre CFL » (noté plus haut N_{CFL}) constant, pour des solutions discontinues (on rappelle que les ordres de convergence sont supérieurs pour les solutions régulières). Ce chapitre correspond à un article paru dans *International Journal of Numerical Methods in Fluids* avec pour coauteurs Thierry Gallouët et Jean-Marc Hérard.

Le chapitre 2 traite de l'analyse et de l'approximation d'une loi de conservation incluant le phénomène de résonnance. Cette équation scalaire est issue de la modélisation des écoulements diphasiques eau-huile en milieu poreux. On rappelle que la résonnance se caractérise pour cette équation par le fait qu'on puisse proposer une réécriture sous forme d'un système 2×2 dont la matrice jacobienne du flux peut devenir non diagonalisable dans $\mathbb{R}$ lorsque ses valeurs propres coïncident. En fait, si on suppose certaines fermetures algébriques sur le système bifluide, le problème de résonnance peut apparaître (là aussi des valeurs propres peuvent s'identifier et la matrice de convection peut devenir non diagonalisable dans $\mathbb{R}$). On montre l'existence et l'unicité de la solution entropique pour une donnée initiale bornée et on exhibe la solution du problème de Riemann associée à cette équation. De plus, deux schémas Volumes Finis « équilibres » au sens de J.M. Greenberg and A.Y. LeRoux [GL96] sont proposés comme alternative aux méthodes déjà existantes dans le contexte industriel pétrolier. Divers tests numériques permettent de comparer qualitativement et quantitativement toutes ces méthodes, dont les résultats sont nettement en faveur des deux nouveaux schémas. On peut d'ailleurs noter que l'un des deux schémas proposés est basé sur une linéarisation du problème qui fait disparaître localement la résonnance et qu'il fournit néanmoins des résultats très satisfaisants pour toute configuration d'écoulement. Ce chapitre correspondant à un travail réalisé avec Julien Vovelle est accepté pour publication dans le journal *Mathematical Models and Methods in Applied Sciences*.

Le chapitre 3 est consacré à l'approximation des termes source dans des systèmes hyperboliques à dominante convective. Il est évident que les modèles bifluides incluent un nombre important de termes source, chacuns de nature différente (termes géométriques, termes de tranfert interfaciaux, termes de relaxation, ...). On s'intéresse dans ce chapitre plus particulièrement à l'approximation des termes géométriques, en se focalisant sur les équations de Saint-Venant avec topographie. Ce système est très proche des modèles monofluides en tuyère, bien qu'il modélise les écoulements hydrauliques incompressibles à surface libre avec un fond non plat. Il possède une particularité intéressante qui est que le vide (zone sèche) est un état licite pour ce modèle, aussi bien en tant que condition initiale comme pour une rupture de barrage sur fond sec ou que zone sèche apparaissant lors de la simulation (bancs découvrants). On retrouve là une problématique déjà évoquée au chapitre 1. Une autre particularité de ce système est qu'il est lui aussi résonnant, lorsque le terme de topographie est considéré comme un terme non conservatif. Enfin, ce système peut être vu comme un système hyperbolique non conservatif dont la structure s'avère proche du modèle à sept équations. Plusieurs schémas Volumes Finis adaptés sont proposés et comparés à la technique de splitting d'opérateur couramment utilisée pour les codes industriels. Ces schémas se basent sur

une linéarisation des schémas « équilibre » d'A.Y. LeRoux (voir [LeR98]) et permettent une prise en compte directe du terme source dans le décentrement. On présente plusieurs tests incluant la convergence en temps vers des états stationnaires et des simulations transitoires incluant des zones sèches. Une technique permettant une augmentation de la précision des schémas et de leur vitesse de convergence est aussi détaillée. Elle est basée sur la technique MUSCL due à B. Van Leer [Van79] utilisant une reconstruction linéaire par morceaux des variables. On montre que la prise en compte de la forme des états stationnaires lors de la reconstruction est nécessaire pour en permettre une approximation précise. Ce travail réalisé avec Thierry Gallouët et Jean-Marc Hérard a fait l'objet d'un article accepté pour publication dans le journal *Computers and Fluids*.

Dans le chapitre 4, on étudie le modèle bifluide à deux pressions évoqué ci-dessus. Sa principale caractéristique par rapport aux modèles généralement utilisés dans les codes industriels est que les pressions phasiques ne sont pas supposées égales en tout point à tout instant [Ish75]. En fait, un terme de relaxation permet de retrouver l'équilibre en un temps infiniment court. L'opérateur de moyenne appliqué à l'équation de suivi d'interface fournit une équation aux dérivées partielles supplémentaire sur la fraction volumique. Elle correspond à l'advection de la fraction volumique à la vitesse V_i, V_i étant la vitesse interfaciale, avec un terme de relaxation en pression permettant d'obtenir asymptotiquement l'équilibre en pression. La forme de cette équation assure le principe du maximum sur la fraction volumique et que le système différentiel du premier ordre est inconditionnellement hyperbolique, mais non conservatif (en raison de la présence de termes de transfert de quantité de mouvement et d'énergie entre phases). En définissant de manière adéquate la vitesse interfaciale et la pression interfaciale, on peut fermer le système au sens algébrique et au sens des relations de saut de Rankine-Hugoniot et on peut montrer que la solution du problème de Riemann est en accord avec le principe du maximum sur la fraction volumique et les principes de positivité de masses partielles et des énergies internes de chaque phase pour des équations phasiques d'état de type gaz parfaits ou Tammann. Sous l'hypothèse de ces fermetures, on retrouve les mêmes phénomènes de résonnance que ceux des chapitres 2 et 3. Les propriétés de positivité sont préservées lors des étapes de relaxation en vitesse et en pression. Pour l'approximation du système, on utilise un splitting d'opérateur séparant le système du premier ordre des différents termes source (relaxation, gravité, ...), comme cela avait été étudié au chapitre 3. Le premier opérateur est discrétisé par des méthodes Volumes Finis. On compare deux schémas, le schéma de Rusanov et le schéma VFRoe-ncv (tous deux déjà présentés dans le premier chapitre), sur des tests de type tube à choc diphasique. On associe à ces schémas une discrétisation des termes de relaxation respectant les différents principes du maximum et de positivité, pour permettre de simuler différents cas tests diphasiques de référence. Ce chapitre a fait l'objet d'une note publiée dans les *Comptes Rendus Mathématique de l'Académie des Sciences de Paris*, Série I-334 (2002), pages 927–932 (dont les coauteurs sont Frédéric Coquel, Thierry Gallouët et Jean-Marc Hérard) ainsi que d'une présentation au congrès « *Third International Symposium on Finite Volume methods for Complex Applications — Problems and perspectives* » à Porquerolles, France, du 24 au 28 juin 2002 (avec Thierry Gallouët et Jean-Marc Hérard).

Enfin, trois annexes viennent compléter ce travail. La première traite de la simulation d'écoulements avec « vide » par des schémas Volumes Finis, dans le cadre des équations de Saint-Venant, des équations d'Euler et du modèle K. L'annexe B traite du principe du maximum et de la positivité des solutions de différents modèles diphasiques. Dans la dernière annexe, on propose une classe de schémas Volumes Finis permettant un traitement précis des discontinuités de contact pour les équations d'Euler avec une loi thermodynamique fortement non linéaire (voire tabulée).

Bibliographie

[BCG+02] P. Bagnerini, F. Coquel, E. Godlewski, C. Marmignon, and S. Rouy. A void fraction relaxation principle for averaged two phase flow models. in preparation, 2002.

[BGH00] T. Buffard, T. Gallouët, and J.M. Hérard. A sequel to a rough Godunov scheme. Application to real gas flows. *Computers and Fluids*, 2000, vol. 29-7, pp. 813–847.

[BN86] M.R. Baer and J.W. Nunziato. A two phase mixture theory for the deflagration to detonation (DDT) transition in reactive granular materials. *Int. J. Multiphase Flow*, 1986, vol. 12-6, pp. 861–889.

[CLL94] G.Q. Chen, C.D. Levermore, and T.P. Liu. Hyperbolic conservation laws with stiff relaxation terms and entropy. *Comm. Pure and Appl. Math.*, 1994, vol. 7, pp. 787–830.

[Col92] J.F. Colombeau, *Multiplication of distributions*, Springer Verlag, 1992.

[Daf99] C. Dafermos, *Hyperbolic conservation laws in continuum physics*, Springer Verlag, Berlin, 1999.

[DL85] R. Dautray and J.L. Lions, *Analyse mathématique et calcul numérique pour les sciences et techniques - Tome III*, Masson, 1985.

[DLM95] G. Dal Maso, P.G. LeFloch, and F. Murat. Definition and weak stability of non conservative products. *J. Math. Pures Appl.*, 1995, vol. 74, pp. 483–548.

[EGH00] R. Eymard, T. Gallouët, and R. Herbin, Finite Volume Methods, In *Handbook of Numerical Analysis* (Vol. VII), editors : P.G. Ciarlet and J.L. Lions, North-Holland, pp. 729–1020, 2000.

[For02] A. Forestier. Pressure relaxation process for multiphase compressible flows. *preprint*, 2002.

[GL96] J.M. Greenberg and A.Y. LeRoux. A well balanced scheme for the numerical processing of source terms in hyperbolic equation. *SIAM J. Numer. Anal.*, 1996, vol. 33-1, pp. 1–16.

[GM96] T. Gallouët and J.M. Masella. A rough Godunov scheme. *C. R. Acad. Sci. Paris*, 1996, vol. I-323, pp. 77–84.

[GR96] E. Godlewski and P.A. Raviart, *Numerical approximation of hyperbolic systems of conservation laws*, Springer Verlag, 1996.

[GS02] S. Gavrilyuk and R. Saurel. Mathematical and numerical modelling of two phase compressible flows with inertia. *J. Comp. Phys.*, 2002, vol. 175-1, pp. 326–360.

[GSS99] J. Glimm, D. Saltz, and D.H. Sharp. Two phase flow modelling of a fluid mixing layer. *Journal of Fluid Mechanics*, 1999, vol. 378, pp. 119–143.

[HL94] X. Hou and P. G. LeFLoch. Why non conservative schemes converge to wrong solutions: error analysis. *Mathematics of computation*, 1994, vol. 62-206, pp. 497–530.

[Ish75] M. Ishii, *Thermo-fluid dynamic theory of two-phase flows*, Collection de la Direction des Etudes et Recherches d'Électicité de France, 1975.

[IT90] E. Isaacson and B. Temple, Nonlinear resonance in inhomogeneous systems of conservation laws, In *Mathematics of nonlinear science (Phoenix, AZ, 1989)*. Amer. Math. Soc., pp. 63–77, Providence, RI, 1990.

[KSB+97] A.K. Kapila, S.F. Son, J.B. Bdzil, R. Menikoff, and D.S. Stewart. Two-phase modeling of DDT: Structure of the velocity-relaxation zone. *Phys. Fluids*, 1997, vol. 9-12.

[LeF88] P.G. LeFloch. Entropy weak solutions to nonlinear hyperbolic systems in nonconservative form. *Comm. PDE*, 1988, vol. 13, pp. 669–727.

[LeR98] A.Y. LeRoux, Discrétisation des termes sources raides dans les problèmes hyperboliques, In *Systèmes hyperboliques : nouveaux schémas et nouvelles applications*. Écoles CEA-EDF-INRIA "problèmes non linéaires appliqués", INRIA Rocquencourt (France), March 1998. Available on
http://www-gm3.univ-mrs.fr/∼leroux/publications/ay.le_roux.html, In French.

[Liu88] T.P. Liu. Hyperbolic conservation laws with relaxation. *Comm. Math. Phys.*, 1988, vol. 108, pp. 153–175.

[Rus61] V.V. Rusanov. Calculation of interaction of non-steady shock waves with obstacles. *J. Comp. Math. Phys. USSR*, 1961, vol. 1, pp. 267–279.

[SA99] R. Saurel and R. Abgrall. A multiphase Godunov method for compressible multifluid and multiphase flows. *J. Comp. Phys.*, 1999, vol. 150, pp. 425–467.

[Sai96] L. Sainsaulieu. Traveling-wave solutions of convection-diffusion systems in nonconservative form. *SIAM J. Math. Anal.*, 1996, vol. 27-5, pp. 1286–1310.

[SM98] A.J. De Souza and D. Marchesin. Resonances for contact wave in systems of conservation laws. *Comp. Appl. Math.*, 1998, vol. 17-3, pp. 317–341.

[Tor97] E.F. Toro, *Riemann solvers and numerical methods for fluid dynamics*, Springer Verlag, 1997.

[Van79] B. VanLeer. Toward the ultimate conservative difference scheme V. A second order sequel to Godunov's method. *J. Comp. Phys.*, 1979, vol. 32, pp. 101–136.

Chapitre 1

Approximation numérique de modèles diphasiques monofluides eau-vapeur

On étudie dans ce chapitre différents schémas Volumes Finis pour l'approximation des écoulements diphasiques eau-vapeur modélisés par une approche monofluide monovitesse avec une loi thermodynamique complexe. Le modèle considéré (Homogeneous Equilibrium Model) s'écrit

$$\begin{array}{l}(\rho_m)_t + \big(\rho_m u_m\big)_x = 0,\\ (\rho_m u_m)_t + \big(\rho_m (u_m)^2 + p_m\big)_x = 0,\\ (E_m)_t + \big(u_m(E_m + p_m)\big)_x = 0,\end{array} \tag{1.1}$$

où ρ_m, u_m et E_m sont respectivement la densité du mélange, la vitesse du mélange et l'énergie totale du mélange. La pression p_m s'exprime suivant une loi thermodynamique de la forme

$$p_m = \varphi\big(\rho_m, E_m - (\rho_m u_m)^2/(2\rho_m)\big). \tag{1.2}$$

On remarque qu'ici les termes sources (pertes de charges, apport externe de chaleur) et les termes visqueux sont négligés et la vitesse relative entre les deux phases est supposée nulle. L'équation d'état (1.2) est dite complexe car, d'un point de vue mathématique, sa forme peut entraîner une perte d'hyperbolicité de (1.1) et les méthodes numériques classiques d'approximation peuvent s'avérer imprécises par rapport au cas de lois d'état plus simples (comme la loi des gaz parfaits par exemple). C'est sur ce dernier point que porte ce chapitre. Ce problème de complexité de loi d'état est dû au fait que celle-ci doit prendre en compte à la fois la thermodynamique de l'eau, de la vapeur et du mélange eau-vapeur. Néanmoins, si on privilégie l'approche bifluide, on peut voir (annexe 4.A du chapitre 4) que seules les lois d'états simples sont autorisées par l'opérateur de moyenne.

L'étude réalisée concerne trois lois d'état : la loi des gaz parfaits, la loi de Tammann et la loi de Van der Waals [LF93]. Cette dernière loi permet de modéliser un mélange diphasique eau-vapeur.

Dans les zones monophasiques de l'espace des etats, on obtient un système hyperbolique, alors que dans la zone de transition de phase, les valeurs propres de la matrice jacobienne du flux sont complexes (comportement elliptique). Ici, la solution des cas tests proposés pour la loi de Van der Waals n'inclut pas d'états pour lesquels le système (1.1) n'est pas hyperbolique. Les schémas sont tous de type Volumes Finis. La plupart de ces méthodes sont basées sur des schémas de Godunov approchés [GM96], [MFG99], [BGH00]. On étudie de plus le schéma de Rusanov [Rus61] et la méthode de relaxation d'énergie [CP98]. Tous ces schémas sont implémentés dans leur forme originale, puis couplés avec la méthode MUSCL d'extension à l'ordre « deux » [Van79]. Les tests sur lesquels les mesures numériques sont effectuées sont de type tube à choc, c'est-à-dire que la condition initiale est composée de deux états constants séparés par une interface située au milieu du domaine. La solution exacte est connue, ce qui permet de comparer la diffusion numérique de chacun des schémas étudiés ici et de mesurer leur vitesse de convergence vers la solution exacte lorsque le maillage est raffiné.

Plusieurs configurations de solutions ont été envisagées permettant d'évaluer la vitesse de convergence des différentes méthodes en présence de discontinuités lorsque le pas d'espace temps vers zéro. Ainsi, pour des ondes associées à des champs vraiment non linéaires, la vitesse de convergence de *tous* les schémas testés ici est 0.8 pour les ondes de raréfaction et de 1 pour les ondes de choc (la vitesse devient 1 dans les deux cas lorsqu'on utilise la méthode MUSCL). Concernant les champs linéairement dégénérés, la vitesse mesurée est d'environ 1/2 (2/3 avec la méthode MUSCL). On rappelle d'ailleurs que ces mesures ne sont pas en contradiction avec les appellations de schémas d'ordre « un » et d'ordre « deux », qui ne font référence qu'aux solutions régulières $\mathcal{C}^\infty$. En effet, même si les ondes de raréfaction sont continues, elles ne sont pas $\mathcal{C}^1$, ce qui suffit à faire chuter la vitesse de convergence des schémas.

Ces mesures permettent de mettre en lumière une difficulté numérique pour la simulation des écoulements diphasiques où la discontinuité de contact correspond souvent à l'interface entre deux mélanges. En effet, c'est pour cette onde que la vitesse de convergence est en pratique la plus faible (ce qui est dû à la forme du spectre). De plus, la condition CFL (Courant Friedrichs Levy) est toujours calculée en fonction de la vitesse maximale des ondes, à savoir $|u_m| + c_m$ (c_m est la vitesse du son du mélange). Cette condition définit le « nombre CFL » (noté N_{CFL}), qui doit être en général inférieur à 1/2 ou 1, selon le schéma numérique considéré, pour assurer la stabilité du calcul. De plus, on rappelle que ce nombre doit être le plus proche de la limite de stabilité (qu'on suppose égale à 1 par la suite) pour que la précision de la méthode numérique soit optimale. En pratique, N_{CFL} est défini par

$$N_{CFL} = \frac{(|u_m| + c_m)\Delta t}{\Delta x}.$$

Or, pour être optimal pour l'approximation de l'onde u_m, le « nombre CFL » associé à cette onde (noté $N_{CFL}^{'}$) devrait être égal à

$$N_{CFL}^{'} = \frac{|u_m|\Delta t}{\Delta x}.$$

Si on note M le nombre de Mach défini par $M = |u_m|/c_m$, on obtient que

$$N_{CFL}^{'} = \frac{M}{1+M} N_{CFL}.$$

Clairement, pour un schéma explicite, le nombre $N_{CFL}^{'}$ est loin d'être optimal en terme de précision pour l'approximation du champ linéairement dégénéré associé à l'onde u_m (dans les configurations

classiques d'écoulements, u_m est petit devant c_m et donc N'_{CFL} de l'ordre de M) et la diffusion numérique pour ce champ est bien plus importante que pour les champs vraiment non linéaires (associés aux ondes $u_m - c_m$ et $u_m + c_m$). Par ailleurs, lorsqu'on s'intéresse à des solutions à vitesse et pression uniforme (en espace), tous les schémas étudiés ici préservent exactement ces deux variables constantes pour des lois d'état simples (loi des gaz parfaits et loi de Tammann). Par contre, si la loi de Van der Waals est utilisée, la vitesse et la pression se mettent alors à varier au cours du calcul (ce problème est d'ailleurs reproduit par tous les schémas classiques [Abg95], [SA99]). Concernant le schéma de Rusanov, ces variations sont en plus amplifiées par son manque de précision sur maillage grossier (voir les figures 1.17-1.18 et 1.23-1.24). Bien sûr, toutes ces variations disparaissent à vitesse 1/2 en raffinant le maillage.

Différentes méthodes existent pour remédier à ces problèmes. Tout d'abord, concernant la diffusion numérique associée au champ linéairement dégénéré, des méthodes de préconditionnement peuvent être utilisées, pour ajuster au mieux la condition CFL (donc le calcul du pas de temps) à la vitesse de la discontinuité de contact. Cependant, celles-ci ne permettent en aucun cas d'augmenter la vitesse de convergence vers des solutions incluant des discontinuités de contact. Pour cela, une modification applicable à certains schémas de Godunov approchés (et bien sûr au schéma de Godunov) est proposée en annexe C. Grâce à ce traitement, la vitesse et la pression sont maintenues constantes sur tout maillage unidimensionnel lorsque la donnée initiale l'implique, quelle que soit la loi d'état considérée (Van der Waals, lois d'état tabulées [RM95], ...). Néanmoins, la vitesse de convergence sur la densité reste au mieux égale à 1/2 (aucune méthode ne permet de régler ce problème ni dans le cadre linéaire ni dans le cadre non linéaire à la connaissance des auteurs). Cette faible vitesse de convergence est d'autant plus gênante que dans le cadre des écoulements diphasiques bifluides à deux pressions du chapitre 4, la solution issue d'un tube à choc contient jusqu'à *trois* discontinuités de contact non superposées. On peut prévoir que les méthodes Volumes Finis classiques seront peu précises (mais toujours convergentes vers la solution faible attendue), notamment au niveau des états intermédiaires.

Some recent Finite Volume schemes to compute Euler equations using real gas EOS

Co-authored with Thierry Gallouët and Jean-Marc Hérard.

Abstract

This paper deals with the resolution by Finite Volume methods of Euler equations in one space dimension, with real gas state laws (namely perfect gas EOS, Tammann EOS and Van Der Waals EOS). All tests are of unsteady shock tube type, in order to examine a wide class of solutions, involving Sod shock tube, stationary shock wave, simple contact discontinuity, occurence of vacuum by double rarefaction wave, propagation of a 1-rarefaction wave over "vacuum", ... Most of methods computed herein are approximate Godunov solvers: VFRoe, VFFC, VFRoe ncv (τ, u, p) and PVRS. The energy relaxation method with VFRoe ncv (τ, u, p) and Rusanov scheme have been investigated too. Qualitative results are presented or commented for all test cases and numerical rates of convergence on some test cases have been measured for first and second order (Runge-Kutta 2 with MUSCL reconstruction) approximations. Note that rates are measured on solutions involving discontinuities, in order to estimate the loss of accuracy due to these discontinuities.

1.1 Introduction

We discuss in this paper the suitability of some Finite Volume schemes to compute Euler equations when dealing with real gas state laws, restricting to the one dimensional framework. Some measured rates of convergence will be presented when focusing on some Riemann problem test cases. This work is based on [Seg00].

Almost all schemes investigated here are approximate Riemann solvers (more exactly approximate Godunov solvers). One may note that comparison with some well known schemes like Godunov scheme or Roe scheme are not provided in this paper; however, one may refer to [BGH98b], [In99b], [Mas97], [MFG99], [Xeu99] for that purpose. Approximate Riemann solvers presented herein may be derived using the general formalism of VFRoe ncv scheme. This only requires defining some suitable variable which is not necessarily the conservative variable, but may be defined on the basis

Paru dans *International Journal for Numerical Methods in Fluids*, volume 39, numéro 12, pages 1073-1138, 2002.

of the solution of the Riemann problem for instance. The first one is obviously VFRoe scheme introduced in [GM96],[Mas97] and [MFG99], where the candidate is the conservative variable. In the second one, which is known as VFFC scheme, and was introduced in [GKL96], [Bou98] and [Kum95], the privileged variable is the flux variable. The third one, which was introduced some years ago in [BGH96] and with more details in [BGH00], suggests to consider the ${}^t(\tau, u, p)$ variable in the Euler framework. Extensions of the latter scheme to the frame of shallow water equations, or to some non conservative hyperbolic systems arising in the "turbulent" literature are described in [BGH98a], [BGH98b] and [BGH99]. The fourth one, which applies for the ${}^t(\rho, u, p)$ variable when computing the Euler equations, was introduced by E. F. Toro in [Tor91], [Tor97] and [ICT98], and is known as PVRS (Primitive Variable Riemann Solver). Note that the latter two rely on (u, p) components, which completely determine the solution of the associated Riemann problem, in the sense that assuming no jump on these in the initial conditions results in "ghost" 1-wave and 3-wave. Thus the latter two schemes, which are based on the use of u and p variables, are indeed quite different from the other two, since the former require no knowledge of the one dimensional Riemann problem solution.

Two slightly different schemes are also used for broader comparison. The first one is the Rusanov scheme ([Rus61]), which is known to be rather "diffusive" but anyway enjoys rather pleasant properties, especially when one aims at computing multi dimensional flows on any kind of unstructured mesh. Recall that for Euler type systems, this scheme ensures the positivity of mass and species, provided that the "cell" CFL number is smaller than 1 ([GHK98]). Even more, it requires no entropy correction at sonic points in rarefaction waves, when restricting to "first" order formulation. The last scheme examined is the energy relaxation method proposed by F. Coquel and B. Perthame in [CP98] (see also [In99a] and [In99b] for applications) applied to the frame of VFRoe scheme with ${}^t(\tau, u, p)$ variable. This one again seems appealing both for its simplicity and for its ability to get rid of entropy correction at sonic points in regular fields.

Both "first order" schemes and "second order" schemes (using RK2 time integration and MUSCL reconstruction with minmod limiter on primitive variables) are examined. This includes three distinct EOS, namely:

- perfect gas EOS,
- Van der Waals EOS,
- Tammann EOS.

Though complex tabulated EOS are not discussed herein, all above mentionned schemes enable computation of EOS such as those detailed in [RM95] or [KMJ]. Numerous unsteady tests are performed, involving a wide variety of initial conditions, so that the solution may be either a 1-rarefaction wave with a 3- shock wave, a double shock wave or a double rarefaction wave. We give emphasis on symetric double rarefaction (or shock) waves, since these allow investigation of wall boundary conditions when the standard mirror technique is applied for. The particular experiment of a single isolated contact discontinuity is also described, since the behaviour highly depends on the nature of the state law (see also [SA99] and [GHS01] on that specific topic). Note also that for almost incompressible fluids, the eigenvalue associated with the LD field is such that the local CFL number varies as $M/(1+M)$, where M stands for the local Mach number, as soon as the overall

CFL number is set to 1. As a result, the accuracy of the prediction of the contact discontinuity is rather poor, which is rather annoying since the vapour quality only varies through this field. Eventually, we note that these test cases include the occurence of vacuum, and the propagation of a shock wave over a (almost) vacuum of gas. The standard stationnary shock is also reported. For completness, we also refer to [LF93] where Godunov scheme [God59] is used to compute Van Der Waals EOS.

Qualitative behaviour of schemes is discussed, and L^1 error norm is plotted in some cases to provide quantitative comparison. Of course, restricting to smooth solutions, "first order" schemes (respectively "second order" schemes) converge at the order 1 (resp. at the order 2), as exposed for instance in [Buf93] and [LeV97]. Solutions investigated here involve some points where the smoothness is only $\mathcal{C}^0$ (at the beginning and at the end of rarefaction waves) and even discontinuities (shocks or contact discontinuities). The quantitative study aims at estimating the rate of convergence in such configurations. Several unsteady solutions are presented:

i. smooth solutions ($\mathcal{C}^\infty$),

ii. pure contact discontinuities,

iii. pure shock waves,

iv. rarefaction waves connected with constant states (solutions are not $\mathcal{C}^1$),

v. shock tube test cases which involve several waves.

Both “first” and “second” order schemes are used on these test cases and associated rates of convergence are measured by refining the mesh (with a constant CFL number).

1.2 Governing equations

1.2.1 Euler equations under conservative form

Governing Euler equations are written in terms of the mean density ρ, the mean pressure p, the mean velocity u and the total energy E as follows:

$$\frac{\partial W}{\partial t} + \frac{\partial F(W)}{\partial x} = 0 \tag{1.3}$$

setting:

$$W = \begin{pmatrix} \rho \\ \rho u \\ E \end{pmatrix} \quad , \quad F(W) = \begin{pmatrix} \rho u \\ \rho u^2 + p \\ u(E+p) \end{pmatrix} \quad \text{and} \quad E = \rho(\frac{1}{2}u^2 + \varepsilon)$$

If ε denotes the internal energy, then some law is required to close the whole system:

$$p = p(\rho, \varepsilon) \tag{1.4}$$

such that the Jacobian matrix may be diagonalized in $\mathbb{R}$ for $W \in \Omega$, Ω the set of admissible states, so that $\hat{\gamma}(p,\rho)p > 0$, $\rho > 0$, where:

$$\rho c^2(p,\rho) = \hat{\gamma}(p,\rho)p = \left(\frac{\partial \varepsilon}{\partial p}_{|\rho}\right)^{-1}\left(\frac{p}{\rho} - \rho\frac{\partial \varepsilon}{\partial \rho}_{|p}\right)$$

Herein, c stands for the speed of acoustic waves.

The Jacobian matrix $A(W) = \dfrac{\partial F(W)}{\partial W}$ may be written:

$$A(W) = \begin{pmatrix} 0 & 1 & 0 \\ K - u^2 & u(2-k) & k \\ (K-H)u & H - ku^2 & u(1+k) \end{pmatrix}$$

setting:

$$\begin{aligned} H &= \frac{E+p}{\rho} \\ k &= \frac{1}{\rho}\frac{\partial p}{\partial \varepsilon}_{|\rho} \\ K &= c^2 + k(u^2 - H) \end{aligned}$$

Eigenvalues of the Jacobian matrix $A(W)$ read:

$$\lambda_1 = u - c,\ \lambda_2 = u,\ \lambda_3 = u + c$$

Associated right eigenvectors are:

$$r_1(W) = \begin{pmatrix} 1 \\ u - c \\ H - uc \end{pmatrix},\ r_2(W) = \begin{pmatrix} 1 \\ u \\ H - \frac{c^2}{k} \end{pmatrix},\ r_3(W) = \begin{pmatrix} 1 \\ u + c \\ H + uc \end{pmatrix}$$

Left eigenvectors of $A(W)$ are:

$$l_1(W) = \frac{1}{2c^2}\begin{pmatrix} K + uc \\ -ku - c \\ k \end{pmatrix},\ l_2(W) = \frac{k}{c^2}\begin{pmatrix} H - u^2 \\ u \\ -1 \end{pmatrix},\ l_3(W) = \frac{1}{2c^2}\begin{pmatrix} K - uc \\ -ku + c \\ k \end{pmatrix}$$

Recall that the 1-wave and the 3-wave are Genuinely Non Linear fields and that the 2-wave is Linearly Degenerated. In an alternative way, Euler equations may be written in a non conservative form, when restricting to smooth solutions.

We only provide herein some useful computations of right and left eigenvectors based on non conservative forms of Euler equations.

1.2.2 Non conservative form wrt (τ, u, p)

Let us set $\tau = 1/\rho$. Thus, Euler equations may written in terms of (τ, u, p) as:

$$\frac{\partial Y_1}{\partial t} + B_1(Y_1)\frac{\partial Y_1}{\partial x} = 0$$

with

$$Y_1 = \begin{pmatrix} \tau \\ u \\ p \end{pmatrix} \quad \text{and} \quad B_1(Y_1) = \begin{pmatrix} u & -\tau & 0 \\ 0 & u & \tau \\ 0 & \hat{\gamma}p & u \end{pmatrix}$$

Obviously, eigenvalues of $B_1(Y_1)$ are still:

$$\lambda_1 = u - c,\ \lambda_2 = u,\ \lambda_3 = u + c$$

Right eigenvectors of matrix $B_1(Y_1)$ are:

$$r_1(Y_1) = \begin{pmatrix} \tau \\ c \\ -\hat{\gamma}p \end{pmatrix},\ r_2(Y_1) = \begin{pmatrix} 1 \\ 0 \\ 0 \end{pmatrix},\ r_3(Y_1) = \begin{pmatrix} \tau \\ -c \\ -\hat{\gamma}p \end{pmatrix}$$

Left eigenvectors of $B_1(Y_1)$ are:

$$l_1(Y_1) = \frac{1}{2c^2}\begin{pmatrix} 0 \\ c \\ -\tau \end{pmatrix},\ l_2(Y_1) = \frac{1}{c^2}\begin{pmatrix} 1 \\ 0 \\ \tau^2 \end{pmatrix},\ l_3(Y_1) = \frac{1}{2c^2}\begin{pmatrix} 0 \\ -c \\ -\tau \end{pmatrix}$$

1.2.3 Non conservative form wrt (ρ, u, p)

In a similar way, we may rewrite Euler equations in terms of (ρ, u, p):

$$\frac{\partial Y_2}{\partial t} + B_2(Y_2)\frac{\partial Y_2}{\partial x} = 0$$

with:

$$Y_2 = \begin{pmatrix} \rho \\ u \\ p \end{pmatrix} \quad \text{et} \quad B_2(Y_2) = \begin{pmatrix} u & \rho & 0 \\ 0 & u & \frac{1}{\rho} \\ 0 & \hat{\gamma}p & u \end{pmatrix}$$

Right eigenvectors of $B_2(Y_2)$ are now:

$$r_1(Y_2) = \begin{pmatrix} 1 \\ -\frac{c}{\rho} \\ c^2 \end{pmatrix},\ r_2(Y_2) = \begin{pmatrix} 1 \\ 0 \\ 0 \end{pmatrix},\ r_3(Y_2) = \begin{pmatrix} 1 \\ \frac{c}{\rho} \\ c^2 \end{pmatrix}$$

Meanwhile, left eigenvectors of matrix $B_2(Y_2)$ read:

$$l_1(Y_2) = \frac{1}{2c^2}\begin{pmatrix} 0 \\ -\rho c \\ 1 \end{pmatrix},\ l_2(Y_2) = \begin{pmatrix} 1 \\ 0 \\ -\frac{1}{c^2} \end{pmatrix},\ l_3(Y_2) = \frac{1}{2c^2}\begin{pmatrix} 0 \\ \rho c \\ 1 \end{pmatrix}$$

1.2.4 Non conservative form wrt $F(W)$

We may rewrite the above mentionned equations in terms of variable $Y = F(W)$. We multiply on the left by $A(W)$ system (1.3):

$$A(W)\frac{\partial W}{\partial t} + A(W)\frac{\partial F(W)}{\partial x} = 0$$

Since $A(W)$ is the Jacobian matrix of flux $F(W)$, we get:

$$A(W)\frac{\partial W}{\partial t} = \frac{\partial F(W)}{\partial t}$$

Hence:

$$\frac{\partial F(W)}{\partial t} + A(W)\frac{\partial F(W)}{\partial x} = 0$$

The associated matrix still is $A(W)$. Eigenstructure is detailed in 1.2.1. We now describe the three equations of state used in our computations.

1.2.5 Considering various EOS

Perfect gas EOS

The closure law is:

$$p = (\gamma - 1)\rho\varepsilon$$

with:

$$\gamma = 1,4$$

Tammann EOS

This law is sometimes used to describe the thermodynamics of the liquid phase (see [Tor91]). It may be simply written as:

$$p = (\gamma_c - 1)\rho\varepsilon - \gamma_c p_c$$

where:

$$\gamma_c = 7,15 \quad p_c = 3.10^8$$

Actually, using some suitable change of variables enables to retrieve Euler equations with perfect gas state law, assuming $\gamma = \gamma_c$. This is an interesting point, since some schemes benefit from nice properties when restricting to perfect gas EOS (see for instance VFRoe with non conservative variable).

Van Der Waals EOS

Van Der Waals EOS is recalled below:

$$(p + \frac{a}{\tau^2})(\tau - b) = RT$$
$$\varepsilon - \varepsilon_0 = c_v T - \frac{a}{\tau}$$
$$c^2 = -2\frac{a}{\tau} + (p\tau^2 + a)(1 + \frac{R}{c_v})/(\tau - b)$$

where:

$$\begin{array}{rclrcl} b & = & 0,001692 & R & = & 461,5 \\ a & = & 1684,54 & c_v & = & 1401,88 \\ \varepsilon_0 & = & 0 & & & \end{array}$$

This identifies with perfect gas EOS while setting $a = b = 0$. This law enables to exhibit some deficiencies of schemes around the contact discontinuity in some cases. We refer to [LF93] which provides some approximation based on Godunov scheme, when focusing on this particular EOS. Initial conditions in shock-tube experiments are taken in this reference. Comparison with some other test cases can be found in [GHK98], [BGH96] and [BGH00].

1.3 Numerical schemes

1.3.1 Framework

Finite Volume schemes

We thus focus herein on some Finite Volume schemes (see for example [GR96] and [EGH00]). Regular meshes are considered, whose size Δx is such that: $\Delta x = x_{i+1/2} - x_{i-1/2}$, $i \in \mathbb{Z}$. Let us denote as usual Δt the time step, where $\Delta t = t^{n+1} - t^n$, $n \in \mathbb{N}$.
We denote $W \in \mathbb{R}^n$ the exact solution of the non degenerate hyperbolic system :

$$\left\{ \begin{array}{l} \dfrac{\partial W}{\partial t} + \dfrac{\partial F(W)}{\partial x} = 0 \\ W(x,0) = W_0(x) \end{array} \right.$$

with $F(W)$ in $\mathbb{R}^n$.
Let W_i^n be the approximate value of $\dfrac{1}{\Delta x}\displaystyle\int_{x_{i-1/2}}^{x_{i+1/2}} W(x,t^n)dx$.
Integrating over $[x_{i-1/2}; x_{i+1/2}] \times [t^n; t^{n+1}]$ provides:

$$W_i^{n+1} = W_i^n - \frac{\Delta t}{\Delta x}\left(\varphi_{i+1/2}^n - \varphi_{i-1/2}^n\right)$$

where $\varphi_{i+1/2}^n$ is the numerical flux through the interface $\{x_{i+1/2}\} \times [t^n; t^{n+1}]$. The time step should comply with some CFL condition in order to guarantee non interaction of numerical waves inside one particular cell, or some other stability requirement. We restrict our presentation to the frame of

three point schemes. Thus $\varphi^n_{i+1/2}$ only depends on W^n_i and W^n_{i+1}, namely $\varphi^n_{i+1/2} = \varphi(W^n_i, W^n_{i+1})$. Whatever the scheme is, the following consistancy relation should hold:

$$\varphi(V, V) = F(V)$$

Hence, we present now approximate numerical fluxes $\varphi(W_L, W_R)$ associated with the 1D Riemann problem:

$$\left\{ \begin{array}{l} \dfrac{\partial W}{\partial t} + \dfrac{\partial F(W)}{\partial x} = 0 \\ W(x,0) = \left\{ \begin{array}{ll} W_L & \text{if } x < 0 \\ W_R & \text{if } x > 0 \end{array} \right. \end{array} \right. \tag{1.5}$$

VFRoe schemes

These are approximate Godunov schemes where the approximate value at the interface between two cells is computed as follows. Let us consider some change of variable $Y = Y(W)$ in such a way that $W_{,Y}(Y)$ is inversible. The counterpart of above system for regular solutions is:

$$\frac{\partial Y}{\partial t} + B(Y)\frac{\partial Y}{\partial x} = 0$$

where $B(Y) = (W_{,Y}(Y))^{-1} A(W(Y))\ W_{,Y}(Y)$ ($A(W)$ stands for the jacobian matrix of flux $F(W)$). Now, the numerical flux $\varphi(W_L, W_R)$ is obtained solving the linearized hyperbolic system:

$$\left\{ \begin{array}{l} \dfrac{\partial Y}{\partial t} + B(\hat{Y})\dfrac{\partial Y}{\partial x} = 0 \\ Y(x,0) = \left\{ \begin{array}{ll} Y_L = Y(W_L) & \text{if } x < 0 \\ Y_R = Y(W_R) & \text{if } x > 0 \end{array} \right. \end{array} \right. \tag{1.6}$$

where $\hat{Y}$ is $(Y_L + Y_R)/2$.

Once the exact solution $Y^*(x/t; Y_L, Y_R)$ of this approximate problem is obtained, the numerical flux is:

$$\varphi(W_L, W_R) = F(W(Y^*(0; Y_L, Y_R)))$$

Notation. *In the following we note ˜ variables which are computed on the basis of $\overline{Y}$ (obviously, if α is one component of $\overline{Y}$, the relation below holds: $\widetilde{\alpha} = \overline{\alpha}$).*

Let us set $\widetilde{l_k}$, $\widetilde{\lambda_k}$ and $\widetilde{r_k}$, $k = 1, ..., n$, left eigenvectors, eigenvalues and right eigenvectors of matrix $B(\overline{Y})$ respectively. If $x/t \neq \lambda_k$, $k = 1, ..., n$, then the solution $Y^*(x/t; Y_L, Y_R)$ of linear problem is:

$$\begin{aligned} Y^*(x/t; Y_L, Y_R) &= Y_L + \sum_{x/t > \widetilde{\lambda_k}} ({}^t\widetilde{l_k}.(Y_R - Y_L))\widetilde{r_k} \\ &= Y_R - \sum_{x/t < \widetilde{\lambda_k}} ({}^t\widetilde{l_k}.(Y_R - Y_L))\widetilde{r_k} \end{aligned}$$

Let us emphasize that all schemes involved by the VFRoe ncv formalism are approximate Godunov schemes. Note that, contrary to the Godunov scheme, VFRoe ncv schemes cannot be interpreted as projection methods. Hence, no theoritical result exists to ensure a good behaviour of the algorithm when dealing with simulations including states near vacuum (see [EMRS91]).

Entropy correction

When one numerical eigenvalue associated with the 1-wave or the 3-wave vanishes, an entropy correction is needed for above mentionned schemes. If a 1-rarefaction wave overlapping the interface is detected, the approximate value at the interface is modified as:

$$Y^*(0; Y_L, Y_R) = \frac{Y_L + Y_1}{2}$$

In a first approach ([BGH96]), we may assume that overlapping occurs if:

$$\lambda_1(W_L) < 0$$

and if in addition $\widetilde{\lambda_1}$ is close to 0.

An alternative way consists in the proposal of A. Harten and J.M. Hyman in [HH83], thus checking whether:

$$\lambda_1(W_L) < 0 < \lambda_1(W_R)$$

This second approach has been applied herein.

1.3.2 Basic VFRoe scheme

This scheme was first proposed in [GM96], [Mas97] and [MFG99]. It is based on the following choice $Y(W) = W$ and thus $B(\overline{Y}) = A(\overline{W})$. Recall that $A(W)$ is the Jacobian matrix of $F(W)$ in the linearized Riemann problem.

1.3.3 VFRoe with non conservative variable (τ, u, p)

We set now $Y(W) = {}^t(\tau, u, p)$, where $\tau = 1/\rho$. This scheme was introduced in [BGH96] (see also [BGH00] and [BGH98b], [GHK98], [BGH99] for various applications).

With help of left eigenvectors of $B(\overline{Y})$ detailed in 1.2.2, and defining $\tilde{\alpha}_1$ and $\tilde{\alpha}_3$ as:

$$\tilde{\alpha}_1 = \frac{1}{2\widetilde{c}^2}(\widetilde{c}\Delta u - \overline{\tau}\Delta p)$$
$$\tilde{\alpha}_3 = -\frac{1}{2\widetilde{c}^2}(\widetilde{c}\Delta u + \overline{\tau}\Delta p)$$

where $\Delta(.) = (.)_R - (.)_L$, intermediate states Y_1 and Y_2 read:

$$Y_1 = \begin{pmatrix} \tau_L + \tilde{\alpha}_1\overline{\tau} \\ u_L + \tilde{\alpha}_1\widetilde{c} \\ p_L - \tilde{\alpha}_1\widetilde{\gamma}\overline{p} \end{pmatrix} \qquad \text{and} \qquad Y_2 = \begin{pmatrix} \tau_R - \tilde{\alpha}_3\overline{\tau} \\ u_R + \tilde{\alpha}_3\widetilde{c} \\ p_R + \tilde{\alpha}_3\widetilde{\gamma}\overline{p} \end{pmatrix}$$

Now:

$$Y_2 = Y_1 + ({}^t\widetilde{l_2}.(Y_R - Y_L))\widetilde{r_2}$$

and last composants of $\widetilde{r_2}$ are null, hence $u_1 = u_2$ and $p_1 = p_2$. The approximate solution is thus in agreement with the exact solution of the Riemann problem. Even more, if we assume that initial conditions agree with $\Delta u = 0$ and $\Delta p = 0$, the following holds $Y_1 = Y_L$ and $Y_2 = Y_R$ (see [BGH00]). This results in the fact that for some particular EOS such as perfect gas EOS and Tammann EOS, cell averages of velocity and pressure are perfectly preserved through the 2-wave, when focusing on single moving contact discontinuity and scheme VFRoe ncv (τ, u, p) (see [BGH99] and appendix 1.A for a general expression of the EOS).

Another property of this scheme is that single 1-shocks (respectively 3-shocks) are preserved in the sense that exact jump conditions and approximate jump conditions arising from linearised system are equivalent, when restricting to perfect gas EOS. In other words, if we set σ the speed of the shock wave and $[\alpha]$ the jump of α through this shock wave, then:

$$-\sigma[W] + [F(W)] = 0$$

and:

$$-\sigma[Y] + B(\overline{Y})[Y] = 0$$

are the same (see [BGH00] for more details). However, note that this scheme does not fulfill the Roe condition (see [Roe81]).

Eventually, we note that strictly speaking, the value $\widetilde{\widetilde{\gamma}}$ is completely determined for given choice of Y. Details concerning the discrete preservation of the positivity of density and pressure intermediate states can be found in [BGH00].

1.3.4 VFRoe with non conservative variable (ρ, u, p) -PVRS-

We now set $Y(W) = {}^t(\rho, u, p)$. This scheme actually identifies with PVRS (Primitive Variable Riemann Solver) scheme proposed by E.F. Toro, in [Tor97] or [ICT98]. Coefficients $\tilde{\alpha}_1$ and $\tilde{\alpha}_3$ are now:

$$\tilde{\alpha}_1 = \frac{1}{2\widetilde{c}^2}(-\overline{\rho}\widetilde{c}\Delta u + \Delta p)$$

$$\tilde{\alpha}_3 = \frac{1}{2\widetilde{c}^2}(\overline{\rho}\widetilde{c}\Delta u + \Delta p)$$

Hence:

$$Y_1 = \begin{pmatrix} \rho_L + \tilde{\alpha}_1 \\ u_L - \tilde{\alpha}_1 \frac{\widetilde{c}}{\overline{\rho}} \\ p_L + \tilde{\alpha}_1 \widetilde{c}^2 \end{pmatrix} \qquad \text{and} \qquad Y_2 = \begin{pmatrix} \rho_R - \tilde{\alpha}_3 \\ u_R - \tilde{\alpha}_3 \frac{\widetilde{c}}{\overline{\rho}} \\ p_R - \tilde{\alpha}_3 \widetilde{c}^2 \end{pmatrix}$$

Once again, we check that:

$$Y_2 = Y_1 + ({}^t\widetilde{l_2}.(Y_R - Y_L))\widetilde{r_2}$$

so that approximate intermediate states mimic the behaviour of the exact Godunov scheme. Moreover, for perfect gas EOS and Tamman EOS, cell averages of Riemann invariants of the 2-wave are perfectly preserved. Above mentionned remark concerning jump conditions no longer holds, even when restricting to perfect gas EOS.

If we turn now to intermediate states of pressure, we note that PVRS scheme computes:

$$p_1 = p_2 = \overline{p}(1 - \frac{\hat{\gamma}(\overline{p},\overline{\rho})\Delta u}{2\tilde{c}})$$

Thus the pressure intermediate states are strictly positive as soon as:

$$\frac{\Delta u}{\tilde{c}} < \frac{2}{\hat{\gamma}(\overline{p},\overline{\rho})}$$

This should be compared with continuous condition for vacuum occurence:

$$\Delta u < X_L + X_R \tag{1.7}$$

where:

$$X_i = \int_0^{\rho_i} \frac{c(\rho, s_i)}{\rho} d\rho$$

where s_i denotes the specific entropy. Thus if we restrict to some symetrical double rarefaction wave with perfect gas EOS, we note that the upper bound of $\frac{\Delta u}{\tilde{c}}$ to avoid occurence of vacuum is $\frac{4}{\gamma-1}$ in the "continuous case" and $\frac{2}{\gamma}$ in the "discrete case" for PVRS scheme. Using the standard value $\gamma = 1.4$ provides 10 and $\frac{10}{7}$ respectively.

1.3.5 VFRoe scheme with flux variable -VFFC-

This corresponds to the choice: $Y(W) = F(W)$. This scheme VFFC was first introduced in [GKL96] (see also [Bou98] and [Kum95] for further details). The associated 1D Riemann problem is now:

$$\begin{cases} \dfrac{\partial F(W)}{\partial t} + A(\overline{W})\dfrac{\partial F(W)}{\partial x} = 0 \\ F(W(x,0)) = \begin{cases} F_L = F(W_L) & \text{if } x < 0 \\ F_R = F(W_R) & \text{if } x > 0 \end{cases} \end{cases}$$

The interface numerical flux F^* is computed with help of eigenstructure of the Jacobian matrix $A(\overline{W})$, as occurs when focusing on basic VFRoe scheme.

1.3.6 Rusanov scheme

Unlike schemes presented above, Rusanov scheme do not solve an approximate Riemann problem at each interface (see [Rus61]). Numerical flux of Rusanov scheme is:

$$\varphi(W_L, W_R) = \frac{F(W_L) + F(W_R)}{2} - \frac{1}{2}\lambda_{i+1/2}^{MAX}(W_R - W_L)$$

with

$$\lambda_{i+1/2}^{MAX} = \max(|u_L| + c_L, |u_R| + c_R)$$

The mean density remains positive as soon as the C.F.L. condition below holds (see [GHK98] for more details):

$$\max_{j\in\mathbb{Z}}(|u_j^n| + c_j^n)\Delta t \leq \Delta x$$

Note that a similar condition is exhibited in [Seg00] for the Rusanov scheme with a MUSCL reconstruction with minmod slope limiter ([Van79]).

1.3.7 Energy relaxation method applied to VFRoe with non conservative variable (τ, u, p)

The energy relaxation method was introduced in [CP98], and used in [In99b] and [In99a]. We refer to these references for further details, and only provide herein an algorithmic version to compute the flux φ, resolving the Riemann problem (1.5) for the Euler equations.

This requires introducing two additional variables γ_1 and ε_2 to the conservative ones. Coefficient γ_1 must fulfill the following conditions to reach convergence of the energy relaxation method:

$$\gamma_1 > \sup_{\rho,\varepsilon} \Gamma(\rho,\varepsilon) \quad \text{where} \quad \Gamma(\rho,\varepsilon) = 1 + \frac{p_{,\varepsilon}}{\rho} \tag{1.8}$$

$$\gamma_1 > \sup_{\rho,\varepsilon} \gamma(\rho,\varepsilon) \quad \text{where} \quad \gamma(\rho,\varepsilon) = \frac{\rho}{p} p_{,\rho} + \frac{p_{,\varepsilon}}{\rho} \tag{1.9}$$

where $\varepsilon = E - \frac{1}{2}\frac{(\rho u)^2}{\rho^2}$ and p is computed using the real EOS (1.4).
Internal energy ε_2 is defined as follows:

$$\varepsilon_2 = \frac{E}{\rho} - \frac{1}{2}\frac{(\rho u)^2}{\rho^2} - \frac{p}{(\gamma_1 - 1)\rho}$$

We may introduce:

$$W_1(\rho,u,p) = \begin{pmatrix} \rho \\ \rho u \\ \frac{1}{2}\rho u^2 + \frac{p}{\gamma_1 - 1} \end{pmatrix}$$

and:

$$F_1(W_1(\rho,u,p)) = \begin{pmatrix} \rho u \\ \rho u^2 + p \\ u(\frac{1}{2}\rho u^2 + \gamma_1 \frac{p}{\gamma_1 - 1}) \end{pmatrix}$$

The four governing equations are:

$$\begin{cases} \dfrac{\partial W_1}{\partial t} + \dfrac{\partial F_1(W_1)}{\partial x} = 0 \\ (\rho\varepsilon_2)_{,t} + (\rho u \varepsilon_2)_{,x} = 0 \end{cases} \tag{1.10}$$

with given initial condition:

$${}^t(\rho,u,p,\varepsilon_2)(x,0) = \begin{cases} {}^t(\rho_L, u_L, p_L, \varepsilon_{2L}) & \text{if } x < 0 \\ {}^t(\rho_R, u_R, p_R, \varepsilon_{2R}) & \text{if } x > 0 \end{cases} \tag{1.11}$$

Thanks to these, one may compute the VFRoe-ncv numerical flux pertaining to the latter system which is an hyperbolic system with three distinct eigenvalues which are those of the Euler system. The numerical flux with three components relative to the mass, momentum and energy equations will eventually be defined as follows:

$$\varphi(W_L, W_R) = \begin{pmatrix} F^*_{1,1} \\ F^*_{1,2} \\ F^*_{1,3} + (\rho u \varepsilon_2)^* \end{pmatrix}$$

noting $F_1^* = {}^t(F_{1,1}^*, F_{1,2}^*, F_{1,3}^*)$.
Since we use the VFRoe ncv (τ, u, p) scheme to solve the four equations system, we get:

$$\begin{aligned}(\rho u \varepsilon_2)^* &= \rho^* u^* \varepsilon_{2L} \quad \text{if } \overline{u}_{LR} > 0 \\ &= \rho^* u^* \varepsilon_{2R} \quad \text{if } \overline{u}_{LR} < 0\end{aligned}$$

Since ε_2 is defined for each Riemann problem resolution, this variable is not continuous in time (a jump occurs at each time step).

1.4 Numerical results

All test cases have been computed for all schemes, but we do not present here all results (see [Seg00], pp.53-451). However, they are all discussed in the following, with some figures to focus on problems in critical configurations. Let us note that VFRoe ncv (τ, u, p) scheme without entropy correction has been investigated too, in order to emphasize the influence of the energy relaxation method.

Following tests are performed using constant CFL number; however, CFL number slightly increases at the beginning of the computation, from $0,1$ to $0,4$ in $t \in [0; T_{MAX}/4]$. Initial conditions refer to different 1D Riemann problems. The regular mesh contains one hundred nodes.

We present results pertaining to perfect gas, focusing first on qualitative behaviour and then on measurement of L^1 error norm of four distinct solutions. Afterwards, some qualitative results are discussed, related to the Tammann EOS. The configurations of these test cases are similar to perfect gas EOS. Eventually, two cases are presented using Van Der Waals EOS, in order to emphasize some numerical problems through the LD field.

Remark 1.1. *Unless otherwise specified, the average of $\hat{\gamma}$ which is used in all test cases is the following: $0.5((\hat{\gamma})_L + (\hat{\gamma})_R)$. The main advantage of this proposal issuing from [BGH96] is that the mean Jacobian matrix has real eigenvalues, provided that initial states have. This is not necessarily true for some non convex EOS when applying for expected value, i.e.: $\widetilde{\hat{\gamma}} = \hat{\gamma}(\overline{Y})$. However, potential drawbacks of the former approach will be discussed when necessary. This remark obviously holds for Tammann EOS and Van der Waals EOS, but not for perfect gas state law.*

1.4.1 Perfect gas EOS - Qualitative behavior

Case 1.1 Perfect gas EOS - Sod shock tube

A 1-rarefaction wave travels to the left and a 3-shock moves to the right end. The contact discontinuity is right going. This case is usually examined but does not provide much information on

schemes since discrepancies can hardly be exhibited between all schemes involved herein. However, one can note that "first-order" Rusanov scheme is a little bit more diffusive than others schemes.

Left State	Right state
$\rho_L = 1$	$\rho_R = 0,125$
$u_L = 0$	$u_R = 0$
$p_L = 10^5$	$p_R = 10^4$

$$T_{MAX} = 6\ ms$$

Case 1.2 Perfect gas EOS - Supersonic 1-rarefaction wave

The 1-rarefaction wave contains a sonic point. As a result, for VFRoe ncv schemes, a wrong shock wave may develop at the origin. This is corrected by introducing an entropy correction at sonic point, when focusing on so called first order scheme. This is no longer compulsory when handling MUSCL type reconstruction, which is usually combined with RK2 time integration in order to avoid loss of stability. Note that VFFC scheme without entropy correction also provides a non entropic shock at sonic point, but this appears to be very small when compared with those arising with VFRoe ncv approach with "physical" variables. Moreover, since the energy relaxation method is applied with VFRoe ncv (τ, u, p) without entropy correction, a small jump can be detected at the sonic point (which vanishes when the mesh is refined). Since first order Rusanov scheme is not based on a linearised Riemann solver, no problem appears at the sonic point. All second order schemes behave in the same way.

Left State	Right state
$\rho_L = 1$	$\rho_R = 0,01$
$u_L = 0$	$u_R = 0$
$p_L = 10^5$	$p_R = 10^3$

$$T_{MAX} = 5\ ms$$

Case 1.3 Perfect gas EOS - Double supersonic rarefaction wave

This case enables to predict the behaviour of the scheme close to wall boundary conditions when applying the mirror technique. Two rarefaction waves are present in the solution when u_R is positive. Due to symetrical initial conditions, the contact discontinuity is a ghost wave. We note that in this particular case VFFC scheme no longer provides a convergent solution since it blows up after a few time steps. Though intermediate states of VFRoe ncv scheme are no longer admissible (see [BGH00]) it however provides a convergent solution. As usual, Rusanov scheme is more diffusive than other schemes, but it provides rather good results.

Left State	Right state
$\rho_L = 1$	$\rho_R = 1$
$u_L = -1200$	$u_R = 1200$
$p_L = 10^5$	$p_R = 10^5$

$$T_{MAX} = 2\ ms$$

Case 1.4 Perfect gas EOS - Double subsonic shock wave

This case is very similar to the previous one, but two shocks are now travelling to the left and to the right since u_R is negative. It corresponds to an inviscid impinging jet on a wall boundary. For supersonic double shock waves with very high initial kinetic energy, small oscillations may occur close to shocks, even when the CFL number is such that waves do not interact. A similar behaviour is observed when computing the case with help of Godunov scheme. Second order schemes create some oscillations, even in a subsonic configuration, except for Rusanov scheme.

Left State	Right state
$\rho_L = 1$	$\rho_R = 1$
$u_L = 300$	$u_R = -300$
$p_L = 10^5$	$p_R = 10^5$

$$T_{MAX} = 5\ ms$$

Case 1.5 Perfect gas EOS - Stationary 1-shock wave

This case is usually considered to evaluate the stability of the (expected) stationary 1-shock wave, especially when the scheme does not comply with Roe's condition. In all cases, no instability arises, and all schemes (except for the energy relaxation method which inserts two points in the stationary shock wave profile and Rusanov scheme which smears the wave) actually perfectly preserve the steadyness, whatever the order is.

Left State	Right state
$\rho_L = 3/4$	$\rho_R = 1$
$u_L = 4/3$	$u_R = 1$
$p_L = 2/3$	$p_R = 1$

$$T_{MAX} = 100\ s$$

Case 1.6 Perfect gas EOS - Unsteady contact discontinuity

This case is interesting since it enables to check whether the Riemann invariants of the 2-wave are preserved from a discrete point of view. This essentially depends on the scheme and the EOS (see appendix 1.A). All (first and second order) computed schemes preserve velocity and pressure exactly constant, whereas density jump at the contact dicontinuity is smeared. Note that Rusanov

scheme is once again more diffusive than schemes based on a linearised Riemann solver and the energy relaxation method.

Left State	Right state
$\rho_L = 1$	$\rho_R = 0,1$
$u_L = 100$	$u_R = 100$
$p_L = 10^5$	$p_R = 10^5$

$$T_{MAX} = 20\ ms$$

Case 1.7 Perfect gas EOS - Supersonic 1-rarefaction wave propagating over "vacuum"

This is one difficult test case for all schemes based on approximate Riemann solvers. Moreover, problems may appear due to the fact that computers have to handle round off errors. The analytical solution is close to a pure 1-rarefaction wave over vacuum, since the variations through the LD field and the 3-shock are not significant. Note that some variables are not defined in vacuum, namely velocity u or specific volume τ. Indeed, for the first order framework, the energy relaxation method applied to VFRoe ncv (τ, u, p) without entropy correction blows up after few time steps. However, VFRoe ncv (τ, u, p) scheme with entropy correction provides good results, except in the vacuum area, where velocity profile becomes less accurate on coarse mesh. Other first order schemes (PVRS, VFFC and Rusanov) provide slightly better profiles, even near vacuum. The second order energy relaxation method and second order VFRoe ncv (τ, u, p) scheme provide good results, though the problem on the velocity profile in the vacuum area remains unchanged. Other second order schemes perform well.

Left State	Right state
$\rho_L = 1$	$\rho_R = 10^{-7}$
$u_L = 0$	$u_R = 0$
$p_L = 10^5$	$p_R = 10^{-2}$

$$T_{MAX} = 1\ ms$$

Case 1.8 Perfect gas EOS - Double rarefaction wave with vacuum

This one too is interesting, since the violation of condition $(\gamma - 1)(u_R - u_L) < 2(c_R + c_L)$ results in a vacuum occurence on each side of the origin. Since this test case provides a double supersonic rarefaction wave, VFFC scheme cannot handle these initial conditions, whatever the order. The energy relaxation method applied to VFRoe ncv (τ, u, p) scheme without entropy correction blows up too, restricting to the first order approximation. However, these two schemes perform well when handling MUSCL reconstruction with RK2 time integration. Moreover, first or second order PVRS, VFRoe and Rusanov schemes preserve density and pressure positivity in this test case and

provide good results too (recall that Rusanov scheme maintains positivity of the density under a standard CFL-like condition).

Left State	Right state
$\rho_L = 1$	$\rho_R = 1$
$u_L = -3000$	$u_R = 3000$
$p_L = 10^5$	$p_R = 10^5$

$$T_{MAX} = 1\ ms$$

1.4.2 Perfect gas EOS - Quantitative behavior

We compute here five test cases (unsteady contact discontinuity, double subsonic shock wave, double subsonic rarefaction wave, Sod shock tube, supersonic 1-rarefaction wave with 3-shock wave) with several meshes: 100, 300, 1000, 3000 and 10000 nodes. Numerical rates of convergence of the L^1 error are measured and presented. Continuous lines refer to first order schemes, whereas dotted lines refer to second order schemes. All results have been obtained using a constant CFL number $\max_i(|u_i|+c_i)\Delta t/h = 0.5$. In order to provide a detailed analysis of true convergence rate, we distinguish:

i. smooth solutions ($\mathcal{C}^\infty$),

ii. pure contact discontinuities,

iii. pure shock waves,

iv. rarefaction waves connected with constant states (solutions are not $\mathcal{C}^1$),

v. shock tube test cases which involve several waves.

When focusing on solutions in $\mathcal{C}^\infty$, three points schemes provide order of convergence close to 1 and five points schemes (with a MUSCL reconstruction) provide rates close to 2. The reader is refered for instance to the work described in references [Buf93] and [LeV97]. In the first reference above, unsteady solutions are simply given by $u(x,t) = \frac{a_0 x + b_0}{t+t_0}$, $u(x,t) - 2\frac{c(x,t)}{\gamma-1} = c_0$, $p(x,t) = (\rho(x,t))^\gamma$, which are basic solutions of Euler equations with perfect gas EOS in a one dimensional framework, and indeed correspond to the inner part of a rarefaction wave. This enables to check that expected rate of convergence is achieved focusing either on first order or second order scheme. This classical result no longer holds when the solution involves rarefaction waves (which are only $\mathcal{C}^0$) or discontinuities such as shock waves or contact discontinuities, which is the case in all the next studied solutions. Therefore, one may expect that the speed of convergence (when Δx tends to 0 with constant CFL number) slows down. Measure of L^1 error norm is achieved for unknowns ρ, u and p since the latter two are not expected to vary through the contact discontinuity whatever the initial conditions are.

Case 2.1 Perfect gas EOS - Unsteady contact discontinuity

We focus here on initial conditions from Case 1.6. Results presented herein have been obtained using VFRoe ncv (τ, u, p). This test aims at measuring the rate of convergence when the solution involves a pure contact discontinuity. Pertaining to first order schemes, the rate is approximatively 1/2 and the addition of the MUSCL reconstruction with a RK2 method leads to a rate around 2/3 (see results of figure 1.49).

This preliminary result is important since it enables to explain the differences between Cases $2.2 - 2.3$ (where no jump of density occurs through the contact discontinuity due to symmetry) and Cases $2.4 - 2.5$ which correspond to classical shock tube experiments.

Case 2.2 Perfect gas EOS - Double subsonic shock wave

The initial conditions of this test case come from the Case 1.4. The contact discontinuity is a "ghost wave" (no variable jumps through this wave). This explains why the rate of convergence of the first order schemes is slightly higher for density than in the following Cases $2.4 - 2.5$. For all schemes, the rates of convergence for density variable are slightly higher with the first order approximation than with the second order approximation, though the error of the first order schemes is more important. It may be explained by the occurence of tiny oscillations on the intermediate state caused by the second order schemes. Here, all rates are close to 1, for both first and second order schemes.

Case 2.3 Perfect gas EOS - Double subsonic rarefaction wave

This concerns Case 1.3, except for the fact that the initial velocity is set to: $u_L = -300$. As a result, the double rarefaction wave is subsonic (hence, the VFFC scheme provides meaningful results). Though the solution of this test case is continuous, connections between rarefaction waves and intermediate states are not regular. Thus, rates of convergence equals to 1 for the "first" order schemes and equals to 2 for the "second" order schemes can hardly be expected. Above mentionned remark concerning the density through the contact discontinuity holds. Nonetheless, unlike in previous case, the rate of convergence for ρ, u and p with first order scheme is smaller than 1. This means that error located at the beginning and at the end of the rarefaction wave affects much the global error, at least on these "coarse" meshes, which is in agreement with description of local L^1 error in [Buf93]. The rates of convergence of second order schemes are with no doubt very close to 1 for all variables. Note that the error associated with the Rusanov scheme is close to the error of other schemes.

We turn now to standard shock tube experiments which involve several waves with true variations of all components. We may expect thus that both u, p will converge with rate 1 when using so called second order scheme, and also that density convergence rate will be close to 2/3.

Case 2.4 Perfect gas EOS - Sod shock tube

Initial conditions of this test case are the same as the Case 1.1. We recall here that local L^1 error has been examined in detail in [Buf93], which confirmed that great part of the error was located not only close to the contact discontinuity and the 3-shock, but also at the beginning and the end of the 1-rarefaction wave. Though Rusanov scheme is less accurate (in terms of error) than other schemes, its rate of convergence is the same. We can note that the rate of convergence of velocity and pressure are the same and higher than the rate of convergence pertaining to density, owing to the contact discontinuity. As expected, the second order schemes converge faster (the slope is close to 1 for velocity and pressure, and a little bit higher than 2/3 for density).

Case 2.5 Perfect gas EOS - Supersonic 1-rarefaction wave

This refers to the Case 1.2. Though the solution of this test case is composed by the same set of waves, we can measure here the influence of entropy correction for the first order schemes. The rates of convergence are the same as above for all schemes, except for the energy relaxation method. Indeed, the first order approximation provides higher rates of convergence than in the Sod shock tube case. The true rate of convergence in L^1 norm is hidden by the error associated with the sonic point due to the parametric entropy correction (which is confirmed by experiments with Godunov scheme on shallow water equations).

To conclude, we emphasize that focusing on the Sod tube test, the loss of accuracy is mainly due to the contact discontinuity, since it has been seen that rates of convergence for rarefaction waves or shock waves are greater than rates of convergence provided for a contact discontinuity. Hence, the main numerical diffusion is located on contact discontinuities and poor rates of convergence when dealing with discontinuous solutions are, again, merely due to contact discontinuities.

1.4.3 Tammann EOS

As mentionned in section 1.2.5, one may retrieve by a suitable change of variables the Euler equations with perfect gas EOS from the Euler equations with Tammann EOS. Hence, the vacuum with the Tamman EOS is $\rho = 0$ and $p + p_c = 0$ and the condition for vacuum occurence (1.7) becomes:

$$\Delta u < \frac{2}{\gamma_c - 1}(c_L + c_R)$$

where $c^2 = \dfrac{\gamma_c(p + p_c)}{\rho}$.
However, this equivalence is only meaningful in the "continuous" framework. Indeed, it no longer holds from a discrete point of view (except for PVRS and VFRoe ncv (τ, u, p)), and numerical results computed with the Tammann EOS are slightly different of previous results, namely with the perfect gas state law.

Case 3.1 Tammann EOS - Subsonic shock tube

This case is somewhat different from its counterpart with perfect gas EOS, and is based on initial conditions provided in [Tor91]. However, the numerical approximation behaves as its counterpart with perfect gas EOS: all schemes provide good results, and Rusanov scheme is more diffusive than the others.

Left State	Right state
$\rho_L = 1100$	$\rho_R = 1000$
$u_L = 500$	$u_R = 0$
$p_L = 5.10^9$	$p_R = 10^5$

$$T_{MAX} = 0.6\ ms$$

Case 3.2 Tammann EOS - Sonic rarefaction wave

Once again, initial conditions are those provided in reference above. Note that the energy relaxation method (with the first order approximation) completely smears the non-entropic shock caused by VFRoe ncv (τ, u, p). All VFRoe ncv schemes have the same behaviour, and the Rusanov scheme is still more diffusive (first order or second order). Figures provided by first order schemes are presented (figures 1.1-1.6).

Left State	Right state
$\rho_L = 10^3$	$\rho_R = 10^3$
$u_L = 2000$	$u_R = 2000$
$p_L = 5.10^8$	$p_R = 10^6$

$$T_{MAX} = 8\ ms$$

Case 3.3 Tammann EOS - Double subsonic rarefaction wave

This test case is the counterpart of the Case 1.3. Note that vacuum (ie $\rho = 0$, $p + p_c = 0$) can occur within subsonic range, though it does not appear in this test case. Except for first order Rusanov scheme, all schemes compute a glitch (or a spike) at the interface (where the contact discontinuity is located) on the density.

Left State	Right state
$\rho_L = 10^3$	$\rho_R = 10^3$
$u_L = -300$	$u_R = 300$
$p_L = 10^9$	$p_R = 10^9$

$$T_{MAX} = 0,5\ ms$$

Case 3.4 Tammann EOS - Double subsonic shock wave

The only difference between this test case and the case presented above is due to the sign of initial velocities. As a result, instead of rarefaction waves, the solution is composed by two shock waves and a ghost contact discontinuity. The same behaviour on the density can be noted, namely a glitch at the interface (even with the first order Rusanov scheme).

Left State	Right state
$\rho_L = 10^3$	$\rho_R = 10^3$
$u_L = 300$	$u_R = -300$
$p_L = 10^9$	$p_R = 10^9$

$$T_{MAX} = 0,5\ ms$$

Case 3.5 Tammann EOS - Stationary 1-shock wave

A very slight difference may be seen when the average value of $\hat{\gamma}$ is chosen as $0.5((\hat{\gamma})_L + (\hat{\gamma})_R)$ instead of $\widetilde{\hat{\gamma}} = \hat{\gamma}(\overline{Y})$ when focusing on VFRoe ncv with variable (τ, u, p). The shock remains steady only if the the latter choice is considered from a theoretical point of view, which is confirmed by computation. However, other VFRoe ncv schemes provide as accurate results. First or second order Rusanov scheme is very diffusive, and the energy relaxation method introduces three or two points in the shock profile, according to the order of approximation.

Left State	Right state
$\rho_L = 2.10^{-10}$	$\rho_R = u_R^{-1}$
$u_L = 5.10^9$	$u_R = \frac{4\gamma_c}{\gamma_c+1} p_c + \frac{\gamma_c-1}{\gamma_c+1} 5.10^9$
$p_L = p_c$	$p_R = p_L + u_L - u_R$

$$T_{MAX} = 10^{-9}\ s$$

Case 3.6 Tammann EOS - Unsteady contact discontinuity

The results provided by all schemes are similar to those provided with the perfect gas EOS (see Case 1.6). Pressure and velocity are exactly preserved (see appendix 1.A), and the jump of density is smeared by all schemes (in particular by the Rusanov scheme).

Left State	Right state
$\rho_L = 10^3$	$\rho_R = 10^2$
$u_L = 10^3$	$u_R = 10^3$
$p_L = 10^8$	$p_R = 10^8$

$$T_{MAX} = 2\ ms$$

Case 3.7 Tammann EOS - Rarefaction wave propagating over vacuum

This test computes a 1-rarefaction wave with a sonic point. The 2-contact discontinuity and the 3-shock wave are not of significant importance, as in Case 1.7. We have used in the following last two cases: $\widetilde{\hat{\gamma}} = \hat{\gamma}(\overline{Y})$. In this case, only VFRoe ncv (τ, u, p) with RK2-MUSCL integration and (first or second order) Rusanov scheme enable computation (see figures 1.7-1.8). Note that the standard choice $0.5((\hat{\gamma})_L + (\hat{\gamma})_R)$ results in a blow up of the computation. Initial conditions make all other schemes blow up. These behaviours confirm the discrete difference between perfect gas EOS and Tammann EOS.

Left State	Right state
$\rho_L = 10^3$	$\rho_R = 10^{-9}$
$u_L = 0$	$u_R = 0$
$p_L = 10^8$	$p_R + p_c = 10^{-2}$

$$T_{MAX} = 0,6\ ms$$

Case 3.8 Tammann EOS - Vacuum occurence

This test results like Case 1.8 in a vacuum occurence in the intermediate state. Recall that vacuum can appear though rarefaction waves are not supersonic. As above, VFRoe ncv (τ, u, p) and Rusanov schemes enable computation. Note that PVRS and VFRoe schemes also perform well in this test (see figures 1.9-1.12).

Left State	Right state
$\rho_L = 10^3$	$\rho_R = 10^3$
$u_L = 1500$	$u_R = 1500$
$p_L = 10^9$	$p_R = 10^9$

$$T_{MAX} = 0,6\ ms$$

1.4.4 Van Der Waals EOS

Results of both computations discussed below were achieved using the standard definition for VFRoe ncv (τ, u, p) and PVRS schemes and the mean of $\hat{\gamma}$: $0.5((\hat{\gamma})_L + (\hat{\gamma})_R)$ instead of: $\widetilde{\hat{\gamma}} = \hat{\gamma}(\overline{Y})$ when focusing on VFRoe ncv scheme. Differences between results for both choices could hardly be noticed for the following.

Case 4.1 Van Der Waals EOS - Subsonic 1-rarefaction wave

Initial conditions below are taken from the paper by Letellier and Forestier [LF93]. The main advantage of this case is that it clearly exhibits the rather unpleasant behaviour around the contact

discontinuity. Though both the exact Godunov scheme and VFRoe scheme with (τ, u, p) variables predict equal velocity and pressure of intermediate states on each side of the LD field, cell values of both u and p are not in equilibrium (this confirms results of appendix 1.A for the VFRoe schemes with (φ, u, p) variable). Obviously this well-known drawback (see [LF93]) tends to vanish when the mesh size decreases, or when time increases. First order results are provided on figures 1.13-1.18.

Left State	Right state
$\rho_L = 333,33$	$\rho_R = 111,11$
$u_L = 0$	$u_R = 0$
$p_L = 37311358$	$p_R = 21770768$

$$T_{MAX} = 5\ ms$$

Case 4.2 Van Der Waals EOS - Moving contact discontinuity

Initial conditions are similar to those given in Case 1.6. Note that the Riemann invariants u and p are not very well preserved around the contact discontinuity when using coarse meshes, and "first" order scheme (see appendix 1.A for more details on VFRoe ncv schemes with (φ, u, p) variable). The "second' order version of the scheme performs much better. Unlike sometimes heard, we emphasize that the approximation is still convergent. Small oscillations apart from the LD scheme which were reported in [LF93] do not arise when using approximate Godunov schemes, which is still unexplained and rather amazing. Due to the very small rate of convergence measured in the LD field (smaller than 2/3), it is clear that this slows down the whole rate of convergence on both velocity and pressure variable, compared with what happens when focusing on perfect gas EOS. Hence, none among schemes presented here are able to preserve velocity and pressure constant on a given mesh (see figures 1.19-1.24 for results performed by first order schemes).

Left State	Right state
$\rho_L = 1$	$\rho_R = 10$
$u_L = 100$	$u_R = 100$
$p_L = 10^5$	$p_R = 10^5$

$$T_{MAX} = 6\ ms$$

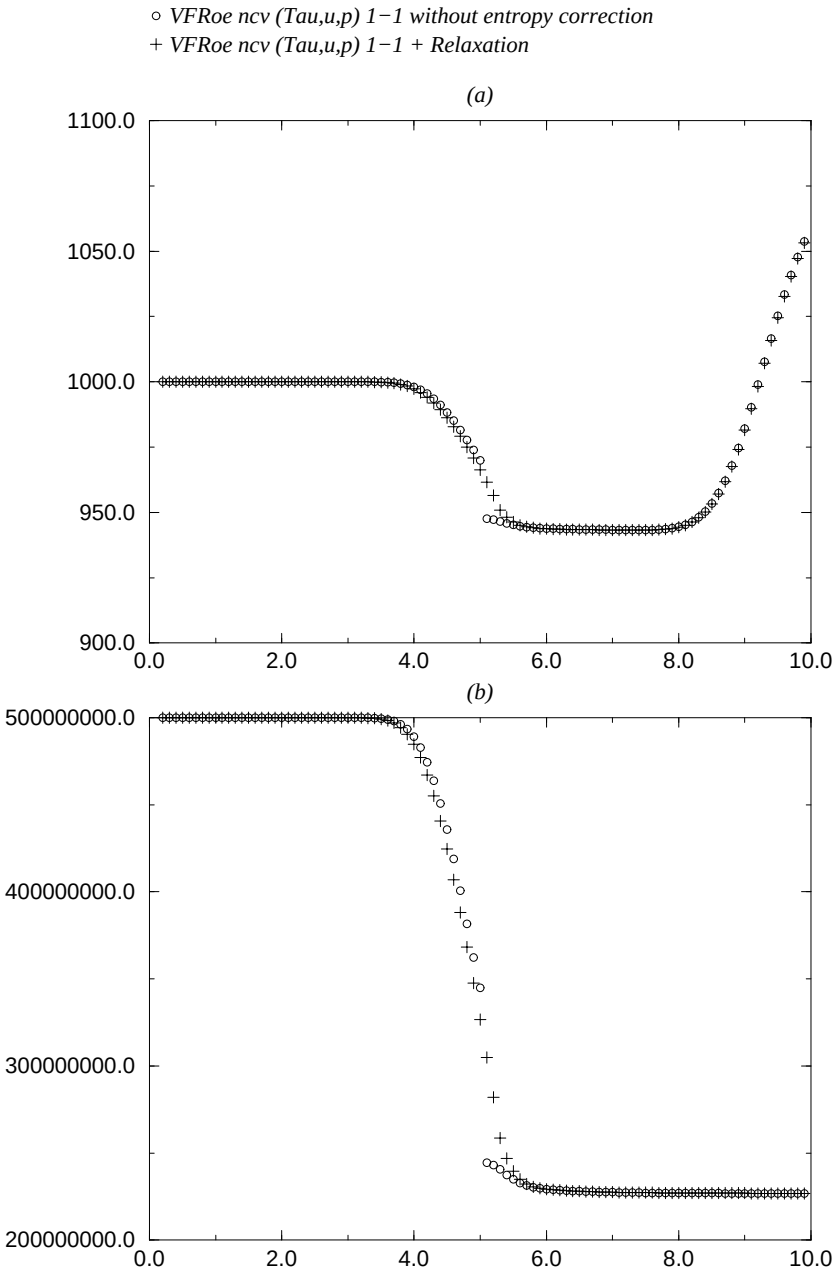

Figure 1.1: Case 3.2: density (a) - $p + p_c$ (b)

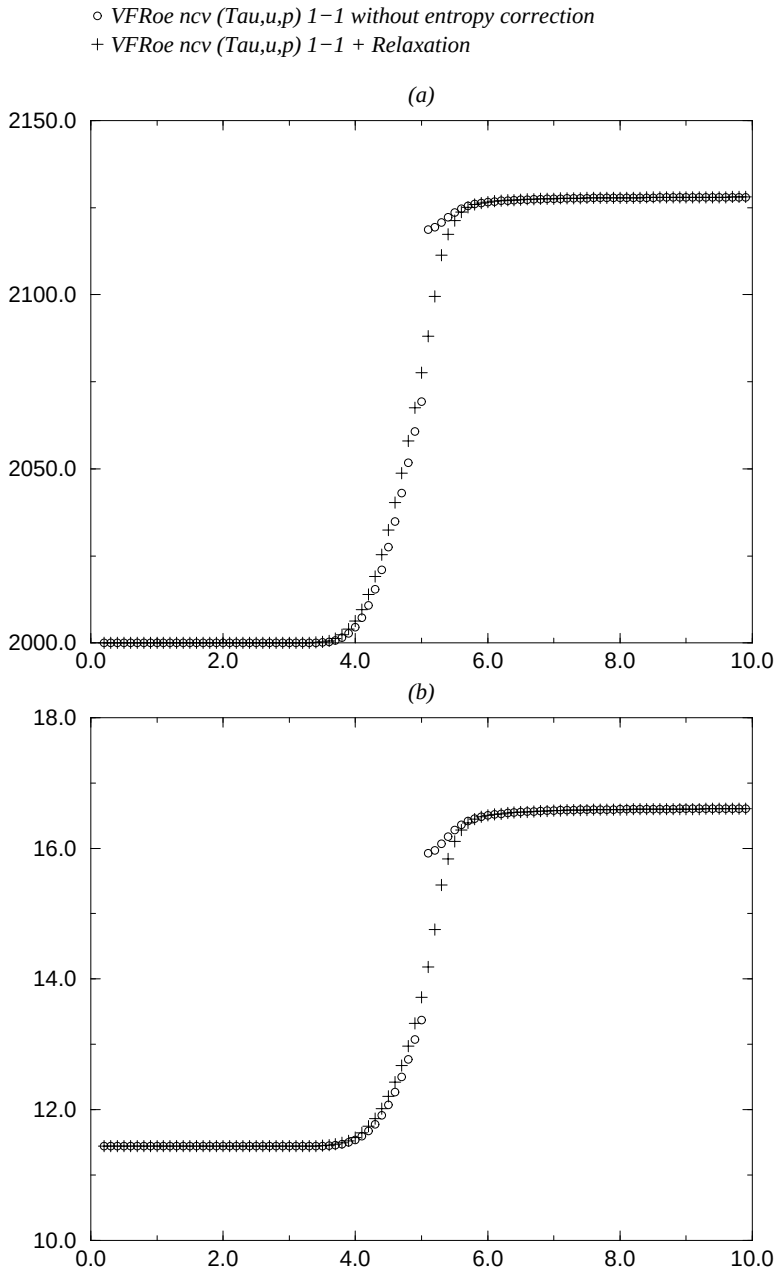

Figure 1.2: Case 3.2: velocity (a) - $\hat{\gamma}(p, \rho)$ (b)

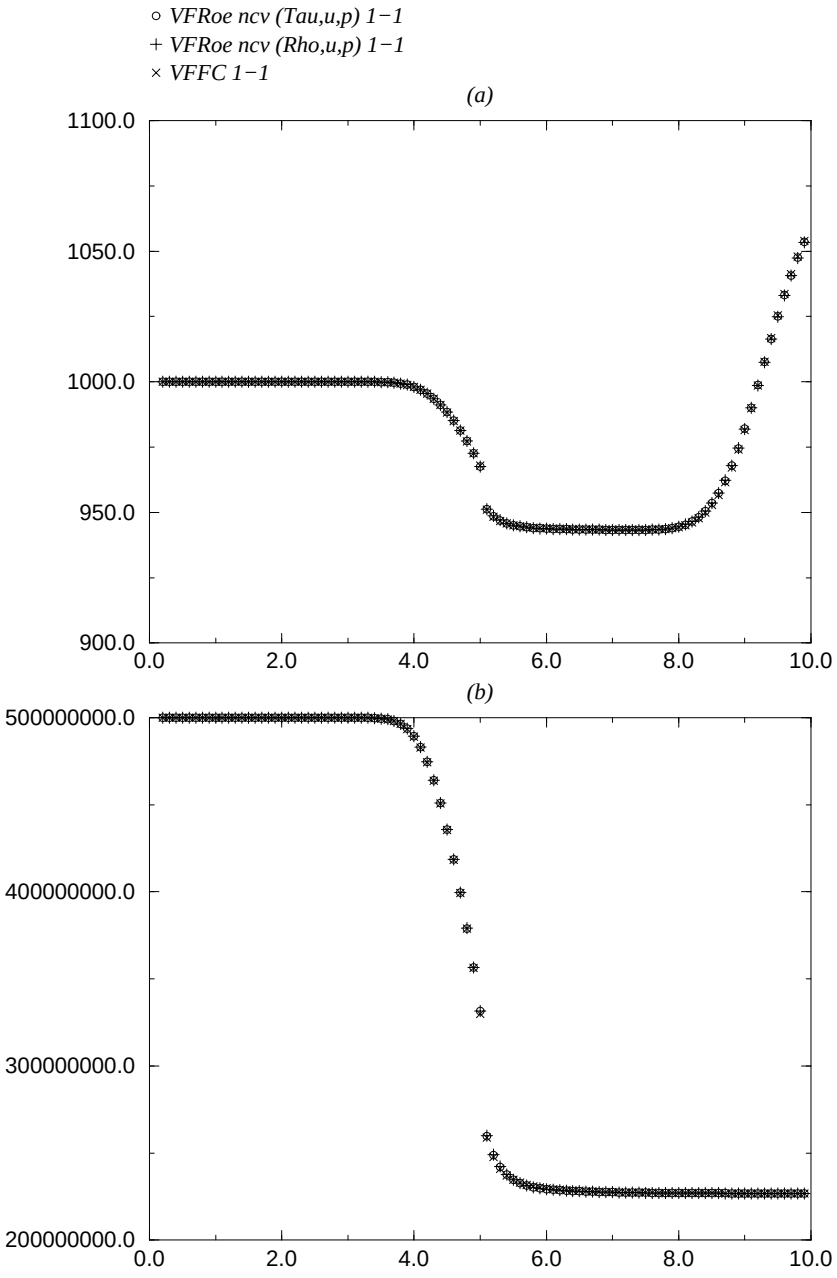

Figure 1.3: Case 3.2: density (a) - $p + p_c$ (b)

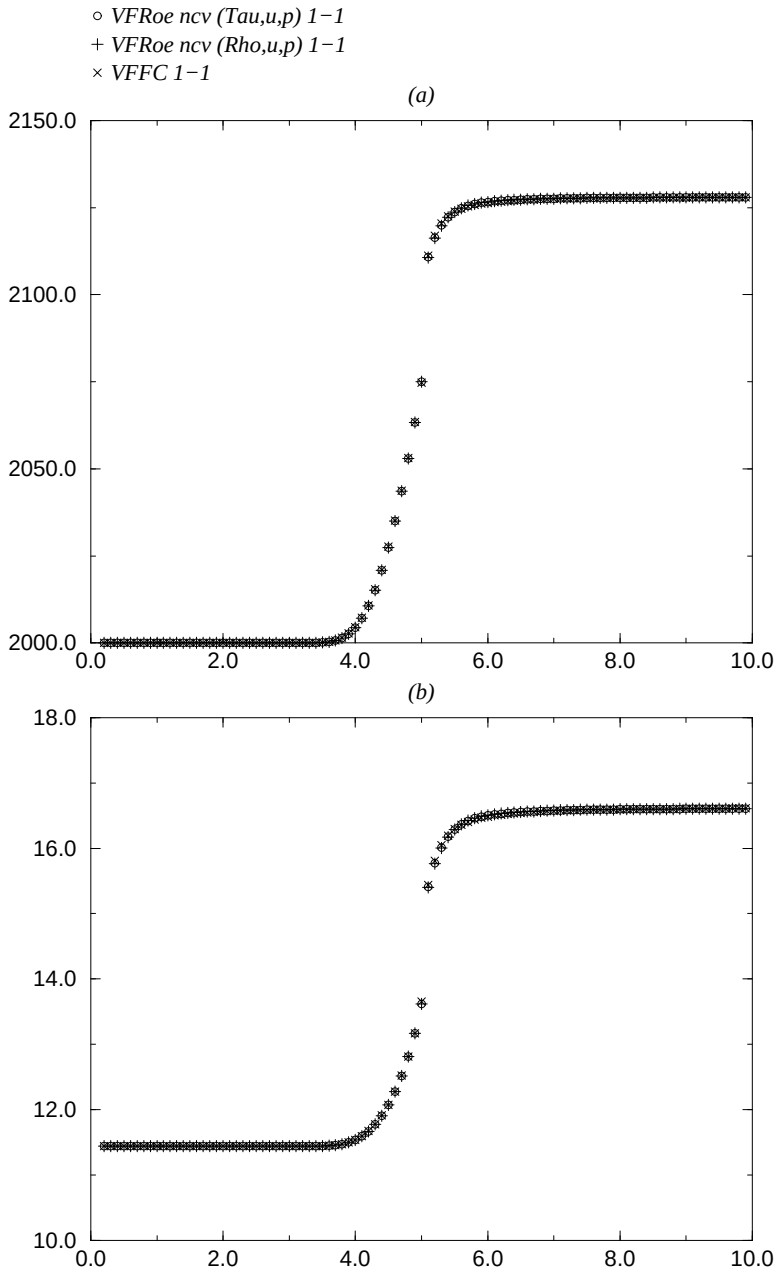

Figure 1.4: Case 3.2: velocity (a) - $\hat{\gamma}(p, \rho)$ (b)

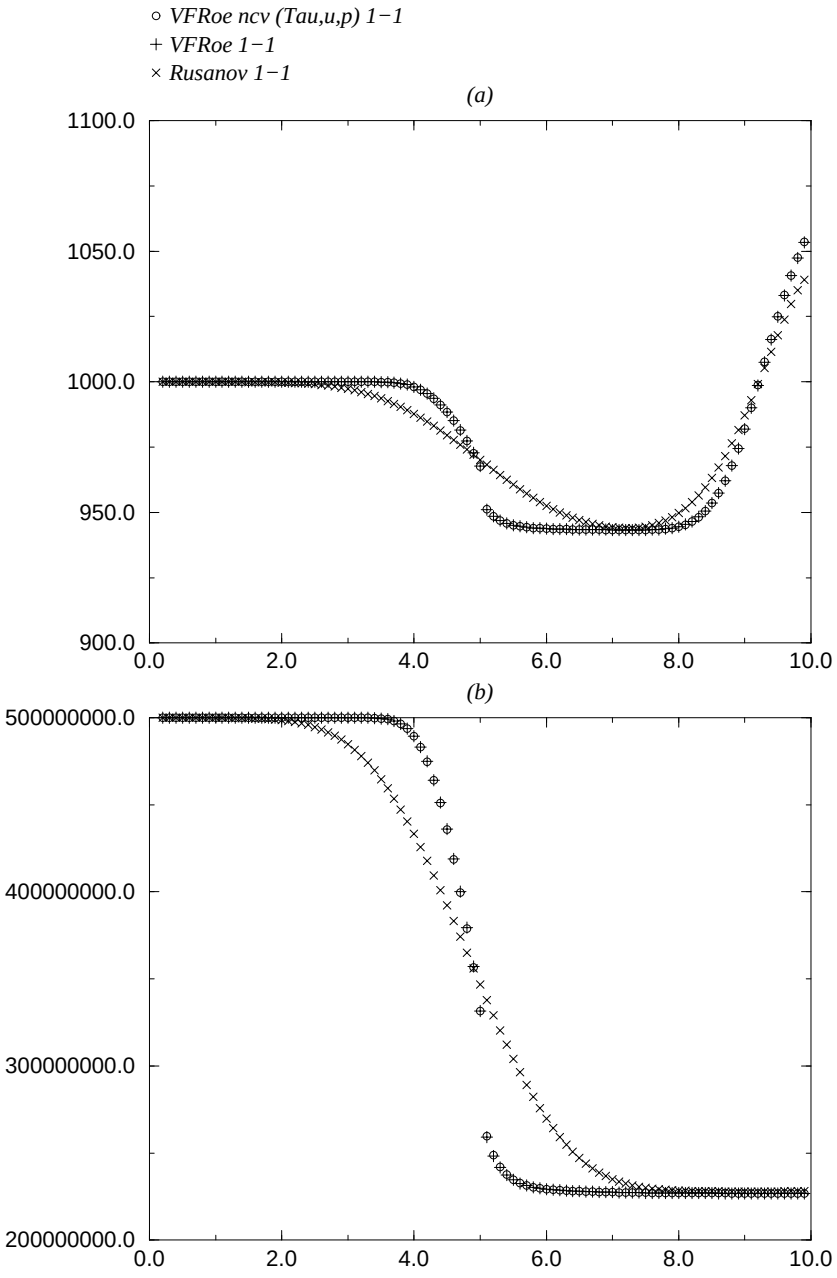

Figure 1.5: Case 3.2: density (a) - $p + p_c$ (b)

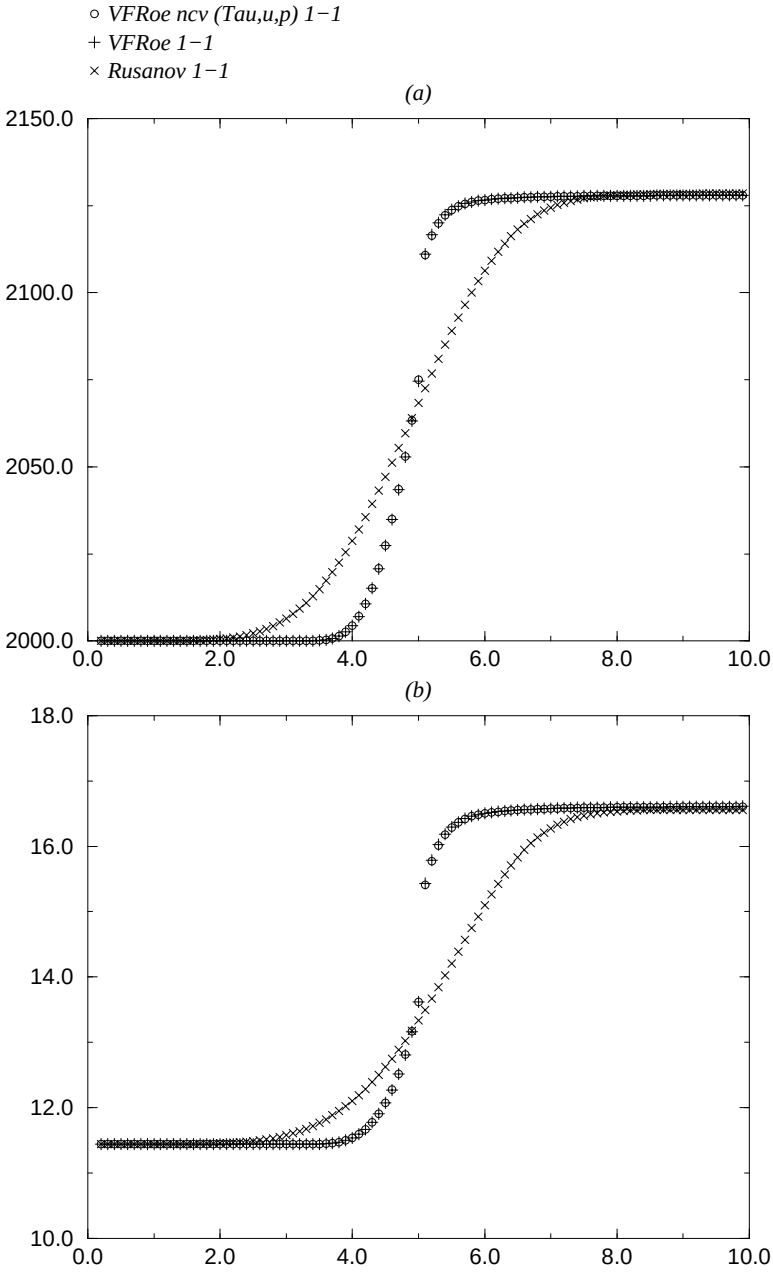

Figure 1.6: Case 3.2: velocity (a) - $\hat{\gamma}(p, \rho)$ (b)

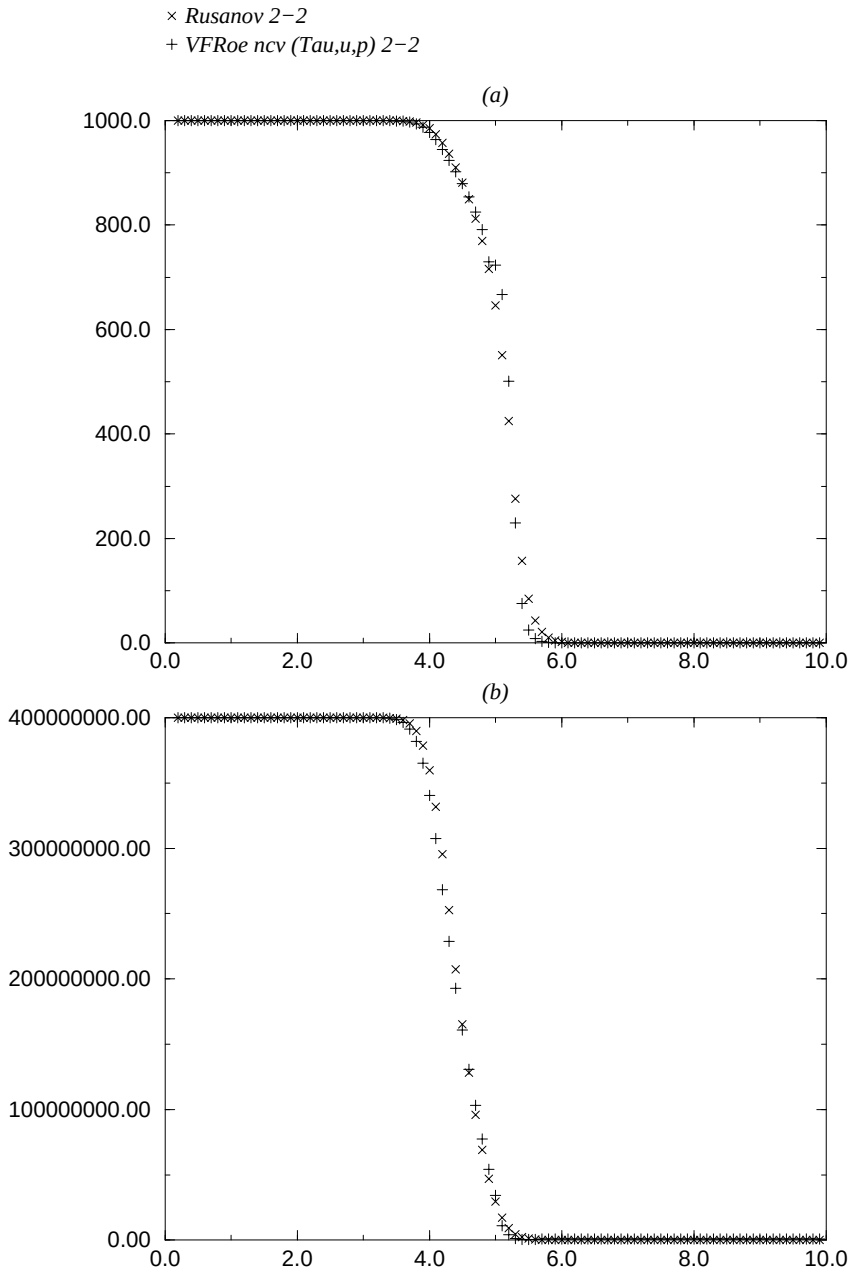

Figure 1.7: Case 3.7: density (a) - $p + p_c$ (b)

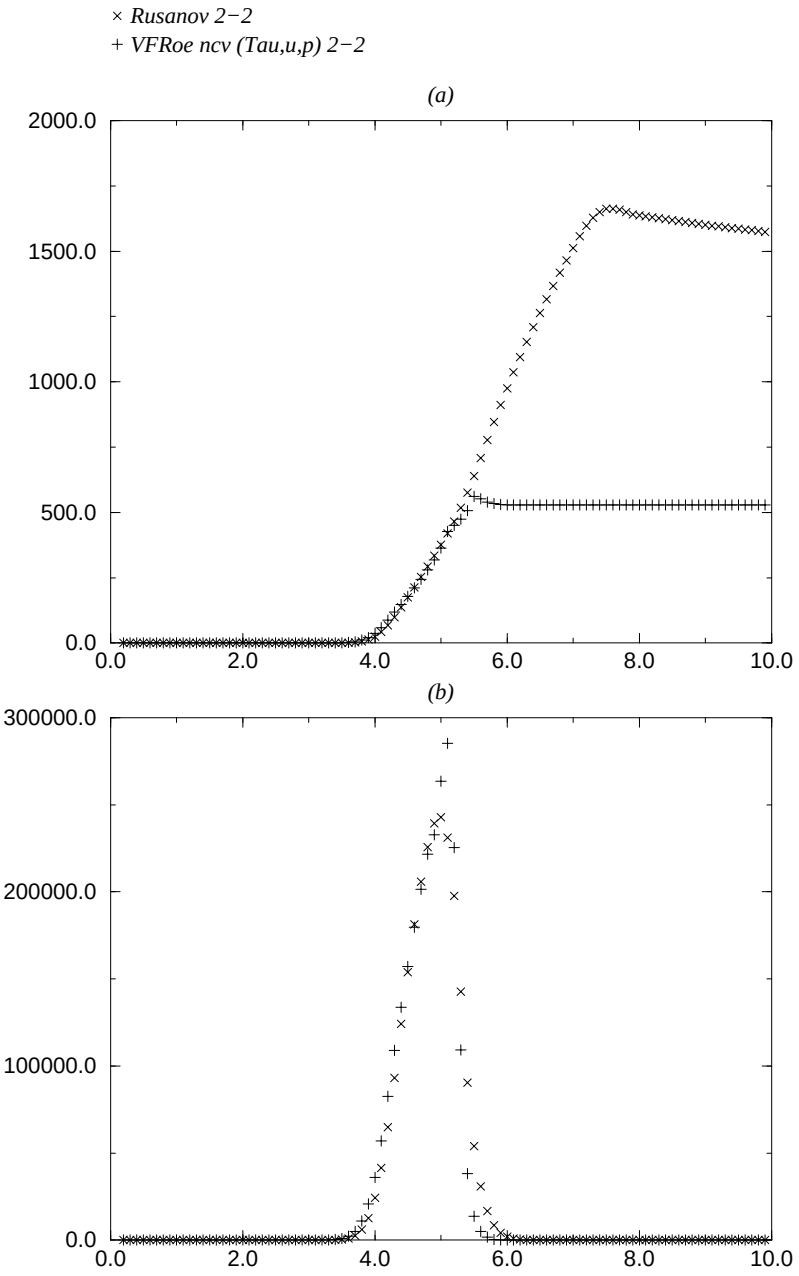

Figure 1.8: Case 3.7: velocity (a) - momentum (b)

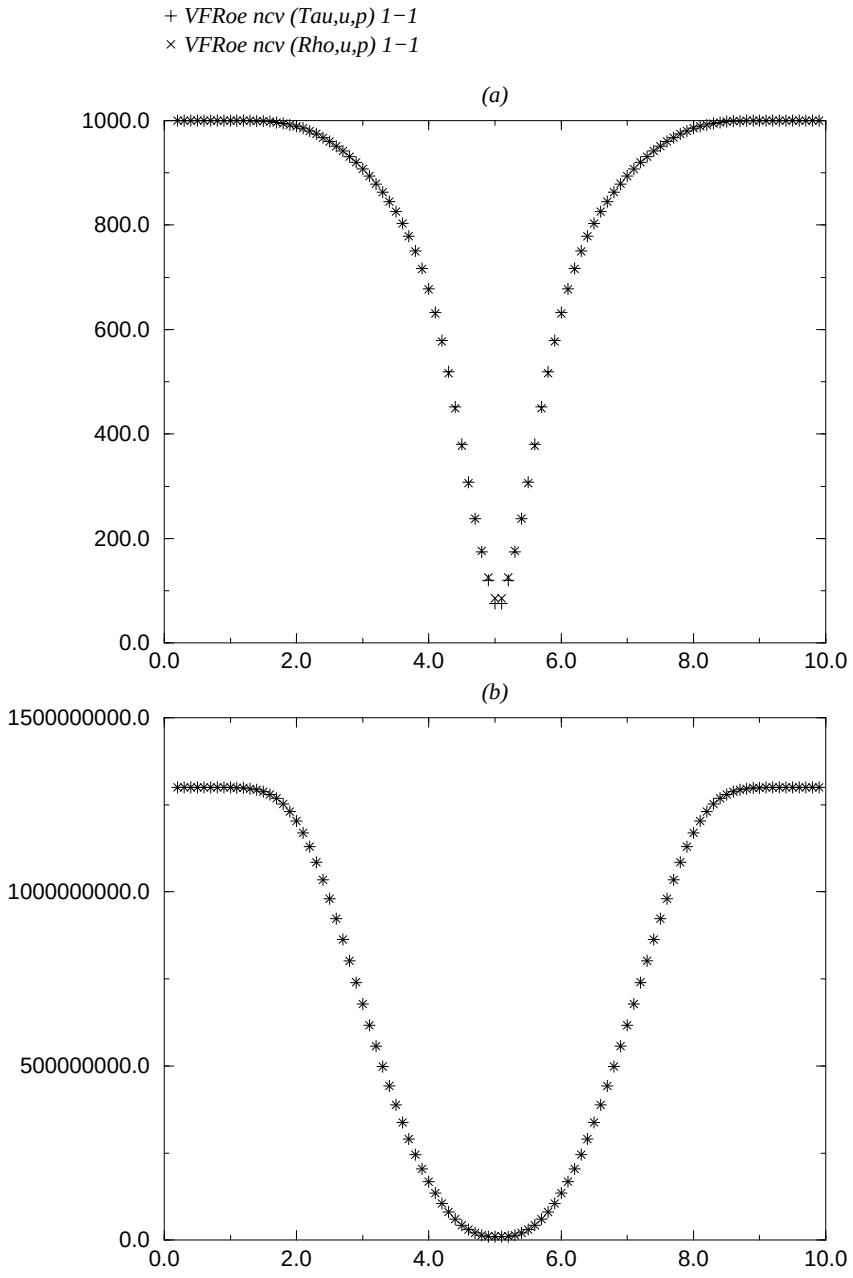

Figure 1.9: Case 3.8: densité (a) - $p + p_c$ (b)

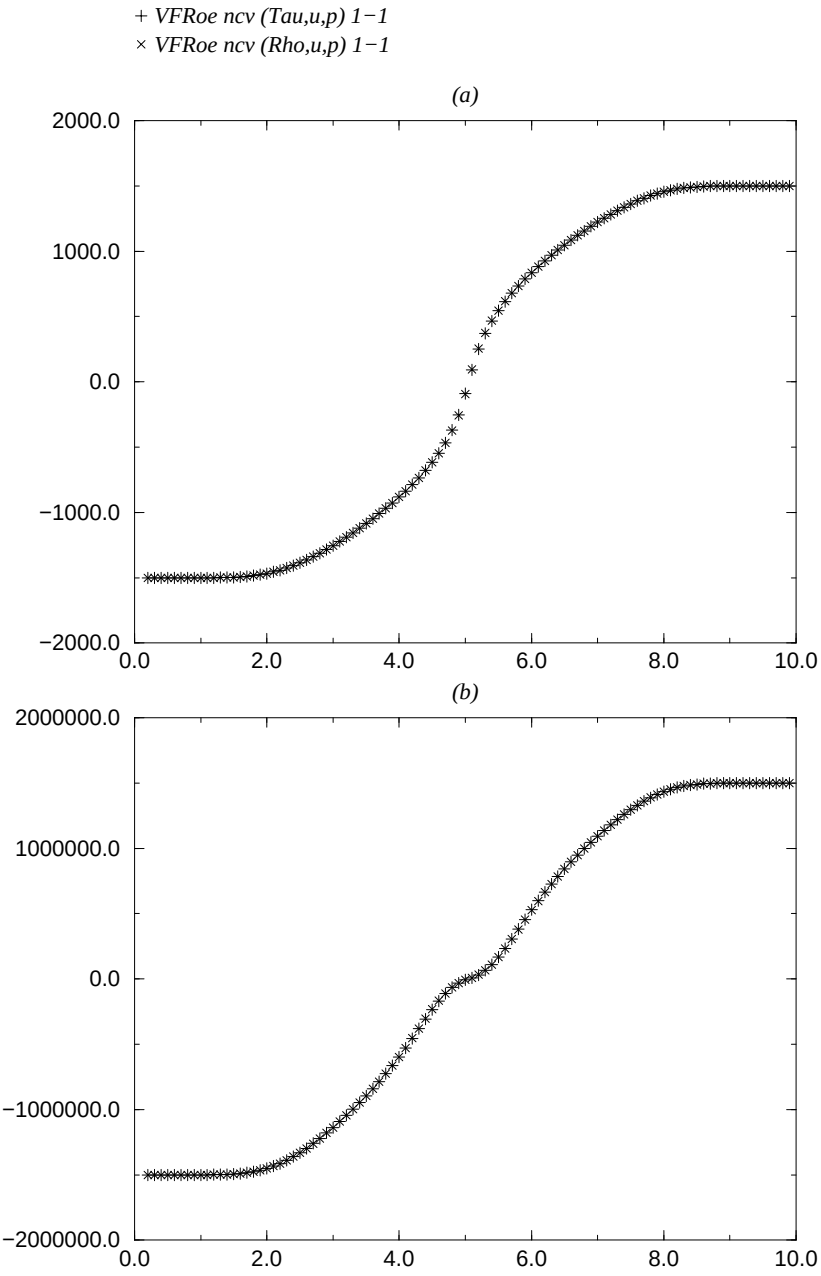

Figure 1.10: Case 3.8: vitesse (a) - momentum (b)

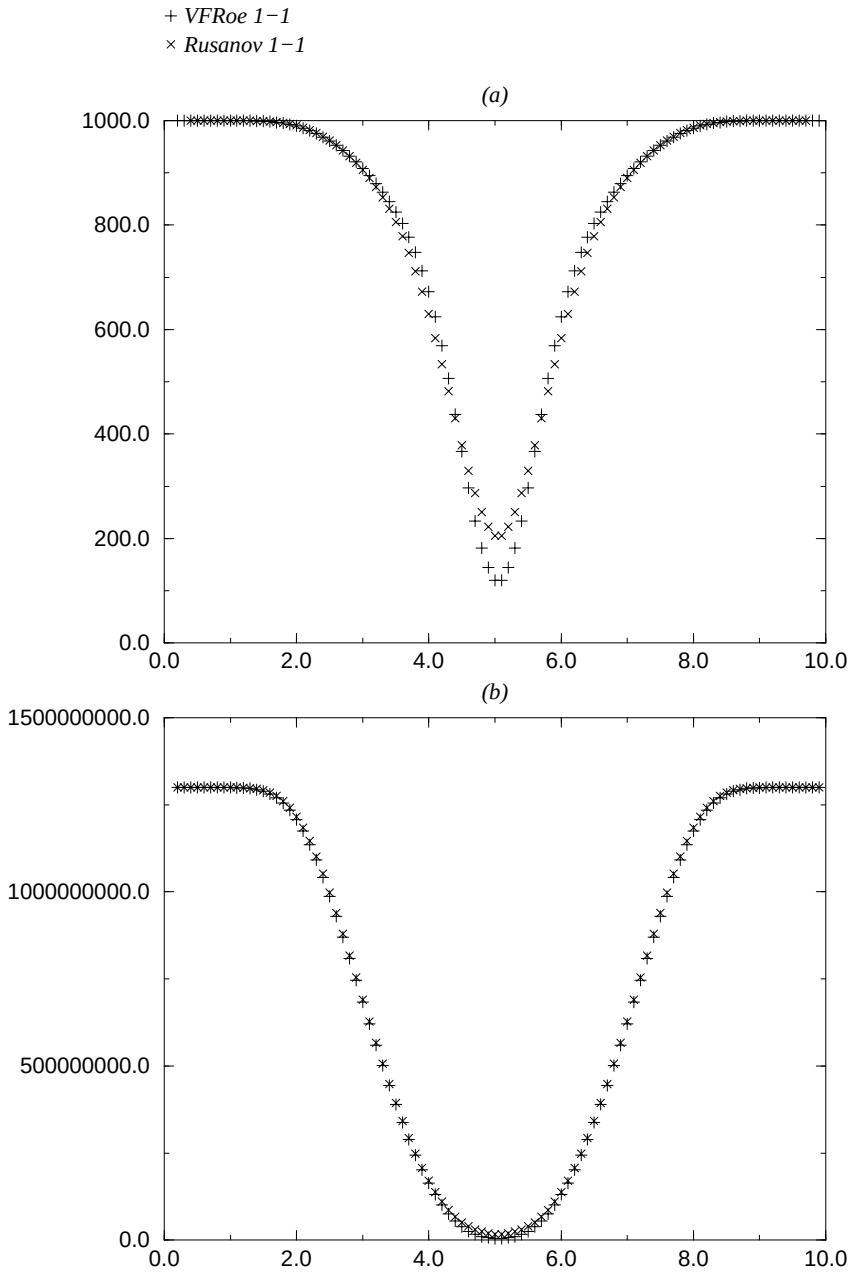

Figure 1.11: Case 3.8: density (a) - $p + p_c$ (b)

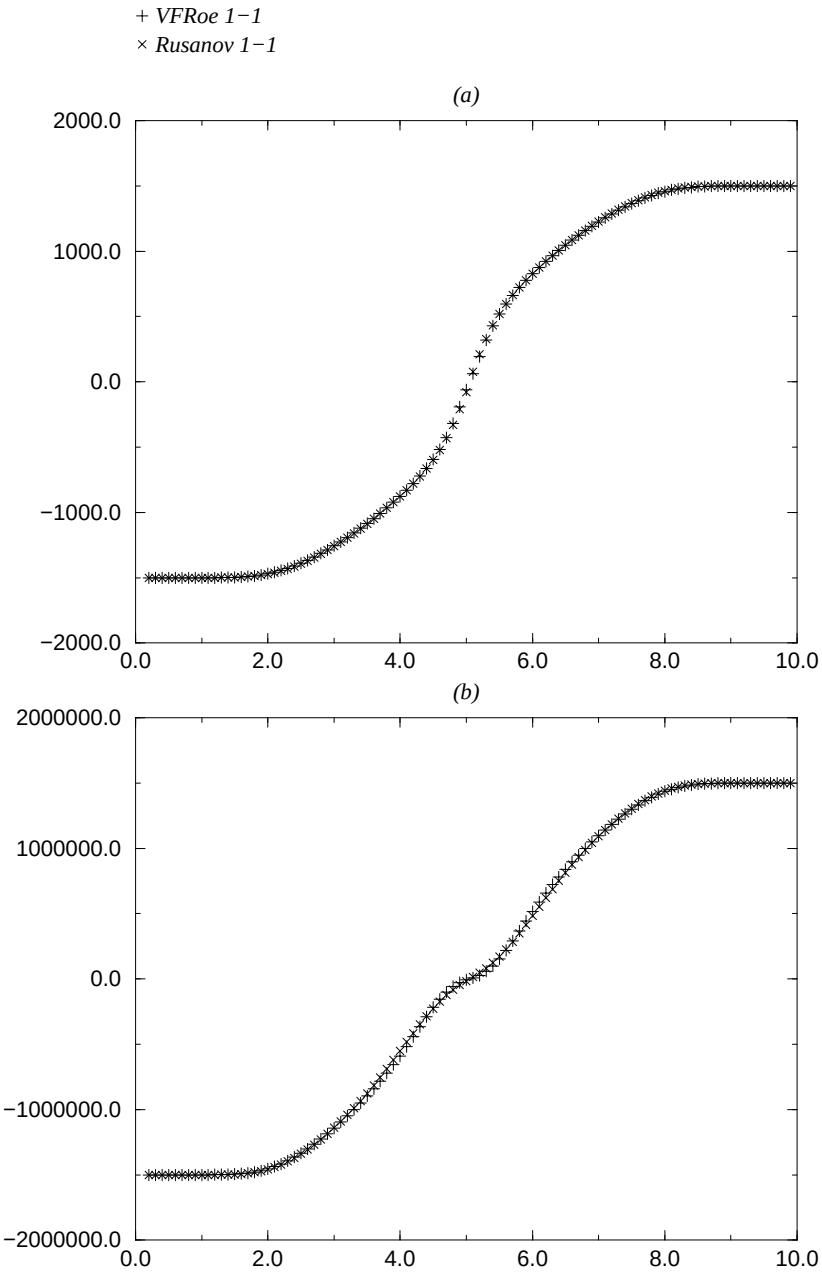

Figure 1.12: Case 3.8: velocity (a) - momentum (b)

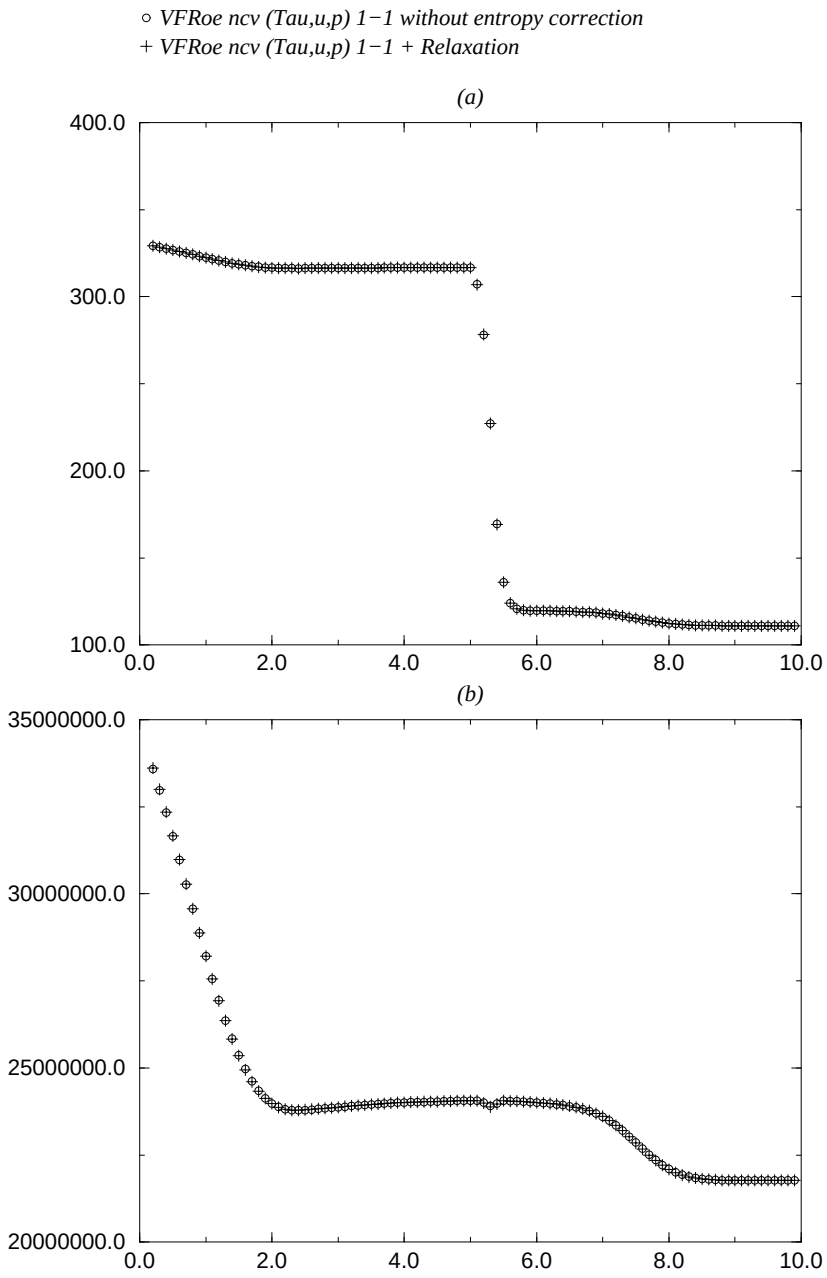

Figure 1.13: Case 4.1: densité (a) - $p + p_c$ (b)

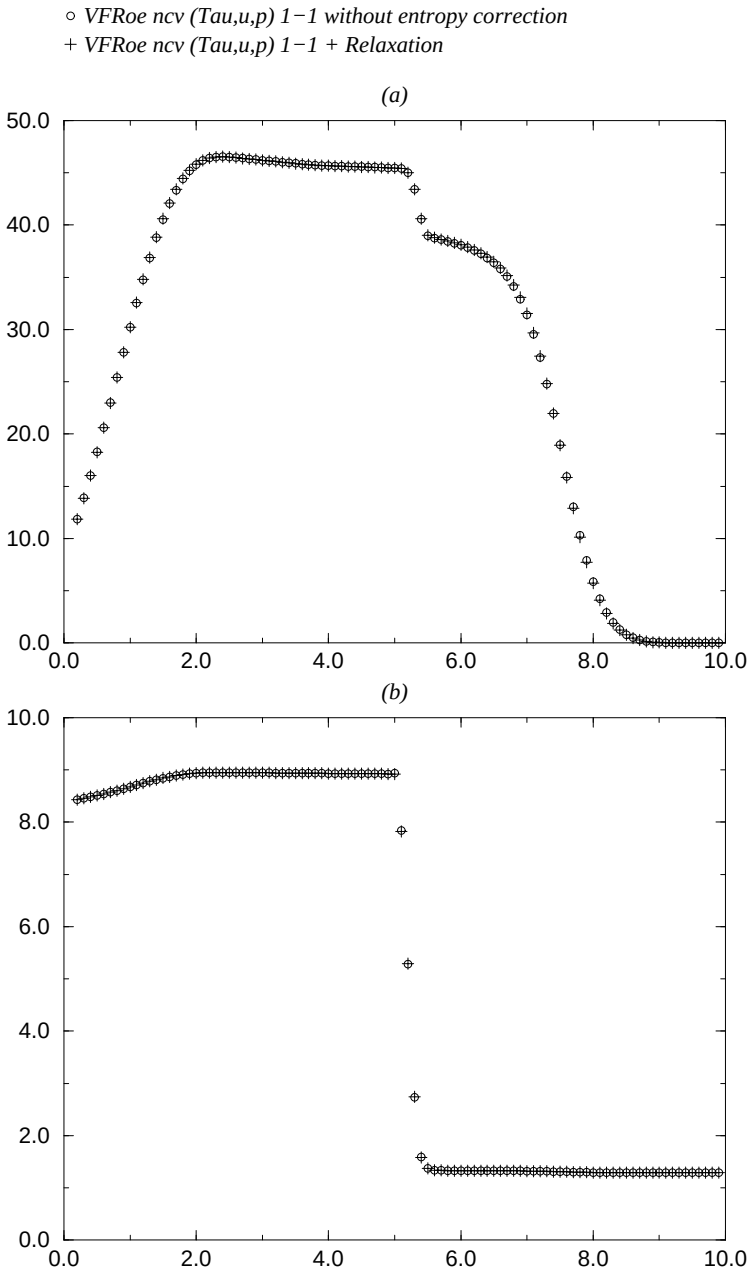

Figure 1.14: Case 4.1: vitesse (a) - $\hat{\gamma}(p,\rho)$ (b)

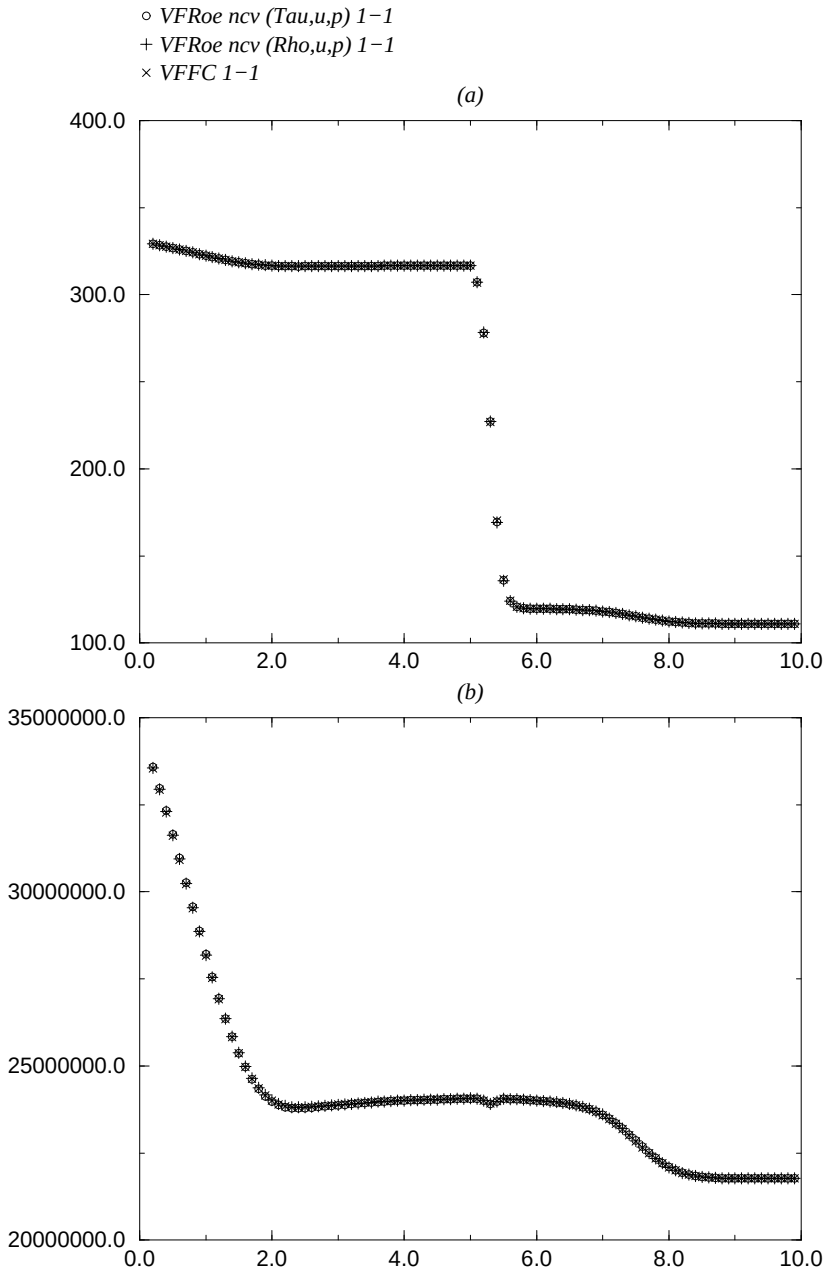

Figure 1.15: Case 4.1: densité (a) - $p + p_c$ (b)

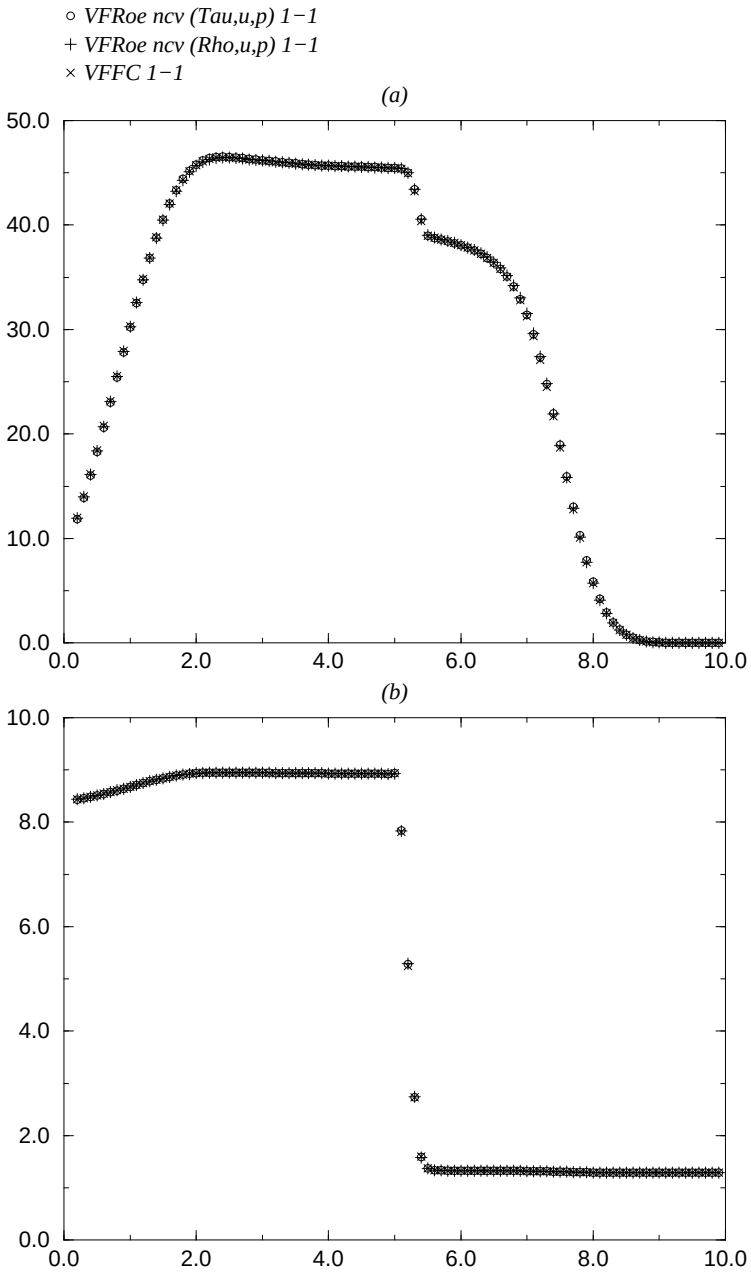

Figure 1.16: Case 4.1: vitesse (a) - $\hat{\gamma}(p,\rho)$ (b)

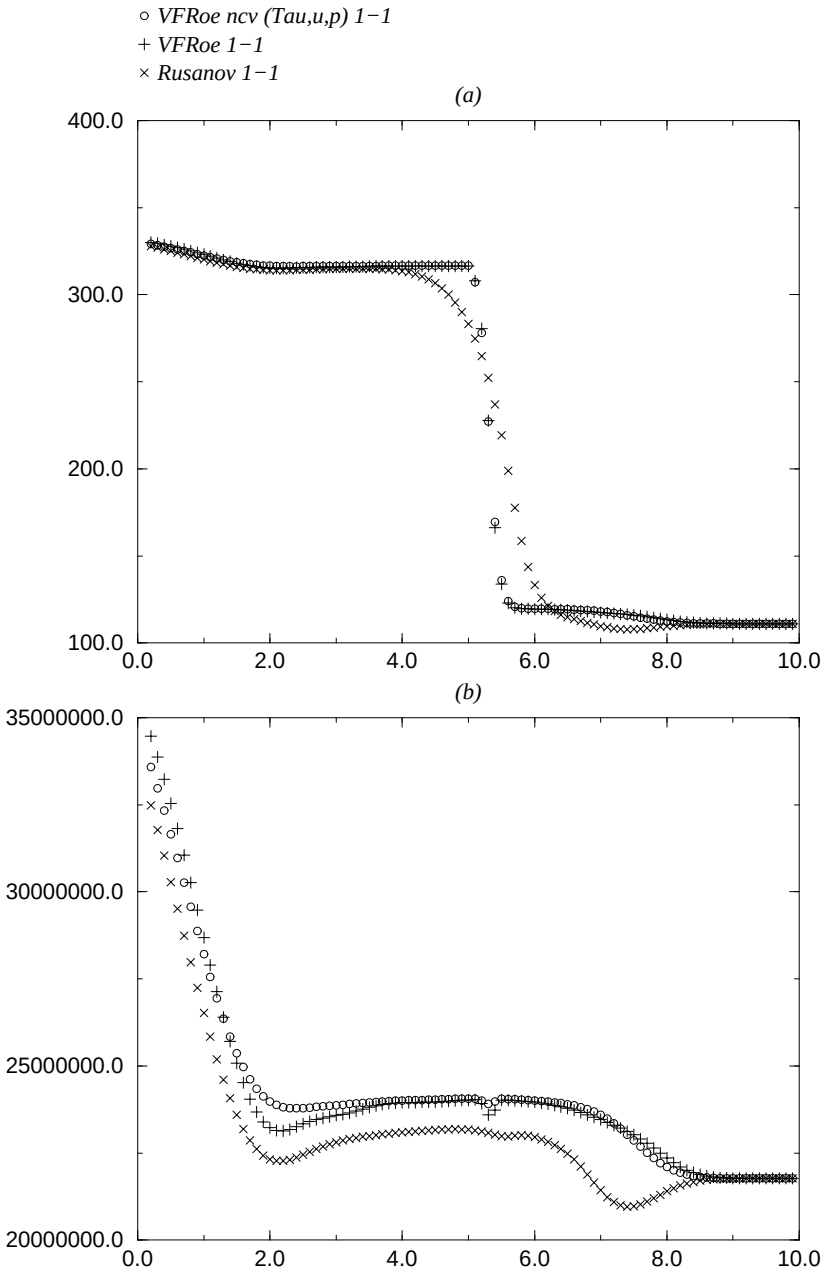

Figure 1.17: Case 4.1: densité (a) - $p + p_c$ (b)

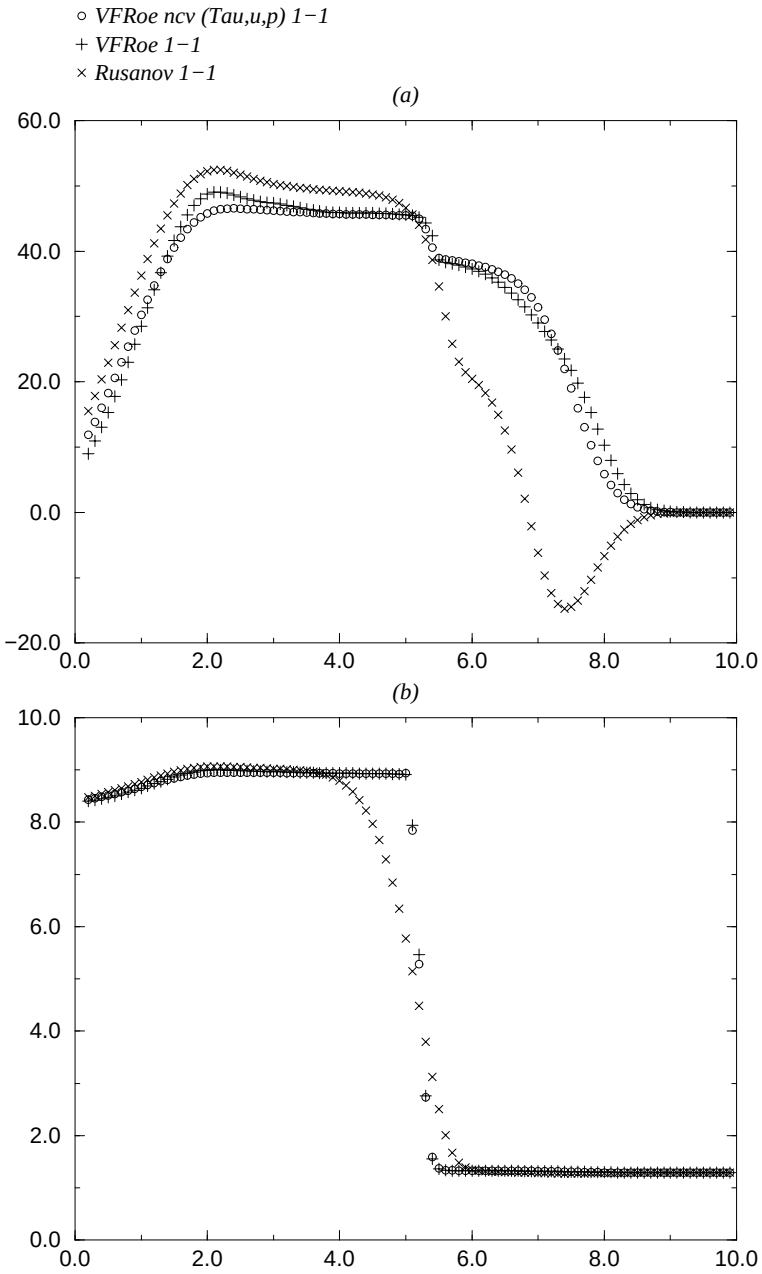

Figure 1.18: Case 4.1: vitesse (a) - $\hat{\gamma}(p,\rho)$ (b)

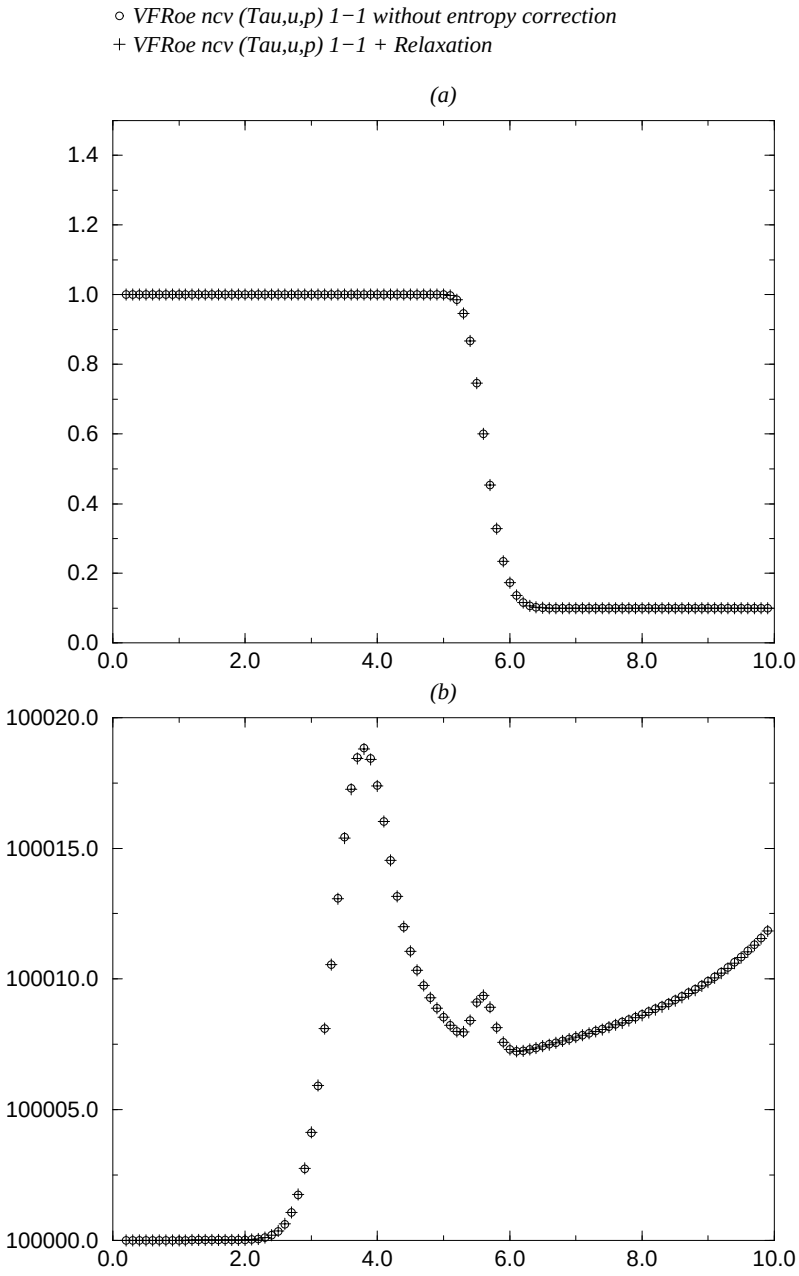

Figure 1.19: Case 4.2: densité (a) - $p + p_c$ (b)

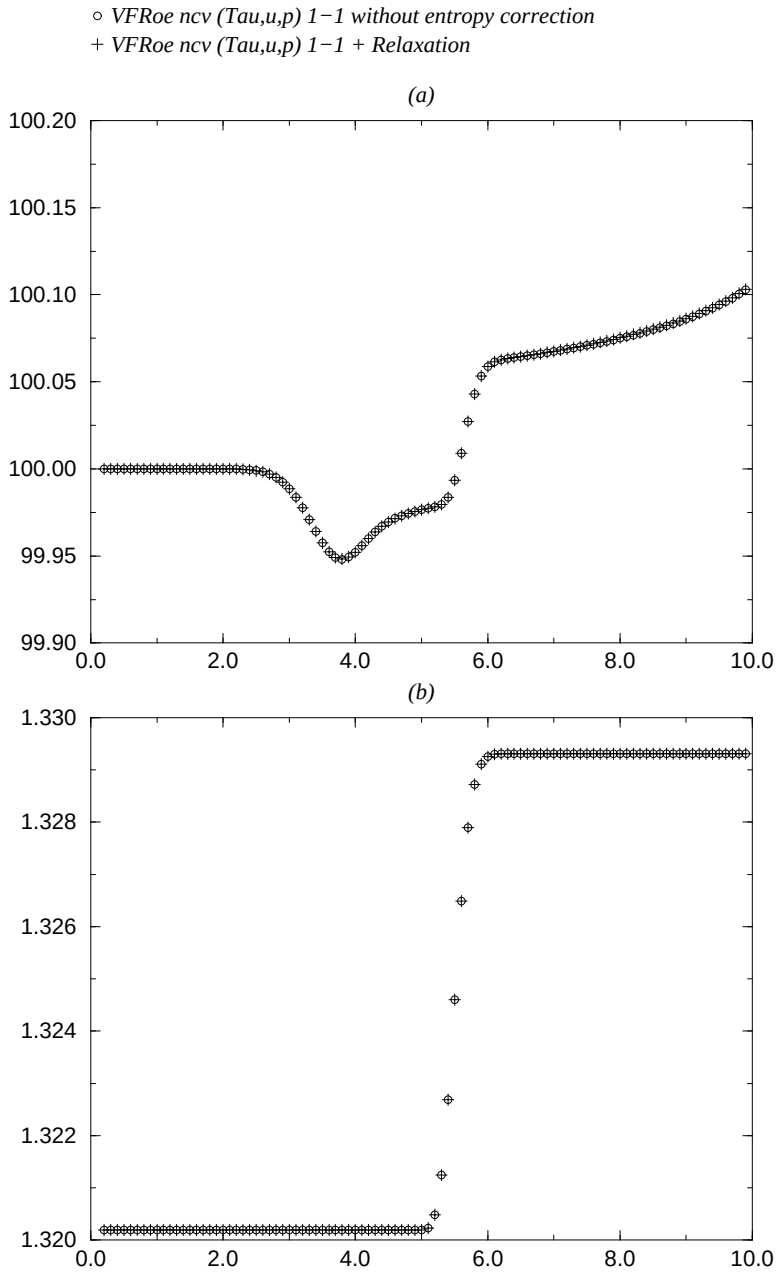

Figure 1.20: Case 4.2: vitesse (a) - $\hat{\gamma}(p,\rho)$ (b)

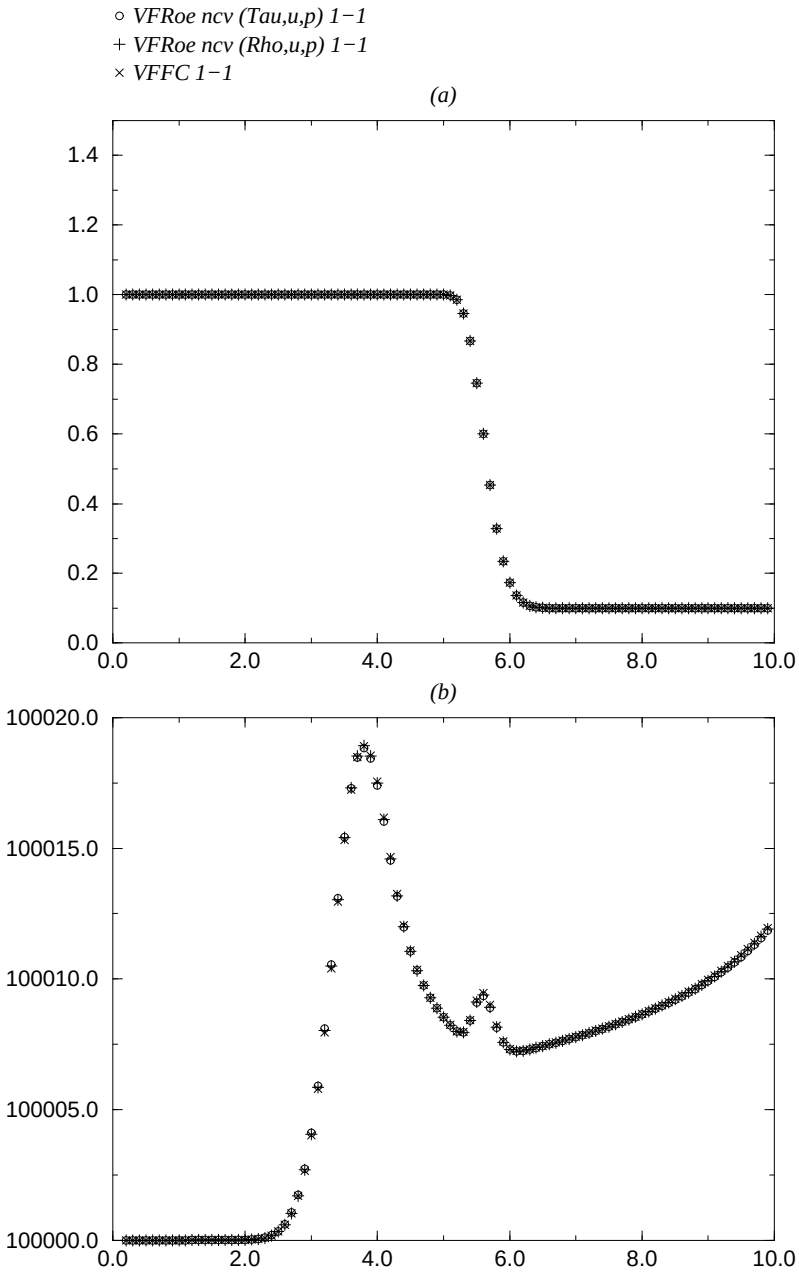

Figure 1.21: Case 4.2: densité (a) - $p + p_c$ (b)

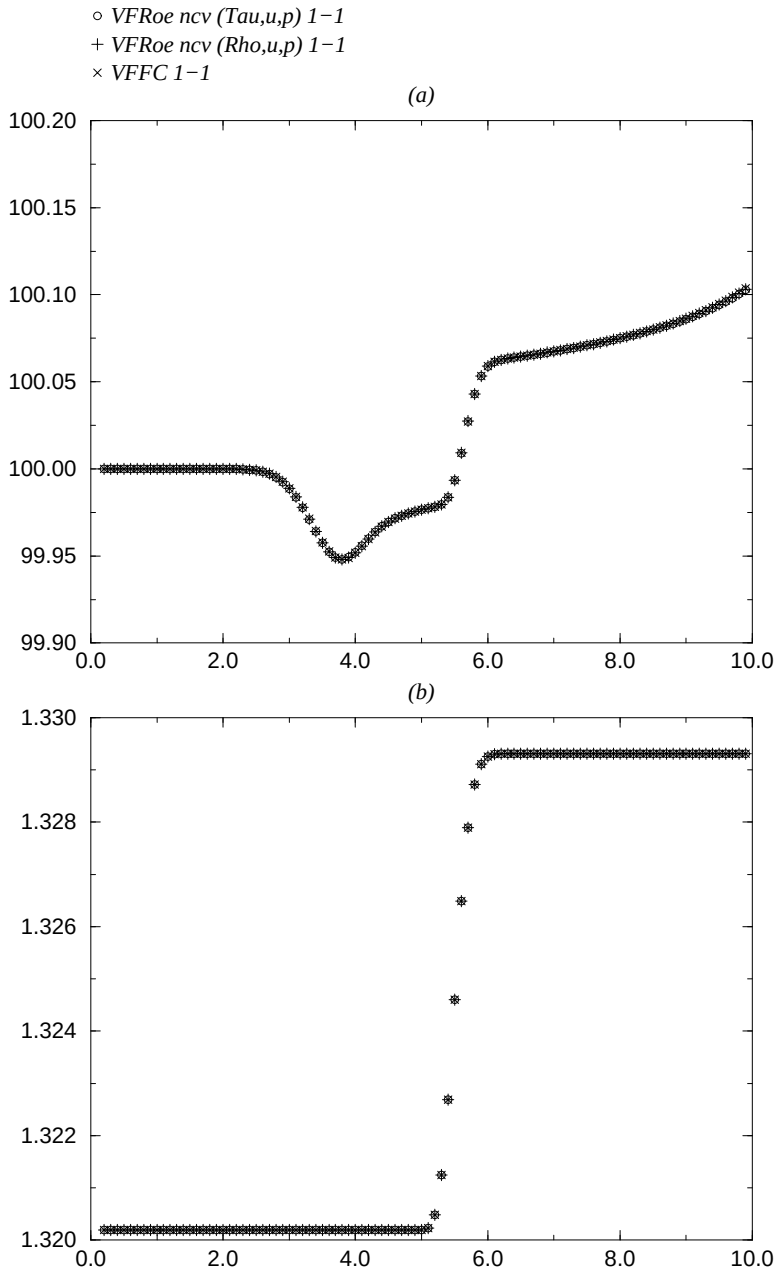

Figure 1.22: Case 4.2: vitesse (a) - $\hat{\gamma}(p,\rho)$ (b)

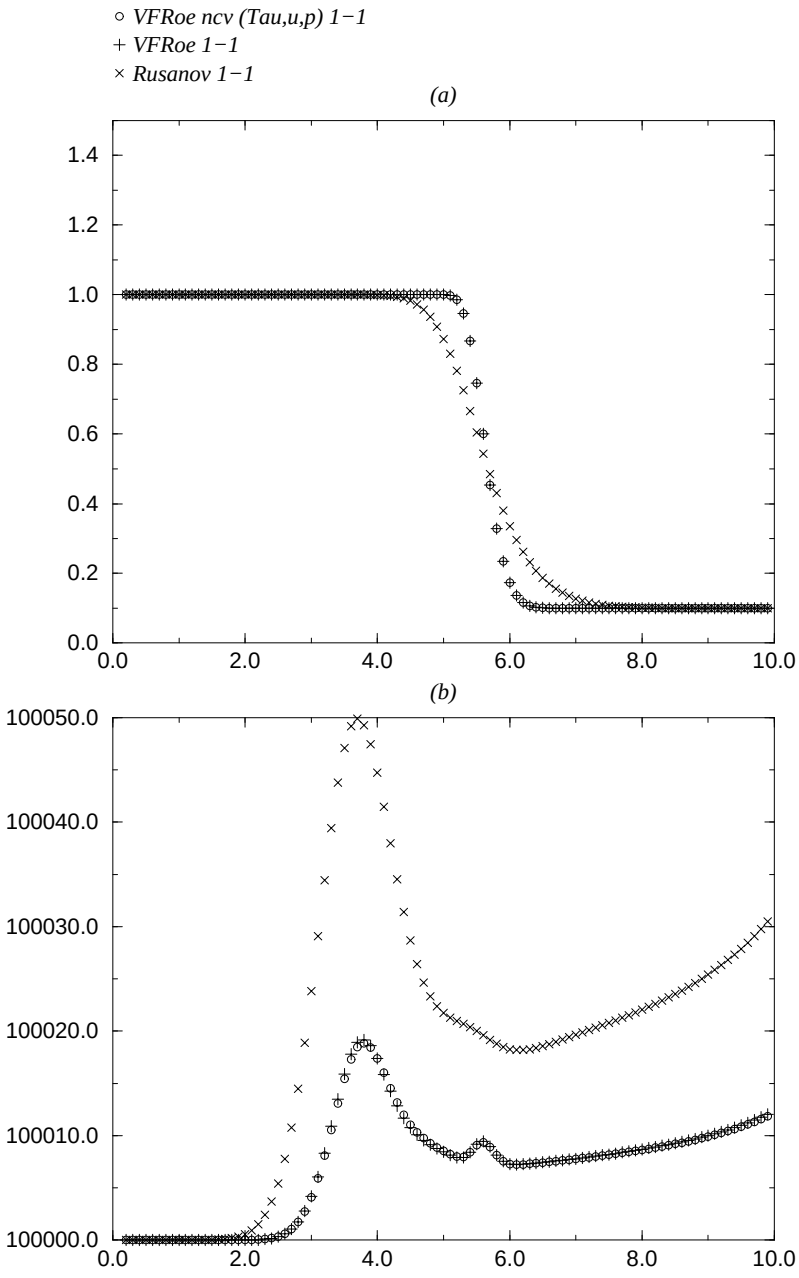

Figure 1.23: Case 4.2: densité (a) - $p + p_c$ (b)

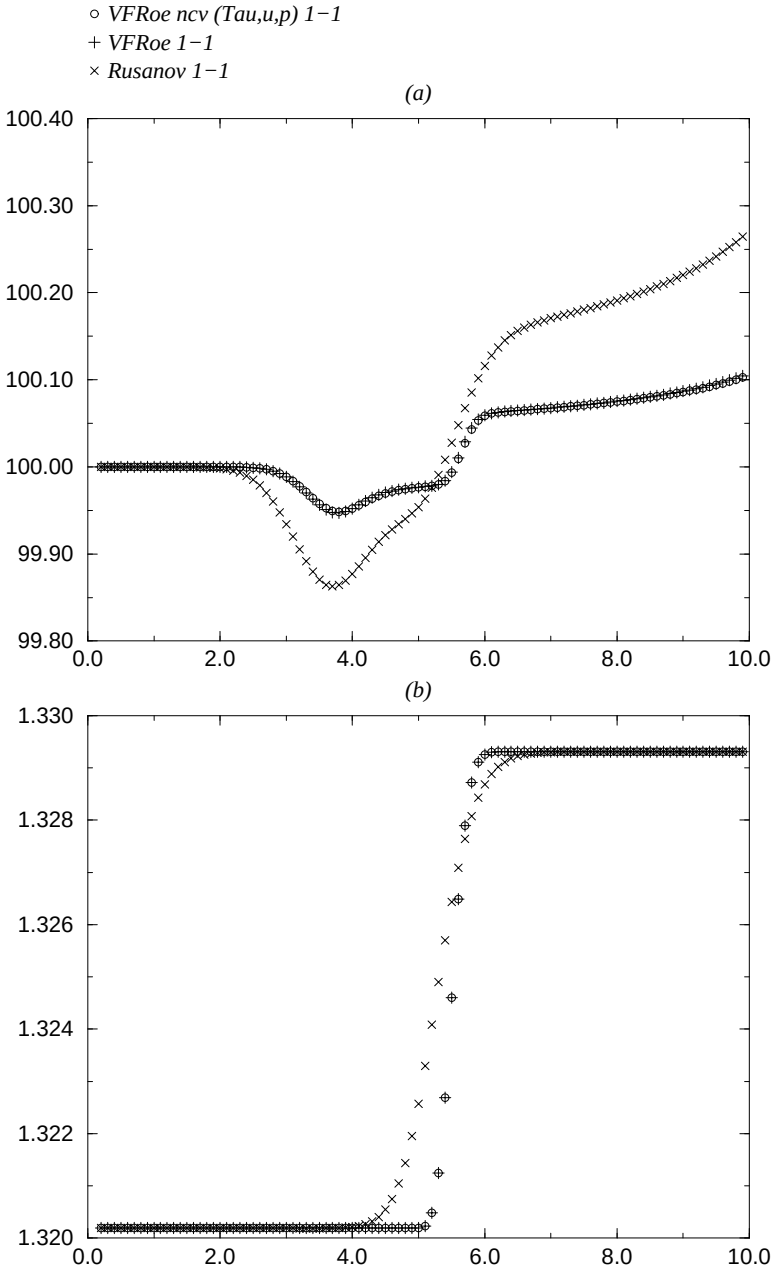

Figure 1.24: Case 4.2: vitesse (a) - $\hat{\gamma}(p, \rho)$ (b)

1.4.5 Actual rates of convergence

Perfect gas EOS - Sod shock tube

- Energy relaxation

	1st order	2nd order
ρ	0.654	0.791
u	0.853	0.967
p	0.812	0.988

- Rusanov

	1st order	2nd order
ρ	0.651	0.780
u	0.842	0.970
p	0.823	0.989

- VFFC

	1st order	2nd order
ρ	0.655	0.792
u	0.855	0.968
p	0.814	0.988

- VFRoe

	1st order	2nd order
ρ	0.654	0.791
u	0.853	0.967
p	0.811	0.988

- VFRoe ncv (ρ, u, p)

	1st order	2nd order
ρ	0.654	0.791
u	0.853	0.967
p	0.811	0.988

- VFRoe ncv (τ, u, p)

	1st order	2nd order
ρ	0.653	0.791
u	0.853	0.967
p	0.812	0.988

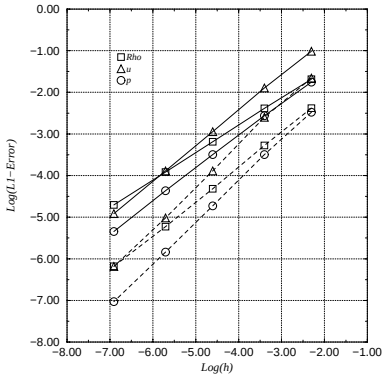

Figure 1.25: Relaxation d'énergie

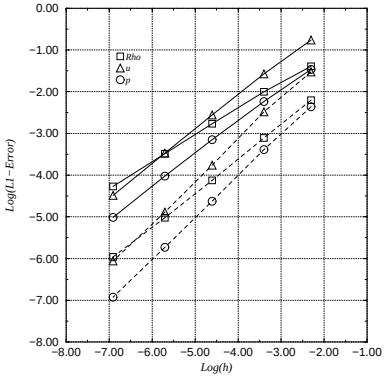

Figure 1.26: Rusanov

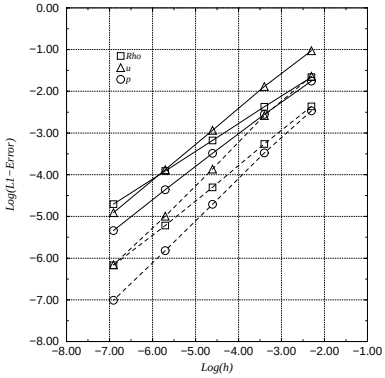

Figure 1.27: VFFC

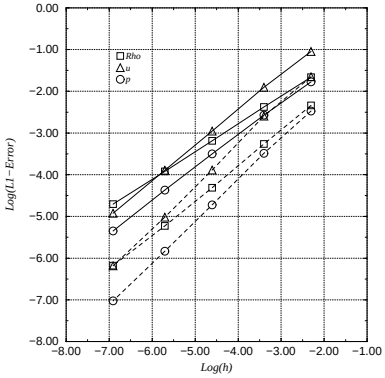

Figure 1.28: VFRoe

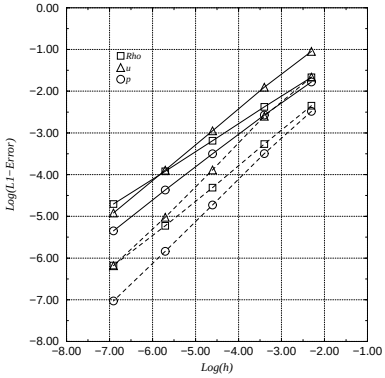

Figure 1.29: VFRoe ncv (ρ, u, p)

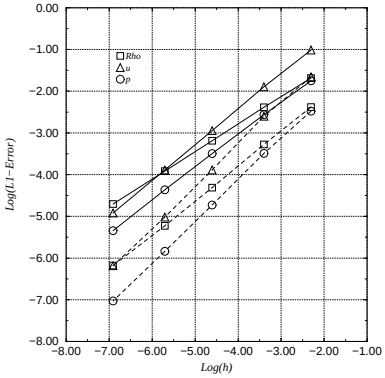

Figure 1.30: VFRoe ncv (τ, u, p)

Perfect gas EOS - Sonic rarefaction wave

- Energy relaxation

	1st order	2nd order
ρ	0.890	0.810
u	0.933	0.973
p	0.927	0.995

- Rusanov

	1st order	2nd order
ρ	0.684	0.827
u	0.794	0.985
p	0.821	0.999

- VFFC

	1st order	2nd order
ρ	0.667	0.819
u	0.808	0.977
p	0.798	0.996

- VFRoe

	1st order	2nd order
ρ	0.669	0.828
u	0.791	0.975
p	0.796	0.996

- VFRoe ncv (ρ, u, p)

	1st order	2nd order
ρ	0.667	0.840
u	0.805	0.977
p	0.796	0.995

- VFRoe ncv (τ, u, p)

	1st order	2nd order
ρ	0.653	0.809
u	0.822	0.973
p	0.802	0.995

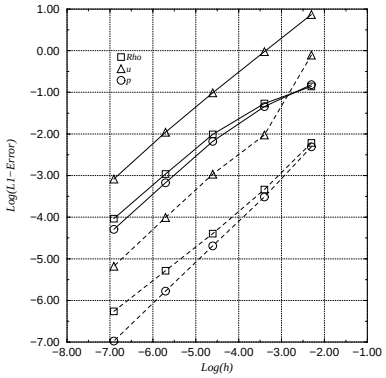

Figure 1.31: Relaxation d'énergie

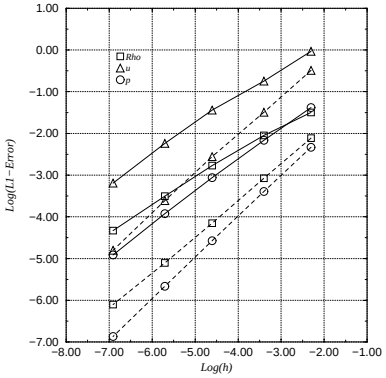

Figure 1.32: Rusanov

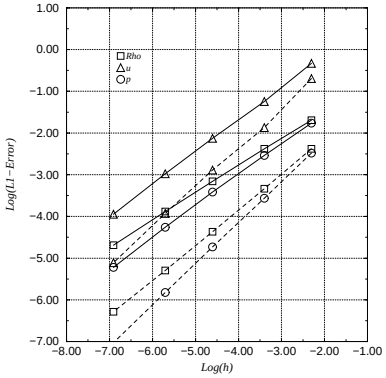

Figure 1.33: VFFC

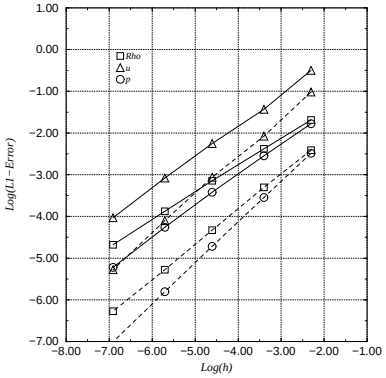

Figure 1.34: VFRoe

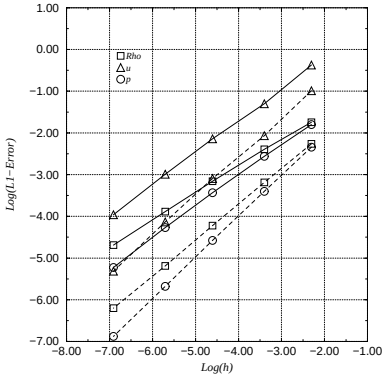

Figure 1.35: VFRoe ncv (ρ, u, p)

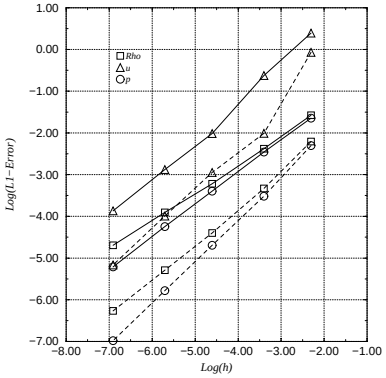

Figure 1.36: VFRoe ncv (τ, u, p)

Perfect gas EOS - Symmetrical double rarefaction wave

- Energy relaxation

	1st order	2nd order
ρ	0.771	0.998
u	0.785	0.999
p	0.775	0.999

- Rusanov

	1st order	2nd order
ρ	0.773	0.999
u	0.787	1.000
p	0.777	0.999

- VFFC

	1st order	2nd order
ρ	0.768	0.998
u	0.782	1.000
p	0.772	0.999

- VFRoe

	1st order	2nd order
ρ	0.771	0.998
u	0.785	0.999
p	0.775	0.999

- VFRoe ncv (ρ, u, p)

	1st order	2nd order
ρ	0.771	0.998
u	0.785	0.999
p	0.775	0.999

- VFRoe ncv (τ, u, p)

	1st order	2nd order
ρ	0.771	0.998
u	0.785	0.999
p	0.775	0.999

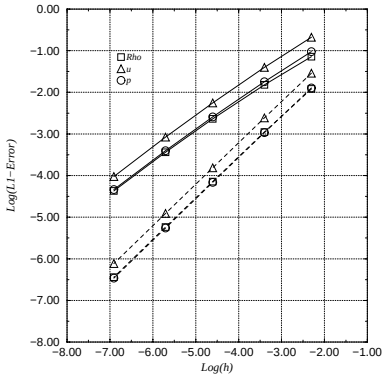

Figure 1.37: Relaxation d'énergie

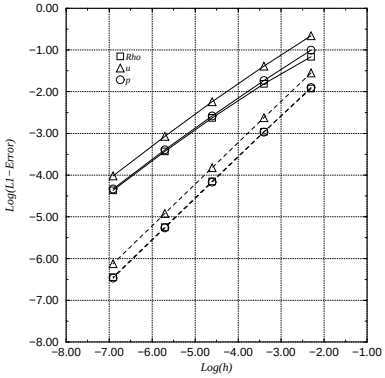

Figure 1.38: Rusanov

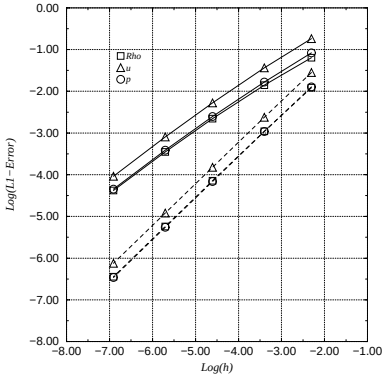

Figure 1.39: VFFC

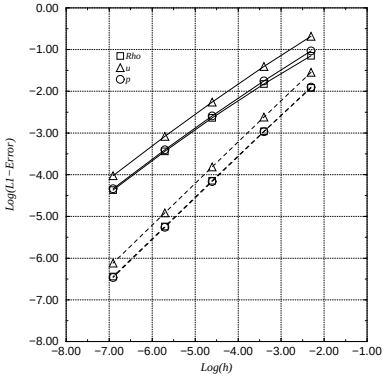

Figure 1.40: VFRoe

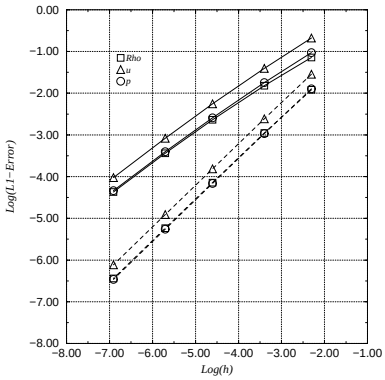

Figure 1.41: VFRoe ncv (ρ, u, p)

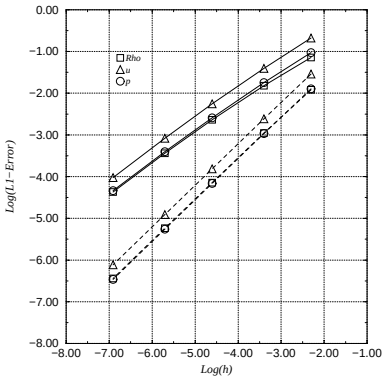

Figure 1.42: VFRoe ncv (τ, u, p)

Perfect gas EOS - Symmetrical double shock wave

- Energy relaxation

	1st order	2nd order
ρ	1.062	0.935
u	1.157	1.156
p	1.050	1.017

- Rusanov

	1st order	2nd order
ρ	1.060	1.028
u	1.056	1.115
p	0.996	1.001

- VFFC

	1st order	2nd order
ρ	1.060	0.905
u	1.157	1.154
p	1.049	1.019

- VFRoe

	1st order	2nd order
ρ	1.063	0.927
u	1.157	1.153
p	1.050	1.019

- VFRoe ncv (ρ, u, p)

	1st order	2nd order
ρ	1.063	0.929
u	1.158	1.154
p	1.050	1.019

- VFRoe ncv (τ, u, p)

	1st order	2nd order
ρ	1.062	0.947
u	1.157	1.153
p	1.050	1.019

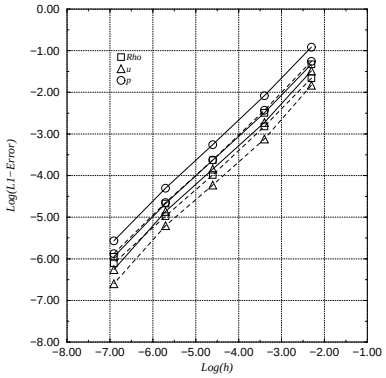

Figure 1.43: Relaxation d'énergie

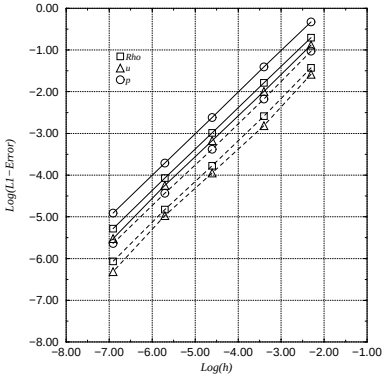

Figure 1.44: Rusanov

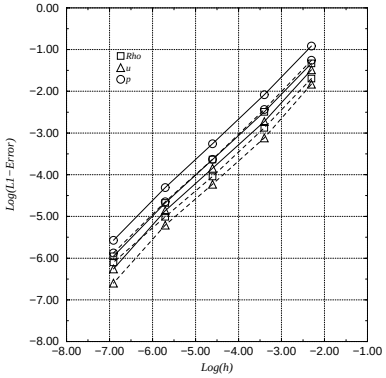

Figure 1.45: VFFC

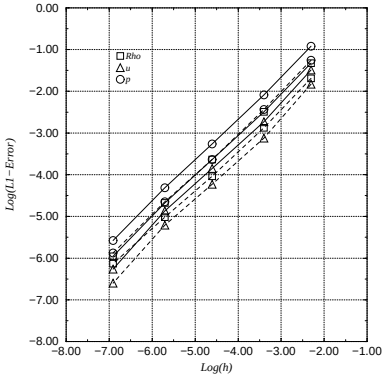

Figure 1.46: VFRoe

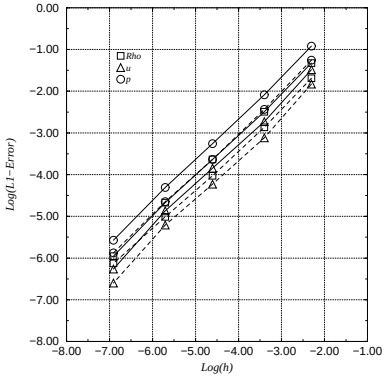

Figure 1.47: VFRoe ncv (ρ, u, p)

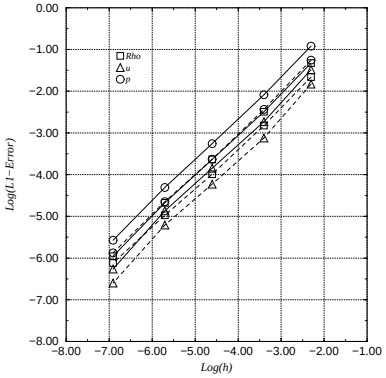

Figure 1.48: VFRoe ncv (τ, u, p)

Perfect gas EOS - Unsteady contact discontinuity

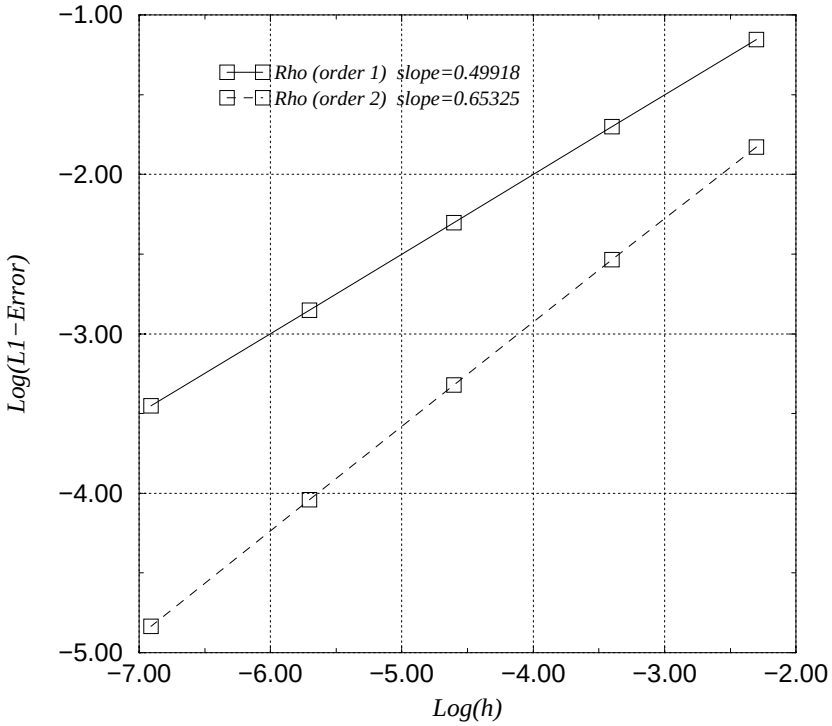

Figure 1.49: Case 2.1: density

1.5 Conclusion

Several approximate Riemann solvers have been compared in this study. Some among them are based on an approximate Godunov scheme, applying various changes of variables in order to compute approximate values of state at the interface. These make use of conservative variable W, flux variable $F(W)$ or variable (ρ, u, p) or (τ, u, p). The latter enables to preserve unsteady contact discontinuites provided the EOS agrees with some conditions (perfect gas EOS, Tammann EOS belong to the latter class). The practical or theoretical behaviour of these schemes when computing steady shock wave, steady contact discontinuity, or vacuum has been investigated. All schemes perform rather well in all experiments, except in vacuum occurence or propagation over vacuum. One drawback of the VFFC scheme can be emphasized: when computing a double supersonic rarefaction wave (with or without vacuum occurence), this scheme blows up after a few time steps. Concerning VFRoe ncv (τ, u, p) and PVRS schemes, changing slightly the average state can increase their robustness and accuracy. The energy relaxation method applied with VFRoe ncv (τ, u, p) scheme has been computed too. The behaviour of this method is nearly the same as the original VFRoe ncv (τ, u, p) scheme. However, the energy relaxation method makes non entropic shocks vanish. The Rusanov scheme provides good results too, though it is slightly less accurate than other schemes investigated, due to important numerical diffusion. But the Rusanov scheme converges as fast as other schemes (in terms of mesh size exponent in the error norm). Moreover, it is the most robust scheme computed here, in particular in test cases with vacuum.

Moreover, a quantitative study has been presented. Solutions involving discontinuities have been investigated for first and second order shemes. Classical rates when restricting to smooth solutions ($\mathcal{C}^\infty$) are around 1 and 2 respectively. When the solution contains rarefaction waves or shock waves (without contact discontinuities), the rate becomes less than or equals to (for the second order schemes) 1. Restricting to a simple unsteady contact discontinuity, first order schemes provide a rate around 1/2 and second order schemes provide a rate around 2/3.

The framework of this paper has been restricted to the computation by Finite Volume schemes of a conservative and hyperbolic system, in one space dimension. Let us recall some extensions of methods used here, in different applications.

Of course, all schemes presented herein can be extended to 2D or 3D problems (see [Buf93]). Rusanov (see [Xeu99]), Godunov (see [Xeu99]), VFFC (see [Bou98]) and VFRoe ncv (τ, u, p) (see [BGH00]) schemes have been applied to Euler equations with real gas EOS, Shallow Water equations (see [BGH98b]) and compressible gas-solid two phase flows (see [CH96]), with structured or unstructured meshes. Since these systems stay unchanged under frame rotation, a multidimensional framework may rely on a one dimension method (see [GR96]).

Some systems arising in CFD cannot be written under a conservative form, and thus, approximate jump relations must be proposed (see [DLM95] and [Col92]). Some of the previous schemes have been extended to the non conservative formalism: Godunov (see [FHL97]), Roe (see [BHJU00], [H95], [HFL94], [Sai95b]), VFRoe ncv (see [BGH98a], [BGH99], [Xeu99]) and VFRoe (see [Mas97], [BCHU01]).

Others non conservative systems are conditionnally hyperbolic, in particular when focusing on two-fluid two-phase flows (see [Sai95a]). Three main directions have been proposed up to now in the literature. The first consists in splitting the jacobian matrix in several matrices, which may

be diagonalised in $\mathbb{R}$ (see [CH99]). The second way consists in using the sign of the real part of eigenvalues to choose the flux direction (see [MBL$^+$99] and [Bou98]). A third approach is based on a development in power series of eigenvalues and eigenvectors in terms of a small parameter (see [Sai95b], [TK96]).

1.A Numerical preservation of velocity and pressure through the contact discontinuity in Euler equations

We discuss in this appendix about schemes and state laws, in order to preserve velocity and pressure on the contact discontinuity, in a one dimension framework. We focus on initial conditions of a Riemann problem, with constant velocity and constant pressure. Schemes investigated here can be derived from the formalism of VFRoe ncv scheme, with variable:

$$Y = {}^t(\varphi, u, p)$$

where $\varphi = \varphi(\rho, s)$ (s denotes the specific entropy) must be independant of pressure p (for instance $\varphi = \rho, \tau, ...$).

Restricting to regular solutions, Euler equations can be written related to $Y = {}^t(\varphi, u, p)$ as follows:

$$Y_{,t} + A(Y)Y_{,x} = 0$$

where:

$$A = \begin{pmatrix} u & \rho\varphi_{,\rho} & 0 \\ 0 & u & \rho^{-1} \\ 0 & \hat{\gamma}p & u \end{pmatrix}$$

At each interface, we linearize the matrix $A(Y)$ to obtain a linear Riemann problem, which may be easily solved. Initial conditions are defined by the average values in cells apart from the considered interface ($i + 1/2$ for instance):

$$\begin{cases} \dfrac{\partial Y}{\partial t} + A(\hat{Y})\dfrac{\partial Y}{\partial x} = 0 \\ Y(x,0) = \begin{cases} Y_L = Y(W_i^n) & \text{if } x < 0 \\ Y_R = Y(W_{i+1}^n) & \text{if } x > 0 \end{cases} \end{cases} \tag{1.12}$$

with $\hat{Y}$ such that $\hat{Y}(Y, Y) = Y$.
To compute the solution at the interface, we need to write the eigenstructure of the matrix A(Y). As usual, the eigenvalues are (c stands for the sound speed):

$$\lambda_1 = u - c,\ \lambda_2 = u,\ \lambda_3 = u + c$$

The associated right eigenvectors are:

$$r_1(Y) = \begin{pmatrix} \rho\varphi_{,\rho} \\ -c \\ \rho c^2 \end{pmatrix},\ r_2(Y) = \begin{pmatrix} 1 \\ 0 \\ 0 \end{pmatrix},\ r_3(Y) = \begin{pmatrix} \rho\varphi_{,\rho} \\ c \\ \rho c^2 \end{pmatrix}$$

Left eigenvectors of $A(Y)$ are:

$$l_1(Y) = \frac{1}{2c^2}\begin{pmatrix} 0 \\ -c \\ \rho^{-1} \end{pmatrix},\ l_2(Y) = \frac{1}{c^2}\begin{pmatrix} 1 \\ 0 \\ -\varphi_{,\rho} \end{pmatrix},\ l_3(Y) = \frac{1}{2c^2}\begin{pmatrix} 0 \\ c \\ \rho^{-1} \end{pmatrix}$$

In the following, we denote $\tilde{}$ variables computed on the basis of $\overline{Y}$. The solution of the linear problem (1.12), when $x/t \neq \lambda_k$, $k = 1, 2, 3$, is:

$$\begin{aligned} Y^*(x/t; Y_L, Y_R) &= Y_L + \sum_{x/t > \widetilde{\lambda_k}} ({}^t\widetilde{l_k}.(Y_R - Y_L))\widetilde{r_k} \\ &= Y_R - \sum_{x/t < \widetilde{\lambda_k}} ({}^t\widetilde{l_k}.(Y_R - Y_L))\widetilde{r_k} \end{aligned}$$

Since the three eigenvalues of the linear system are distinct, two intermediate states Y_1 and Y_2 may occur:

$$\begin{aligned} Y_1 &= Y_L + \widetilde{\alpha_1}\widetilde{r_1} \\ Y_2 &= Y_R - \widetilde{\alpha_3}\widetilde{r_3} \end{aligned}$$

with:

$$\begin{aligned} \widetilde{\alpha_1} &= -\frac{1}{2\tilde{c}}\Delta u + \frac{1}{2\tilde{\rho}\tilde{c}^2}\Delta p \\ \widetilde{\alpha_3} &= \frac{1}{2\tilde{c}}\Delta u + \frac{1}{2\tilde{\rho}\tilde{c}^2}\Delta p \end{aligned}$$

where $\Delta(.) = (.)_R - (.)_L$. Note that the two intermediate states Y_1 and Y_2 do not depend on the choice of φ.
Recall that initial conditions investigated herein are unsteady contact discontinuity. Thus:

$$\begin{aligned} \Delta u = \Delta p = 0 &\Rightarrow \widetilde{\alpha_1} = \widetilde{\alpha_3} = 0 \\ &\Rightarrow Y_1 = Y_L \text{ and } Y_2 = Y_R \end{aligned}$$

Note that these equalities are verified at each interface of the mesh. Hence, if we denote $\rho_{i+1/2}$ the numerical density of the problem (1.12) at the interface $i + 1/2$, u_0 and p_0 initial velocity and pressure, the Finite Volume scheme applied to the mass conservation equation gives:

$$\begin{aligned} \rho_i^{n+1} &= \rho_i^n - \frac{\Delta t}{\Delta x}((\rho u)_{i+1/2} - (\rho u)_{i-1/2}) \\ &= \rho_i^n - \frac{\Delta t}{\Delta x} u_0(\rho_{i+1/2} - \rho_{i-1/2}) \end{aligned}$$

Now, if we apply the Finite Volume scheme to the momentum conservation equation, it gives:

$$\begin{aligned} (\rho u)_i^{n+1} &= (\rho u)_i^n - \frac{\Delta t}{\Delta x}((\rho u^2 + p)_{i+1/2} - (\rho u^2 + p)_{i-1/2}) \\ &= (\rho u)_i^n - \frac{\Delta t}{\Delta x}((\rho_{i+1/2} u_0^2 + p_0) - (\rho_{i-1/2} u_0^2 + p_0)) \\ &= (\rho u)_i^n - \frac{\Delta t}{\Delta x} u_0^2(\rho_{i+1/2} - \rho_{i-1/2}) \\ &= u_0\left(\rho_i^n - \frac{\Delta t}{\Delta x} u_0(\rho_{i+1/2} - \rho_{i-1/2})\right) \\ &= u_0 \rho_i^{n+1} \end{aligned}$$

Thus, we have $u_i^{n+1} = u_0$, $\forall i \in \mathbb{Z}$.
To study the discrete preservation of pressure, let us write the Finite Volume scheme applied to energy conservation equation:

$$\begin{aligned} E_i^{n+1} &= E_i^n - \frac{\Delta t}{\Delta x}((u(E+p))_{i+1/2} - (u(E+p))_{i-1/2}) \\ &= E_i^n - \frac{\Delta t}{\Delta x} u_0 (E_{i+1/2} - E_{i-1/2}) \end{aligned}$$

Energy is defined by $E = \rho\varepsilon + \frac{1}{2}\rho u^2$. Thus, we have:

$$(\rho\varepsilon)_i^{n+1} = (\rho\varepsilon)_i^n - \frac{\Delta t}{\Delta x} u_0 ((\rho\varepsilon)_{i+1/2} - (\rho\varepsilon)_{i-1/2})$$

Let us assume that the equation of state can be written under the form:

$$\rho\varepsilon = f(p) + b\rho + c \tag{1.13}$$

where b and c are real constants, and f a inversible function (for instance perfect gas EOS, Tammann EOS, ...). If we introduce this equation of state in the previous equation, it gives:

$$\begin{aligned} (f(p) + b\rho + c)_i^{n+1} &= (f(p) + b\rho + c)_i^n \\ &\quad - \frac{\Delta t}{\Delta x} u_0 ((f(p) + b\rho + c)_{i+1/2} - (f(p) + b\rho + c)_{i-1/2}) \\ f(p_i^{n+1}) + b\rho_i^{n+1} + c &= f(p_0) + b\rho_i^n + c \\ &\quad - \frac{\Delta t}{\Delta x} u_0 ((f(p_0) - f(p_0)) + b(\rho_{i+1/2} - \rho_{i-1/2}) + (c - c)) \\ f(p_i^{n+1}) &= f(p_0) \end{aligned}$$

Thus, $p_i^{n+1} = p_0$.

Hence, if a state law can be written under the form (1.13), then a VFRoe ncv scheme with variable (φ, u, p) maintains velocity and pressure constant.

Moreover, if the contact discontinuity is steady (ie $u_0 = 0$), we can remark that the VFRoe ncv (φ, u, p) scheme preserves pressure and velocity exactly constant, whatever the state law considered.

Bibliography

[Abg95] R. Abgrall. How to prevent pressure oscillations in multicomponent flow calculations: a quasi conservative approach. *J. Comp. Phys.*, 1995, vol. 125, pp. 150–160.

[BCHU01] C. Berthon, F. Coquel, J.M. Hérard, and M. Uhlmann. An approximate solution of the Riemann problem for a realizable second moment turbulent closure. accepted for publication in *Shock Waves*, 2001.

[BGH96] T. Buffard, T. Gallouët, and J.M. Hérard, *Schéma VFRoe en variables caractéristiques. Principe de base et applications aux gaz réels*, EDF-DER Report HE-41/96/041/A, 1996. In French.

[BGH98a] T. Buffard, T. Gallouët, and J.M. Hérard. A naive Godunov scheme to compute a non-conservative hyperbolic system. *Int. Series Num. Math.*, 1998, vol. 129, pp. 129–138.

[BGH98b] T. Buffard, T. Gallouët, and J.M. Hérard. A naive Godunov scheme to solve shallow-water equations. *C. R. Acad. Sci. Paris*, 1998, vol. I-326, pp. 885–890.

[BGH99] T. Buffard, T. Gallouët, and J.M. Hérard. An approximate Godunov scheme to compute turbulent real gas flow models. *AIAA paper 99-3349*, 1999.

[BGH00] T. Buffard, T. Gallouët, and J.M. Hérard. A sequel to a rough Godunov scheme. Application to real gas flows. *Computers and Fluids*, 2000, vol. 29-7, pp. 813–847.

[BHJU00] G. Brun, J.M. Hérard, D. Jeandel, and M. Uhlmann. An approximate Roe-type Riemann solver for a class of realizable second order closures. *Int. J. of Comp. Fluid Dyn.*, 2000, vol. 13-3, pp. 233–249.

[Bou98] M. Boucker, *Modélisation numérique multidimensionnelle d'écoulements diphasiques liquide–gaz en régimes transitoire et permanent : méthodes et applications*, Ph.D. thesis, École Normale Supérieure de Cachan, France, December 1998.

[Buf93] T. Buffard, *Analyse de quelques méthodes de volumes finis non structurés pour la résolution des équations d'Euler*, Ph.D. thesis, Université Paris VI, France, 1993.

[CH96] L. Combe and J.M. Hérard, *Principe du maximum pour un modèle diphasique gaz-solide à trois équations*, EDF-DER Report HE-41/96/045/A, 1996. In French.

[CH99] L. Combe and J.M. Hérard. Finite volume algorithm to compute dense compressible gas-solid flows. *AIAA journal*, 1999, vol. 37, pp. 337–345.

[Col92] J.F. Colombeau, *Multiplication of distributions*, Springer Verlag, 1992.

[CP98] F. Coquel and B. Perthame. Relaxation of energy and approximate Riemann solvers for general pressure laws in fluid dynamics equations. *SIAM J. Numer. Anal.*, 1998, vol. 35-6, pp. 2223–2249. In Memory of Ami Harten.

[DLM95] G. Dal Maso, P.G. LeFloch, and F. Murat. Definition and weak stability of non conservative products. *J. Math. Pures Appl.*, 1995, vol. 74, pp. 483–548.

[EGH00] R. Eymard, T. Gallouët, and R. Herbin, Finite Volume Methods, In *Handbook of Numerical Analysis* (Vol. VII), editors : P.G. Ciarlet and J.L. Lions, North-Holland, pp. 729–1020, 2000.

[EMRS91] B. Einfeldt, C.D. Munz, P.L. Roe, and B. Sjögreen. On Godunov-type methods near low densities. *J. Comp. Phys.*, 1991, vol. 92-2, pp. 273–295.

[FHL97] A. Forestier, J.M. Hérard, and X. Louis. A Godunov type solver to compute turbulent compressible flows. *C. R. Acad. Sci. Paris*, 1997, vol. I-324, pp. 919–926.

[GHK98] B. Gest, J.M. Hérard, and L. Kloetzer, *Validation d'un algorithme implicite volumes finis pour gaz réels*, EDF-DER Report HE-41/98/041/A, 1998. In French.

[GHS01] T. Gallouët, J.M. Hérard, and N. Seguin, *A hybrid scheme to compute contact discontinuities in Euler systems*, EDF-DRD Report HI-81/01/011/A, *submitted for publication*, 2001.

[GKL96] J.M. Ghidaglia, A. Kumbaro, and G. LeCoq. Une approche volume fini à flux caractéristiques pour la résolution numérique des systèmes hyperboliques de lois de conservation. *C. R. Acad. Sci. Paris*, 1996, vol. I-322, pp. 981–988.

[GM96] T. Gallouët and J.M. Masella. A rough Godunov scheme. *C. R. Acad. Sci. Paris*, 1996, vol. I-323, pp. 77–84.

[God59] S.K. Godunov. A difference method for numerical calculation of discontinuous equations of hydrodynamics. *Mat. Sb.*, 1959, pp. 271–300. In Russian.

[GR96] E. Godlewski and P.A. Raviart, *Numerical approximation of hyperbolic systems of conservation laws*, Springer Verlag, 1996.

[Hé95] J.M. Hérard, *Solveur de Riemann approché pour un système hyperbolique non conservatif issu de la turbulence compressible*, EDF-DER Report HE-41/95/009/A, 1995. In French.

[HFL94] J.M. Hérard, A. Forestier, and X. Louis, *A non strictly hyperbolic system to describe compressible turbulence*, EDF-DER Report HE-41/94/011/A, 1994.

[HH83] A. Harten and J.M. Hyman. A self-adjusting grid for the computation of weak solutions of hyperbolic conservation laws. *J. Comp. Phys.*, 1983, vol. 50, pp. 235–269.

[ICT98] M.J. Ivings, D.M. Causon, and E.F. Toro. On Riemann solvers for compressible flows. *Int. J. Num. Meth. Fluids*, 1998, vol. 28, pp. 395–418.

[In99a] A. In, *Méthodes numériques pour les équations de la dynamique des gaz complexes et écoulements diphasiques*, Ph.D. thesis, Université Paris VI, France, October 1999.

[In99b] A. In. Numerical evaluation of an energy relaxation method for inviscid real fluids. *SIAM J. Sci. Comp.*, 1999, vol. 21-1, pp. 340–365.

[KMJ] R. Kee, J. Miller, and T. Jefferson, *Chemkin: a general purpose, problem independant transportable fortran chemical kinetics code package*, SAND Report 80-8003, Sandia National Laboratories.

[Kum95] A. Kumbaro, *Schéma volume fini à flux caractéristiques - implémentation, tests et résultats numériques*, EDF-DER Report HT-30/95/017/A, 1995. In French.

[LeV97] R.J. LeVeque. Wave propagation algorithms for multidimensional hyperbolic systems. *J. Comp. Phys.*, 1997, vol. 131, pp. 327–353.

[LF93] A. Letellier and A. Forestier, *Le problème de Riemann en fluide quelconque*, CEA-DMT Report 93/451, 1993. In French.

[Mas97] J.M. Masella, *Quelques méthodes numériques pour les écoulements diphasiques bi-fluides en conduites pétrolières*, Ph.D. thesis, Université Paris VI, France, May 1997.

[MBL+99] S. Mimouni, M. Boucker, G. LeCoq, J.M. Ghidaglia, and al., *An overview of the VFFC-methods and tools for the simulation of two-phase flows*, EDF-DER Report HT-33/99/006/A, 1999.

[MFG99] J.M. Masella, I. Faille, and T. Gallouët. On an approximate Godunov scheme. *Int. J. of Comp. Fluid Dyn.*, 1999, vol. 12, pp. 133–149.

[RM95] P. Rascle and O. Morvant, *Interface utilisateur de Thetis - THErmodynamique en Tables d'InterpolationS*, EDF-DER Report HT-13/95021B, 1995. In French.

[Roe81] P.L. Roe. Approximate Riemann solvers, parameter vectors and difference schemes. *J. Comp. Phys.*, 1981, vol. 43, pp. 357–372.

[Rus61] V.V. Rusanov. Calculation of interaction of non-steady shock waves with obstacles. *J. Comp. Math. Phys. USSR*, 1961, vol. 1, pp. 267–279.

[SA99] R. Saurel and R. Abgrall. A simple method for compressible multifluid flows. *SIAM J. Sci. Comp.*, 1999, vol. 21-3, pp. 1115–1145.

[Sai95a] L. Sainsaulieu, *Contribution à la modélisation mathématique et numérique des écoulements diphasiques constitués d'un nuage de particules dans un écoulement de gaz*, Thèse d'habilitation, Université Paris VI, France, 1995.

[Sai95b] L. Sainsaulieu. Finite volume approximations of two phase-fluid flows based on approximate Roe-type Riemann solver. *J. Comp. Phys.*, 1995, vol. 121, pp. 1–28.

[Seg00] N. Seguin, *Comparaison numérique de schémas Volumes Finis pour les équations d'Euler en gaz parfaits et réels*, EDF-DRD Report HI-81/00/010/A, 2000, pp. 1–451. In French.

[TK96] I. Toumi and A. Kumbaro. An approximate linearized Riemann solver of a two-fluid model. *J. Comp. Phys.*, 1996, vol. 124, pp. 286–300.

[Tor91] E.F. Toro. A linearised Riemann solver for time-dependent Euler equations of gas dynamics. *Proc. R. Soc. Lond. A.*, 1991, vol. 434, pp. 683–693.

[Tor97] E.F. Toro, *Riemann solvers and numerical methods for fluid dynamics*, Springer Verlag, 1997.

[Van79] B. VanLeer. Toward the ultimate conservative difference scheme V. A second order sequel to Godunov's method. *J. Comp. Phys.*, 1979, vol. 32, pp. 101–136.

[Xeu99] E. Xeuxet, *Comparaison de solveurs numériques pour le traitement de la turbulence bifluide*, Ph.D. thesis, Université d'Evry, France, June 1999.

Chapitre 2

Un modèle simplifié pour la simulation d'écoulements diphasiques eau-huile en milieu poreux

On étudie ici un écoulement unidimensionnel eau-huile dans un milieu poreux hétérogène. On suppose que les deux phases sont immiscibles et incompressibles et que les effets capillaires sont négligés (mais on conserve les effets de la gravité). Le modèle se compose de deux lois de conservation de la masse (sans échange de masse à l'interface),

$$(\varphi u \rho_e)_t + (V_e)_x = 0, \tag{2.1}$$
$$(\varphi(1-u)\rho_h)_t + (V_h)_x = 0, \tag{2.2}$$

où φ est la porosité du milieu (elle ne dépend que de la variable espace et elle est comprise entre 0 et 1), ρ_e et ρ_h sont des constantes positives et représentent respectivement les densités de l'eau et de l'huile, V_e et V_h sont les vitesses de filtration de chacune des phases et u est la saturation de l'eau (ces trois dernières variables dépendent du temps et de l'espace). On ajoute les deux équations suivantes, issues de la loi de Darcy généralisée à un écoulement diphasique :

$$V_e + k f_e(u)(p_x - \rho_e g) = 0, \tag{2.3}$$
$$V_h + k f_h(u)(p_x - \rho_h g) = 0, \tag{2.4}$$

avec k (dépendant seulement de l'espace) la perméabilité du milieu, p la pression (qui dépend du temps et de l'espace) du mélange et f_e et f_h les mobilités de l'eau et de l'huile (ce sont en fait les rapports des perméabilités relatives des phases sur les viscosités des phases). Si on introduit (2.3) dans (2.1) et (2.4) dans (2.2), on obtient le système

$$(\varphi u)_t - (k f_e(u)(p_x - \rho_e g))_x = 0, \tag{2.5}$$
$$(\varphi(1-u))_t - (k f_h(u)(p_x - \rho_h g))_x = 0. \tag{2.6}$$

En additionnant les équations (2.5) et (2.6), on peut en déduire l'équation

$$\Big(-k(f_e(u)+f_h(u))p_x+(kf_e(u)\rho_e+kf_h(u)\rho_h)g\Big)_x=0$$

que l'on intègre :

$$-k(f_e(u)+f_h(u))p_x+(kf_e(u)\rho_e+kf_h(u)\rho_h)g=\alpha$$

où α est une fonction qui ne dépend que du temps (elle correspond au débit volumique total). On peut ainsi écrire que

$$p_x=\frac{-\alpha+(kf_e(u)\rho_e+kf_h(u)\rho_h)g}{k(f_e(u)+f_h(u))}$$

et en soustrayant $\rho_e g$, on a

$$p_x-\rho_e g=\frac{-\alpha}{k(f_e(u)+f_h(u))}+\frac{kf_h(u)(\rho_h-\rho_e)g}{k(f_e(u)+f_h(u))}.$$

En injectant cette équation dans (2.5), on aboutit finalement à l'équation sur la saturation de l'eau u suivante (u est l'inconnue) :

$$(\varphi u)_t+f(t,x,u)_x=0 \quad \text{où} \quad f(t,x,u)=\frac{f_e(u)(-\alpha(t)+k(x)f_h(u)(\rho_h-\rho_e)g)}{f_e(u)+f_h(u)}. \tag{2.7}$$

Si $\rho_e=\rho_h$, on peut retrouver à partir de cette équation l'équation de Buckley-Leverett. La fonction f_e est croissante régulière et vérifie $f_e(0)=0$ et la fonction f_h est décroissante régulière et vérifie $f_h(1)=0$.

Pour simplifier, on prendra $\varphi\equiv 1$, $f_e(s)=s$ et $f_h(s)=1-s$ ainsi que $\alpha=0$, $g=1$ et $\rho_h-\rho_e=1$ (le cas $\alpha=1$ et $\rho_e=\rho_h$ étant connu). On obtient donc l'équation scalaire

$$u_t+(ku(1-u))_x=0$$

à laquelle on adjoint la perméabilité

$$k(x)=\begin{cases}k_L & \text{si } x<0,\\ k_R & \text{si } x>0,\end{cases}$$

avec k_L et k_R positifs et non égaux. Toute la difficulté est située à l'interface $x=0$. Ce type d'équations conservatives avec un coefficient discontinu a déjà été étudié par plusieurs auteurs [KR99], [KR95], [LTW95a], [Tem82], ... On peut remarquer que cette équation peut être réécrite comme un système :

$$k_t=0, \qquad u_t+(ku(1-u))_x=0.$$

Cette écriture permet de mettre en évidence le caractère « résonnant » de ce problème, c'est-à-dire que les deux valeurs propres de ce système, 0 et $k(1-2u)$, peuvent s'identifier et la matrice jacobienne du flux n'est plus diagonalisable dans $\mathbb{R}$. Ce modèle est donc un bon candidat pour la compréhension des problèmes hyperboliques dont les ondes ne sont pas ordonnées et peuvent se superposer, comme les systèmes étudiés dans les chapitres 3 et 4. En effet, le système des équations de Saint-Venant avec terme source de topographie comporte lui aussi un terme géométrique (le

gradient de la topographie, qui dépend de la variable d'espace) que l'on suppose discontinu en $x = 0$ lors de l'étude du problème de Riemann associé. Néanmoins, ce système n'est pas conservatif (à cause du terme source) et le problème des fermetures des relations de saut peut se poser. Concernant le système bifluide à deux pressions du chapitre 4 (avec les fermetures *ad hoc*), on peut retrouver le même type de problématique bien qu'il n'y ait pas de terme géométrique dans le système convectif. Dans ce cas, c'est la fraction volumique qui va jouer le rôle du terme géométrique et le caractère « résonnant » ne se situe plus à l'interface $x = 0$ mais au niveau de la discontinuité de contact qui transporte la fraction volumique. Il paraît donc nécessaire de comprendre au mieux cette équation scalaire pour pouvoir, d'une part, justifier différents travaux existants pour les équations de Saint-Venant avec topographie [LeR99] et [Seg99] et, d'autre part, étendre cette analyse au système du chapitre 4.

On montre ici que le problème de Cauchy associé (avec une donnée initiale u_0 dans $L^\infty(\mathbb{R})$) admet une unique solution faible entropique (dans un sens précisé par la suite). On remarque que l'analyse s'appuie sur une condition (déjà évoquée dans [KR95] et [Tow00] par exemple) de type condition entropique au niveau de l'interface $x = 0$ correspondant à la discontinuité de la perméabilité k. Cette condition est obtenue en raccordant k_L et k_R par une chemin monotone régulier k_ε sur $-\varepsilon \leq x \leq \varepsilon$. Il faut noter que si on considère l'équation scalaire comme un système 2×2, l'interface $x = 0$ correspond à un champ linéairement dégénéré. Or, dans le cadre classique des systèmes de lois de conservation, les champs linéairement dégénérés ne nécessitent pas de condition entropique. En fait, la condition entropique obtenue ici s'explique par la présence d'un choc superposé à l'interface $x = 0$ que l'on peut mettre en évidence en étudiant les solutions stationnaires admissibles (au sens des chocs entropiques) pour le problème régularisé dans l'intervalle $[-\varepsilon; \varepsilon]$. Cette approche peut être étendue aux systèmes résonnants, elle rejoint (et justifie) l'étude initiée dans [LeR99] et [Seg99] pour les équations de Saint-Venant avec un terme source de topographie.

Dans une seconde partie, on étudie numériquement quatre schémas Volumes Finis. Deux schémas sont issus de l'industrie, utilisant une moyenne harmonique du flux $ku(1-u)$. Ensuite, en suivant les idées développées dans [LTW95a] et [LTW95b] et dans [GL96] pour les lois de conservation avec terme source, on introduit le schéma de Godunov et le schéma de Godunov approché VFRoe-ncv qui se basent sur l'écriture en système 2×2 (ces deux schémas sont dits « équilibres » [GL96]). Les résultats obtenus par ces deux derniers schémas sont nettement plus précis que ceux des deux schémas industriels (mais les vitesses de convergence restent identiques). Il est intéressant de remarquer que même pour les simulations où le phénomène de résonnance apparaît, le schéma VFRoe-ncv se comporte aussi bien que le schéma de Godunov, bien que les solutions de la linéarisation locale effectuée pour le schéma VFRoe-ncv n'incluent pas le concept de résonnance. On propose de plus une technique de montée en ordre, qui n'est en fait qu'une modification de la technique des limiteurs de pentes [Van79] où la reconstruction prend en compte la forme de solutions stationnaires de l'équation scalaire. Différents tests de convergence en maillage et en temps témoignent de l'apport en précision et en vitesse de convergence dû à cette technique. Cette technique a été aussi appliquée dans le cadre des équations de Saint-Venant avec terme source (chapitre 3), où la convergence des méthodes vers des états permanents est une problématique importante.

Analysis and approximation of a scalar conservation law with a flux function with discontinuous coefficients

Co-authored with Julien Vovelle.

Abstract

We study here a model of conservative nonlinear conservation law with a flux function with discontinuous coefficients, namely the equation $u_t + (k(x)u(1-u))_x = 0$. It is a particular entropy condition on the line of discontinuity of the coefficient k which ensures the uniqueness of the entropy solution. This condition is discussed and justified. On the other hand, we perform a numerical analysis of the problem. Two Finite Volume schemes, the Godunov scheme and the VFRoe-ncv scheme, are proposed to simulate the conservation law. They are compared with two Finite Volume methods classically used in an industrial context. Several tests confirm the good behavior of both new schemes, especially through the discontinuity of permeability k (whereas a loss of accuracy may be detected when industrial methods are performed). Moreover, a modified MUSCL method which accounts for stationary states is introduced.

2.1 Introduction

Consider the Cauchy Problem associated with the following conservation law with discontinuous coefficient:

$$\begin{cases} \dfrac{\partial u}{\partial t} + \dfrac{\partial}{\partial x}\big(k(x)u(1-u)\big) = 0 \qquad x \in \mathbb{R},\, t \in \mathbb{R}_+\,, \\ u(0,x) = u_0(x)\,, \\ k(x) = \begin{cases} k_L & \text{if } x < 0 \\ k_R & \text{if } x > 0\,, \end{cases} \end{cases} \tag{2.8}$$

with k_L, $k_R > 0$ and $k_L \neq k_R$.

À paraître dans *Mathematical Models and Methods in Applied Sciences*, volume 5, numéro 13, 2003.

This problem can be seen as a model for the governing equation of the saturation of a fluid in a gravity field flowing in a one dimensional porous media with discontinuous permeability k. It is also one of the simplest example of resonant system [IT86], [IT90]: indeed, it can be written as the system

$$u_t + (kg(u))_x = 0\,, \quad k_t = 0 \tag{2.9}$$

whose eigenvalues 0 and $kg'(u)$ can intersect each other if the function g' vanishes for a certain value of u. Resonant systems, including systems as the system (2.9) have been studied by several authors. We refer to [Tem82], [LTW95a], [KR99], [KR95] and references therein.

One of the main difficulty in the analysis of Problem (2.8) is the correct definition of a solution. Let us briefly justify this assertion: consider the Cauchy problem

$$u_t + (f(x,u))_x = 0 \quad (t>0\,,\ x\in\mathbb{R}) \qquad u(0,x) = u_0(x) \quad (x\in\mathbb{R})\,. \tag{2.10}$$

Suppose that the function f is not continuous with respect to x. Actually, suppose that

$$f(x,u) = \begin{cases} -u & \text{if } x<0 \\ u & \text{if } x>0\,. \end{cases}$$

An easy computation (thanks to the method of the characteristics) ensures that the solution u of Problem (2.10) is known in the domain $\{|x|>t\}$ but is not determined at all in the domain $\{|x|<t\}$. Otherwise speaking, the problem (2.10) cannot be well-posed for every function f ! In the case where the flux writes $f(x,u)=k(x)g(u)$ (k being discontinuous) and when the function g is convex (or concave) some definitions of solutions have been proposed. First, in [KR95], Klingenberg and Risebro define a weak solution which is shown to be unique and stable [KR99] under a wave entropy condition. Secondly, in [Tow00], Towers define a notion of entropy solution and prove the uniqueness of piecewise smooth entropy solutions. The definition of Towers (see Definition 2.1) is a global definition (in the sense that the entropy conditions are enclosed in the weak formulation and not required as local conditions) and, therefore, adapted to the study of the convergence of approximations to Problem (2.8). In this article [Tow00] is given the "entropy condition" on the line of discontinuity of the function k (see Eq. (2.20)) which, actually, plays a central role in the study of the well-posedness of Problem (2.8). A justification for this condition is given here (see Section 2.3).

Assuming that the function $g : u \mapsto u(1-u)$ is concave and, therefore, has only one global maximum, is not insignificant. The study of Problem (2.8) or (2.9) in the case where the function g has more than one local extremum remains difficult. Some steps forward have been made by Klingenberg, Risebro and Towers in particular [KR01], [Tow01]. Nevertheless, one of the stake in the study of Problem (2.8) in the case where the function g has more than one global optimum, probably remains the design of a global definition of entropy solution.

The understanding of the Riemann Problem is one of the basis of all the theory of one-dimensional systems of conservation laws. It is also a useful tool to make the problem (2.8) more intelligible (the question of uniqueness of a solution in particular) while it is necessary to define properly the Godunov scheme. The Riemann Problem for resonant systems has been studied, near a hyperbolic singularity, by Isaacson, Marchesin, Plohr and Temple [IMPT88], [IT88]. The Riemann Problem for scalar conservation laws as (2.8) has been completely solved by Gimse and Risebro [GR91],

[Die95]. In Appendix 2.A we present a new way to visualize the solution of the Riemann Problem (see Fig. 2.9 and 2.10).

Different approximations of Problem (2.8) have been studied. In [KR95], Klingenberg and Risebro prove the convergence of the front-tracking method applied to (2.8) to the weak solution defined in [KR95]. The first result of convergence of a numerical scheme has been established by Temple [Tem82] who proves the convergence of the Glimm Scheme associated to Problem (2.9). In [LTW95a] and [LTW95b], Lin, Temple and Wang prove the convergence to a weak solution of the Godunov method applied to Problem (2.9). Some Finite Volume schemes associated to Problem (2.8) have also been studied by Towers. In [Tow00], the author proves the convergence of the Godunov scheme and the Engquist-Osher scheme, by considering a discretization of k staggered with respect to that of u. Here, we study the qualitative behavior of the Godunov scheme (with a discretization of k superimposed on that of u), of an approximate Godunov scheme and show that they behave much better than two schemes classically implemented in industrial codes. Notice that this study is close to some works that have been performed to investigate the behavior of the Finite Volume method applied to (systems of) conservation laws with source terms by J.M. Greenberg and A.Y. LeRoux [GL96], or Gallouët, Hérard, Seguin [GHS03].

A somewhat related subject is the study of a transport equation with a discontinuous coefficient [BJ98]. Also notice that, forgetting the conservative form of Eq. (2.8), this latter can be rewritten

$$\frac{\partial u}{\partial t} + k(x)\frac{\partial}{\partial x}\big(u(1-u)\big) = -(k_R - k_L)\delta_0(x)\, u(1-u).$$

This underlines its relation with the study of the behavior, as $\varepsilon \to 0$, of the solution u_ε of the problem

$$\frac{\partial u_\varepsilon}{\partial t} + \frac{\partial}{\partial x} A(u_\varepsilon) + z_\varepsilon(x) B(u_\varepsilon) = 0\,,$$

where $z_\varepsilon \to \delta_0$, performed by A. Vasseur [Vas02].

Besides, degenerate parabolic equations of the kind $u_t + (k(x)g(u))_x - A(u)_{xx} = 0$, where the coefficient k is discontinuous have been studied by Karlsen, Risebro and Towers (see [KRT01] and references therein).

Eventually, Godlewski and Raviart recently provide a study of the consistence and the numerical approximation of Problem (2.8) when a condition of continuity is set on the variable u [GR02]. Notice that it is a point of view different from the point of view of Karlsen, Klingenberg, Risebro, Towers and us: we impose a condition of continuity of the flux, $kg(u)$, at the interface $\{x = 0\}$.

This paper is organized as follows. In Section 2.2, we give an overview of the notion of entropy solution to Problem (2.8) as defined by Towers and prove that uniqueness holds for general L^∞ solutions. In Section 2.3, we discuss the entropy condition (2.20). Then, we present several Finite Volume schemes (Section 2.4), which may be seen as the adaptation to space-dependent flux of the well balanced scheme [GL96] (initially designed for conservation laws with source terms). The first one is called the Godunov scheme, since it is based on the exact solution of the Riemann problem associated with the conservation law. This Riemann problem may be linearized to simplify its resolution, which leads to the second scheme studied here, namely the VFRoe-ncv scheme. Moreover, two other schemes are introduced, which are derivated from methods classically used in the industrial context. Furthermore, a higher order method based on the MUSCL formalism is

described. Indeed, stationary solutions are no longer uniform states, because the permeability k is not constant. Hence, in the implementation of the slope limiters, the characterization of stationary states has to be taken into account . The higher order method may then be implemented to simulate the convergence in time towards stationary solutions.

In Section 2.5, several numerical tests are given. First, some solutions of Riemann problems are computed to compare the four "first order" schemes. Afterwards, quantitative results are shown. Measurements of rates of convergence when the mesh is refined are presented, with or without MUSCL reconstruction. Convergence in time towards stationary states is performed too.

Finally, a new visualization of the Riemann problem, additional tests to illustrate the resonance phenomenon and some BV estimates are available in appendix.

2.2 Entropy solution

In the case where the function k is regular, the accurate notion of solution to the problem (2.8), namely the one which ensures existence and uniqueness, is the notion of entropy solution. Here, also, a notion of entropy solution can be defined. According to Towers [Tow00], we have

Definition 2.1. Let $u_0 \in L^\infty(\mathbb{R})$, with $0 \leq u_0 \leq 1$ a.e. on $\mathbb{R}$. A function u of $L^\infty(\mathbb{R}_+ \times \mathbb{R})$ is said to be an entropy solution of the problem (2.8) if it satisfies the following entropy inequalities: for all $\kappa \in [\,0,1]$, for all non-negative function $\varphi \in \mathcal{C}_c^\infty(\mathbb{R}_+ \times \mathbb{R})$,

$$\begin{aligned} &\int_0^\infty\!\!\int_{\mathbb{R}} |u(t,x)-\kappa|\,\varphi_t(t,x) + k(x)\,\Phi(u(t,x),\kappa)\,\varphi_x(t,x)\,dx\,dt \\ &+ \int_{\mathbb{R}} |u_0(x)-\kappa|\,\varphi(0,x)\,dx + |k_L-k_R| \int_0^\infty g(\kappa)\,\varphi(t,0)\,dt \;\geq 0\,, \end{aligned} \tag{2.11}$$

where Φ denotes the entropy flux associated with the Kruzkov entropy,

$$\Phi(u,\kappa) = \operatorname{sgn}(u-\kappa)(g(u)-g(\kappa))\,,$$

with

$$g(u) = u(1-u)$$

and

$$\operatorname{sgn}(a) = \begin{cases} +1 & \text{if } a > 0 \\ 0 & \text{if } a = 0 \\ -1 & \text{if } a < 0 \end{cases}.$$

Remark 2.1. *This definition can be adapted in the case where the function k has finitely many jumps. It would be interesting to study the case where, more generally, the function k has a bounded total variation. However, we restricted our study to the case where the function k has one jump, keeping in view that this framework is rich enough to point out the different phenomena that occur in the numerical analysis of such problems.*

Remark 2.2. *Notice that this definition is pertinent only if the flux function g is concave (or convex). To our knowledge, no definition of solution to Problem (2.8) of this type has been given in the case where the flux g has two or more local maxima; however, the resolution of the Riemann Problem, the convergence of the front-tracking method and of the smoothing method to the same solution has been proved in [KR01] while the convergence of an Engquist-Osher scheme to a weak solution has been proved by Towers in [Tow01].*

Actually, the flux function $u \mapsto u(1-u)$ being considered, existence and uniqueness hold for an entropy solution as defined in Def.2.1. More precisely, the following theorem can be proved.

Theorem 2.1. *Suppose that $u_0 : \mathbb{R} \to \mathbb{R}$ is a measurable function such that $0 \leq u_0 \leq 1$ a.e. on $\mathbb{R}$. Then there exists a unique entropy solution u of the problem (2.8) in $L^\infty((0,T)\times\mathbb{R})$. The solution u satisfies $0 \leq u \leq 1$ a.e. on $(0,T)\times\mathbb{R}$. Besides, if the function $v \in L^\infty((0,T)\times\mathbb{R})$ is an other entropy solution of the Problem (2.8) with initial condition $v_0 \in L^\infty(\mathbb{R},[0,1])$ then, for every R, $T > 0$, the following result of comparison holds true*

$$\int_0^T \int_{(-R,R)} |u(t,x) - v(t,x)|\, dx\, dt \leq T \int_{(-R-KT,R+KT)} |u_0(x) - v_0(x)|\, dx \tag{2.12}$$

where $K = \max\{k_L, k_R\}$.

A natural way to get the existence of an entropy solution to Problem (2.8) is to check the consistence of Def.2.1 with the usual definition of an entropy solution given in the case where the function k is regular [Vol67], [Kru70]: let $(k_\varepsilon)_\varepsilon$ be a sequence of approximation of the function k such that: $\forall \varepsilon > 0$, the function k_ε is a regular function, it is monotone non-decreasing or non-increasing, according to the sign of $k_R - k_L$ and it verifies

$$\begin{cases} k_\varepsilon(x) = k_L & \text{if } x \leq -\varepsilon\,, \\ k_\varepsilon(x) = k_R & \text{if } \varepsilon \leq x\,. \end{cases}$$

For any initial condition $u_0 \in L^\infty(\mathbb{R}\,;[0,1])$ there exists a unique entropy solution u_ε of the problem (2.13):

$$\begin{cases} \dfrac{\partial u}{\partial t} + \dfrac{\partial}{\partial x}\big(k_\varepsilon(x) g(u)\big) = 0 \qquad x \in \mathbb{R},\, t \in \mathbb{R}_+\,, \\ u(0,x) = u_0(x)\,, \end{cases} \tag{2.13}$$

which satisfies (2.14) and $0 \leq u_\varepsilon \leq 1$ a.e. Moreover, the sequence (u_ε) converges in $L^1_{\text{loc}}([\,0,T]\times\mathbb{R})$ to a function $u \in L^\infty([\,0,T]\times\mathbb{R},[0,1])$. To begin with, this result can be proved up to a subsequence, and when the initial condition additionally satisfies $u_0 \in BV(\mathbb{R})$. The compactness of the sequence (u_ε) is deduced from the following list of arguments. First, for every $\kappa \in [0,1]$, the distribution

$$|u_\varepsilon - \kappa|_t + (k_\varepsilon\, \Phi(u_\varepsilon,\kappa))_x + k'_\varepsilon(x) g(\kappa) \mathrm{sgn}(u_\varepsilon - \kappa)$$

is non-positive and, therefore, is a bounded measure. The distribution $|u_\varepsilon - \kappa|_t$ and the distribution $k'_\varepsilon(x) g(\kappa)\mathrm{sgn}(u_\varepsilon - \kappa)$ are also bounded measures because, respectively, the distribution $\partial_t u_\varepsilon$ is a bounded measure (since $u_0 \in BV(\mathbb{R})$) and $TV(k_\varepsilon) \leq |k_R - k_L|$. Eventually, and consequently, the distribution $(k_\varepsilon\, \Phi(u_\varepsilon,\kappa))_x$ is also a bounded measure. From these facts, one can deduce that the

function $\Phi(u_\varepsilon,\kappa)$ is BV with a BV-norm uniformly bounded with respect to ε (a rigorous proof of this estimate is given in Appendix 2.C). Notice that this estimate on $\Phi(u_\varepsilon,\kappa)$ remains true even when the function g has more than one local maximum. Now, Helly's Theorem [Giu84] ensures that a subsequence of $(\Phi(u_\varepsilon,\kappa))$ is converging in $L^1_{\rm loc}([\,0,T]\times\mathbb{R})$. The convergence of a subsequence of (u_ε) is deduced from the dominated convergence theorem and from the fact that the function $\Phi(\cdot,1/2)$ is an invertible function with a continuous inverse. Thus, the function $\Phi(\cdot,1/2)$ plays the role of a Temple function [Tem82]. These tools are those used by Towers in [Tow00] to prove the convergence of a Godunov scheme to the entropy solution of Problem (2.8). In [Tow01], the same author studies the convergence of an Engquist-Osher scheme associated to the problem (2.9) in the case where the flux-function g is not necessarily convex and introduces a new Temple function, also in order to get compactness on the sequence of numerical approximations.

These estimates *via* the use of a Temple function play a central role; then, the fact that every limit u of a subsequence of (u_ε) is an entropy solution to Problem (2.8) is quite natural in view of Definition 2.1. Indeed, let $\kappa\in[\,0,1]$ and φ be a non-negative function of $\mathcal{C}^\infty_c(\mathbb{R}_+\times\mathbb{R})$. Suppose that T is such that $\varphi(t,x)=0$ for every $(t,x)\in[\,T,+\infty)\times\mathbb{R}$. For every $\varepsilon>0$, the function u_ε satisfies the following entropy inequality:

$$\begin{array}{l}\displaystyle\int_0^\infty\!\!\int_{\mathbb{R}} |u_\varepsilon(t,x)-\kappa|\,\varphi_t(t,x)+k(x)\,\Phi(u_\varepsilon(t,x),\kappa)\,\varphi_x(t,x)\,dx\,dt\\ \displaystyle+\int_{\mathbb{R}}|u_0(x)-\kappa|\,\varphi(0,x)\,dx-\int_0^\infty\!\!\int_{\mathbb{R}} k'_\varepsilon(x)\,\mathrm{sgn}(u_\varepsilon(t,x)-\kappa)\,g(\kappa)\,\varphi(t,x)\,dx\,dt\ \geq 0\,,\end{array}\tag{2.14}$$

As u_ε converges to u in $L^1_{\rm loc}([\,0,T]\times\mathbb{R})$, the first term of Ineq. (2.14) converges to the first term of Ineq. (2.11) when $\varepsilon\to 0$ so that one has to focus on the study of the last term. The estimate $|\mathrm{sgn}(u_\varepsilon-\kappa)|\leq 1$ yields $\int_0^\infty\!\!\int_{\mathbb{R}} k'_\varepsilon(x)\,\mathrm{sgn}(u_\varepsilon-\kappa)\,g(\kappa)\,\varphi\,dx\,dt\ \leq\ I_\varepsilon$ where $I_\varepsilon=\int_0^\infty\!\!\int_{\mathbb{R}}|k'_\varepsilon(x)|\;g(\kappa)\,\varphi\,dx\,dt$. To conclude, one uses the fact that the monotony of the function k_ε is set by the sign of k_L-k_R and several integrations by parts to get

$$\begin{array}{rcl} I_\varepsilon &=& \mathrm{sgn}(k_R-k_L)\displaystyle\int_0^\infty\!\!\int_{\mathbb{R}} k'_\varepsilon(x)\,g(\kappa)\,\varphi\,dx\,dt\\ &=& -\mathrm{sgn}(k_R-k_L)\displaystyle\int_0^\infty\!\!\int_{\mathbb{R}} k_\varepsilon(x)\,g(\kappa)\,\partial_x\varphi\,dx\,dt\\ &\to& -\mathrm{sgn}(k_R-k_L)\displaystyle\int_0^\infty\!\!\int_{\mathbb{R}} k(x)\,g(\kappa)\,\partial_x\varphi\,dx\,dt\\ &=& \mathrm{sgn}(k_R-k_L)\,(k_R-k_L)\displaystyle\int_0^\infty g(\kappa)\,\varphi(t,0)\,dt\\ &=& |k_R-k_L|\displaystyle\int_0^\infty g(\kappa)\,\varphi(t,0)\,dt\,.\end{array}$$

To sum up, when the initial condition satisfies $u_0\in BV(\mathbb{R})$, the sequence (u_ε) is compact in $L^1_{\rm loc}([\,0,T]\times\mathbb{R})$ and has at least one adherence value u, which is an entropy solution of Problem (2.8). It is the result of comparison exposed in Theorem 2.1 which ensures that the whole sequence $(u_\varepsilon)_\varepsilon$ converges to u. Notice that this result of comparison (2.12) also yields the existence of an entropy solution of the Problem (2.8) when the initial condition is merely a function of $L^\infty(\mathbb{R}\,;[0,1])$. Indeed, suppose $u_0\in L^\infty(\mathbb{R}\,;[0,1])$ and set

$$u_0^\alpha=\rho_\alpha\star(\chi_{(-1/\alpha,1:/\alpha)}u_0)$$

where (ρ_α) is a classical sequence of mollifiers. Then $u_0^\alpha \in L^\infty(\mathbb{R}\,;[0,1]) \cap BV(\mathbb{R})$ and $\lim_{\alpha\to 0} u_0^\alpha = u_0$ in $L^1_{loc}(\mathbb{R})$. Therefore, if u^α denotes the corresponding entropy solution, then the sequence (u^α) is a Cauchy sequence in $L^1_{\rm loc}(\mathbb{R}_+ \times \mathbb{R})$ since the comparison

$$\int_0^T\!\!\int_{(-R,R)} |u^\alpha(t,x) - u^{\alpha'}(t,x)|\,dx\,dt \;\le T \int_{(-R-KT,R+KT)} |u_0^\alpha(x) - u_0^{\alpha'}(x)|\,dx$$

holds for every R, $T>0$. Consequently, this sequence (u^α) is convergent, and denoting by u its limit in $L^1_{loc}(\mathbb{R}_+ \times \mathbb{R})$, the function u is an entropy solution of the Problem (2.8).

Thus, the result of comparison (2.12) not only entails uniqueness or continuous dependence on the data, but is also a key point to show the existence of an entropy solution in the general framework of L^∞ functions. How to prove it ?

The classical proof of uniqueness of Kruzkov [Kru70] applies without changes to prove that, if u and v are two entropy solutions of Problem (2.8), if φ is a non-negative function of $\mathcal{C}^\infty_c([\,0,T)\times\mathbb{R})$ *which vanishes in a neighborhood of the line* $\{x=0\}$ *of discontinuity of the function* k, then the following inequation holds true

$$\int_0^\infty\!\!\int_{\mathbb{R}} |u(t,x)-v(t,x)|\varphi_t(t,x) + k(x)\Phi(u(t,x),v(t,x))\varphi_x(t,x)\,dx\,dt \\ + \int_{\mathbb{R}} |u_0(x)-v_0(x)|\,\varphi(0,x)\,dx \ge 0\,. \quad (2.15)$$

In order to remove this additional hypothesis on the test function φ, a particular entropy condition on the line of discontinuity of the function k will be used. Consider any non-negative function ψ of $\mathcal{C}^\infty_c([\,0,T)\times\mathbb{R})$ and, for $\varepsilon>0$, set $\varphi(t,x) = \psi(t,x)\,(1-\omega_\varepsilon(x))$ in Ineq. (2.15), the cut-off function ω_ε being defined by

$$\omega_\varepsilon(x) = \begin{cases} 0 & \text{if } 2\varepsilon < |x| \\ \frac{-|x|+2\varepsilon}{\varepsilon} & \text{if } \varepsilon \le |x| \le 2\varepsilon \\ 1 & \text{if } |x| < \varepsilon \end{cases}.$$

Passing to the limit $\varepsilon \to 0$ in the inequality obtained in this way, one gets

$$\int_0^\infty\!\!\int_{\mathbb{R}} |u-v|\psi_t + k(x)\Phi(u,v)\psi_x\,dx\,dt \;+ \int_{\mathbb{R}} |u_0-v_0|\,\psi(0)\,dx - J \ge 0\,, \quad (2.16)$$

where

$$J = \lim_{\varepsilon\to 0} \int_0^\infty\!\!\int_{\mathbb{R}} k(x)\Phi(u,v)\psi\,\omega_\varepsilon'(x)\,dx\,dt\,.$$

The last term J of Ineq. (2.16) will turn to be non-negative (so that Ineq. (2.15) will turn to be indeed right for any non-negative function $\varphi \in \mathcal{C}^\infty_c([\,0,T)\times\mathbb{R})$). In order to estimate this term J, one uses the result of existence of strong traces for solutions of non-degenerate conservation laws by Vasseur [Vas01]. In this article [Vas01] is proved that, given a conservation law

$$u_t + (A(u))_x = 0\,,$$

set on a domain $\Omega \subset \mathbb{R}_+ \times \mathbb{R}^d$ with a flux satisfying: for all $(\tau,\zeta) \in \mathbb{R}_+ \times \mathbb{R}^d \setminus \{(0,0)\}$, the measure of the set $\{\xi\,;\ \tau + \zeta\cdot A(\xi) = 0\}$ is zero, then the entropy solution u has strong traces on $\partial\Omega$. Applying

this result to Problem (2.8) on the sets $\Omega^- = (0,+\infty)\times(-\infty,0)$ and $\Omega^+ = (0,+\infty)\times(0,+\infty)$ respectively, we get:

Lemma 2.1. *Let $u \in L^\infty(\mathbb{R}_+\times\mathbb{R})$ be an entropy solution to the problem (2.8) with initial condition $u_0 \in L^\infty(\mathbb{R})$, $0 \le u_0 \le 1$ a.e. Then the function u admits strong traces on the line $\{x=0\}$, that is: there exists some functions γu^- and γu^+ in $L^\infty(0,+\infty)$ such that, for every compact K of $(0,+\infty)$,*

$$\operatorname*{ess\,lim}_{s\to 0^\pm} \int_K \left| u(t,s) - \gamma u^\pm \right| \, dt = 0\,. \tag{2.17}$$

Coming back to the definition of the cut-off function ω_ε, one gets

$$J = \int_0^\infty \left(k_L\, \Phi(\gamma u^-(t), \gamma v^-(t)) - k_R\, \Phi(\gamma u^+(t), \gamma v^+(t)) \right) \psi(t,0)\, dt\,.$$

As already said, the sign of J is actually determined, considering that a Rankine-Hugoniot relation and an entropy inequality occur on the line of discontinuity of the function k (see Eq.(2.19) and (2.20)). As usual, the Rankine-Hugoniot relation is derived from the weak formulation of Problem (2.8) (every entropy solution is a weak solution) whereas the entropy condition is a consequence of the entropy inequality (2.11) set with the parameter κ equal to the point where the function g reaches its maximum, that is $\kappa = 1/2$ here. Precisely: set $\varphi := \varphi\omega_\varepsilon$ in Ineq. (2.11) and pass to the limit $\varepsilon \to 0$ in the inequality obtained in this way. Using Lemma 2.1 again, this yields the inequality

$$\int_0^\infty \left(k_L\, \Phi(\gamma u^-(t), \kappa) - k_R\, \Phi(\gamma u^+(t), \kappa) \right) \varphi(t,0)\, dt + |k_L - k_R| \int_0^\infty g(\kappa)\varphi(0,t) \ge 0$$

for every $\kappa \in [0,1]$, or, still:

$$\forall \kappa \in [0,1]\,, \text{ for a.e. } t > 0\,,\ k_L\, \Phi(\gamma u^-(t), \kappa) - k_R\, \Phi(\gamma u^+(t), \kappa) + |k_L - k_R| g(\kappa) \ge 0\,. \tag{2.18}$$

By choosing successively $\kappa = 0$ and $\kappa = 1$ in Ineq. (2.18), one derives the Rankine-Hugoniot relation

$$k_L\, g(\gamma u^-) = k_R\, g(\gamma u^+)\,. \tag{2.19}$$

By choosing $\kappa = 1/2$ in Ineq. (2.18), one derives the following "entropy condition": denote by a the derivative of the function g, then for a.e. $t > 0$,

$$a(\gamma u^+(t)) > 0 \Rightarrow a(\gamma u^-(t)) \ge 0\,. \tag{2.20}$$

(We refer to [Tow00] for the rigorous proof of this result). This condition (2.20) can be seen as a limit of entropy conditions (*cf.* Section 2.3). This justifies the denomination which it has been given. As the study of the Riemann Problem suggests it, this condition has to be specified in order to distinguish between several potential solutions. For example, if the initial condition u_0 is defined by

$$u_0(x) = \begin{cases} 0 & \text{if } x < 0\,, \\ 1 & \text{if } x > 0\,, \end{cases}$$

then the stationary function $u(t,x) = u_0(x)$ seems to be an acceptable solution of Problem (2.8): it is an entropy solution apart from the line of discontinuity of k while it satisfies the Rankine-Hugoniot relation (2.19) on this line. Nevertheless, it is not the admissible solution to Problem (2.8) (see Appendix 2.A for the description of this latter). Technically, the discussion of the respective positions of γu^-, γu^+, γv^- and γv^+, combined with the use of Eq. (2.19) and (2.20) allows to prove that $J \geq 0$ (see the proof of Theorem 4.6 in [Tow00]). It is then classical to conclude to (2.12).

2.3 Derivation of the entropy condition (2.20)

Suppose that $u \in L^\infty \cap BV((0,T) \times \mathbb{R})$ is a solution of the problem (2.8), in accordance with a definition that we would like to determine. It is rather natural to suppose that the function u is, at least, a weak solution, that is to say satisfies:

$$\int_0^\infty \int_{\mathbb{R}} u\, \varphi_t + k(x)\, g(u)\, \varphi_x = 0 \tag{2.21}$$

for all $\varphi \in \mathcal{C}_c^\infty(]\,0, +\infty[\times\mathbb{R})$. We also suppose that the function u is a "classical" entropy solution outside the line $\{x = 0\}$, which means that for all $\kappa \in \mathbb{R}$, for all non-negative function $\varphi \in \mathcal{C}_c^\infty(]\,0, +\infty[\times\mathbb{R})$ such that $\varphi(t,0) = 0$, $\forall t \in [0,T]$,

$$\int_0^\infty \int_{\mathbb{R}} |u(t,x) - \kappa|\, \varphi_t(t,x) + k(x)\, \Phi(u(t,x),\kappa)\, \varphi_x(t,x)\, dx\, dt \\ + \int_{\mathbb{R}} |u_0(x) - \kappa|\, \varphi(0,x)\, dx \geq 0\,. \tag{2.22}$$

Denoting by γu^- and γu^+ the traces of the function u on $\{x = 0-\}$ and $\{x = 0+\}$ respectively, we deduce from (2.21) the following Rankine-Hugoniot condition:

$$k_L\, g(\gamma u^-) = k_R\, g(\gamma u^+)\,. \tag{2.23}$$

Actually, if $u \in L^\infty \cap BV((0,T)\times\mathbb{R})$ satisfies (2.23) and (2.22) then Eq. (2.21) holds. Nevertheless, these two conditions are inadequate for a complete characterization of the solution: the study of the Riemann Problem shows that there may be more than one single function in $L^\infty \cap BV((0,T)\times\mathbb{R})$ satisfying both (2.23) and (2.22). Thus, condition (2.23) has to be enforced with an other condition, interpreted as an entropy condition on the line $\{x = 0\}$. Two possible approaches of the question are exposed here.

2.3.1 The characteristics method approach

Suppose that the values of the solution u are sought through the use of the characteristics method. Let $t_\star$ be in $(0,T)$ and $x_\star$ be in $\mathbb{R}$, for example $x_\star > 0$. Two cases have to be distinguished.

First case : $a(u(t_*, x_*)) \leq 0$

In the (x,t)-plane the equation of the half characteristic line is

$$x = x_* + k_R\, a(u(t_*,x_*))\,(t-t_*)\,, t \le t_*\,.$$

Therefore, it does not intersect the line $\{x=0\}$. The value of $u(t_*,x_*)$ is given by the value of the initial condition u_0 at the foot of the characteristic denoted by y on fig.2.1.

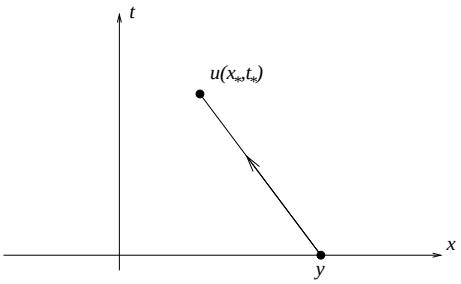

Figure 2.1: $a(u(t_*,x_*)) \le 0$

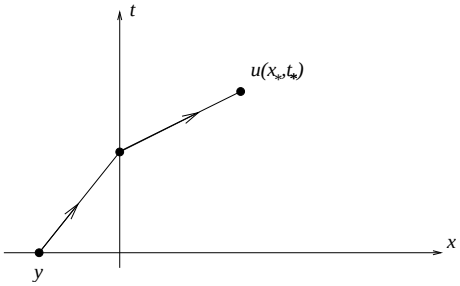

Figure 2.2: $a(u(t_*,x_*)) > 0$

Second case : $a(u(t_*,x_*)) > 0$

The half characteristic line may intersect the line $\{x=0\}$. Suppose that it happens, at time $t=\tau$. Denoting by $\gamma u^+ = u(\tau,0+)$ and $\gamma u^- = u(\tau,0-)$ the traces of the function u, one has $u(t_*,x_*) = \gamma u^+$ (and $a(\gamma u^+) > 0$) for the solution u is constant along the characteristic lines. Thus, the aim is to determine γu^+. The Rankine-Hugoniot condition (2.23) ensures $k_R\, g(\gamma u^+) = k_L\, g(\gamma u^-)$, which provides two possible values of γu^-, one such that $a(\gamma u^-) < 0$ and the other such that $a(\gamma u^-) \ge 0$. Besides, the calculus along the characteristics should be pursued, now starting from the point $(\tau, 0-)$. If $a(\gamma u^-) \ge 0$, then it is possible: the equation of the half characteristic line is

$$x = k_L\, a(u^-)(t-\tau)\,, t \le \tau\,;$$

its slope is non-negative, thus it intersects the line $\{t=0\}$ at a point y and $u(t_*,x_*) = u_0(y)$. It is this configuration which is described on fig.2.2.

If $a(u^+) < 0$, then there exists an indetermination and this lack of information makes the calculus of the value $u(t_*,x_*)$ impossible by the characteristics method.

2.3.2 Interaction of waves

Again, a function $u \in L^\infty \cap BV((0,T)\times\mathbb{R})$ is supposed to satisfy (2.23) and (2.22). To understand which entropy condition could be imposed on the line $\{x=0\}$, that line is "thickened": let ε be a positive number, we consider the continuous approximation k_ε of the function k define by:

$$k_\varepsilon(x) = \begin{cases} k_L & \text{if } x \le -\varepsilon \\ \dfrac{k_R - k_L}{2\,\varepsilon} x + \dfrac{k_R + k_L}{2} & \text{if } -\varepsilon \le x \le \varepsilon \\ k_R & \text{if } \varepsilon \le x \end{cases}$$

and seek for a *stationary* solution of the problem

$$\begin{cases} \dfrac{\partial}{\partial t}u_\varepsilon + \dfrac{\partial}{\partial x}\big(k_\varepsilon\, u_\varepsilon\,(1-u_\varepsilon)\big) = 0 \\ u_\varepsilon(x \le -\varepsilon) = u_L \\ u_\varepsilon(x \ge \varepsilon) = u_R \end{cases}.$$

Let us denote by K_0 the quantity

$$K_0 = k_L\,\gamma u^-(1-\gamma u^-) = k_R\,\gamma u^+\,(1-\gamma u^+)\,. \tag{2.24}$$

Then the function $u_\varepsilon = u_\varepsilon(x)$ has to satisfy the equation

$$k_\varepsilon(x)\,u_\varepsilon(x)(1-u_\varepsilon(x)) = K_0, \quad x \in [-\varepsilon;\varepsilon]\,. \tag{2.25}$$

This equation defines two curves, whose parameterizations are denoted by u_1 and u_2, such that (see fig.2.3):

$$\begin{aligned} x \in [-\varepsilon;\varepsilon], \quad u_1(x) &= \frac{1}{2} - \frac{\sqrt{k_\varepsilon(x)^2 - 4k_\varepsilon(x)K_0}}{2k_\varepsilon(x)}, \\ x \in [-\varepsilon;\varepsilon], \quad u_2(x) &= \frac{1}{2} + \frac{\sqrt{k_\varepsilon(x)^2 - 4k_\varepsilon(x)K_0}}{2k_\varepsilon(x)}. \end{aligned} \tag{2.26}$$

It is clear that:

$$\forall x \in [-\varepsilon;\varepsilon], \quad 0 \le u_1(x) \le \frac{1}{2} \le u_2(x) \le 1.$$

The numbers γu^- and γu^+ satisfy Eq. (2.24); consequently, if $(1-2\gamma u^+)(1-2\gamma u^-) \ge 0$, that is to say:

$$a(\gamma u^+)a(\gamma u^-) \ge 0\,, \tag{2.27}$$

then γu^+ and γu^- can be linked by one of the two curves u_1 or u_2. Now, suppose that condition (2.27) is not fulfilled. Then, in order to link γu^- to γu^+, one has to introduce a stationary discontinuity between the two curves so that the following Rankine-Hugoniot condition may be satisfied:

$$k_\varepsilon(x_0)u_\varepsilon(x_0^-)\big(1-u_\varepsilon(x_0^-)\big) = k_\varepsilon(x_0)u_\varepsilon(x_0^+)\big(1-u_\varepsilon(x_0^+)\big),$$

the point x_0 denoting the point where the discontinuity occurs (see fig.2.3). As the function $g : u \mapsto u(1-u)$ is concave, this discontinuity is admissible (in the entropy sense) if $u(x_0^+) > u(x_0^-)$. Letting ε tend to zero, this yields the condition

$$\gamma u^+ > \gamma u^-\,. \tag{2.28}$$

Eventually, we are led to the following condition:

$$\begin{cases} \text{either } a(\gamma u^+)a(\gamma u^-) \ge 0\,, \\ \text{either } a(\gamma u^+)a(\gamma u^-) < 0 \text{ and } \gamma u^+ > \gamma u^-\,. \end{cases}$$

This condition implies condition (2.20) (and is equivalent to it, in fact). Indeed, suppose $a(\gamma u^+) > 0$. Then, either $a(\gamma u^-) \ge 0$ holds, and in that case condition (2.27) is fulfilled, either $a(\gamma u^-) < 0$, and in that case

$$0 \le \gamma u^+ < 1/2 < \gamma u^- \le 1\,,$$

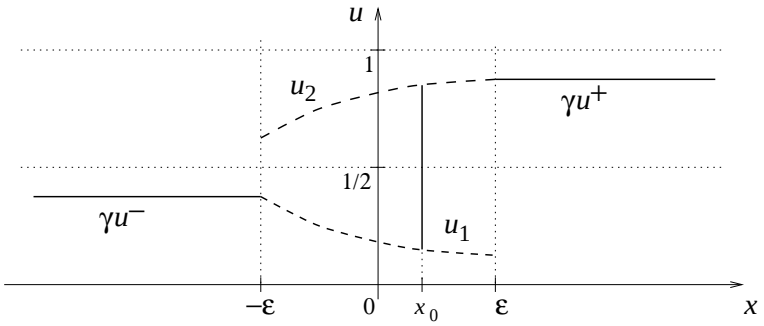

Figure 2.3: stationary connection between γu^- and γu^+ with $k(x) = k_\varepsilon(x)$.

which contradicts condition (2.28). Notice that, here, condition (2.20) is derived by considering the limit of an entropy condition: this justifies the denomination of "entropy" condition to design the condition (2.20).

To conclude, condition (2.20) can be interpreted as the admissibility condition for the superposition of a stationary shock with a contact discontinuity. In several applications, shallow-water equations with topography (see [Seg99] and [LeR99]) for instance, the construction of the solution of the Riemann problem is closely related to this condition. In fact, it is the resonance of the studied system which permits to select the solution of the related Riemann problem. This kind of phenomenon may also be observed in the study of two-phase flows, with two-fluid two-pressure models.

2.4 Numerical methods

All the methods presented in this section are Finite Volume methods (see [EGH00] and [GR96]). For the sake of simplicity, the presentation is restricted to regular meshes (though all methods may be naturally extended to irregular meshes). Let Δx be the space step, with $\Delta x = x_{i+1/2} - x_{i-1/2}$, $i \in \mathbb{Z}$, and let Δt be the time step, with $\Delta t = t^{n+1} - t^n$, $n \in \mathbb{N}$. Besides, let u_i^n denote the approximation of $\frac{1}{\Delta x}\int_{x_{i-1/2}}^{x_{i+1/2}} u(t^n, x)dx$.
Integrating Eq. (2.8) over the cell $]x_{i-1/2}; x_{i+1/2}[\times[t^n; t^{n+1})$ yields:

$$u_i^{n+1} = u_i^n - \frac{\Delta t}{\Delta x}\left(\varphi_{i+1/2}^n - \varphi_{i-1/2}^n\right)$$

where $\varphi_{i+1/2}^n$ is the numerical flux through the interface $\{x_{i+1/2}\} \times [t^n; t^{n+1})$. Let us emphasize that the permeability $k(x)$ is approximated by a piecewise constant function:

$$k_i = \frac{1}{\Delta x}\int_{x_{i-1/2}}^{x_{i+1/2}} k(x)dx, \quad i \in \mathbb{Z}\,. \tag{2.29}$$

The numerical flux $\varphi_{i+1/2}^n$ depends on k_i, k_{i+1}, u_i^n and u_{i+1}^n, and a consistency criterion is imposed:

$$u_i^n = u_{i+1}^n = u_0 \text{ and } k_i = k_{i+1} = k_0 \quad \Longrightarrow \quad \varphi_{i+1/2}^n = k_0 u_0(1-u_0)\,.$$

Moreover, a C.F.L. condition is associated with the time step Δt to ensure the stability of the scheme. Notice that all the methods presented here rely on conservative schemes, since the problem is conservative. The four schemes introduced are three-points schemes, as mentioned above. A higher order extension is also presented (five-point schemes), in order to increase the accuracy of the methods and their rates of convergence (when $\Delta x \to 0$).

2.4.1 Scheme 1

The first scheme is defined by the following numerical flux:

$$\varphi^n_{i+1/2} = \frac{2k_i k_{i+1}}{(k_i + k_{i+1})} \frac{u^n_i (1 - u^n_{i+1})}{(u^n_i + (1 - u^n_{i+1}))} \,. \tag{2.30}$$

The C.F.L. condition associated with this scheme is the classical condition which limits the time step Δt, according to the maximal speed of waves, computed on each cells:

$$\lambda_{MAX} \frac{\Delta t}{\Delta x} < \frac{1}{2}, \quad \text{where } \lambda_{MAX} = \max_{i \in \mathbb{Z}, n \in \mathbb{N}} (k_i (1 - 2u^n_i)) \,. \tag{2.31}$$

For this scheme, the design of the fluxes is based on methods usually implemented in industrial codes.

2.4.2 Scheme 2

Physical considerations drive the conception of the second scheme:

$$\varphi^n_{i+1/2} = \frac{k_i u^n_i k_{i+1} (1 - u^n_{i+1})}{k_i u^n_i + k_{i+1} (1 - u^n_{i+1})} \,. \tag{2.32}$$

Indeed, the physical variables are ku and $k(1-u)$, rather than k and u. The C.F.L. condition is the same as condition (2.31), associated with the scheme 1.

2.4.3 The Godunov scheme

The Godunov scheme [God59] is based on the resolution of the Riemann problem at each interface of the mesh. The application of the Godunov scheme to the framework of space-dependent flux may be seen as an extension of the works of J.M. Greenberg and A.Y. LeRoux to deal with conservation laws with source terms (see [GL96] and [LeR99]). The Godunov Method applied to resonant systems like (2.9) has been studied by Lin, Temple and Wang ([LTW95a], [LTW95b]). A specific Godunov scheme associated to Problem (2.8) has been defined by Towers by considering a discretization of k staggered with respect to that of u [Tow00]. Here, we consider the Godunov Method applied to the 2×2 system (2.9).

$$\begin{cases} \dfrac{\partial k}{\partial t} = 0 \,, \quad \dfrac{\partial u}{\partial t} + \dfrac{\partial}{\partial x}\big(ku(1-u)\big) = 0, \qquad t > t^n,\, x \in \mathbb{R} \,, \\ u(0,x) = \begin{cases} u^n_i & \text{if } x < x_{i+1/2} \\ u^n_{i+1} & \text{if } x > x_{i+1/2} \end{cases}, \quad k(x) = \begin{cases} k_i & \text{if } x < x_{i+1/2} \\ k_{i+1} & \text{if } x > x_{i+1/2} \end{cases} . \end{cases} \tag{2.33}$$

Let $u^n_{i+1/2}\big((x-x_{i+1/2})/(t-t^n);k_i,k_{i+1},u^n_i,u^n_{i+1}\big)$ be the exact solution of this Riemann problem (see Appendix 2.A for an explicit presentation of the solution). Since the function k is discontinuous through the interface $\{x_{i+1/2}\}\times[t^n;t^{n+1})$, the solution $u^n_{i+1/2}$ is discontinuous through this interface too. However, as the problem is conservative, the flux is continuous through this interface, and writes:

$$\begin{aligned}\varphi^n_{i+1/2} &= k_i g\big(u^n_{i+1/2}(0^-;k_i,k_{i+1},u^n_i,u^n_{i+1})\big)\\ &= k_{i+1} g\big(u^n_{i+1/2}(0^+;k_i,k_{i+1},u^n_i,u^n_{i+1})\big)\end{aligned} \tag{2.34}$$

where $g(u)=u(1-u)$. Here, the C.F.L. condition is based on the maximal speed of waves associated with each local Riemann problem.

Remark 2.3. *Since the problem involves a homogeneous conservation law, the definition of the flux is not ambiguous. Indeed, in the framework of shallow-water equations with topography for instance (see [LeR99] and [GHS03]), the source term "breaks" the conservativity of the system and the flux becomes discontinuous through the interface. Moreover, the approximation of the topography by a piecewise constant function introduces a product of distributions, which is not defined (contrary to what happen in the current framework, where all jumps relations are well defined).*

2.4.4 The VFRoe-ncv scheme

We present herein an approximate Godunov scheme, based on the exact solution of a linearized Riemann problem. A VFRoe-ncv scheme is defined by a change of variables (see [BGH00] and [GHS02]), the new variable is denoted by $\theta(k,u)$. The choice of θ is motivated by the properties of the VFRoe-ncv scheme induced from this change of variables. Here, we set $\theta(k,u)=ku(1-u)$ to be the new variable. If v is defined by $v(t,x)=\theta(k(x),u(t,x))$, then the VFRoe-ncv scheme is based on the exact resolution of the following linearized Riemann problem:

$$\begin{cases}\dfrac{\partial v}{\partial t}+\big(\hat{k}(1-2\hat{u})\big)\dfrac{\partial v}{\partial x}=0, \qquad t>t^n,\ x\in\mathbb{R}\,,\\ v(0,x)=\begin{cases}\theta(k_i,u^n_i) & \text{if } x<x_{i+1/2}\\ \theta(k_{i+1},u^n_{i+1}) & \text{if } x>x_{i+1/2}\end{cases},\end{cases} \tag{2.35}$$

where $\hat{k}=(k_i+k_{i+1})/2$ and $\hat{u}=(u^n_i+u^n_{i+1})/2$.
The (non-linear) initial problem thus becomes a classical convection equation, and the VFRoe-ncv scheme is reduced to the well-known upwind scheme for problem (2.35). Hence, as the Godunov scheme, the flux (which is represented by v) is continuous through the interface $\{x_{i+1/2}\}\times[t^n;t^{n+1})$ (this property is provided by the choice of θ; another choice would lead to a jump of the flux v through the local interface). If $v^n_{i+1/2}\big((x-x_{i+1/2})/(t-t^n);k_i,k_{i+1},u^n_i,u^n_{i+1}\big)$ is the exact solution of the Riemann problem (2.35), the numerical flux of the VFRoe-ncv scheme is:

$$\varphi^n_{i+1/2}=v^n_{i+1/2}(0;k_i,k_{i+1},u^n_i,u^n_{i+1})\,. \tag{2.36}$$

The C.F.L. condition is determined by the speed waves generated by the local Riemann problems, like the Godunov scheme (but the speed computed by the two methods are *a priori* different). Since

the VFRoe-ncv scheme relies on the resolution of a linearized Riemann problem, an entropy fix has to be applied to avoid the occurrence of non-entropic shock when dealing with sonic rarefaction wave [HH83].

Remark 2.4. *For some initial conditions, the VFRoe-ncv scheme may compute exactly the same numerical results as the Godunov scheme. Indeed, if each local Riemann problem can be solved by an upwinding on v (*ie *no sonic point arises), both methods compute the same numerical flux (since it is completely defined by one of the two initial states).*

2.4.5 A higher order extension

Classical methods to increase the accuracy and the rate of convergence (when $\Delta x \to 0$) of Finite Volume schemes call for a piecewise linear reconstruction by cell. A second order Runge-Kutta method (also known as the Heun scheme) is associated with the reconstruction to approximate time derivatives. The linear reconstruction introduced here lies within a framework introduced by B. Van Leer in [Van79], namely MUSCL (monotonic upwind schemes for conservation laws), with the minmod slope limiter. This formalism is usually applied to homogeneous conservation laws (see [GHS02] for numerical results and measurements, dealing with the Euler system). However, a classical reconstruction applied in our context may penalize results provided by the initial algorithm, when simulating convergence in time (*ie* when $t \to +\infty$) towards stationary states. This phenomenon will be pointed out later by numerical results, and a method to avoid it is proposed (see [GHS03] for a presentation of this method adapted to the approximation of the shallow-water equations with topography).

A MUSCL scheme may be described by the following three steps algorithm:

i. Let $\{u_i^n\}_{i\in\mathbb{Z}}$ be a piecewise constant approximation, compute $u^{lin}(t^n, x)$, a piecewise linear function.

ii. Solve the conservation law with $u^{lin}(t^n, x)$ as initial condition and thus obtain $u^{lin}(t^{n+1}, x)$.

iii. Compute $\{u_i^{n+1}\}_{i\in\mathbb{Z}}$, averaging $u^{lin}(t^{n+1}, x)$.

The method proposed in this section only modifies the first step. It requires the use of the minmod slope limiter and preserves its main properties (see [GR96] and references inside). See Remark 2.5 for details about the computation of steps 2 and 3.

In the following of this section, we drop the time dependance for all variables. Let $\{w_i\}_{i\in\mathbb{Z}}$ be a variable constant on each cell $I_i = [x_{i-1/2}; x_{i+1/2}]$ and $x_i = (x_{i+1/2} + x_{i-1/2})/2$. Let $\delta_i(w)$ be the slope associated with w_i on the cell I_i. Moreover, let $w_i^{lin}(x)$, $x \in I_i$, the linear function defined by:

$$w_i^{lin}(x) = w_i - \delta_i(x - x_i) \qquad x \in I_i\,.$$

To compute the slope $\delta_i(w)$, the minmod slope limiter is used:

$$\delta_i(w) = \begin{cases} s_{i+1/2}(w)\min\big(|w_{i+1} - w_i|, |w_i - w_{i-1}|\big)/\Delta x & \text{if } s_{i-1/2}(w) \\ & \quad = s_{i+1/2}(w)\,, \\ 0 & \text{else}\,, \end{cases} \tag{2.37}$$

where $s_{i+1/2}(w) = \mathrm{sgn}(w_{i+1} - w_i)$. This linear reconstruction fulfills:

Proposition 2.1. *If w^{cst} and w^{lin} respectively denote the functions defined by the constant and linear piecewise approximations of w,*

$$\begin{array}{ll} w^{cst}(x) = w_i & i \in \mathbb{Z} \text{ such that } x \in I_i, \\ w^{lin}(x) = w_i^{lin} & i \in \mathbb{Z} \text{ such that } x \in I_i, \end{array}$$

then w^{lin}, defined by the minmod slope limiter (2.37) from w^{cst}, verifies

$$|w^{lin}|_{BV(\mathbb{R})} = |w^{cst}|_{BV(\mathbb{R})}. \tag{2.38}$$

When dealing with a classical scalar conservation law $\partial_t u + \partial_x f(u) = 0$, the reconstruction is performed on the conservative variable $w = u$. Hence, Proposition 2.1 ensures that the method does not introduce oscillations on the modified variable.

Though the equation studied here is a conservation law, some properties deeply differ from the classical framework $\partial_t u + \partial_x f(u) = 0$, due to the space-dependence of the flux. Indeed, focusing on stationary states, the characterization of thess latter is quite different ; whereas piecewise constant functions represent stationary states for $\partial_t u + \partial_x f(u) = 0$, their form closely depends on the shape of $k(x)$ here, since stationary states have to verify $\partial_x(ku(1-u)) = 0$. Using the classical Finite Volume formalism, this equation becomes the following discrete equation:

$$\forall i \in \mathbb{Z}, \quad k_i u_i (1 - u_i) = k_{i+1} u_{i+1} (1 - u_{i+1}) \,. \tag{2.39}$$

Thus, if the previous reconstruction with $w = u$ is computed in the current framework, a discrete stationary state (2.39) is not maintained by the whole algorithm (even assuming that the initial scheme is able to maintain it). Furthermore, convergence in time towards a stationary state may be altered (some numerical tests illustrate this numerical phenomenon in the following).

A way to avoid this problem is to take into account relation (2.39) in the linear reconstruction. Recalling the notation $v(x) = \theta(k(x), u(x)) = k(x)u(x)(1-u(x))$, (2.39) becomes $v_i = v_{i+1}, \forall i \in \mathbb{Z}$. A natural idea is to use the linear reconstruction with $w = v$, to ensure that oscillations do not occur when dealing with stationary states. Indeed, such a reconstruction implies the constraint (2.38) on the total variation of v (Proposition 2.1). However, the change of variables from (k, u) to (k, v) is not invertible, which forbids the use of this reconstruction (see Remark 2.6 for more details). Moreover, Proposition 2.1 on u is lost if the minmod reconstruction is only computed on v.

We propose here to keep the linear reconstruction on u with the minmod slope limiter (2.37), and to add a BV-like constraint on v (following equality (2.38)). Let us first introduce the function ϑ_i defined for $x \in I_i$ by

$$\vartheta_i(x) = \begin{cases} \dfrac{2(x_i - x)}{\Delta x}\, \theta(k_i, u^{lin}(x^+_{i-1/2})) \\ \qquad + \dfrac{2(x - x_{i-1/2})}{\Delta x}\, \theta(k_i, u^{lin}(x_i)) & \text{if } x \in]x_{i-1/2}; x_i] \,, \\ \dfrac{2(x - x_i)}{\Delta x}\, \theta(k_i, u^{lin}(x^-_{i+1/2})) \\ \qquad + \dfrac{2(x_{i+1/2} - x)}{\Delta x}\, \theta(k_i, u^{lin}(x_i)) & \text{if } x \in]x_i; x_{i+1/2}[\,, \end{cases}$$

and the function ϑ defined for $x \in \mathbb{R}$ by

$$\vartheta(x) = \vartheta_i(x) \quad i \in \mathbb{Z} \text{ such that } x \in I_i.$$

This function represents the linear interpolation provided by the values of u^{lin} at each interface of the mesh and at each center of cells (see Fig. 2.4). The function ϑ is linear on each interval $]x_{i-1/2}; x_i[$ and $]x_i; x_{i+1/2}[$, $\forall i \in \mathbb{Z}$. Moreover, the function ϑ is discontinuous at each interface $x_{i+1/2}$ and continuous at each center of cell x_i. We want to impose that the reconstruction on u verifies the *a posteriori* criterion:

$$|\vartheta|_{BV(\mathbb{R})} = |\theta(k^{cst}, u^{cst})|_{BV(\mathbb{R})}\,, \tag{2.40}$$

where $\theta(k^{cst}, u^{cst})$ represents the function v computed from the piecewise constant approximations of k and u. Equality (2.40) may be seen as the counterpart of equality (2.38) for v. In practice, equality (2.40) becomes:

$$\begin{aligned} &\forall i \in \mathbb{N}\,, \quad 0 \leq |\vartheta(x_i) - \vartheta(x_{i-1/2}^-)| \leq |\vartheta(x_i) - \vartheta(x_{i-1})|/2\,, \\ &\forall i \in \mathbb{N}\,, \quad 0 \leq |\vartheta(x_{i+1/2}^+) - \vartheta(x_i)| \leq |\vartheta(x_{i+1}) - \vartheta(x_i)|/2\,. \end{aligned} \tag{2.41}$$

In fact, (2.41) only implies (2.40). If condition (2.41) is not fulfilled, the slope is reset to $\delta_i(u) = 0$ (for instance, function ϑ represented on Fig. (2.4) fulfills conditions (2.41)).

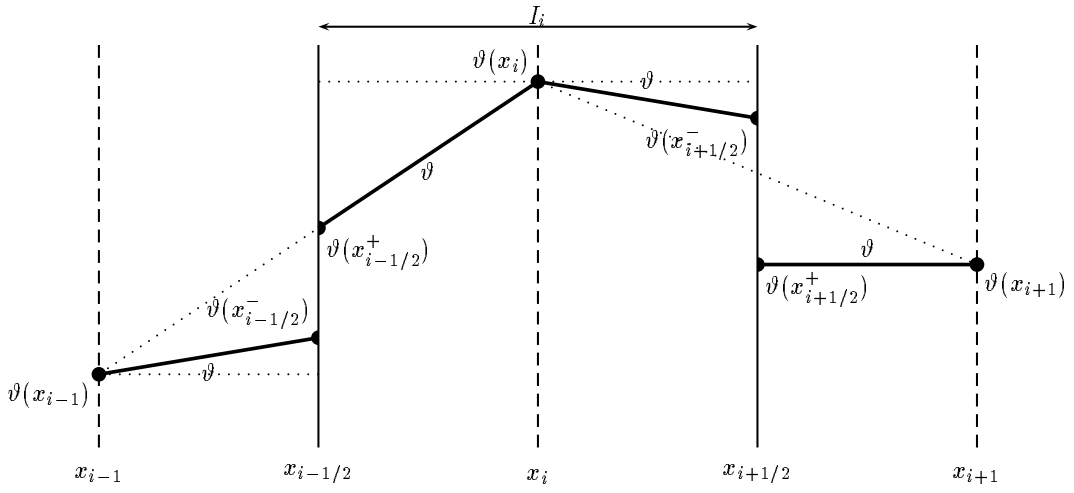

Figure 2.4: A BV-like reconstruction to deal with stationary states.

Thus, one may sum up the reconstruction on u with the following algorithm:

i. Computation of $\delta_i(u)$ by the minmod slope limiter:

$$\delta_i(u) = \begin{cases} s_{i+1/2}(u) \min\big(|u_{i+1} - u_i|, |u_i - u_{i-1}|\big)/\Delta x & \text{if } s_{i-1/2}(u) \\ & \quad = s_{i+1/2}(u)\,, \\ 0 & \text{else}\,. \end{cases}$$

ii. If condition (2.41) is not fulfilled by the linear approximation of u provided by this computation of $\delta_i(u)$, the slope is reset to $\delta_i(u) = 0$, else, the slope is not modified.

Hence, using this method, the two constraints on the total variation of u and v, namely (2.38) and (2.40), are fulfilled. The algorithm of reconstruction is not optimal focusing on condition (2.40), since $|\vartheta|_{BV(\mathbb{R})} \leq |\theta(k^{lin}, u^{lin})|_{BV(\mathbb{R})}$, but it minimizes the number of logical tests.

Some numerical results are presented in the next section. Rates of convergence when the mesh is refined and measurements of the convergence to stationary states are provided. These tests are performed without reconstruction, with the minmod reconstruction on u, with the modified reconstruction, and with the reconstruction on v for the VFRoe-ncv scheme (see Remark 2.6).

Remark 2.5. *A modification of the minmod slope limiter has been proposed here to take into account stationary states when the MUSCL formalism is applied. Hence, steps 2 and 3 are not modified and properties enumerated in [GR96] related to the minmod limiter are maintained. However, most of these properties are obtained using generalized Riemann problems in step 2 and exact Finite Volume integration in step 3. Here, classical Riemann problems have been used to compute numerical fluxes $\varphi^n_{i+1/2}$ and the Heun scheme is used to approximate time derivatives.*

Remark 2.6. *Since the change of variables from (k, u) to (k, v) is not invertible, the reconstruction on v cannot be performed with a standard scheme. However, due to the specific form of the VFRoe-ncv scheme presented in Section 2.4.4, one may compute the linear reconstruction with the minmod slope limiter (2.37) on v with this scheme. Some numerical tests are presented in the following to illustrate the validity of this first idea.*

2.5 Numerical experiments

Several numerical tests are presented here, as well as qualitative results and quantitative results. All the schemes introduced are performed using no reconstruction, reconstruction on u, modified reconstruction and reconstruction on v with the VFRoe-ncv scheme.

2.5.1 Qualitative results

The two following tests correspond to Riemann problems. The length of the domain is $10\,m$. The mesh is composed of 100 cells and the C.F.L. condition is set to 0.45 for all schemes (recall however that the computation of speed of waves is different according to the scheme). The variables u and $v = ku(1-u)$ are plotted, in order to estimate the behavior of all schemes through the interface $\{x/t = 0\}$. Notice that no reconstruction has been used here.

The initial conditions of the first Riemann problem are $k_L = 2$, $k_R = 1$, $u_L = 0.5$ and $u_R = 0.3$. The results of Fig. 2.5 are plotted at $t = 4\,s$. The analytic solution of this Riemann problem may be found in Appendix 2.A. The numerical approximations provided by scheme 1 and scheme 2 are very close each to other. One may notice that these two schemes are very diffusive, and that the intermediate state on the left of the interface is not well approximated (though the difference with the exact solution tends to 0 when the mesh is refined). On the other hand, the results provided

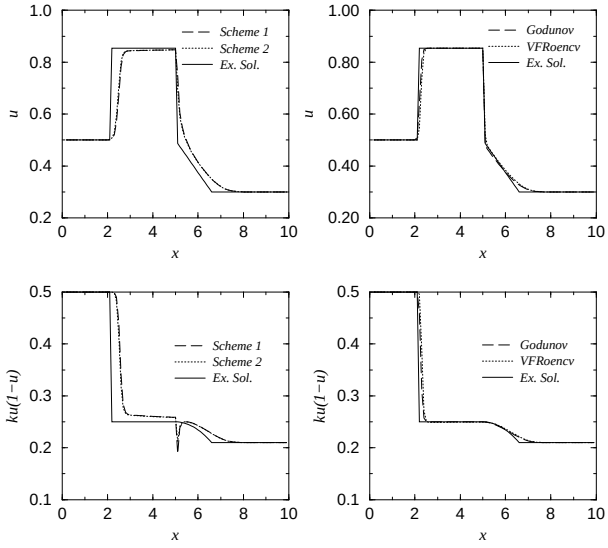

Figure 2.5: 100 cells - $k_L = 2$, $k_R = 1$, $u_L = 0.5$, $u_R = 0.3$.

by the VFRoe-ncv scheme and the Godunov scheme are very similar, and more accurate than the results provided by the latter two schemes. Moreover, contrary to scheme 1 and scheme 2, the VFRoe-ncv scheme and the Godunov scheme do not introduce oscillation on v at the interface $\{x/t = 0\}$.

The initial conditions of the second Riemann problem are $k_L = 2$, $k_R = 1$, $u_L = 0.95$ et $u_R = 0.8$. The results at $t = 2\,s$ are presented on Fig. 2.6. Same comments may be made about scheme 1 and scheme 2, in particular about their behavior at the interface $\{x/t = 0\}$, where an undershoot is detected on the variable v (its length represents about 60% of $v_R - v_L$ for scheme 1 and about 25% of $v_R - v_L$ for scheme 2). Furthermore, the two schemes (in particular scheme 1) introduce a loss of monotonicity at the end of the rarefaction wave. Approximations provided by the VFRoe-ncv scheme and the Godunov scheme are better. Moreover, the two schemes exactly compute here the same results. As noticed in the previous test, the contact discontinuity is perfectly approximated (no point is introduced in the discontinuity) and the monotonicity of the rarefaction wave is maintained.

2.5.2 Quantitative results

We study in this section the ability of the schemes to converge towards the entropy solution. The first case provides measurements of the rates of convergence of the methods in the L^1 norm when the mesh is refined. The second test gives some results about the variation in time in the L^2 norm of the numerical approximations when dealing with a transient simulation which converges towards a stationary state.

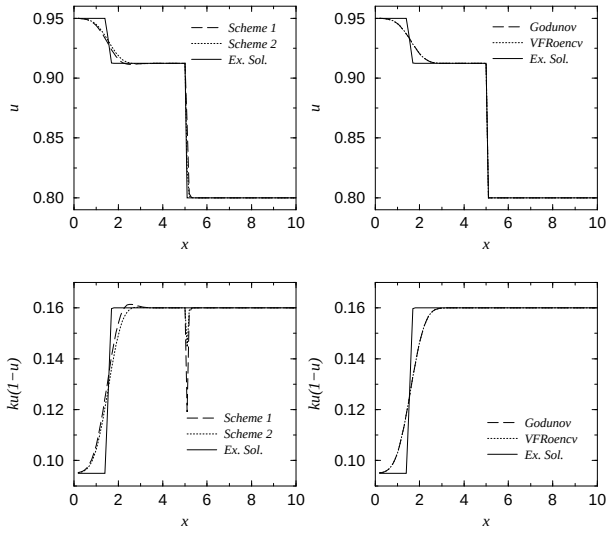

Figure 2.6: 100 cells - $k_L = 2$, $k_R = 1$, $u_L = 0.95$, $u_R = 0.8$.

Convergence related to the space step

The computations of this test are based on the first of the two Riemann problem exposed just above. The simulations are stopped at $t = 4\,s$. The main interest of this test is that the analytic solution is composed of a shock wave, a contact discontinuity and a rarefaction wave (see Fig. 2.5). Some measurements of the numerical error provided by the methods when Δx tends to 0 are exposed. Let us define the L^1 norm of the numerical error by $\Delta x \sum_{i=1,..,N} |u_i^{app} - u^{ex}(x_i)|$. Several meshes are considered: involving 1000, 3000, 10000 and 30000 cells. Fig. 2.7 represents, in a logarithmic scale, the profiles of the error provided by the different schemes with the different reconstructions. Moreover, Table 2.1 enumerates the different rates of convergence computed between the meshes with 10000 and 30000 nodes. The four schemes have been tested without reconstruction, with the minmod reconstruction on u, with the modified reconstruction, and with the minmod reconstruction on v for the VFRoe-ncv scheme. As expected, all the methods converge towards the entropy solution (see Fig. 2.7). Notice first that, with any reconstruction, the Godunov scheme is much more accurate that scheme 1 and scheme 2. Indeed, if the Godunov scheme is performed on a mesh with N cells, scheme 1 and scheme 2 must be performed on a mesh containing between $7N$ and $8N$ cells, in order to obtain the same L^1 error (with the same C.F.L. condition for all schemes),– notice that the CPU time required is about the same for all schemes. Comparing the VFRoe-ncv scheme and the Godunov scheme, one may remark that the results are very close each to other when no reconstruction is active. On the other hand, if a reconstruction is added to the latter two schemes, the Godunov scheme becomes twice more accurate than the VFRoe-ncv scheme (and remains about four times more accurate than scheme 1 or scheme 2). Notice that the difference between the reconstruction on u and the modified reconstruction is not significant.

In Table 2.1 are listed the rates of convergence provided by all the methods. A reconstruction

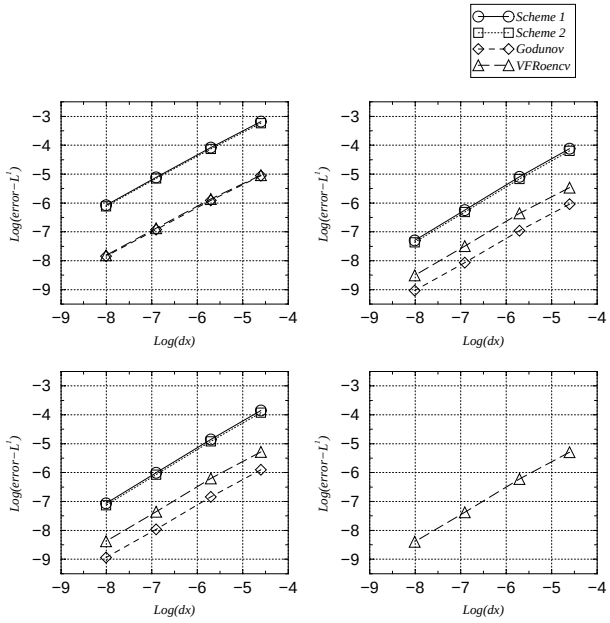

Figure 2.7: Profiles of convergence for variable u. top-left: no reconstruction - top-right: reconstruction on u - bottom-left: modified reconstruction - bottom-right: reconstruction on v.

Table 2.1: Rates of convergence for variable u.

Reconstruction	Scheme 1	scheme 2	Godunov	VFRoe-ncv
No reconstruction	0.88	0.87	0.82	0.85
Reconstruction on u	0.96	0.95	0.87	0.92
Modified reconstruction	0.96	0.96	0.89	0.93
Reconstruction on v	-	-	-	0.93

increase the rates of convergence. Moreover, the reconstruction on u and the modified reconstruction provide similar rates. Notice that, the more accurate a method is, the less important the convergence rate is, but differences are not significant. As above, the results provided by the reconstruction on u and the modified reconstruction are very similar (the reconstruction on v with the VFRoe-ncv scheme provides the same behavior). Hence, the computation of one of the reconstructions enables to obtain much more accurate results (see Fig. 2.7) and to increase the rate of convergence associated with a scheme.

Convergence towards a stationary state

The test studied herein simulates a transient flow which converges towards a stationary state when t tends to $+\infty$. The initial conditions are:

$$k(x) = \begin{cases} 2 & \text{if } 0 \leq x \leq 2,5 \\ \frac{25-2x}{10} & \text{if } 2,5 < x < 7,5 \\ 1 & \text{if } 7,5 \leq x \leq 10 \end{cases} \quad \text{and} \quad u_0(x) = \begin{cases} 0,9 & \text{if } 0 \leq x \leq 2,5 \\ \frac{1+\sqrt{0,28}}{2} & \text{if } 2,5 < x \leq 10 \end{cases}.$$

The stationary solution writes

$$u(t=+\infty, x) = \begin{cases} 0,9 & \text{if } 0 \leq x \leq 2,5 \\ \frac{1}{2} + \frac{\sqrt{k(x)^2 - 0,72k(x)}}{2k(x)} & \text{if } 2,5 < x < 7,5 \\ \frac{1+\sqrt{0,28}}{2} & \text{if } 7,5 \leq x \leq 10 \end{cases}. \tag{2.42}$$

The mesh used for this test contains 100 cells, the C.F.L. condition is set to $0,45$. We define the L^2 norm of the variation in time by $(\Delta x \sum_{i=1,\ldots,100} |u_i^{n+1} - u_i^n|^2)^{1/2}$. The variation along the time is represented on Fig. 2.8 for all methods and reconstructions. Notice that all methods converge towards the stationary state (2.42) without any reconstruction (see Fig. 2.8-top-left). Moreover, the profiles computed by the VFRoe-ncv scheme and the Godunov scheme are superposed, and provide rates of convergence more important than the profiles computed by scheme 1 and scheme 2 (which are both superposed too). If the classical MUSCL reconstruction on u is performed (Fig. 2.8-top-right), rates of convergence are altered (all schemes nonetheless converge), in particular for the VFRoe-ncv scheme and the Godunov scheme. On the other hand, when the modified version of the MUSCL reconstruction is used (Fig. 2.8-bottom-left), the behavior of all algorithms is quite better, and the rates of convergence are close to (but slightly less important than) the rates obtained without any reconstruction. Hence, taking into account stationary states in the MUSCL reconstruction enables to improve the behavior of the methods when dealing with convergence towards steady states. To confirm it, see the last figure (Fig. 2.8-bottom-right). It represents the results computed by the VFRoe-ncv scheme with the minmod reconstruction on v. Here, the rates of convergence are the greatest of those obtained by all other approximations. Similar results are obtained when the stationary solution contains a stationary shock. Similar simulations (convergence towards a steady state) have been performed with the VFRoe-ncv scheme for shallow-water equations with topography [GHS03]. Nevertheless, in that case, the gap between the results computed with the classical reconstruction and the modified version is quite important. Indeed, the classical minmod reconstruction provides non-convergent results (the L^2 variation in time does

not decrease) whereas the modified reconstruction gives convergent and accurate results. This phenomenon may be due to the non-conservativeness of the whole system of shallow-water equations with topography.

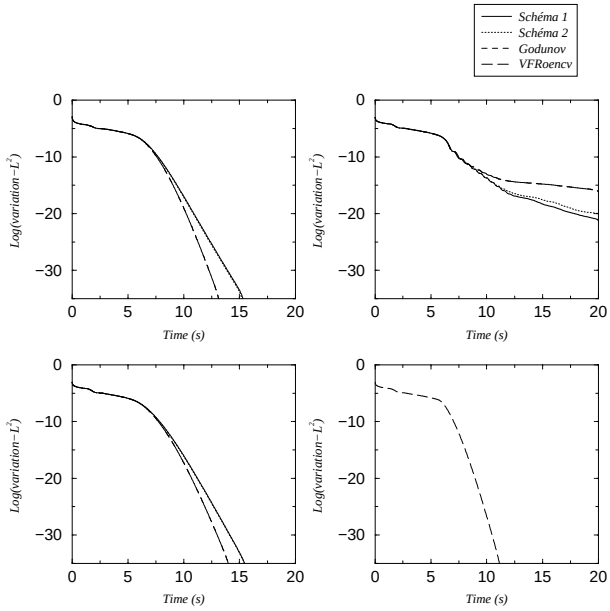

Figure 2.8: Variation in time for variable u. top-left: no reconstruction - top-right: reconstruction on u - bottom-left: modified reconstruction - bottom-right: reconstruction on v.

2.6 Conclusion

A scalar conservation is studied here. Its flux depends not only on the conservative variable u but on the space variable x *via* the permeability k which is a discontinuous function. Thanks to the conservative form of the equation, some jump relations are classically defined (whereas a product of distribution may occur when dealing with source terms or non-conservative equations). Existence and uniqueness of the entropy solution hold. The particular entropy admissibility criterion (namely Condition (2.20)) has been discussed. Notice that this condition is independent of the choice of the integration path on k, contrary to the non-conservative framework [DLM95] (here, the path is only assumed to be regular and monotone). Several ways have been presented to recover this condition (or to clarify it). One of them deals with the superposition of two waves, namely the discontinuity on $\{x = 0\}$ and a shock wave. To this purpose, the jump of k is replaced by a linear connection k_ε in $]-\varepsilon;+\varepsilon[$. Stationary states are investigated inside this "thickness". These solutions may be totally smooth, or they may involve a stationary shock wave. Obviously, this shock wave must agree with the entropy condition (which is classical, since k_ε is continuous).

Hence, passing to the limit, the condition on the stationary shock wave remains for the solution u and is equivalent to Condition (2.20). This point of view may be very useful in the study of some problems. For instance, focusing on shallow-water equations with topography, a similar phenomenon occurs when dealing with a discontinuous bottom (though the system is restricted to smooth topography, a bottom step is used to study the associated Riemann problem). Indeed, the solution of the Riemann problem (completely described in [Seg99]) may be defined without any ambiguity only as soon as the resonant case is completely understood. Furthermore, such a problem of resonance arises in two-phase flows, with a two-fluid two-pressure approach [GHS01]. Since these two problems are non-conservative, the derivation of the limit $[\varepsilon \to 0]$ is not so clear and the condition on the discontinuity becomes no more than a conjecture.

Several numerical schemes have been provided too, in order to simulate the conservation law. Two Finite Volume schemes have been introduced, derived from those used in the industrial context. Two other schemes have been proposed, following the ideas of J.M. Greenberg and A.Y. LeRoux [GL96], the first one based on the exact solution of the Riemann problem and the other based on the exact solution of a linearized Riemann problem, respectively the Godunov scheme [God59] and the VFRoe-ncv scheme [BGH00]. Some qualitative and quantitative tests confirm the good behavior of the latter two schemes, in comparison with the two others. A great difference of accuracy may be detected, especially trough the discontinuity of permeability. Notice however that the rates of convergence (when the mesh is refined) of all the schemes are very close each to other. To increase the accuracy and the speed of convergence of all schemes, a higher order method is presented too. Though a classical MUSCL method can fulfill all these requirements, if we focus on convergence towards stationary states, the convergence may be perturbed by a classical reconstruction (even lost for shallow-water equations with topography). Hence, a modification of the reconstruction is proposed and tested (see [GHS03] for the application to shallow-water equations with topography). The good behavior is recovered, without any significant loss of accuracy.

2.A The Riemann problem

We present in this appendix the exact solution of the following Riemann problem:

$$\begin{cases} \dfrac{\partial u}{\partial t} + \dfrac{\partial}{\partial x}\big(ku(1-u)\big) = 0 \qquad x \in \mathbb{R},\, t \in \mathbb{R}_+\,, \\ u(t=0,x) = \begin{cases} u_L & \text{if } x < 0 \\ u_R & \text{if } x > 0 \end{cases}, \quad k(x) = \begin{cases} k_L & \text{if } x < 0 \\ k_R & \text{if } x > 0 \end{cases}, \end{cases} \tag{2.43}$$

where $k_L, k_R \in \mathbb{R}_+$ and $u_L, u_R \in [0;1]$.

2.A.1 Properties of the solution of the Riemann problem

The Riemann problem (2.43) may be seen as two separated problems, $\{t \geq 0; x < 0\}$ and $\{t \geq 0; x > 0\}$, coupled by some interface conditions at $\{t \geq 0; x = 0\}$. Let us define $u^- = u(t > 0, x = 0^-)$ and $u^+ = u(t > 0, x = 0^+)$ ($u^-, u^+ \in [0;1]$). The entropy solution u of (2.43) is self-similar (which implies that u^- and u^+ are constant), and verifies the following relations:

In $t \geq 0$, $x < 0$:

- u is the (unique) entropy solution of:

$$\begin{cases} \dfrac{\partial u}{\partial t} + \dfrac{\partial}{\partial x}\big(k_L u(1-u)\big) = 0 & t \in \mathbb{R}_+,\, x \in \mathbb{R}_-^*\,, \\ u(t=0,x) = u_L & x \in \mathbb{R}_-^*\,, \\ u(t, x=0^-) = u^- & t \in \mathbb{R}_+\,. \end{cases}$$

- If u contains a rarefaction wave, $u(t,x) \geq \frac{1}{2}$, $t \in \mathbb{R}_+$, $\forall x \in \mathbb{R}_-^*$.
- If u contains a shock wave, $u_L + u^- \geq 1$.

In $t \geq 0$, $x > 0$:

- u is the (unique) entropy solution of:

$$\begin{cases} \dfrac{\partial u}{\partial t} + \dfrac{\partial}{\partial x}\big(k_R u(1-u)\big) = 0 & t \in \mathbb{R}_+,\, x \in \mathbb{R}_+^*\,, \\ u(t=0,x) = u_R & x \in \mathbb{R}_+^*\,, \\ u(t, x=0^+) = u^+ & t \in \mathbb{R}_+\,. \end{cases}$$

- If u contains a rarefaction wave, $u(t,x) \leq \frac{1}{2}$, $t \in \mathbb{R}_+$, $\forall x \in \mathbb{R}_+^*$.
- If u contains a shock wave, $u_R + u^+ \leq 1$.

In $t \geq 0$, $x = 0$:

- $k_L u^-(1-u^-) = k_R u^+(1-u^+)$.
- Either $\quad u^-, u^+ \leq \frac{1}{2} \quad$ or $\quad u^-, u^+ \geq \frac{1}{2} \quad$ or $\quad u^- < u^+$.

Thanks to all these properties, one may now describe explicitly the solution u of the whole Riemann problem (2.43).

2.A.2 The explicit form of the solution of the Riemann problem

We first present the construction of the solution when the permeability is constant $k(x) = k_0$. Let u_l and u_r two different states in $[0;1]$. One may link u_l and u_r by a rarefaction wave or by a shock wave.

If $u_l > ur$: u_l and u_r are linked by a rarefaction wave defined by:

$$u(t,x) = \begin{cases} u_l & \text{if } x/t \leq k_0(1-2u_l)\,, \\ \frac{k_0 - x/t}{2k_0} & \text{if } k_0(1-2u_l) < x/t < k_0(1-2u_r)\,, \\ u_r & \text{if } x/t \geq k_0(1-2u_r)\,. \end{cases} \tag{2.44}$$

If $u_l < ur$: u_l and u_r are linked by a shockwave defined by:

$$u(t,x) = \begin{cases} u_l & \text{if } x/t \leq k_0(1-(u_l+u_r))\,, \\ u_r & \text{if } x/t > k_0(1-(u_l+u_r))\,. \end{cases} \tag{2.45}$$

So, the construction of the solution of the Riemann problem (2.43) is reduced to the determination of u^- and u^+. Indeed, since $k(x)$ is constant in $\{t \geq 0; x < 0\}$ and in $\{t \geq 0; x > 0\}$, the previous characterization gives the profile of u (by (2.44) or (2.45)). We first focus on the case $k_L > k_R$.

If $u_R < 1/2$:

- $0 \leq u_L < 1/2$ and $k_L g(u_L) \leq k_R g(u_R)$:
  - $u^- = u_L$,
  - u^+ is the smallest root of $k_L g(u_L) = k_R g(u^+)$, and u^+ and u_R are linked by a shock wave (defined by (2.45), with $u_l = u^+$ and $u_r = u_R$).
- $k_L g(u_L) \leq k_R g(u_R)$ and $k_L g(u_L) \leq k_R g(1/2)$:
  - $u^- = u_L$,
  - u^+ is the smallest root of $k_L g(u_L) = k_R g(u^+)$, and u^+ and u_R are linked by a rarefaction wave (defined by (2.44), with $u_l = u^+$ and $u_r = u_R$).
- $k_L g(u_L) > k_R g(1/2)$:
  - u^- is the greatest root of $k_L g(u^-) = k_R g(1/2)$, and u_L and u^- are linked by a shock wave (defined by (2.45), with $u_l = u_L$ and $u_r = u^-$),
  - $u^+ = 1/2$, and u^+ and u_R are linked by a rarefaction wave (defined by (2.44), with $u_l = u^+$ and $u_r = u_R$).
- $1/2 < u_L \leq 1$ and $k_L g(u_L) \leq k_R g(u_R)$:
  - u^- is the greatest root of $k_L g(u^-) = k_R g(1/2)$, and u_L and u^- are linked by a rarefaction wave (defined by (2.44), with $u_l = u_L$ and $u_r = u^-$),

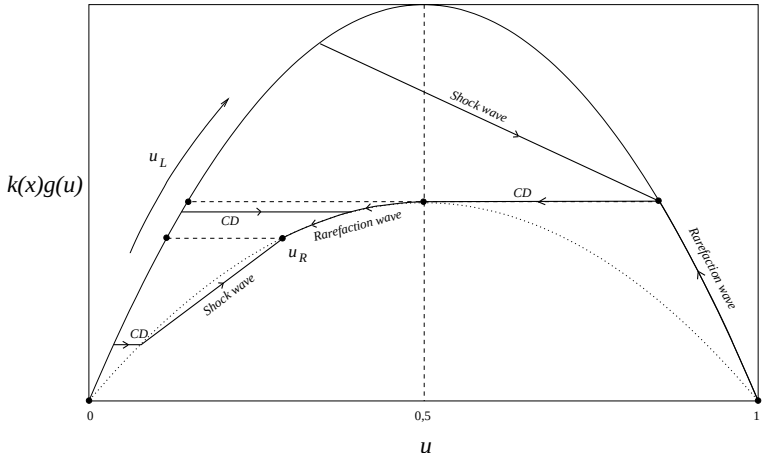

Figure 2.9: $k_L > k_R$ and $u_R < 1/2$.

– $u^+ = 1/2$, and u^+ and u_R are linked by a rarefaction wave (defined by (2.44), with $u_l = u^+$ and $u_r = u_R$).

The previous cases are represented on Fig. 2.9 (where CD denotes the contact discontinuity at the interface of the Riemann problem).

If $u_R > 1/2$:

- $0 \leq u_L < 1/2$ and $k_L g(u_L) \leq k_R g(u_R)$:
  - $u^- = u_L$,
  - u^+ is the smallest root of $k_L g(u_L) = k_R g(u^+)$, and u^+ and u_R are linked by a shock wave (defined by (2.45), with $u_l = u^+$ and $u_r = u_R$).
- $k_L g(u_L) > k_R g(u_R)$:
  - u^- is the greatest root of $k_L g(u^-) = k_R g(u_R)$, and u_L and u^- are linked by a shock wave (defined by (2.45), with $u_l = u_L$ and $u_r = u^-$),
  - $u^+ = u_R$.
- $1/2 < u_L \leq 1$ and $k_L g(u_L) \leq k_R g(u_R)$:
  - u^- is the greatest root of $k_L g(u^-) = k_R g(u_R)$, and u_L and u^- are linked by a rarefaction wave (defined by (2.44), with $u_l = u_L$ and $u_r = u^-$),
  - $u^+ = u_R$.

The previous cases are represented on Fig. 2.10. The case where $u_R = 1/2$ may be directly deduced from the two previous cases.

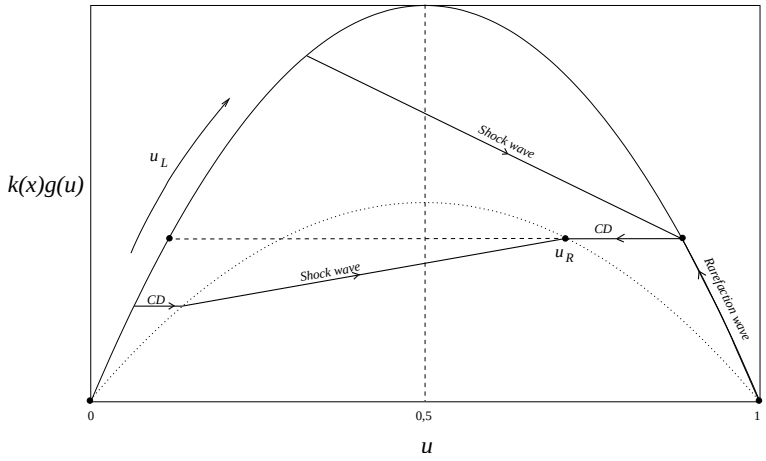

Figure 2.10: $k_L > k_R$ and $u_R > 1/2$.

Furthermore, if $k_L < k_R$, the construction of the solution u is the same as above. Indeed, setting $1 - u_L$ instead of u_L and $1 - u_R$ instead of u_R, and exchanging k_L and k_R, the solution may be constructed in the same way.

Remark 2.7. *Let us emphasize on some interesting cases of the previous description. Assume that $k_L > k_R$. Choosing u_L such that $k_L g(u_L) > k_R g(1/2)$, one cannot find a state u_R separated to u_L just by a simple wave (namely a contact discontinuity). Hence, an other wave (a shock wave or a rarefaction wave) must be introduced to allow the construction of the solution. For classical non-resonant systems (Euler equations for instance), such a problem does not occur. Now, we focus on the two last cases described when $u_R < 1/2$. The profile of u (see Fig. 2.5 and Fig. 2.12) seems to be composed of three different waves. In fact, two of them compose only one wave, and the constant state between them belongs to the same wave too. The third corresponds to the discontinuity of k.*

2.B Approximation of the resonance phenomenon

Here, we present two interesting tests computed using the Godunov scheme (2.34) with the higher order extension on a domain of $10\,m$ divided in 500 cells.

2.B.1 A wave reflecting on a discontinuity of the permeability

The initial condition for this test is

$$k(x) = \begin{cases} 1 & \text{if } 0 < x < 7,5 \\ 2 & \text{if } 7,5 < x < 10 \end{cases} \quad \text{and} \quad u_0(x) = \begin{cases} 0,45 & \text{if } 0 < x < 2,5 \\ 0,3 & \text{if } 2,5 < x < 7,5 \\ 0,5 + \frac{\sqrt{2,32}}{4} & \text{if } 7,5 < x < 10 \end{cases}.$$

The discontinuity of u_0 at $x = 2,5\,m$ generates a rarefaction wave moving to the right while the discontinuity in $x = 7,5\,m$ is in agreement with Conditions (2.19) and (2.20). At time $t = 12\,s$, the rarefaction wave starts to imping on the discontinuity in $x = 7,5\,m$ and for $t > 12\,s$, it is reflected and becomes a shock wave, see Fig. 2.11.

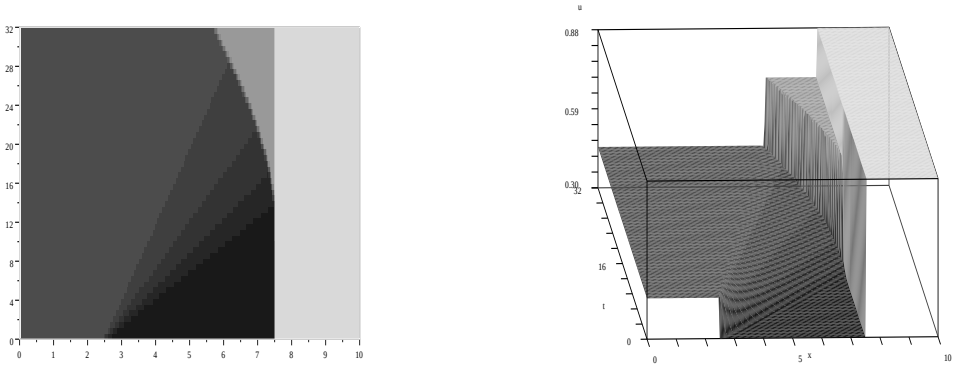

Figure 2.11: A rarefaction wave reflecting on a discontinuity of the permeability

2.B.2 A bifurcation test case

Here, the initial condition is

$$k(x) = \begin{cases} 2 & \text{if } 0 < x < 6 \\ 1 & \text{if } 6 < x < 10 \end{cases} \quad \text{and} \quad u_0(x) = \begin{cases} 0,4 & \text{if } 0 < x < 2 \\ 0,13 & \text{if } 2 < x < 6 \\ 0,5 - \frac{\sqrt{0,0952}}{2} & \text{if } 6 < x < 10 \end{cases}.$$

It generatess a rarefaction wave at $x = 2\,m$ which moves to the right while the discontinuity in $x = 6\,m$ is in agreement with Conditions (2.19) and (2.20). When the rarefaction wave meets the other discontinuity, it is separated in "two" waves: a shock wave which is reflected towards the left and a rarefaction wave bounded by the speeds 0 and $\sqrt{0,0952}$ (see Fig. 2.12). Note that these "two" waves correspond to the same eigenvalue, namely $k(1-2u)$. It is called a "bifurcation" phenomenon.

2.C BV estimates

Lemma 2.2. *Suppose $u_0 \in L^\infty \cap BV(\mathbb{R})$ and $0 \leq u_0 \leq 1$ a.e. on $\mathbb{R}$. Then the solution u_ε of the problem (2.13) satisfies the following maximum principle*

$$0 \leq u_\varepsilon(t,x) \leq 1 \text{ for a.e. } (t,x) \in \mathbb{R}_+ \times \mathbb{R} \tag{2.46}$$

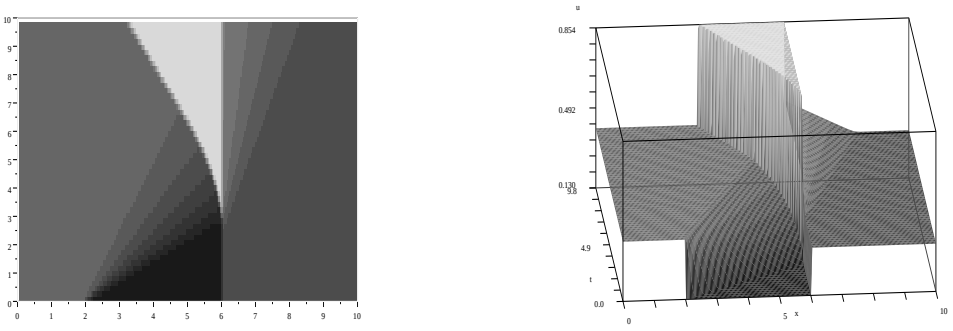

Figure 2.12: A rarefaction wave dividing in two waves

as well as the following BV estimate: for any $T > 0$*, for any* $\kappa \in [0,1]$*, there exists a constant* $C > 0$*, depending on* T*,* k_L*,* k_R *and not on* ε *such that*

$$|\Phi(u_\varepsilon, \kappa)|_{BV((0,T)\times\mathbb{R})} \leq C(|u_0|_{BV(\mathbb{R})} + |k_\varepsilon|_{BV(\mathbb{R})})\,. \tag{2.47}$$

Here, we suppose that u_0 is smooth with compact support: $u_0 \in \mathcal{C}_c^\infty(\mathbb{R})$, and that the bound $0 \leq u_0 \leq 1$ still holds. Let v^μ denotes the solution of the viscous approximation of Problem (2.13), that is

$$v_t + (k_\varepsilon(x)\, g(v))_x - \mu\, v_{xx} = 0\,, \tag{2.48}$$

with initial condition u_0. Then, as (2.48) is a parabolic equation, the solution v^μ is smooth. We state several results put together in the following lemma.

Lemma 2.3. *i. Let* w^μ *be an other smooth solution of Eq.(2.48) with initial condition* w_0*, such that* $g(w^\mu(t, \pm\infty)) = 0$*. Then the following result of comparison holds*

$$\int_{\mathbb{R}} (v^\mu(t,x) - w^\mu(t,x))^+\, dx \leq \int_{\mathbb{R}} (u_0(x) - w_0(x))^+\, dx \quad \textit{for every } t \geq 0\,. \tag{2.49}$$

ii. As the initial condition u_0*, the solution* v^μ *satisfies* $0 \leq v^\mu \leq 1$*.*

iii. For every $T > 0$*,* $R > 0$*, there exists a constant* $C_{T,R}$ *depending only on* T *and* R *such that*

$$\mu \int_0^T \int_{-R}^R |v_x^\mu|^2\, dx\, dt \leq C_{T,R}\,. \tag{2.50}$$

PROOF OF LEMMA 2.3: for the proof of the first point see Dafermos [Daf99], pp. 92-93. For the sake of completeness, we detail it.

Let η_α denote the smooth approximation of the function $v \mapsto v^+$ defined by

$$\eta_\alpha(v) = \begin{cases} 0 & \text{if } v \leq 0\,, \\ v^2/4\alpha & \text{if } 0 \leq v \leq 2\alpha\,, \\ v - \alpha & \text{if } 2\alpha \leq v\,. \end{cases}$$

Multiplying the equation

$$(v^\mu - w^\mu)_t + (k_\varepsilon\, g(v^\mu) - k_\varepsilon\, g(w^\mu))_x = \mu(v^\mu - w^\mu)_{xx}$$

by $\eta'_\alpha(v^\mu - w^\mu)$ and noting

$$\begin{aligned} A^\mu =& \partial_t \eta_\alpha(v^\mu - w^\mu) + \partial_x \left(\eta'_\alpha(v^\mu - w^\mu)[k_\varepsilon\, g(v^\mu) - k_\varepsilon\, g(w^\mu)]\right) \\ & - \eta''_\alpha(v^\mu - w^\mu)[k_\varepsilon\, g(v^\mu) - k_\varepsilon\, g(w^\mu)]\partial_x(v^\mu - w^\mu) \end{aligned}$$

we get

$$A^\mu = \mu\partial_{xx}\eta_\alpha(v^\mu - w^\mu) - \mu\eta''_\alpha(v^\mu - w^\mu)[\partial_x(v^\mu - w^\mu)]^2 \le \mu\partial_{xx}\eta_\alpha(v^\mu - w^\mu)\,.$$

Integrating this last inequality on $(0,t)\times\mathbb{R}$ yields

$$\begin{aligned} \int_{\mathbb{R}} \eta_\alpha(v^\mu(t) - w^\mu(t))\,dx - \int_{\mathbb{R}} \eta_\alpha(u_0(t) - w_0(t))\,dx & \\ \le \int_0^t \int_{\mathbb{R}} \eta''_\alpha(v^\mu - w^\mu)[k_\varepsilon\, g(v^\mu) - k_\varepsilon\, g(w^\mu)]\partial_x(v^\mu - w^\mu)\,dx\,dt & \\ \le \mathrm{Lip}(g)\int_0^t \int_{\mathbb{R}} \eta''_\alpha(v^\mu - w^\mu)\, k_\varepsilon\, |v^\mu - w^\mu| \cdot |\partial_x(v^\mu - w^\mu)|\,dx\,dt\,. & \end{aligned}$$

Notice that $g(v^\mu(t,\pm\infty)) = 0$ because $g(0) = 0$ and $v(t,\cdot)$ decreases rapidly to zero when $x \to \pm\infty$ (for the initial condition u_0 has a compact support), while $g(w^\mu(t,\pm\infty)) = 0$ by hypothesis. Eventually, letting α tend to zero yields (2.49).

We use this result of comparison to prove the L^∞ estimate on v^μ. As $g(1) = 0$, the constant function 1 is a solution to (2.48) with initial condition 1, therefore, one has

$$\int_{\mathbb{R}} (v^\mu(t,x) - 1)^+\,dx \le \int_{\mathbb{R}} (u_0(x) - 1)^+\,dx \quad \text{for every } t \ge 0\,.$$

As $0 \le u_0 \le 1$ by hypothesis, there holds $(u_0 - 1)^+ = 0$ and $v^\mu(t,x) \le 1$. Considering the function $s \mapsto s^-$ instead of $s \mapsto s^+$ and choosing $w^\mu = 0$ would give, in the same way, $v^\mu \ge 0$. Then the function v^μ satisfies the maximum principle (2.46).

Once an L^∞ estimate on the function v^μ is available, it is not really difficult to prove the energy estimate (2.50) (multiply Eq.(2.48) by v^μ and integrate by parts).

Now we turn to the BV-estimate on $\Phi(v^\mu,\kappa)$ and, to this purpose, we first give a bound on the L^1-norm of v^μ_t. For h a positive number, the function $w^\mu(t,x) = v^\mu(t+h,x)$ is a solution of Eq. (2.48) with initial condition $v^\mu(h,\cdot)$. Using the result of comparison (2.49) with $s \mapsto |s|$ instead of $s \mapsto s^+$ (it is still true), we get

$$\int_{\mathbb{R}} |v^\mu(t+h,x) - v^\mu(t,x)|\,dx \le \int_{\mathbb{R}} |v^\mu(h,x) - v^\mu(0,x)|\,dx \quad \text{for every } t \ge 0\,.$$

Dividing the result by h and letting h tend to $0+$, we get

$$\int_{\mathbb{R}} |v^\mu_t(t,x)|\,dx \le \int_{\mathbb{R}} |v^\mu_t(0,x)|\,dx \quad \text{for every } t \ge 0\,.$$

Besides, $v_t^\mu(0,x) = -k_\varepsilon'(x)\, g(u_0(x)) - k_\varepsilon(x)\, g'(u_0(x))\, u_0'(x) + \mu\, u_0''(x)$, and, since $\sup\{|g(u)|\,;\ u \in [0,1]\} = 1/4$, $\sup\{|g'(u)|\,;\ u \in [0,1]\} = 1$, and $|k_\varepsilon|_{BV(\mathbb{R})} = \displaystyle\int_{\mathbb{R}} |k_\varepsilon'(x)|\, dx$, we have

$$\int_{\mathbb{R}} |v_t^\mu(t,x)|\, dx \le \frac{1}{4}|k_\varepsilon|_{BV(\mathbb{R})} + \max\{k_L, k_R\}\, |u_0|_{BV(\mathbb{R})} + \mu \int_{\mathbb{R}} |u_0''(x)|\, dx\,. \tag{2.51}$$

Let $\kappa \in [0,1]$. Multiplying Eq.(2.48) by $\operatorname{sgn}(v^\mu - \kappa)$ yields $\partial_x(k_\varepsilon\, \Phi(v^\mu,\kappa)) \le S_1^\mu + S_2^\mu + S^\mu$ in $\mathcal{D}'((0,T)\times\mathbb{R})$, with

$$S_1^\mu = -\partial_t|v^\mu - \kappa|\,, \quad S_2^\mu = k_\varepsilon'\operatorname{sgn}(v^\mu - \kappa)\, g(\kappa) \quad \text{and} \quad S^\mu = \mu\partial_{xx}|v^\mu - \kappa|\,.$$

We evaluate each distribution S^μ against a test-function φ of $\mathcal{C}_c^\infty((0,T)\times\mathbb{R})$ such that $0 \le \varphi \le 1$. From the estimate on the L^1-norm of v_t^μ, we deduce

$$< S_1^\mu, \varphi > \le T\left(\frac{1}{4}|k_\varepsilon|_{BV(\mathbb{R})} + \max\{k_L, k_R\}\, |u_0|_{BV(\mathbb{R})} + \mu \int_{\mathbb{R}} |u_0''(x)|\, dx\right). \tag{2.52}$$

Moreover, we have

$$< S_2^\mu, \varphi > \le \frac{T}{4}|k_\varepsilon|_{BV(\mathbb{R})}\,, \tag{2.53}$$

and, from the energy estimate (2.50) and from the Cauchy-Schwarz inequality, we deduce

$$< S^\mu, \varphi > \le C_\varphi\, ||\varphi||_{L^2(\mathbb{R})}\sqrt{\mu} \tag{2.54}$$

where C_φ depends on the support of φ.

Now, it is known that $\lim\limits_{\mu\to 0} v^\mu = u_\varepsilon$ in $L^1_{loc}((0,+\infty)\times\mathbb{R})$. Therefore, each of the preceding distributions converges in $\mathcal{D}'((0,T)\times\mathbb{R})$. From (2.54), we deduce $S^\mu \to 0$ so that there holds $\partial_x(k_\varepsilon\, \Phi(u_\varepsilon,\kappa)) \le S_1 + S_2$ with

$$\begin{aligned} &< S_1, \varphi > \le T\left(\frac{1}{4}|k_\varepsilon|_{BV(\mathbb{R})} + \max\{k_L, k_R\}\, |u_0|_{BV(\mathbb{R})}\right), \\ &< S_2, \varphi > \le \frac{T}{4}|k_\varepsilon|_{BV(\mathbb{R})}\,, \end{aligned}$$

for every φ in $\mathcal{C}_c^\infty((0,T)\times\mathbb{R})$ such that $0 \le \varphi \le 1$. Therefore $k_\varepsilon\, \Phi(u_\varepsilon,\kappa) \in BV((0,T)\times\mathbb{R})$ and

$$\begin{aligned} \big|k_\varepsilon\, \Phi(u_\varepsilon,\, \kappa)\big|_{BV((0,T)\times\mathbb{R})} &\le 2\, \sup\{< \partial_x(k_\varepsilon\, \Phi(u_\varepsilon,\kappa)), \varphi >\,;\ \varphi \in \mathcal{C}_c^\infty((0,T)\times\mathbb{R};[0,1])\} \\ &\le T\left(|k_\varepsilon|_{BV(\mathbb{R})} + 2\, \max\{k_L, k_R\}\, |u_0|_{BV(\mathbb{R})}\right). \end{aligned}$$

Writing

$$\partial_x(k_\varepsilon\, \Phi(u_\varepsilon,\kappa)) = k_\varepsilon \partial_x(\Phi(u_\varepsilon,\kappa)) + k_\varepsilon'\, \Phi(u_\varepsilon,\kappa)$$

and using the estimates $|k_\varepsilon'\, \Phi(u_\varepsilon,\kappa)|_{L^1((0,T)\times\mathbb{R})} \le T\, |k_\varepsilon|_{BV(\mathbb{R})}$ and $k_\varepsilon \ge \min\{k_L, k_R\}$, we get $\Phi(u_\varepsilon,\kappa) \in BV((0,T)\times\mathbb{R})$ and

$$|\Phi(u_\varepsilon,\kappa)|_{BV((0,T)\times\mathbb{R})} \le \frac{2\,T}{\min\{k_L, k_R\}}\left(|k_\varepsilon|_{BV(\mathbb{R})} + \max\{k_L, k_R\}\, |u_0|_{BV(\mathbb{R})}\right).$$

By classical results of approximation, this is still true if $u_0 \in BV(\mathbb{R})$ and $0 \le u_0 \le 1$ a.e. This ends the proof of Lemma 2.2.

Bibliography

[BGH00] T. Buffard, T. Gallouët, and J.M. Hérard. A sequel to a rough Godunov scheme. Application to real gas flows. *Computers and Fluids*, 2000, vol. 29-7, pp. 813–847.

[BJ98] F. Bouchut and F. James. One-dimensional transport equations with discontinuous coefficients. *Nonlinear Anal.*, 1998, vol. 32-7, pp. 891–847.

[Daf99] C. Dafermos, *Hyperbolic conservation laws in continuum physics*, Springer Verlag, Berlin, 1999.

[Die95] S. Diehl. On scalar conservation laws with point source and discontinuous flux function. *SIAM J. Math. Anal.*, 1995, vol. 26-6, pp. 1425–1451.

[DLM95] G. Dal Maso, P.G. LeFloch, and F. Murat. Definition and weak stability of non conservative products. *J. Math. Pures Appl.*, 1995, vol. 74, pp. 483–548.

[EGH00] R. Eymard, T. Gallouët, and R. Herbin, Finite Volume Methods, In *Handbook of Numerical Analysis* (Vol. VII), editors : P.G. Ciarlet and J.L. Lions, North-Holland, pp. 729–1020, 2000.

[GHS01] T. Gallouët, J.M. Hérard, and N. Seguin, *Numerical modeling of two phase flows using the two fluid two pressure approach*, EDF-DRD Report HI-81/01/043/A, 2001.

[GHS02] T. Gallouët, J.M. Hérard, and N. Seguin. Some recent Finite Volume schemes to compute Euler equations using real gas EOS. *Int. J. Num. Meth. Fluids*, 2002, vol. 39-12, pp. 1073–1138.

[GHS03] T. Gallouët, J.M. Hérard, and N. Seguin. Some approximate godunov schemes to compute shallow-water equations with topography. *Computers and Fluids*, 2003, vol. 32-4, pp. 479–513.

[Giu84] E. Giusti, *Minimal surfaces and functions of bounded variation*, Monograph in Math., Birkhauser, 1984.

[GL96] J.M. Greenberg and A.Y. LeRoux. A well balanced scheme for the numerical processing of source terms in hyperbolic equation. *SIAM J. Numer. Anal.*, 1996, vol. 33-1, pp. 1–16.

[God59] S.K. Godunov. A difference method for numerical calculation of discontinuous equations of hydrodynamics. *Mat. Sb.*, 1959, pp. 271–300. In Russian.

[GR91] T. Gimse and N.H. Risebro, Riemann problems with a discontinuous flux function, In *Third International Conference on Hyperbolic Problems, Vol. I, II (Uppsala, 1990).* Studentlitteratur, pp. 488–502, Lund, 1991.

[GR96] E. Godlewski and P.A. Raviart, *Numerical approximation of hyperbolic systems of conservation laws*, Springer Verlag, 1996.

[GR02] E. Godlewski and P.A. Raviart. The numerical coupling of nonlinear hyperbolic systems of conservation laws: I. The scalar case. submitted for publication, 2002.

[HH83] A. Harten and J.M. Hyman. A self-adjusting grid for the computation of weak solutions of hyperbolic conservation laws. *J. Comp. Phys.*, 1983, vol. 50, pp. 235–269.

[IMPT88] E. Isaacson, D. Marchesin, B. Plohr, and B. Temple. The Riemann problem near a hyperbolic singularity: the classification of solutions of quadratic Riemann problems. I. *SIAM J. Applied Math.*, 1988, vol. 48-5, pp. 1009–1032.

[IT86] E. Isaacson and B. Temple. Analysis of a singular hyperbolic system of conservation laws. *J. Diff. Equations*, 1986, vol. 65-2, pp. 250–268.

[IT88] E. Isaacson and B. Temple. The Riemann problem near a hyperbolic singularity. II, III. *SIAM J. Applied Math.*, 1988, vol. 48-6, pp. 1287–1318.

[IT90] E. Isaacson and B. Temple, Nonlinear resonance in inhomogeneous systems of conservation laws, In *Mathematics of nonlinear science (Phoenix, AZ, 1989)*. Amer. Math. Soc., pp. 63–77, Providence, RI, 1990.

[KR95] C. Klingenberg and N.H. Risebro. Convex conservation laws with discontinuous coefficients. Existence, uniqueness and asymptotic behavior. *Comm. Part. Diff. Equations*, 1995, vol. 20-11-12, pp. 1959–1990.

[KR99] R.A. Klausen and N.H. Risebro. Stability of conservation laws with discontinuous coefficients. *J. Diff. Equations*, 1999, vol. 157-1, pp. 41–60.

[KR01] C. Klingenberg and N.H. Risebro. Stability of a resonant system of conservation laws modeling polymer flow with gravitation. *J. Diff. Equations*, 2001, vol. 170-2, pp. 344–380.

[KRT01] K.H. Karlsen, N.H. Risebro, and J.D. Towers, *On a nonlinear degenerate parabolic transport-diffusion equation with a discontinuous coefficient*, 2001. Available in the conservation law preprint server
http://www.math.ntnu.no/conservation/.

[Kru70] S. Kruzkov. First-order quasilinear equations in several space variables. *Mat. Sb.*, 1970, vol. 123, pp. 228–255.

[LeR99] A.Y. LeRoux, Riemann solvers for some hyperbolic problems with a source term, In *Actes du 30ème Congrès d'Analyse Numérique, CANum '98 (Arles, 1998)*. Soc. Math. Appl. Indust., pp. 75–90, Paris (France), 1999.

[LTW95a] L. Lin, B. Temple, and J. Wang. A comparison of convergence rates for Godunov's method and Glimm's method in resonant nonlinear systems of conservation laws. *SIAM J. Numer. Anal.*, 1995, vol. 32-3, pp. 824–840.

[LTW95b] L. Lin, B. Temple, and J. Wang. Suppression of oscillations in Godunov's method for a resonant non-strictly hyperbolic system. *SIAM J. Numer. Anal.*, 1995, vol. 32-3, pp. 841–864.

[Seg99] N. Seguin, *Génération et validation de Rozavel, un code équilibre en hydraulique 2D.* Mémoire de D.E.A., Université de Bordeaux I, 1999.
Available on http://www-gm3.univ-mrs.fr/∼leroux/publications/n.seguin.html.

[Tem82] B. Temple. Global solution of the Cauchy problem for a class of 2×2 nonstrictly hyperbolic conservation laws. *Adv. in Appl. Math.*, 1982, vol. 3-3, pp. 335–375.

[Tow00] J.D. Towers. Convergence of a difference scheme for conservation laws with a discontinuous flux. *SIAM J. Numer. Anal.*, 2000, vol. 38-2, pp. 681–698.

[Tow01] J.D. Towers. A difference scheme for conservation laws with a discontinuous flux: the nonconvex case. *SIAM J. Numer. Anal.*, 2001, vol. 39-4, pp. 1197–1218.

[Van79] B. VanLeer. Toward the ultimate conservative difference scheme V. A second order sequel to Godunov's method. *J. Comp. Phys.*, 1979, vol. 32, pp. 101–136.

[Vas01] A. Vasseur. Strong traces for weak solutions to multidimensional conservation laws. *Arch. of Rat. Mech. Anal.*, 2001, vol. 160-3, pp. 181–193.

[Vas02] A. Vasseur. Well-posedness of scalar conservation laws with singular sources. *preprint*, 2002.

[Vol67] A.I. Vol'pert. The space BV and quasilinear equations. *Math. USSR Sb.*, 1967, vol. 73-115, pp. 225–267.

Chapitre 3

Traitement numérique de termes sources raides dans un système convectif par splitting d'opérateur ou par décentrement

On s'intéresse maintenant au traitement numérique des termes sources pour les systèmes hyperboliques. Dans le cadre des écoulements diphasiques, ces termes sources peuvent avoir différentes échelles de temps caractéristiques, c'est-à-dire que le retour à l'équilibre (qui correspond pour les processus de relaxation à un modèle homogène ayant un nombre d'équations aux dérivées partielles inférieur à celui du modèle initial) nécessite des temps plus ou moins longs suivant les termes considérés. Bien sûr, ces échelles de temps peuvent être complètement distinctes du pas de temps utilisé lors de la simulation. Donc, le traitement numérique pour être précis et stable doit tenir compte de ces échelles de temps.

Pour cela, on va s'intéresser ici à des systèmes de la forme

$$W(t,x)_t + F(W(t,x))_x = S(W(t,x))a(x)_x \tag{3.1}$$

où $W = W(t,x)$ est l'inconnue, à valeurs dans $\mathbb{R}^d$. On restreint cette présentation au cas unidimensionnel, mais sa généralisation au cas multidimensionnel est directe. De plus, on a $F : \mathbb{R}^d \to \mathbb{R}^d$, $S : \mathbb{R}^d \to \mathbb{R}^d$ et $a : \mathbb{R} \to \mathbb{R}$. On compare deux techniques différentes d'approximation des solutions (avec discontinuités) du système (3.1). La première correspond à la technique classique de splitting d'opérateur [Yan68]. Celle-ci décompose le système (3.1) en deux systèmes:

$$W_t + F(W)_x = 0 \tag{3.2}$$

$$\text{et } W_t = S(W)a(x)_x. \tag{3.3}$$

Ainsi, lors d'un pas de temps Δt, le système (3.2) est résolu par une méthode Volumes Finis

classique (voir plus loin pour les notations)

$$\Delta x\big(W_i^{n+1/2} - W_i^n\big)) + \Delta t\big(F_{i+1/2}^n - F_{i-1/2}^n\big)) = 0 \tag{3.4}$$

et la solution obtenue est alors utilisée comme condition initiale pour la résolution numérique du système d'équations différentielles (3.3), par exemple :

$$\Delta x(W_i^{n+1} - W_i^{n+1/2}) = \Delta t S(W_i^{n+1/2}) \frac{a(x_{i+1}) - a(x_{i-1})}{2}.$$

Bien que cette technique de prise en compte des termes sources n'ait pas une précision optimale, en particulier pour l'approximation des états stationnaires (*i.e.* les états W vérifiant $F(W(t,x))_x = S(W(t,x))a(x)_x$), elle peut s'avérer très robuste pour chaque pas. D'ailleurs, cette technique est abondamment utilisée dans les codes indutriels. La seconde technique a été introduite par A.Y. LeRoux [GL96b], [LeR98]. Celle-ci introduit tout d'abord une discrétisation du terme $a(x)$ notée $a_{\Delta x}(x)$ définie par

$$a_{\Delta x}(x) = \frac{1}{\Delta x} \int_{x_{i-1/2}}^{x_{i+1/2}} a(x)\, dx, \quad \text{pour } x \text{ dans }]x_{i-1/2}; x_{i+1/2}[.$$

Le système (3.1) devient alors

$$V(t,x)_t + C(V(t,x))V(t,x)_x = 0 \tag{3.5}$$

où

$$V = \begin{pmatrix} a_{\Delta x} \\ W \end{pmatrix} \quad \text{et} \quad C(V) = \begin{pmatrix} 0 & 0 \\ S(W) & \dfrac{\partial F(W)}{\partial W} \end{pmatrix}.$$

Comme $(a_{\Delta x})_t = 0$, le schéma Volumes Finis associé au système (3.5) s'écrit alors

$$\Delta x(W_i^{n+1/2} - W_i^n) + \Delta t\big(F(W_{i+1/2}^-) - F(W_{i-1/2}^+)\big) = 0 \tag{3.6}$$

où $W_{i+1/2}^-$ et $W_{i+1/2}^+$, $i \in \mathbb{Z}$ sont calculés à partir du problème de Riemann associé au système non conservatif (3.5). Les exposants $-$ et $+$ font respectivement référence à la solution à gauche et à droite de l'interface $x_{i+1/2}$, car la donnée $a_{\Delta x}$ y est discontinue, ce qui induit un saut de la solution à travers l'interface $x_{i+1/2}$. Si $W_{i+1/2}^-$ et $W_{i+1/2}^+$ correspondent à la solution exacte le schéma (3.6) est dit « équilibre » car il maintient tous les états définis par la forme discrète de l'équation $F(W(t,x))_x = S(W(t,x))a(x)_x$. De plus, le terme source est pris en compte directement dans le calcul de $W_{i+1/2}^-$ et $W_{i+1/2}^+$, d'où l'appellation de « décentrement du terme source ». On note que $S(W)(a_{\Delta x})_x$ n'apparaît pas explicitement dans le schéma (3.6) car cette écriture est obtenue par intégration sur $]x_{i-1/2}; x_{i+1/2}[$ et $(a_{\Delta x})_x$ est nul sur cet intervalle. Cette approche permet une résolution précise et robuste, puisqu'elle est l'extension naturelle du schéma de Godunov [God59] au cadre des systèmes avec termes sources.

Dans le cadre des écoulements diphasiques, les termes sources sont en général de la forme

$$S(W(t,x)), \text{ voire } S(W(t,x),x).$$

Pour appliquer la technique précédente, il suffit alors de définir la fonction

$$a_{\Delta x}(x) = \frac{x_{i-1/2} + x_{i+1/2}}{2}, \quad \text{pour } x \text{ dans }]x_{i-1/2}; x_{i+1/2}[$$

qui correspond à la discrétisation de la fonction $a(x) = x$. Les deux méthodes, splitting d'opérateur et schéma équilibre, s'étendent naturellement au cas multidimensionnel.

Le système qui est étudié dans ce chapitre est le système de Saint-Venant (ou *shallow-water equations*) avec un terme source de topographie. Ce système est de la forme (3.1) et la partie homogène est identique aux équations d'Euler dans le cas isentropique avec une loi d'état particulière. Néanmoins, à la différence de la dynamique des gaz, le cas du vide (appelé assèchement dans le contexte hydraulique) doit être pris en compte, aussi bien en tant que condition initiale qu'en tant qu'état pouvant apparaître lors d'un écoulement. D'ailleurs, ce type de configuration d'écoulement est le plus souvent dû à la présence du terme source de topographie. Ce système est donc un bon candidat pour tester la robustesse et la précision des deux méthodes numériques citées précédemment puisque les simulations les plus complexes vont de pair avec la présence du terme source. En outre, dans un souci de gain de temps calcul, le schéma Volumes Finis (3.4) et le calcul de $W^-_{i+1/2}$ et $W^+_{i-1/2}$ dans (3.6) sont basés sur une linéarisation du problème de Riemann (tous deux sont donc des schémas de Godunov approchés, comme ceux étudiés au chapitre 1). De ce fait, la robustesse en présence de zones sèches (bancs découvrants) ne semble plus garantie. Dans l'annexe A on étudie le comportement du schéma linéarisé pour le système de Saint-Venant homogène (ainsi qu'en dynamique des gaz, avec ou sans turbulence) en présence de zones sèches. De même, dans ce chapitre sont présentés différents cas où des zones sèches apparaissent, soit par un phénomène convectif (mais avec une topographie non constante), soit par le terme source et la condition limite. Malgré le caractère linéarisé des deux algorithmes, le vide est bien reproduit, sans recours au « clipping » (c'est-à-dire à l'ajustement de valeurs de mailles non physiques, qui consiste à utiliser $h_i^n = \max(0,h_i^n)$ où h correspond à la hauteur d'eau). Par contre, du point de vue de la précision, la technique basée sur la réécriture (3.5) est bien supérieure, notamment lors de la simulation d'écoulements convergeant vers un état stationnaire [GM97]. Pour améliorer la vitesse de convergence par rapport au raffinement du maillage, une technique basée sur la méthode MUSCL [Van79] est introduite. Celle-ci correspond exactement à celle du chapitre 2, en prenant en compte la forme des solutions régulières stationnaires. Cependant, contrairement à l'étude du chapitre 2, le système ici est non homogène et on peut assister à une perte de « stationnarité » (quand $t \to +\infty$) si la méthode MUSCL ne subit pas la modification proposée, c'est-à-dire que la norme L^2 de la variation en temps de l'approximation ne tend pas vers zéro au cours du temps.

Un autre intérêt des équations de Saint-Venant avec topographie approchées par le système (3.5) est que cette écriture introduit le phénomène de résonnance, déjà détecté dans le modèle du chapitre 2 et qui intervient dans le système bifluide à deux pressions du chapitre 4. L'étude numérique dans ce chapitre est donc d'autant plus utile qu'elle permet d'apprécier le comportement des schémas de Godunov approchés VFRoe-ncv pour un système résonnant mais non conservatif (contrairement au cas traité dans le chapitre 2).

Some approximate Godunov schemes to compute shallow-water equations with topography

Co-authored with Thierry Gallouët and Jean-Marc Hérard.

Abstract

We study here the computation of shallow-water equations with topography by Finite Volume methods, in a one-dimensional framework (though all methods introduced may be naturally extended in two dimensions). All methods are based on a dicretisation of the topography by a piecewise function constant on each cell of the mesh, from an original idea of A.Y. LeRoux *et al.*. Whereas the Well-Balanced scheme of A.Y. LeRoux is based on the exact resolution of each Riemann problem, we consider here approximate Riemann solvers. Several single step methods are derived from this formalism, and numerical results are compared to a fractional step method. Some test cases are presented: convergence towards steady states in subcritical and supercritical configurations, occurence of dry area by a drain over a bump and occurence of vacuum by a double rarefaction wave over a step. Numerical schemes, combined with an appropriate high order extension, provide accurate and convergent approximations.

3.1 Introduction

We study in this paper some approximate Godunov schemes to compute shallow-water equations with a source term of topography, in a one-dimensional framework. All methods presented may be extended naturally to the 2D model.

Shallow-water equations are based on conservation laws and provide a hyperbolic system. However, topography introduces some source term related to the unknown. Hence, analytic properties of the model of isentropic Euler equations are deeply modified, in comparison with the homogeneous case. For instance, a well-known problem is the occurence of other equilibrium states (or steady states), due to the presence of the source term.

Several ways to compute conservation laws with source term have already been investigated. The main problem is the approximation of the source term and the numerical preservation of properties

À paraître dans *Computers and Fluids*, volume 32, numéro 4, pages 479-513, 2003.

fulfilled by the continuous system. Some Finite Volume method have been proposed, in particular the Well Balanced schemes, which can maintain *all* steady states. These schemes have been initially introduced by J.M. Greenberg and A.Y. LeRoux in [GL96b] and [GLBN97] in the scalar case (see also [GL96a] and [BPV02]). Well Balanced schemes have been recently extended to shallow-water equations with topography in [Bon97] and [LeR98] and friction in [CL99]. Since the Well Balanced scheme is based on an exact Riemann solver as the Godunov scheme (see [God59]), its main drawbacks are its calculation cost and the need to compute the "exact" solution of the Riemann problem. Other Finite Volume methods to deal with source terms exist too, for instance based on the Roe scheme (see [Roe81] and [GNVC00]), or based on another approximation of the source term, like in [LeV98].

Some properties of the continuous model (Riemann invariants, jump relations, ...) are first exposed, and a study of the Riemann problem is briefly recalled. Thereafter, some approximate Gudunov methods are introduced to compute shallow-water equations, derived from the VFRoe-ncv formalism. VFRoe-ncv stands for the scheme VFRoe using a non conservative variable. Finite Volume scheme VFRoe should not be confused with Roe scheme. VFRoe-ncv schemes are Finite Volume schemes, based on a linearised Riemann problem written with respect to a non conservative variable. Some applications of VFRoe-ncv schemes are provided for the Euler equations (in [MFG99], [BGH00] and [GHS00]), for shallow-water equations with a flat bottom in [BGH98b] and for turbulent compressible flows [BGH98a]. The VFRoe-ncv schemes are based on an arbitrary change of variable, and on a linearisation of each interface Riemann problem. In the homogeneous case, the numerical flux is defined using the exact solution of the linearised Riemann problem and the conservative flux. However, the source term "breaks" the conservativity of the model. Thus, using a piecewise constant function to approximate the bottom, some approximate Riemann solvers are presented. The main advantages of this approach are the natural integration of the source term in the numerical methods and the use of a linearised Riemann problem, which minimizes the CPU time. Note that a scheme which exactly preserves a large class of steady states is obtained. In addition, a fractional step method is performed, based on the VFRoe-ncv scheme introduced in [BGH98b]. This method enables to deal with vacuum and provides good results, too. To complete this presentation, a higher order extension is provided, to increase the accuracy of the schemes when computing unsteady configurations or flows at rest.

Several numerical experiments are presented. All the test cases are one-dimensional, and are based on a non trivial topography. Indeed, applications of shallow-water equations are one-dimensional or two-dimensional configurations. Hence, computational limitations are rather different from the gas dynamics frame where the main applications are 2D and 3D. Therefore, numerical experiments in an industrial context may be here performed on mesh containing several hundreds nodes. The tests include subcritical and transcritical flows over a bump [GM97] and a drain with a non flat bottom. The convergence towards steady states is measured. A vacuum occurence by a double rarefaction wave over a step is tested too. All the numerical tests confirm the good behaviour of the numerical methods, including the fractional step method.

Eventually, some complementary tests with the Godunov and the VFRoe method are provided in the appendix.

3.2 The shallow-water equations with topography

3.2.1 Governing equations

The shallow-water equations represent a free surface flow of incompressible water. The two-dimensional system may be written as follows:

$$h_{,t} + (hu)_{,x} + (hv)_{,y} = 0 \tag{3.7a}$$

$$(hu)_{,t} + (hu^2)_{,x} + (huv)_{,y} + g\Big(\frac{h^2}{2}\Big)_{,x} = -gh(Z_f)_{,x} \tag{3.7b}$$

$$(hv)_{,t} + (huv)_{,x} + (hv^2)_{,y} + g\Big(\frac{h^2}{2}\Big)_{,y} = -gh(Z_f)_{,y} \tag{3.7c}$$

where h denotes the water height, $\mathbf{u} = {}^t(u, v)$ the velocity, g the gravity constant and ∇Z_f the bed slope (g and $Z_f(x, y)$ are given, and Z_f must be at least $\mathcal{C}^0(\mathbb{R}^2)$) (see figure 3.1).

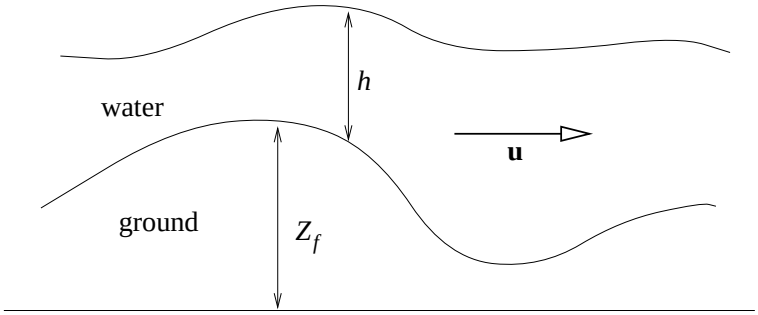

Figure 3.1: Mean variables

This study is restricted to the computation by Finite Volume schemes (see [EGH00]). Since the hyperbolic system (3.7) remains unchanged under frame rotation, this two-dimensional problem may be solved considering on each interface of the mesh the following system:

$$h_{,t} + (hu_n)_{,n} = 0 \tag{3.8a}$$

$$(hu_n)_{,t} + \left(hu_n^2 + g\frac{h^2}{2}\right)_{,n} = -gh(Z_f)_{,n} \tag{3.8b}$$

$$(hu_\tau)_{,t} + (hu_n u_\tau)_{,n} = 0 \tag{3.8c}$$

where $u_n = \mathbf{u}.n$, $u_\tau = \mathbf{u}.\tau$, n and τ the normal and the tangential vector to the interface ($||n|| = ||\tau|| = 1$), and $(\ )_{,n}$ the derivate along the normal vector n.

The pure one-dimensional shallow-water equations may be written as follows:

$$h_{,t} + (hu)_{,x} = 0 \tag{3.9a}$$

$$(hu)_{,t} + \left(hu^2 + g\frac{h^2}{2}\right)_{,x} + ghZ_f'(x) = 0. \tag{3.9b}$$

We focus in this paper on the numerical resolution of the one-dimensional system (3.9).
Let us note that h and hu (also denoted Q in the following) are the conservative variables. So, vacuum (or dry bed) may be represented by $h = hu = 0$, which implies that u is not defined.

Remark 3.1. *The change of variable from (h, Q) to (h, u) leads to the following equations for smooth solutions:*

$$\begin{aligned} h_{,t} + Q_{,x} &= 0 \\ u_{,t} + \psi_{,x} &= 0. \end{aligned}$$

where $\psi = (u^2/2 + g(h + Z_f))$.
These equations enable to define some stationary smooth solutions as follows:

$$Q_{,x} = 0 \quad \textit{and} \quad \psi_{,x} = 0. \tag{3.10}$$

One may add to these equations Rankine Hugoniot relations (on smooth topography) for stationary shocks to complete the definition of stationary states.

3.2.2 The Riemann problem on a flat bottom

Assuming that the river bed is flat (ie $Z_f'(x) = 0$), the system (3.9) becomes homogeneous. Hence, we obtain a conservative system, which leads to the following Riemann problem:

$$\begin{cases} h_{,t} + Q_{,x} = 0 \\ Q_{,t} + \left(\dfrac{Q^2}{h} + g\dfrac{h^2}{2}\right)_{,x} = 0 \\ (h, Q)(x, 0) = \begin{cases} (h_L, Q_L) & \text{if } x < 0, \\ (h_R, Q_R) & \text{if } x > 0. \end{cases} \end{cases} \tag{3.11}$$

This problem, which is also the Riemann problem for isentropic Euler equations (for a particular state law) may be classically solved. Its solution is a similarity solution (ie a function of x/t) composed by three constant states, (h_L, Q_L), (h_1, Q_1) and (h_R, Q_R) separated by two Genuinely Non Linear (GNL) fields associated with eigenvalues $u - c$ and $u + c$ (where $c = \sqrt{gh}$). The intermediate state (h_1, Q_1) may be computed using through the 1-wave:

$$u_1 = \begin{cases} u_L - 2(\sqrt{gh_1} - \sqrt{gh_L}) & \text{if } h_1 < h_L, \\ u_L - (h_1 - h_L)\sqrt{g\dfrac{h_1 + h_L}{2h_1h_L}} & \text{if } h_1 > h_L. \end{cases} \tag{3.12}$$

and through the 2-wave:

$$u_1 = \begin{cases} u_R + 2(\sqrt{gh_1} - \sqrt{gh_R}) & \text{if } h_1 < h_R, \\ u_R + (h_1 - h_R)\sqrt{g\dfrac{h_1 + h_R}{2h_1h_R}} & \text{if } h_1 > h_R. \end{cases} \tag{3.13}$$

The latter two curves are derived from the Riemann invariants (when $h_1 < h_L$ and $h_1 < h_R$) for rarefaction waves and from the Rankine Hugoniot relations (when $h_1 > h_L$ and $h_1 > h_R$) for shock waves. Note that the intermediate velocity u_1 is defined only if:

$$u_R - u_L < 2(\sqrt{gh_R} + \sqrt{gh_L}). \tag{3.14}$$

Otherwise, h_1 and Q_1 become null, and u_1 is undefined.

3.2.3 The Riemann problem with a piecewise constant topography

Following the idea developed by A.Y. LeRoux in [LeR98], the topography is described by a piecewise constant function. Therefore, adding the "partial" differential equation concerning Z_f, the following Riemann problem may be obtained:

$$\begin{cases} Z_{f,t} = 0 \\ h_{,t} + (hu)_{,x} = 0 \\ Q_{,t} + \left(\dfrac{Q^2}{h} + g\dfrac{h^2}{2}\right)_{,x} + gh(Z_f)_{,x} = 0 \\ (h, Q, Z_f)(x,0) = \begin{cases} (h_L, Q_L, Z_{f\,L}) & \text{if } x < 0, \\ (h_R, Q_R, Z_{f\,R}) & \text{if } x > 0. \end{cases} \end{cases} \tag{3.15}$$

Note that this Riemann problem does not correspond to the Riemann problem associated with the system (3.9), since the topography is not smooth. The jump of topography along the curve $x/t = 0$ introduces a problem for the definition of the product of distributions, focusing on non smooth solutions (see [Col92] and [DLM95] for more details). So, the jump relations across the discontinuity $x/t = 0$ are not defined. Assuming that $h > 0$ and restricting to smooth solutions, the system (3.15) may be written:

$$Z_{f,t} = 0 \tag{3.16a}$$
$$h_{,t} + Q_{,x} = 0 \tag{3.16b}$$
$$u_{,t} + \left(\frac{u^2}{2} + g(h + Z_f)\right)_{,x} = 0. \tag{3.16c}$$

We note $\psi = (u^2/2 + g(h + Z_f))$ in the following. One may deduce the conservation law on entropy for non viscous smooth solutions:

$$\eta_{,t} + (Q\psi)_{,x} = 0 \tag{3.17}$$
$$\eta = h\frac{u^2}{2} + g\frac{h^2}{2} + ghZ_f. \tag{3.18}$$

Moreover, system (3.16) provides the Riemann invariants through the stationary wave. Since the wave located at $x/t = 0$ is a contact discontinuity, we assume that the Rankine Hugoniot relations identify with the Riemann invariants. Thus, the Riemann problem (3.15) admits a Linearly Degenerated field of speed 0 such that:

$$[\![Q]\!] = 0 \tag{3.19a}$$
$$[\![\psi]\!] = 0 \tag{3.19b}$$

where $[\![\alpha]\!]$ represents the jump of α across the wave.

Two Genuinely Non Linear fields also compose the solution of the Riemann problem (3.15), which are the same as in the flat bottom case. Hence, to connect a state W to a state W_a through the wave $u - c$, one may use the following relations (a rarefaction wave occurs when $h < h_a$, and a

shock wave occurs when $h > h_a$):

$$Z_f = Z_{f_a} \tag{3.20a}$$

$$u = \begin{cases} u_a - 2(\sqrt{gh} - \sqrt{gh_a}) & \text{if } h < h_a, \\ u_a - (h - h_a)\sqrt{g\dfrac{h + h_a}{2hh_a}} & \text{if } h > h_a. \end{cases} \tag{3.20b}$$

In the same way, to connect a state W to a state W_b through the wave $u + c$, one may use the following relations (a rarefaction wave occurs when $h < h_b$, and a shock wave occurs when $h > h_b$):

$$Z_f = Z_{f_b} \tag{3.21a}$$

$$u = \begin{cases} u_b + 2(\sqrt{gh} - \sqrt{gh_b}) & \text{if } h < h_b, \\ u_b + (h - h_b)\sqrt{g\dfrac{h + h_b}{2hh_b}} & \text{if } h > h_b. \end{cases} \tag{3.21b}$$

Moreover, to connect a state W to a state W_c through the stationary wave, one uses the Riemann invariants:

$$Q = Q_c \tag{3.22a}$$

$$\psi = \psi_c \tag{3.22b}$$

Remark 3.2. *Several remarks about the resolution of the Riemann problem* (3.15) *follow.*

i. Since equation (3.9b) *is not conservative when the bottom Z_f is discontinuous, the associated jump relation* (3.19b) *is just the sense we give to the third equation of* (3.15) *at the discontinuity of Z_f. Since this discontinuity is a contact discontinuity for* (3.15)*, this choice is quite natural because it corresponds to the Riemann invariants in the associated field.*

ii. Even assuming (3.19b)*, the resolution of the Riemann problem* (3.15) *remains undetermined. Indeed, combining equations* (3.22a) *and* (3.22b)*, the connection through the stationary wave results in looking for solution (h, Q) of the couple of equations $Q = Q_c$ and $Q_c^2/(2h^2) + g(h + Z_f) = \psi_c$ where Z_f, Q_c and ψ_c are given. This equation may admit zero, one or two solutions. Therefore, without additionnal informations, the solution remains unknown.*

iii. Let us emphasize that the Riemann problem (3.15) *may be resonant, that is, a GNL wave may be superposed with the stationary wave. Moreover, waves are not ordered which renders the resolution of the Riemann problem much more complex than in the flat bottom case.*

At this stage, it clearly appears that the classical method to solve the Riemann problem (described in [GR96] for instance) is not sufficient to construct the solution of (3.15)*, owing to items 1, 2 and 3.*

iv. A.Y. LeRoux et al. *have proposed an original method to solve the Riemann problem in [LeR98], [Seg99] and [CL99]. It is based on a linear connection between Z_{f_L} and Z_{f_R} and the study of stationary solutions of* (3.9) *inside the connection. Some relations naturally appear and allow the complete resolution of the Riemann problem* (3.15)*. In particular, except when a stationary shock wave occurs, states on each side of the discontinuity $x/t = 0$*

must be either both subcritical or both supercritical. Therefore, no ambiguity remains when the parametrisation (3.22) *admits two solutions because one of the two solutions is subcritical while the other is supercritical.*

v. *Note that, in a simpler framework (see [SV03]), a similar method may provide existence and uniqueness of the entropy solution.*

We will discuss below two families of schemes which are intended to provide a convergent approximation of the above mentioned system. The first series is based on straightforward approximate Godunov schemes which account for topography. The second series is based on the fractional step method.

3.3 Single step methods

We present in this section several ways to solve the shallow-water equations with source term by Finite Volume schemes (see [EGH00] and [Tor97] for instance). The description of the methods computed herein is split in two steps: the Finite Volume scheme provided by integration of (3.9) and the solver at each interface.

3.3.1 An approximate Godunov-type scheme

We introduce herein a Finite Volume scheme following the idea proposed by J.M. Greenberg, A.Y. LeRoux *et al.* in [GL96b] and [GLBN97].

Focusing on system (3.9), it consists in using a piecewise bottom, flat on each cell, in the "continuous" framework (see [LeR98] and [CL99]). Thus, the source term $-ghZ_f'(x)$ is reduced to a sum of Dirac masses occuring on each interface [Col92]. Hence, since the Finite Volume formalism is based on the integration of the system (3.9) on a cell $]x_{i-1/2};x_{i+1/2}[\times[t^n;t^{n+1}[$, the source term does not appear explicitly (contrary to the scheme investigated in [GNVC00] for instance). As mentioned above, such an approximation of the topography introduces a stationary wave at the interface of each local Riemann problem. Though the Well Balanced scheme of J.M. Greenberg and A.Y. LeRoux is based on the exact solution of (3.15), we focus here on approximate Riemann solvers. These Riemann solvers are based on an approximate solution of the problem (3.15), and the numerical flux is computed from the conservative flux and the approximate solution at each interface.

Let us note $W = {}^t(Z_f, h, Q)$ the conservative variable, $F(W) = {}^t(0, Q, hu^2+gh^2/2)$ the associated conservative flux and Δx_i and Δt the space and time steps. We denote W_i^n the approximation de $\frac{1}{\Delta x_i}\int_{x_{i-1/2}}^{x_{i+1/2}} W(x,t^n)dx$.
So, the Finite Volume scheme may be written as follows:

$$W_i^{n+1} = W_i^n - \frac{\Delta t}{\Delta x_i}\Big(F\big(W^*_{i+1/2}(0^-;W_i,W_{i+1})\big) - F\big(W^*_{i-1/2}(0^+;W_{i-1},W_i)\big)\Big) \tag{3.23}$$

where $W^*_{i+1/2}(x/t; W_i, W_{i+1})$ is the (exact or approximate) solution of the Riemann problem (3.15) with $L = i$ and $R = i+1$. As mentioned above, the source term only contributes to the computation of the (exact or approximate) solutions $W^*_{i+1/2}(x/t; W_i, W_{i+1})$ but it does not appear explicitly in the expression of the scheme (3.23). However, the approximation of the topography by a piecewise constant function implies that the numerical flux is not continuous through each interface of the mesh, contrary to the homogeneous and conservative case. So, whereas the numerical flux associated with equation (3.9a) has to be continuous (since this equation is homogenous and conservative), the numerical flux associated with equation (3.9b) becomes discontinuous in the non flat bottom case, according to the relations (3.19). In order to obtain a constant numerical flux for equation (3.9a), we will have, in some cases, to modify the scheme (3.23) (see (3.27) for instance).

Note that the Finite Volume scheme (3.23) associated with the exact interface Riemann solver (ie the Well-Balanced scheme presented in [LeR98]) is able to maintain all steady states. Moreover, let us emphasize that the scheme (3.23) may be easily extended to a multi-dimensional framework (indeed, the formalism presented is very similar to Finite Volume schemes).

3.3.2 The VFRoe-ncv formalism

Since the Well Balanced scheme [LeR98] is based on an exact Riemann solver as the Godunov scheme [God59], its main drawbacks are its calculation cost and the need to compute the exact solution of the Riemann problem (3.15). Thus, we suggest to compute the state $W^*_{i+1/2}(x/t; W_i, W_{i+1})$ by approximate Riemann solvers.

All the Riemann solvers presented here may be derived from the VFRoe-ncv formalism [BGH00, GHS00]. The VFRoe-ncv schemes are based on the exact solution of a linearised Riemann problem. Their construction may be split in three steps. The first step consists in writting the initial system under a non-conservative form, by an arbitrary change of variable $Y(W)$ (we denote by $W(Y)$ the inverse change of variable). Afterwards, the Riemann problem (3.15) is linearised averaging the convection matrix:

$$\begin{cases} Y_{,t} + B(\widehat{Y})Y_{,x} = 0 \\ Y(x,0) = \begin{cases} Y_L = Y(W_L) & \text{if } x < 0 \\ Y_R = Y(W_R) & \text{if } x > 0 \end{cases} \end{cases} \tag{3.24}$$

where $B(Y) = (W_{,Y}(Y))^{-1} F_{,W}(W(Y))\, W_{,Y}(Y)$ and $\widehat{Y} = \dfrac{Y_L + Y_R}{2}$.
As a result, the Riemann problem (3.15) becomes a linear Riemann problem, which is solved exactly. Denoting $(\widetilde{l_k})_{k=1,2,3}$ and $(\widetilde{r_k})_{k=1,2,3}$ respectively left and right eigenvectors of $B(\widehat{Y})$, $(\widetilde{\lambda_k})_{k=1,2,3}$ eigenvalues of $B(\widehat{Y})$, the exact solution $Y^*(x/t; Y_L, Y_R)$ of (3.24) is defined by:

$$\begin{aligned} Y^*\left((x/t)^-; Y_L, Y_R\right) &= Y_L + \sum_{x/t > \widetilde{\lambda_k}} \left({}^t\widetilde{l_k}.[\![Y]\!]_L^R\right)\widetilde{r_k} \\ Y^*\left((x/t)^+; Y_L, Y_R\right) &= Y_R - \sum_{x/t < \widetilde{\lambda_k}} \left({}^t\widetilde{l_k}.[\![Y]\!]_L^R\right)\widetilde{r_k}. \end{aligned} \tag{3.25}$$

where $[\![\alpha]\!]_L^R = \alpha_R - \alpha_L$. Both are equal when $x/t \neq \widetilde{\lambda_k}$ and $x/t = \widetilde{\lambda_k}$ corresponds to a discontinuity of Y^*, $k = 1, 2, 3$. Thus, the solution written in terms of the conservative variable is

$$W^*\left(x/t; W_L, W_R\right) = W\left(Y^*\left(x/t; Y_L, Y_R\right)\right). \tag{3.26}$$

Therefore numerical fluxes in (3.23) are computed using (3.26). In a conservative and homogeneous framework, the numerical flux is defined by the conservative flux computed with the approximate solution at the interface $x/t = 0$. However, the Riemann problem (3.15) provides a stationary wave at the interface, which introduces a jump of the numerical flux across it (which appears even when the exact solution of (3.15) is computed).

We emphasize that the source term of topography $-gZ_f'(x)$ appears naturally and explicitly in the expression of intermediate states computed by the following schemes.

3.3.3 The VFRoe (Z_f, h, Q) scheme

We consider first the conservative variable $W = {}^t(Z_f, h, Q)$. Note that this solver corresponds to the initial VFRoe scheme [MFG99]. The main interest of this interface Riemann solver is the discrete continuity of Q through the stationary wave, in agreement with the Riemann invariant (3.19a).

If we develop the system (3.9), we can write the convection matrix (which identifies with the jacobian matrix of the numerical flux $F_{,W}(W)$):

$$B(Y) = \begin{pmatrix} 0 & 0 & 0 \\ 0 & 0 & 1 \\ c^2 & c^2 - u^2 & 2u \end{pmatrix}.$$

Eigenvalues of the matrix $B(Y)$ are:

$$\lambda_1 = 0,\ \lambda_2 = u - c,\ \lambda_3 = u + c.$$

The associated matrix of right eigenvectors is:

$$\Omega = \begin{pmatrix} c^2 - u^2 & 0 & 0 \\ -c^2 & 1 & 1 \\ 0 & u - c & u + c \end{pmatrix}.$$

If we refer to the exact solution (3.25) of the linearised Riemann problem (3.24), we can write:

$$W^*\left(0^+; W_L, W_R\right) = W^*\left(0^-; W_L, W_R\right) + \frac{[\![Z_f]\!]_L^R}{\tilde{c}^2 - \tilde{u}^2} \begin{pmatrix} \tilde{c}^2 - \tilde{u}^2 \\ -\tilde{c}^2 \\ 0 \end{pmatrix}$$

where $\tilde{u} = u(\widehat{Y})$ and $\tilde{c} = c(\widehat{Y})$. This implies that the discharge Q is continuous through the stationary wave, according to relation (3.19a). So, the scheme associated to h is conservative. By

the same way, one may write the relations to connect a state W to a state W_a through the $u-c$ wave:

$$W = W_a + \frac{1}{2}\left(\frac{\tilde{c}[\![Z_f]\!]_L^R}{\tilde{c}-\tilde{u}} + \frac{(\tilde{c}+\tilde{u})[\![h]\!]_L^R}{\tilde{c}} - \frac{[\![Q]\!]_L^R}{\tilde{c}}\right)\begin{pmatrix}0\\1\\\tilde{u}-\tilde{c}\end{pmatrix}$$

and the relations to connect a state W to a state W_b through the $u+c$ wave:

$$W = W_b + \frac{1}{2}\left(\frac{\tilde{c}[\![Z_f]\!]_L^R}{\tilde{c}+\tilde{u}} + \frac{(\tilde{c}-\tilde{u})[\![h]\!]_L^R}{\tilde{c}} + \frac{[\![Q]\!]_L^R}{\tilde{c}}\right)\begin{pmatrix}0\\1\\\tilde{u}+\tilde{c}\end{pmatrix}.$$

3.3.4 The VFRoe-ncv $(Z_f, 2c, u)$ scheme

We consider herein the change of variable $Y(W) = {}^t(Z_f, 2c, u)$. The choice of variable Y was motivated by the form of Riemann invariants associated with waves of speed $u-c$ and $u+c$ which are respectively $u+2c$ and $u-2c$ (see (3.12) and (3.13)). Moreover, in the flat bottom case (3.11), variable ${}^t(2c, u)$ provides a symmetrical convection matrix and the condition to maintain a positive intermediate sound speed is formally the same as the condition of vacuum occurence (3.14) (see for more details [GHS02] and [BGH98b]).

The system (3.9) may be written related to Y as follows:

$$\begin{aligned}&Z_{f,t} = 0\\&(2c)_{,t} + u(2c)_{,x} + cu_{,x} = 0\\&u_{,t} + c(2c)_{,x} + uu_{,x} + gZ_{f,x} = 0.\end{aligned}$$

Note that this system is defined only if $h > 0$ and focusing on smooth solutions. The convection matrix $B(Y)$ is:

$$B(Y) = \begin{pmatrix}0 & 0 & 0\\0 & u & c\\g & c & u\end{pmatrix}.$$

Eigenvalues of matrix $B(Y)$ read:

$$\lambda_1 = 0,\ \lambda_2 = u-c,\ \lambda_3 = u+c.$$

If we denote by Ω the matrix of right eigenvectors, we may write:

$$\Omega = \begin{pmatrix}u^2-c^2 & 0 & 0\\gc & 1 & 1\\-gu & -1 & 1\end{pmatrix}.$$

The solution provided by the linearised Riemann problem verify through the stationary wave:

$$Y^*\left(0^+; Y_L, Y_R\right) = Y^*\left(0^-; Y_L, Y_R\right) + \frac{[\![Z_f]\!]_L^R}{\tilde{u}^2-\tilde{c}^2}\begin{pmatrix}\tilde{c}^2-\tilde{u}^2\\g\tilde{c}\\-g\tilde{u}\end{pmatrix}.$$

The relation between a state Y and a state Y_a through the $u-c$ wave may be written:

$$Y = Y_a + \left(\frac{-g}{2(\tilde{u}-\tilde{c})} [\![Z_f]\!]_L^R + [\![c]\!]_L^R - \frac{[\![u]\!]_L^R}{2} \right) \begin{pmatrix} 0 \\ 1 \\ -1 \end{pmatrix}$$

and the relation to connect a state Y to a state Y_b through the $u+c$ wave is:

$$Y = Y_b + \left(\frac{g}{2(\tilde{u}+\tilde{c})} [\![Z_f]\!]_L^R + [\![c]\!]_L^R + \frac{[\![u]\!]_L^R}{2} \right) \begin{pmatrix} 0 \\ 1 \\ 1 \end{pmatrix}.$$

One may easily note that the discharge Q computed by the VFRoe-ncv $(Z_f, 2c, u)$ solver is different on both sides of the interface. Hence, the scheme (3.23) is not conservative according to the equation (3.9a). To avoid this problem, a new Finite Volume approximation of (3.9a) may be introduced:

$$h_i^{n+1} = h_i^n - \frac{\Delta t}{2\Delta x_i} \left((Q_{i+1/2}^- + Q_{i+1/2}^+) - (Q_{i-1/2}^- + Q_{i-1/2}^+) \right) \tag{3.27}$$

where $Q_{i+1/2}^-$ and $Q_{i+1/2}^+$ refer respectively to values at the left and the right side of the interface $x_{i+1/2}$. The scheme obtained from this approximate Riemann solver is able to deal with vacuum in the flat bottom case, according to tests provided in [BGH98b]. Moreover, some numerical results are provided in the last section with occurence of dry area on a non trivial topography.

3.3.5 The VFRoe-ncv (Z_f, Q, ψ) scheme

This approximate Riemann solver follows the same formalism as above. We consider herein the variable $Y(W) = {}^t(Z_f, Q, \psi)$ (with $Q = hu$ and $\psi = u^2/2 + g(h + Z_f)$). However, we may remark that this change of variable is not inversible, which may cause some problems to define the numerical flux. The choice of Y is related to the form of the Riemann invariants associated with the null velocity wave (3.19).

The system (3.9) written related to Y is:

$$\begin{aligned} &Z_{f,t} = 0 \\ &Q_{,t} + uQ_{,x} + h\psi_{,x} = 0 \\ &\psi_{,t} + gQ_{,x} + u\psi_{,x} = 0. \end{aligned}$$

As a result, the convection matrix $B(Y)$ is:

$$B(Y) = \begin{pmatrix} 0 & 0 & 0 \\ 0 & u & h \\ 0 & g & u \end{pmatrix}.$$

As above, eigenvalues of matrix $B(Y)$ are:

$$\lambda_1 = 0,\ \lambda_2 = u - c,\ \lambda_3 = u + c.$$

If Ω is the matrix of right eigenvectors, we may write:

$$\Omega = \begin{pmatrix} 1 & 0 & 0 \\ 0 & -c & c \\ 0 & g & g \end{pmatrix}.$$

The approximate Riemann problem to solve is the same as (3.24), whose solution $Y^*(x/t; Y_L, Y_R)$ is defined in (3.25). We have the following relation through the stationary wave:

$$Y^*(0^+; Y_L, Y_R) = Y^*(0^-; Y_L, Y_R) + \begin{pmatrix} [\![Z_f]\!]_L^R \\ 0 \\ 0 \end{pmatrix}.$$

Thus, the solution computed by this Riemann solver is in agreement with the Riemann invariants (3.19a) and (3.19b). Hence, this approximate Riemann solver associated with the scheme (3.23) is able to maintain a large class of steady states, ie those based on the Riemann invariants (3.19) (see remark 3.5). A state Y may be connected to a state Y_a through the $u - c$ wave by:

$$Y = Y_a + \left(\frac{-1}{2\tilde{c}} [\![Q]\!]_L^R + \tilde{c} [\![\psi]\!]_L^R \right) \begin{pmatrix} 0 \\ -\tilde{c} \\ g \end{pmatrix}$$

and a state Y is connected to a state Y_b through the $u + c$ wave by:

$$Y = Y_b + \left(\frac{1}{2\tilde{c}} [\![Q]\!]_L^R + \tilde{c} [\![\psi]\!]_L^R \right) \begin{pmatrix} 0 \\ \tilde{c} \\ g \end{pmatrix}$$

Remark 3.3. *The convection matrix $B(Y)$ may be written in a symmetrical form, as follows:*

$$B(Y) = \begin{pmatrix} 0 & 0 & 0 \\ 0 & u & h \\ 0 & g & u \end{pmatrix} = \begin{pmatrix} 1 & 0 & 0 \\ 0 & 1 & 0 \\ 0 & 0 & h/g \end{pmatrix}^{-1} \begin{pmatrix} 0 & 0 & 0 \\ 0 & u & h \\ 0 & h & hu/g \end{pmatrix}$$

Remark 3.4. *Note that the system* (3.16) *provides a pseudo-conservative form for smooth solutions. Thus, one could use this form to define a Finite Volume scheme from it (with the VFRoe-ncv (Z_f, Q, ψ) solver for instance). However, one can easily verify that, even in the flat bottom case, the Rankine Hugoniot relations are not equivalent. Indeed, noting $v = u - \sigma$ (σ the shock speed) and $\overline{\alpha}$ the arithmetic average, the jump relations provided by the (real) system in the flat bottom case* (3.11) *are:*

$$[\![hv]\!] = 0 \tag{3.28}$$

$$\overline{hv}[\![v]\!] + g\overline{h}[\![h]\!] = 0 \tag{3.29}$$

whereas the jump relations provided by the pseudo-conservative system (3.16) *in the flat bottom case write:*

$$[\![hv]\!] = 0 \tag{3.30}$$

$$\overline{v}[\![v]\!] + g[\![h]\!] = 0 \tag{3.31}$$

which are not equivalent to the previous relations.

Remark 3.5. *According to remark 3.1 and relations* (3.19) *(assuming that the Riemann invariants and the Rankine Hugoniot relations identify through le LD field), one can define the following discrete steady states:*

$$[\![Q]\!]_i^{i+1} = 0 \tag{3.32a}$$

$$[\![\psi]\!]_i^{i+1} = 0. \tag{3.32b}$$

Moreover, these states strictly include steady states with $u \equiv 0$*:*

$$u_i = 0 \tag{3.33a}$$

$$[\![h + Z_f]\!]_i^{i+1} = 0. \tag{3.33b}$$

Remark 3.6. *Steady states* (3.32) *are exactly preserved by the VFRoe-ncv* (Z_f, Q, ψ)*. Moreover, all VFRoe-ncv schemes presented here preserve exactly steady states* (3.33)*.*

Remark 3.7. *All VFRoe-ncv schemes presented above are conservative schemes when the bottom is flat, except when dealing with a stationary shock wave superposed with an interface of the mesh. To avoid this loss of conservativity, the numerical flux in* $x_{i+1/2}$ *becomes* $F((W_{i+1/2}(0^-) + W_{i+1/2}(0^+))/2)$ *to compute* W_i^{n+1} *and* W_{i+1}^{n+1}*. Hence, this correction provides a conservative scheme which guarantees the correct shock speeds for all shock waves.*

We turn now to the second class of methods based on the splitting method.

3.4 Fractional step method

We present now a new scheme, based on a fractional step method (see [Tor97], [LM79] and [Yan68]). The system (3.9) is split in two parts. The first one is the conservative and homogenous system of P.D.E.:

$$h_{,t} + (hu)_{,x} = 0 \tag{3.34a}$$

$$(hu)_{,t} + \left(hu^2 + g\frac{h^2}{2}\right)_{,x} = 0. \tag{3.34b}$$

The second one is the system of O.D.E.:

$$h_{,t} = 0 \tag{3.35a}$$

$$(hu)_{,t} = -ghZ_f'(x). \tag{3.35b}$$

The effects of the source term are decoupled from the conservative system. So, a robust method may be applied to compute the system (3.34) (ensuring positivity of h), and a classical method is used to solve the O.D.E. (3.35).

3.4.1 The VFRoe-ncv $(2c, u)$ scheme

To compute the (strictly) hyperbolic, conservative and homogenous system (3.34), we propose the VFRoe-ncv $(2c, u)$ scheme (see [GHS02] and [BGH98b]). This system may be written in terms of non conservative variable $Y(W) = {}^t(2c, u)$. Hence comes:

$$\frac{\partial Y}{\partial t} + B(Y)\frac{\partial Y}{\partial x} = 0$$

with:

$$B(Y) = \begin{pmatrix} u & c \\ c & u \end{pmatrix}.$$

Matrix $B(Y)$ is symmetric. The intermediate state is given by (we set here $\hat{Y} = \overline{Y}$):

$$u_s = \overline{u} - [\![c]\!]_L^R \tag{3.36a}$$

$$c_s = \overline{c} - \frac{[\![u]\!]_L^R}{4} \tag{3.36b}$$

where $[\![\alpha]\!]_L^R$ represents $\alpha_R - \alpha_L$, for each interface Riemann problem. Note that the linearization has been made around the state $(2\overline{c},\overline{u})$.

Vacuum arises in the intermediate state of linearized Godunov solver if and only if initial data makes vacuum occur in the exact solution of the Riemann problem associated with the non linear set of equations (see the condition (3.14)). Actually, when focusing on the solution of the Riemann problem, vacuum may only occur when initial data is such that two rarefaction waves develop. Riemann invariants are preserved in that case, hence $u + 2c$ (respectively $u - 2c$) is constant in the 1-rarefaction wave (respectively the 2-rarefaction wave). Due to the specific form of the linearized system written in terms of non conservative variable Y, one gets from a discrete point of view:

$$u_R - 2c_R = u_s - 2c_s \tag{3.37a}$$

$$u_L + 2c_L = u_s + 2c_s. \tag{3.37b}$$

Thus, the linearized solver is well suited to handle double rarefaction waves in the solution of the exact Riemann problem. Hence, the discrete condition to ensure the positivity of c_s is:

$$u_R - u_L < 2(\sqrt{gh_R} + \sqrt{gh_L})$$

which exactly identifies with the continuous condition (3.14).

3.4.2 The fractional step method

The Finite Volume scheme which computes the homogenous system (3.34) may be written as follows:

$$\begin{aligned} W_i^{n+\frac{1}{2}} = W_i^n - \frac{\Delta t}{\Delta x_i}\Big(& F\big(W^*_{i+\frac{1}{2}}(0; W_i, W_{i+1})\big) \\ & - F\big(W^*_{i-\frac{1}{2}}(0; W_{i-1}, W_i)\big)\Big) \end{aligned} \tag{3.38}$$

where $W^*_{i+\frac{1}{2}}(x/t; W_i, W_{i+1})$ is the solution of the Riemann problem at the interface $x_{i+\frac{1}{2}}$, approximated by the VFRoe-ncv $(2c, u)$ solver.

The system of O.D.E. (3.35) is approximated by an explicit Euler method for the time part, and by a centered discretisation for the space part :

$$\begin{aligned} h_i^{n+1} &= h_i^{n+\frac{1}{2}} \\ Q_i^{n+1} &= Q_i^{n+\frac{1}{2}} - \frac{\Delta t}{\Delta x_i}\, g h_i^{n+\frac{1}{2}} \left(\frac{Z_{f\,i+1} - Z_{f\,i-1}}{2} \right). \end{aligned} \tag{3.39}$$

Note that the property of the VFRoe-ncv $(2c, u)$ scheme concerning the occurence of vacuum is not modified by step (3.39). Some numerical results with dry area provided in the following confirm the good behaviour of the fractional step method over vacuum.

Note that neither steady states (3.32) nor steady states (3.33) are maintained by the whole algorithm. This phenomenon is well known and will be discussed in the following, based on some numerical experiments, to emphasize that the algorithm is able to converge towards steady states.

Remark 3.8. *In the flat bottom case, the fractional step method* (3.38)-(3.39) *and the VFRoe-ncv* $(Z_f, 2c, u)$ *scheme presented before provide the same algorithm.*

Remark 3.9. *The two steps may be recast in one single step form, as follows:*

$$\begin{aligned} h_i^{n+1} &= h_i^n - \frac{\Delta t}{\Delta x_i}\Big(Q^*_{i+\frac{1}{2}} - Q^*_{i-\frac{1}{2}} \Big) \\ Q_i^{n+1} &= Q_i^n - \frac{\Delta t}{\Delta x_i}\Big(\big(hu^2 + gh^2/2\big)^*_{i+\frac{1}{2}} - \big(hu^2 + gh^2/2\big)^*_{i-\frac{1}{2}} \Big) - \frac{\Delta t}{\Delta x_i}\, g h_i^{n+1} \frac{Z_{f\,i+1} - Z_{f\,i-1}}{2} \end{aligned}$$

where $(\ )^*_{i+\frac{1}{2}}$ *denotes the variable computed by the VFRoe-ncv* $(2c, u)$ *scheme at the interface* $x_{i+\frac{1}{2}}$.

3.5 A higher order extension

All schemes previously presented are derived from "first order" methods. We introduce in this section an extension to obtain more accurate results and to increase rate of convergence (related to the mesh size). This method is based on a linear reconstruction on each cell by the method introduced by B. Van Leer in [Van79], namely MUSCL (Monotonic Upwind Schemes for Conservation Laws). This formalism is usually applied in a conservative and homogeneous framework (see [GHS00] for numerical measures with some VFRoe-ncv schemes on Euler system, with non smooth solutions). However, the source term of topography deeply modifies the structure of the solutions.

When applied to the shallow-water equations on a flat bottom, the MUSCL method would limit the slope of variables h and u for instance. However, the source term of topography must be taken into account. Indeed, refering to a steady state such that $h + Z_f \equiv C^{ste}$ and $u \equiv 0$, a classical MUSCL reconstruction breaks the balance of the state. Since a general class of steady states are defined by Q and ψ constant (see remark 3.5), one may require that the reconstruction does not modify these states. Moreover, the method must be able to deal with vacuum. We present here a slope limiter which verifies these requirements.

For a sake of simplicity, all variables used in this section are supposed to be time-independent. Indeed, the MUSCL method is applied at each time step, ie t is locally fixed to t^n at the n^{th} time step. Moreover, though this MUSCL method may be computed on irregular meshes, we restrict this presentation to constant space step Δx.

Some notations are first introduced. Let $\{\alpha_i\}_{i\in\mathbb{Z}}$ a variable, constant on each cell, where a cell is $I_i = [x_{i-1/2}; x_{i+1/2}]$. Let $x_i = (x_{i+1/2} + x_{i-1/2})/2$ and $\delta_i(\alpha)$ the (constant) slope associated to α_i on the cell I_i. Let $\alpha_i^{lin}(x)$, $x \in I_i$, the function defined on I_i by:

$$\alpha_i^{lin}(x) = \alpha_i - \delta_i(x - x_i) \qquad x \in I_i.$$

Thus, to compute numerical flux at an interface $x_{i+1/2}$, the initial data become $\alpha_i^{lin}(x_{i+1/2})$ and $\alpha_{i+1}^{lin}(x_{i+1/2})$ of the local Riemann problem instead of α_i and α_{i+1}. This step is the same as in the classical framework.

The modification of the algorithm to take into account the topography is thus restricted to the choice of variables for which the MUSCL reconstruction is applied to and to the computation of the slope δ_i. The first variable is the momentum Q. A classical minmod slope limiter is used (see for instance [LeV90]):

$$\delta_i(Q) = \begin{cases} s_{i+1/2}(Q)\min\big(|Q_{i+1} - Q_i|, |Q_i - Q_{i-1}|\big)/\Delta x & \text{if } s_{i-1/2}(Q) = s_{i+1/2}(Q), \\ 0 & \text{else,} \end{cases} \tag{3.40}$$

where

$$s_{i+1/2}(\alpha) = \text{sign}\,(\alpha_{i+1} - \alpha_i).$$

Such a slope limiter is TVD (Total Variation Diminishing) in the following sense:

Property 3.1. *Let Ω an open subset of $\mathbb{R}$ (here $\Omega = \mathbb{R}$).*
Let us define the total variation of a function $v \in L^1_{loc}(\Omega)$:

$$||v|| = sup\left\{\int_\Omega v \ div\ \varphi\, dx,\ \varphi \in \mathcal{C}_0^1(\Omega),\ ||\varphi||_{L^\infty(\Omega)} \le 1\right\}.$$

If v^{cst} and v^{lin} are the functions which respectively represent the constant and linear piecewise approximations of v:

$$v^{cst}(x) = v_i \quad i \in \mathbb{Z} \text{ such that } x \in I_i,$$
$$v^{lin}(x) = v_i^{lin} \quad i \in \mathbb{Z} \text{ such that } x \in I_i,$$

then v^{lin} defined by the minmod slope limiter verifies:

$$||v^{lin}|| \le ||v^{cst}||. \tag{3.41}$$

The linear reconstruction on Q based on (3.40) verifies property 3.1.

As mentioned above, stationary states must be preserved by the method, in order to permit convergence in time to steady states. To satisfy this requirement, one may choose to apply the reconstruction on ψ and to verify the property 3.1 for ψ. However, the change of variable from

(h, Q) to (Q, ψ) is not inversible. Thus, the slope limitation is made on the water height, but the computation of the slope $\delta_i(h)$ is modified to take into account ψ. Let us first define:

$$\delta_i(h) = \begin{cases} s_{i+1/2}(h+Z_f)\min\Big(& h_i, & \text{if } s_{i-1/2}(h+Z_f) \\ & |(h+Z_f)_{i+1} - (h+Z_f)_i|, & \quad = s_{i+1/2}(h+Z_f) \\ & |(h+Z_f)_i - (h+Z_f)_{i-1}| \ \Big)/\Delta x & \\ 0 & & \text{else.} \end{cases} \tag{3.42}$$

The term h_i in the minimum enables the method to deal with vacuum. The profile of ψ does not appear in the computation of $\delta_i(h)$ (though ψ and $g(h+Z_f)$ identify when $u \equiv 0$). Hence, when the source term is locally non null (ie $Z_{f\,i-1} \neq Z_{f\,i}$ or $Z_{f\,i} \neq Z_{f\,i+1}$), $\delta_i(h)$ must be modified, according to values of ψ_{i-1}, ψ_i and ψ_{i+1}. Since the slope limiters are based on a TVD requirement for the linear reconstruction, we impose a TVD-like condition on ψ, for the computation of $\delta_i(h)$. Let Ψ be the function:

$$\Psi(Z_f, h, Q) = \frac{Q^2}{2h^2} + g(h+Z_f).$$

All methods presented in this paper use the following values, $\forall i \in \mathbb{Z}$:

$$\begin{aligned} \Psi_i^- &= \Psi\Big(Z_{f\,i}, h_i - \delta_i(h)\frac{\Delta x}{2}, Q_i - \delta_i(Q)\frac{\Delta x}{2}\Big), \\ \Psi_i &= \Psi\Big(Z_{f\,i}, h_i, Q_i\Big) \quad (= \psi_i), \\ \Psi_i^+ &= \Psi\Big(Z_{f\,i}, h_i + \delta_i(h)\frac{\Delta x}{2}, Q_i + \delta_i(Q)\frac{\Delta x}{2}\Big). \end{aligned}$$

Following these notations, Ψ_i is the value of Ψ at the center of each cell I_i, Ψ_i^- is the value of Ψ at the right of each interface $x_{i-1/2}$ and Ψ_i^+ is the value of Ψ at the left of each interface $x_{i+1/2}$, $i \in \mathbb{Z}$. The computation of numerical flux at an interface $x_{i+1/2}$ needs Ψ_i^+ and Ψ_{i+1}^-. Following notations previously introduced, let Z_f^{cst}, h^{cst} and Q^{cst} be the piecewise constant approximations and let Z_f^{lin}, h^{lin} and Q^{lin} be the piecewise linear approximations. Thus, one can easily verify that $||\Psi(Z_f^{lin}, h^{lin}, Q^{lin})||$ is less than or equal to $||\Psi(Z_f^{cst}, h^{cst}, Q^{cst})||$. Hence, the reconstructions (3.40) and (3.42) do not imply that Ψ verifies property 3.1. An idea to solve this problem should be limiting "strongly" h (ie computing $\delta_i(h) = 0$) if $\Psi(Z_f^{lin}, h^{lin}, Q^{lin})$ does not verify the TVD requirement. However, this condition may be considered too restrictive. Thus, we introduce the following condition:

$$\begin{aligned} 0 \leq |\Psi_i - \Psi_i^-| \leq |\Psi_i - \Psi_{i-1}|/2, \\ 0 \leq |\Psi_i^+ - \Psi_i| \leq |\Psi_{i+1} - \Psi_i|/2, \end{aligned} \tag{3.43}$$

illustrated by figure 3.2.

Condition (3.43) imposes a TVD-like condition on Ψ. Indeed, assuming that Ψ_i^-, Ψ_i and Ψ_i^+ fulfill condition (3.43) $\forall i \in \mathbb{Z}$, if Φ denotes the linear interpolation computed from Ψ_i^-, Ψ_i and Ψ_i^+ $\forall i \in \mathbb{Z}$, then Φ verifies the following TVD property:

$$||\Phi|| \leq ||\Psi(Z_f^{cst}, h^{cst}, Q^{cst})||,$$

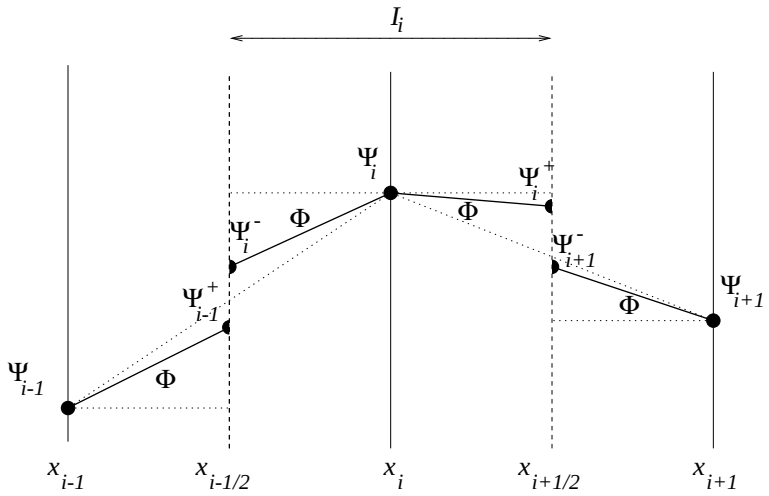

Figure 3.2: a TVD-like reconstruction for Ψ

which may be seen as the counterpart of (3.41).

We recall now all the steps of the algorithm used to compute slopes $\delta_i(h)$ and $\delta_i(Q)$, $\forall i \in \mathbb{Z}$:

i. Computation of $\delta_i(Q)$:

$$\delta_i(Q) = \begin{cases} s_{i+1/2}(Q)\min\big(|Q_{i+1}-Q_i|, |Q_i - Q_{i-1}|\big)/\Delta x & \text{if } s_{i-1/2}(Q) = s_{i+1/2}(Q), \\ 0 & \text{else.} \end{cases}$$

ii. Computation of $\delta_i(h)$:

- if $Z_{f\,i-1} = Z_{f\,i} = Z_{f\,i+1}$, then the minmod slope limiter is applied to compute $\delta_i(h)$:

$$\delta_i(h) = \begin{cases} s_{i+1/2}(h)\min\big(|h_{i+1}-h_i|, |h_i - h_{i-1}|\big)/\Delta x & \text{if } s_{i-1/2}(h) = s_{i+1/2}(h), \\ 0 & \text{else,} \end{cases}$$

- else, $\delta_i(h)$ is first computed by a classical minmod limiter on $h + Z_f$:

$$\delta_i(h) = \begin{cases} s_{i+1/2}(h+Z_f)\min\Big(& h_i, & \text{if } s_{i-1/2}(h+Z_f) \\ & |(h+Z_f)_{i+1} - (h+Z_f)_i|, & = s_{i+1/2}(h+Z_f), \\ & |(h+Z_f)_i - (h+Z_f)_{i-1}| \Big)/\Delta x & \\ 0 & & \text{else,} \end{cases}$$

- but if condition (3.43) is not fulfilled, then we reset $\delta_i(h)$ to

$$\delta_i(h) = 0.$$

Let us emphasize that, when $\delta_i(h)$ is set to 0, conditions (3.43) may not be verified (because of the limitation on Q).

This slope limiter is combined with a second order Runge-Kutta integration wrt time (namely the Heun scheme). Some numerical results are described in the following and point out the good behaviour of the slope limiter obtained. A comparison with a classical recontruction is presented in section 3.6.3 (figure 3.13) which shows that the method may fail to converge towards a steady state when t tends to $+\infty$, if the modification described above is not computed.

3.6 Numerical results

Though several VFRoe-ncv schemes have been previously discussed, only numerical results performed by the VFRoe-ncv $(Z_f, 2c, u)$ scheme with the higher order extension and by the fractional step method are presented here (some complementary tests are provided in the appendix). Some experiments tested herein come from a workshop on dam-break wave simulation [GM97]. Most of them deal with steady states on non trivial bottom. The ability of the methods to compute dry area is tested too. Let us emphasize that all the numerical results have been obtained without any "clipping" treatment (ie non-physical values such as negative *cell* water height are not artificially set to 0).

The first four tests are performed with the same topography. The channel length is $l = 25m$. The bottom Z_f is defined as follows:

$$Z_f(x) = \begin{cases} 0,2 - 0,05(x-10)^2 & \text{if } 8\,m < x < 12\,m, \\ 0 & \text{else.} \end{cases}$$

Only initial and boundary conditions are modified.
All tests cases are computed with a CFL number set to $0,4$. Results of the flow at rest, the subcritical flow over a bump and the transcritical flow over a bump are plotted at $T_{MAX} = 200\,s$.

3.6.1 Flow at rest

The initial condition of this test case is a flow at rest. Thus, numerically, it fulfills conditions (3.33), where $h > 0$. Since we compute a flow at rest, we impose $h + Z_f = \max(Z_f; 0,15)\,m$ and $Q = 0\,m^2/s$ all along the mesh, which contains 300 nodes. As expected, the VFRoe-ncv scheme exactly preserves the steady state (figures 3.3 and 3.4). Moreover, though it is not plotted here, we may emphasize that the behaviour of this scheme remains good in this case when the initial conditions are $h + Z_f = 0,5\,m$ (no dry cells) or $h = 0\,m$ (no water). The fractional step method (FSM) does not maintain $h + Z_f$ and Q constant on the wet cells. The slope of topography introduces a convection of water. The fractional step method nonetheless converges towards the right solution when the mesh is refined.

The interest of the next three tests (extracted from [GM97]) is to study the convergence of this scheme towards a steady state. All these tests are performed on 300 cells. The boundary conditions are a positive imposed discharge Q_{in} on the left boundary, and a imposed height h_{out} on the right

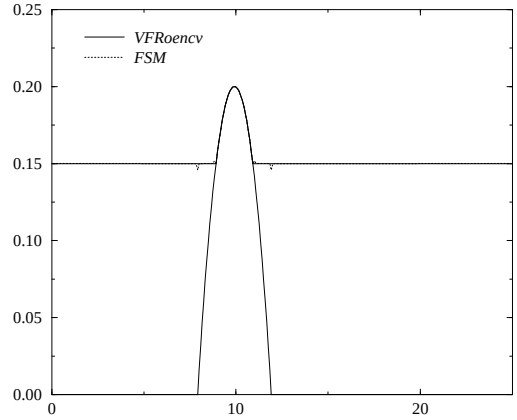

Figure 3.3: Flow at rest: water height

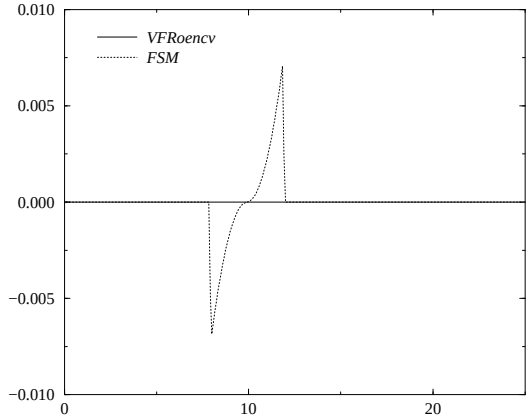

Figure 3.4: Flow at rest: discharge

boundary (except in the case of a supercritical flow). The initial condition is set to $h = h_{out}$ and $Q = 0$. To discuss results, several profiles are plotted, namely h, Q and ψ *vs* space (in meters). Moreover, to illustrate the quantitative convergence of the methods, the normalised time variation in L^2-norm is plotted too (see figure 3.6 for instance): time t in seconds for x-axis and $\ln \frac{||h^{n+1}-h^n||_{L^2}}{||h^3-h^2||_{L^2}}$ for y-axis.

3.6.2 Subcritical flow over a bump

Here, the boundary conditions are $h_{out} = 2\,m$ and $Q_{in} = 4,42\,m^2/s$. The two solutions provided by the VFRoe-ncv scheme and the fractional step method seem very close to each other, according to figure 3.5 (they are in agreement with the analytic solution). However, figures 3.7 and 3.8 focus on some differences between the two methods: whereas Q and ψ seem to be constant in the case of the VFRoe-ncv scheme, the fractional step method makes occur oscillations near variations of topography. The two profiles on figure 3.6 are superposed, and show that the two methods converge to steady state.

3.6.3 Transcritical flow over a bump

The boundary conditions are $Q_{in} = 1,53\,m^2/s$ and $h_{out} = 0,66\,m$. The analytic solution of this test is smooth, with a decreasing part, beginning at the top of the bump and a critical (sonic) point on the decreasing part of h. The solution at the right of the decreasing part is supercritical (the boundary condition h_{out} is only used when the flow is subcritical, during the transient part of the simulation). Figure 3.9 shows that results provided by the VFRoe-ncv scheme and the fractional step method are similar and the critical point induces no problem (though methods are based on approximate Godunov schemes). According to figure 3.10, the time variation of the VFRoe-ncv scheme decreases slowlier than the one of the FSM. On figures 3.11 and 3.12, one may notice

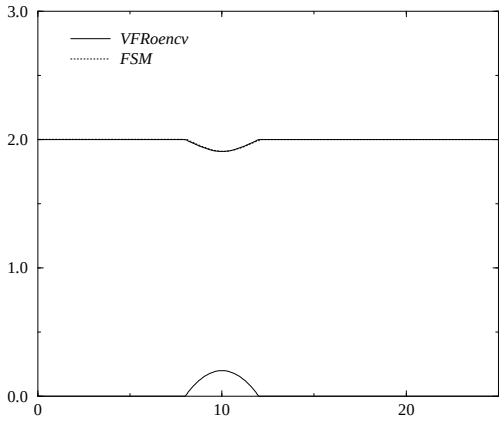

Figure 3.5: Subcritical flow: water height

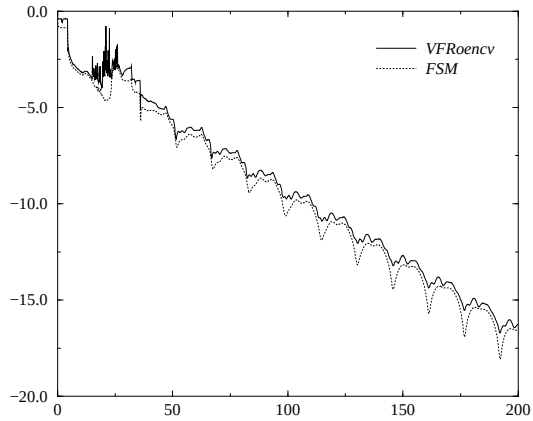

Figure 3.6: Subcritical flow: normalised time variation in L^2-norm

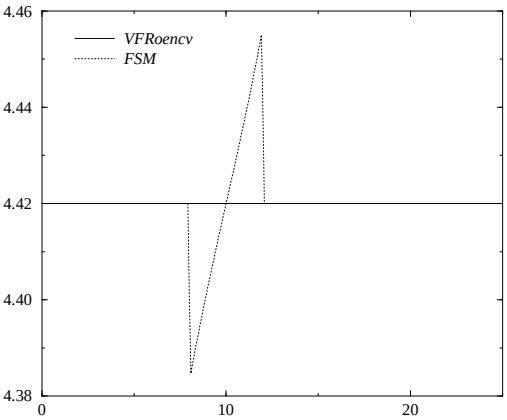

Figure 3.7: Subcritical flow: discharge

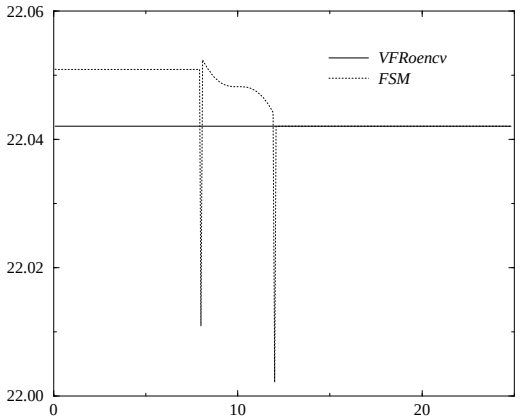

Figure 3.8: Subcritical flow: ψ

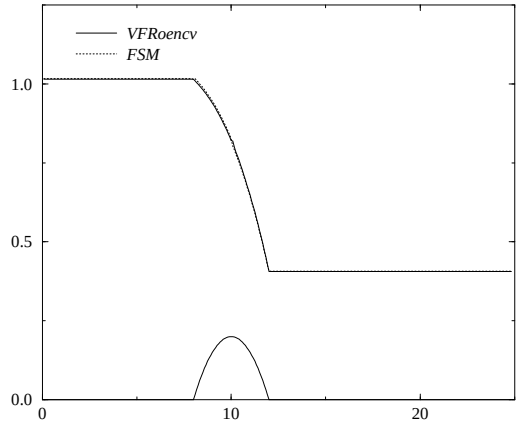

Figure 3.9: Transcritical flow: water height

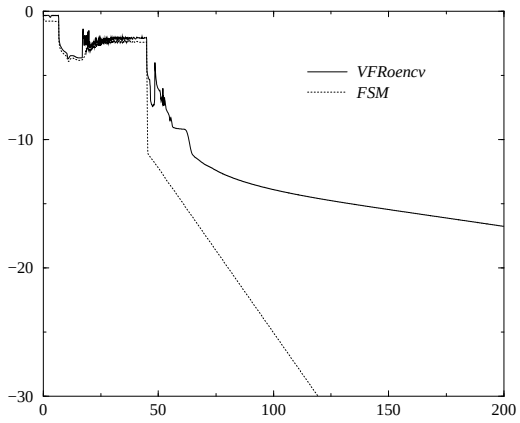

Figure 3.10: Transcritical flow: normalised time variation in L^2-norm

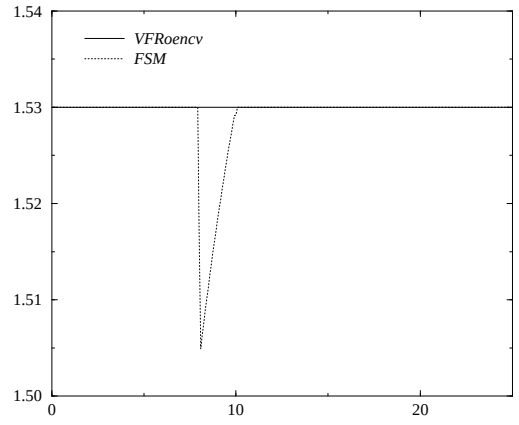

Figure 3.11: Transcritical flow: discharge

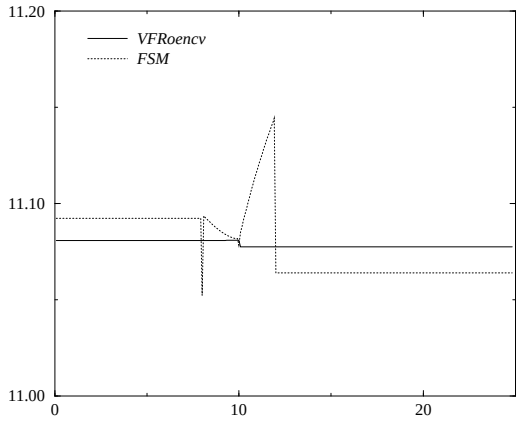

Figure 3.12: Transcritical flow: ψ

that results performed by the VFRoe-ncv scheme are more accurate, since Q and ψ seem almost constant.

We present now the counterpart of figure 3.10, using the VFRoe-ncv scheme (with the non conservative variable $(Z_f, 2c, u)$) associated to several reconstructions: the original three-points scheme without any reconstruction, the second order scheme presented in section 3.5 and the classical second order scheme (*ie* the minmod limiter without modification). Results are plotted on figure 3.13. Whereas the first two schemes provide a similar profile, the second order scheme with no modifi-

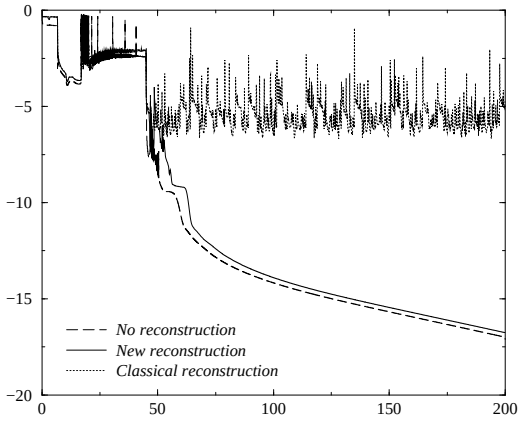

Figure 3.13: Transcritical flow: normalised time variation in L^2-norm

cation does not converge very well on the coarse mesh. Nonetheless, oscillations remains bounded. Note that this surprising behaviour can appear since the problem is not in conservative form. In a conservative framework, the second order scheme with the classical reconstruction converges but the speed of convergence slows down compared with both other schemes (see [SV03]).

3.6.4 Drain on a non flat bottom

The topography of this test case is the same as all cases previously presented. The left boundary condition is a "mirror state"-type condition, and the right boundary condition is an outlet condition on a dry bed [BGH00]. The initial condition is set to $h+Z_f = 0,5\,m$ and $Q = 0\,m^2/s$. The solution of this test case at $t = +\infty$ is a state at rest on the left part of top of the bump with $h+Z_f = 0,2\,m$ and $Q = 0\,m^2/s$ and a dry state (ie $h = 0\,m$ and $Q = 0\,m^2/s$) on the right side of the bump. Results are presented at several times: $t = 0$, 10, 20, 100 and $1000\,s$ on figures 3.14, 3.16 and 3.17. Note that, since a dry zone is expected at the downstream side of the bump, variable ψ is not defined in this zone (thus, results plotted on figure 3.17 in this zone must not be taken in account). Figure 3.14 represents the water height computed by the VFRoe-ncv scheme ("plus" symbols) and the fractional step method ("circle" symbols). Results at intermediate times are slightly different, but denote the same behaviour. However, if the final time T_{MAX} is increased, the fractional step method computes a level of water slightly lower than the level expected at the left of the bump, namely $h + Z_f = 0,2\,m$. This numerical phenomenon has already been pointed

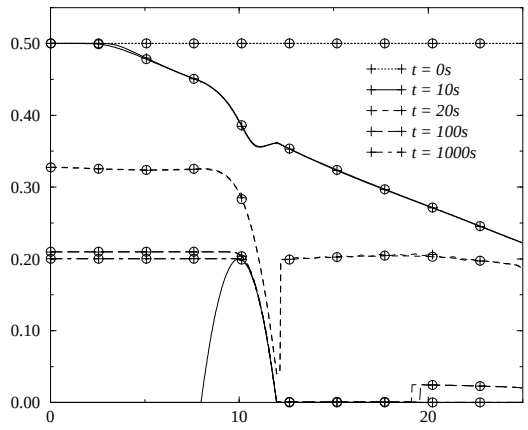

Figure 3.14: Drain on a non flat bottom: water height

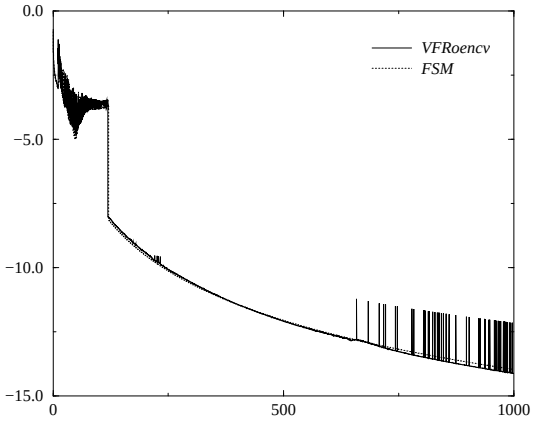

Figure 3.15: Drain on a non flat bottom: normalised time variation in L^2-norm

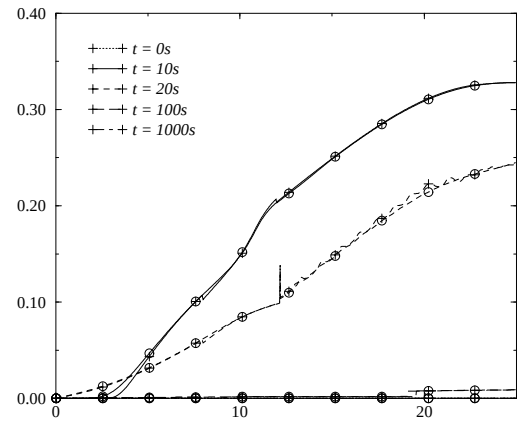

Figure 3.16: Drain on a non flat bottom: discharge

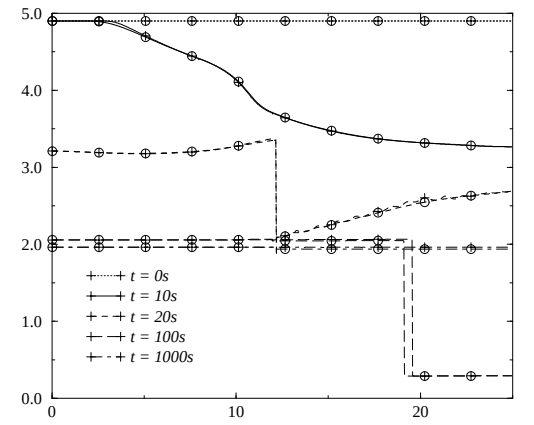

Figure 3.17: Drain on a non flat bottom: ψ

out by A.Y. LeRoux [LeR98]. It is due to the non preservation of discrete steady states (3.33) by the fractional step method. Note however that, when the mesh is refined, the level computed tends to $h + Z_f = 0,2\,m$. Results performed by the VFRoe-ncv scheme are rather good, the expected steady state is well approximated, as shown on figures 3.14, 3.16 and 3.17. Furthermore, the time variation is decreasing for both methods.

3.6.5 Vacuum occurence by a double rarefaction wave over a step

This numerical test is different from previous tests. Indeed, we do not study here the convergence towards a steady state but the ability of the numerical scheme to compute vacuum (ie dry bed). Moreover, the topography is not smooth (which indeed is not in agreement with initial assumptions). This test is based on a test proposed by E.F. Toro [GM97], but we introduce here a non trivial topography: $Z_f = 1\,m$ if $25/3\,m < x < 12,5\,m$, and $Z_f = 0\,m$ otherwise (the total length is still $25\,m$). The initial water height is initialised to $10\,m$ and the initial discharge is set to

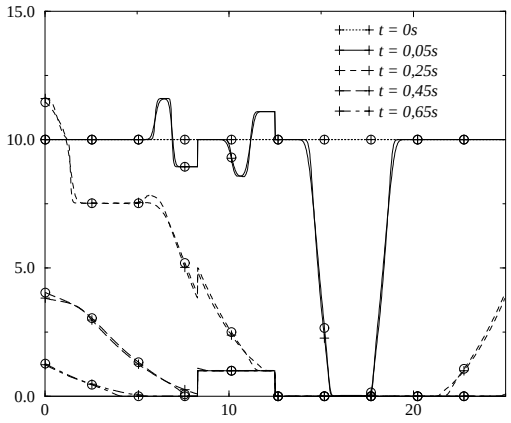

Figure 3.18: Vacuum occurence: water height

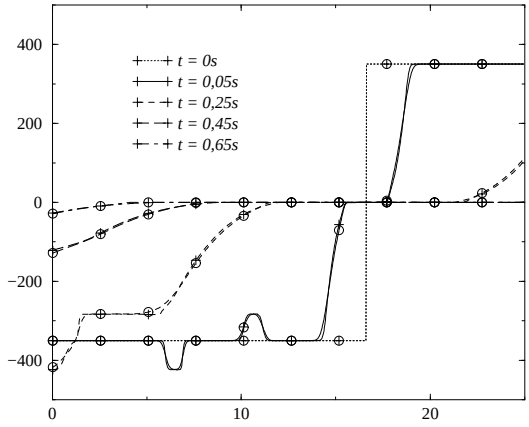

Figure 3.19: Vacuum occurence: discharge

$-350\,m^2/s$ if $x < 50/3\,m$ and to $350\,m^2/s$ otherwise. Results at several times are presented: $0\,s$, $0,05\,s$, $0,25\,s$, $0,45\,s$ and $0,65\,s$. In the case of a flat bottom, the solution would be composed of two rarefaction waves, with a dry zone occuring between the two waves. Here, since the topography is not flat, the two algorithms introduce waves, located on the jumps of topography (see figures 3.18 and 3.19, where sign "plus" represents the VFRoe-ncv scheme and the sign "circle" represents the fractional step method). Moreover, one may note that results computed by the two methods are close to each other, but more diffusive for the FSM method (since no MUSCL reconstruction has been performed for this algorithm).

3.7 Conclusion

Some Finite Volume schemes have been studied in this paper to compute shallow-water equations with topography. Some relations of the system have been recalled, in the case of a piecewise con-

stant function to approximate the topography. So, according to this approximation, several Finite Volume schemes have been introduced, based on the VFRoe-ncv formalism [BGH00], [GHS00], namely the VFRoe-ncv schemes, in variable (Z_f, h, Q), $(Z_f, 2c, u)$ and (Z_f, Q, ψ). All the previous schemes are able to maintain steady states with $u \equiv 0$ and the latter can preserve a larger class of steady states. Moreover, a fractional step method based on the VFRoe-ncv $(2c, u)$ scheme (initially proposed in [BGH98b]) is presented. A higher order extension is also presented, based on the minmod slope limiter, which takes into account steady states.

Refering to numerical results included in [GM97], one may conclude that the VFRoe-ncv $(Z_f, 2c, u)$ scheme (with the higher order extension in space and a second order Runge-Kutta time integration) provides accurate and convergent results. Moreover, the robustness of the method has been emphasized too, dealing with two tests with occurence of dry area on non trivial topography, though no clipping treatment has been introduced (ie no non-conservative treatment of negative water heights has been computed). The "first order" fractional step method behaves well (in particular over vacuum), but does not approximate steady states as accurately as the VFRoe-ncv scheme.

Considering results performed by the Well-Balanced scheme, the expected accuracy is shown on some tests. This scheme has been compared with the VFRoe-ncv $(Z_f, 2c, u)$ scheme and numerical results confirm the good behaviour of the latter scheme. However, the Well-Balanced scheme is (several times) more expensive than a usual Godunov method, since the resolution of the Riemann problem is not obvious and many configurations must be considered (this essential difficulty is due to the stationary wave). Indeed, the CPU time required by the "higher" order VFRoe-ncv $(Z_f, 2c, u)$ scheme is between 10 and 100 times lower than the CPU time required by the "first" order Well-Balanced scheme.

We have also presented the basic VFRoe scheme (in variable (Z_f, h, Q)), with some results provided in the appendix. The behaviour of this scheme is as good as the VFRoe-ncv $(Z_f, 2c, u)$ scheme. However, unlike the VFRoe-ncv $(Z_f, 2c, u)$ scheme, this method fails to deal with occurence of a critical point, provided by an upstream boundary condition. Such a drawback has been emphasized too with the R.J. LeVeque scheme [LeV98].

An interesting potential extension of the method presented here is to take into account a variable section $S(x, h)$ in the one-dimensional framework. In this case, the same technique may be used to approximate the corresponding source term.

3.A Comparison with the Well-Balanced scheme

This appendix is devoted to the numerical comparison of the VFRoe-ncv scheme $Z_f, 2c, u)$ with the Well-Balanced scheme presented in [LeR98]. Note that the VFRoe-ncv scheme is computed with the higher order extension and a second order Runge-Kutta method whereas the Well-Balanced scheme tested is the original "first" order scheme. Two tests are presented: a subcritical flow over a bump and a trancritical flow over a bump. The same topography is used for both tests:

$$Z_f(x) = \begin{cases} 0,2 - 0,05(x-10)^2 & \text{if } 8\,m < x < 12\,m, \\ 0 & \text{else.} \end{cases}$$

Moreover, all results are plotted at $T_{MAX} = 200\,s$. The CFL number is set to $0,4$. Computations are performed on a mesh with 300 nodes. Only initial and boundary conditions differ between the two following tests.

3.A.1 Subcritical flow over a bump

This test computes a transient flow, which tends to become a steady subcritical flow (see test 3.6.2). The imposed boundary conditions are $Q_{in} = 4,42\,m^2/s$ and $h_{out} = 2\,m$. The initial conditions are $Q(t=0,x) = 0\,m^2/s$ and $h(t=0,x) = h_{out}\,m$. Figure 3.20 represents the water height. Results

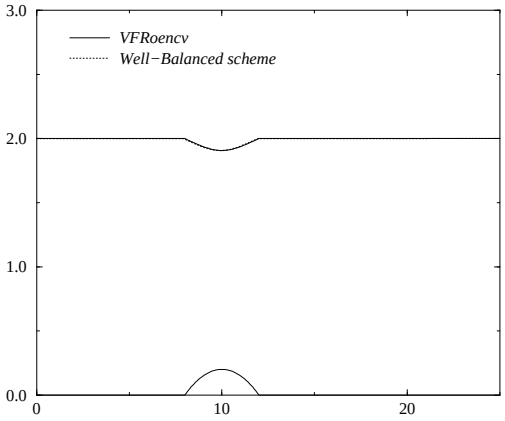

Figure 3.20: Subcritical flow: water height

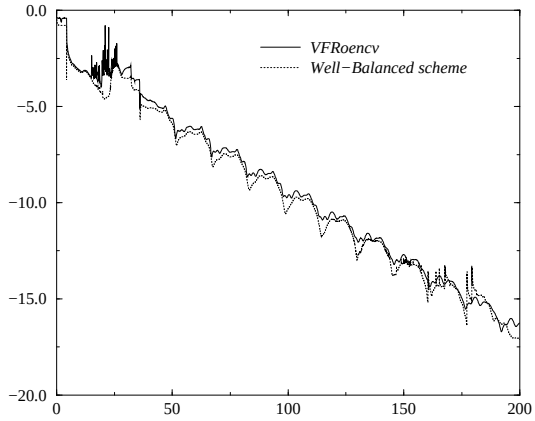

Figure 3.21: Subcritical flow: normalised time variation in L^2-norm

performed by the two schemes are very close to each other. The normalised variation is plotted on figure 3.21. The x-axis is the time and the y-axis is $\ln \frac{||h^{n+1}-h^n||_{L^2}}{||h^3-h^2||_{L^2}}$. One may remark that the two profiles are similar and both methods provide a stationary result. This confirms the good behaviour of the VFRoe-ncv scheme. Figures 3.22 and 3.23 present Q and ψ. Whereas figure 3.22 shows that the two methods provide almost the same results, one can note that the two profiles are slightly different. The analytic solution is $\psi = 22,04205$. The slightly different values provided by

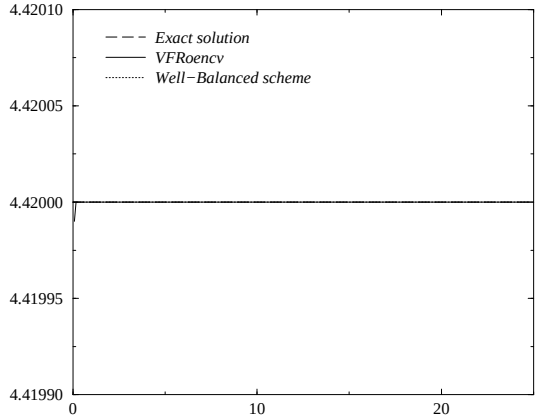

Figure 3.22: Subcritical flow: discharge

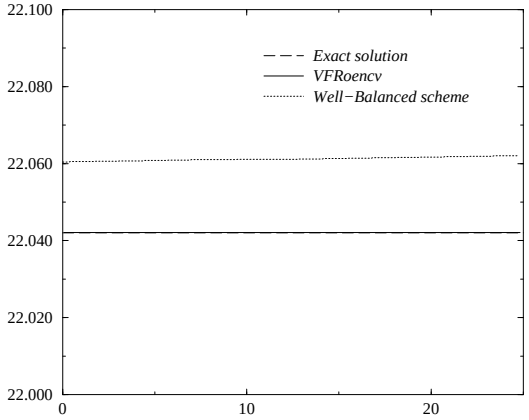

Figure 3.23: Subcritical flow: ψ

the Well-Balanced scheme is due to iterative methods (Newton, dichotomy, ...) used to compute the exact solution of each interface Riemann problem. Indeed, these methods stop when the relative error is 10^{-5} or when the number of iterations is larger than 500.

3.A.2 Transcritical flow over a bump

The solution of this test case is a regular profile for the water height, with a subcritical flow upstream of the bump and a supercritical flow downstream of the bump (see test 3.6.3). The

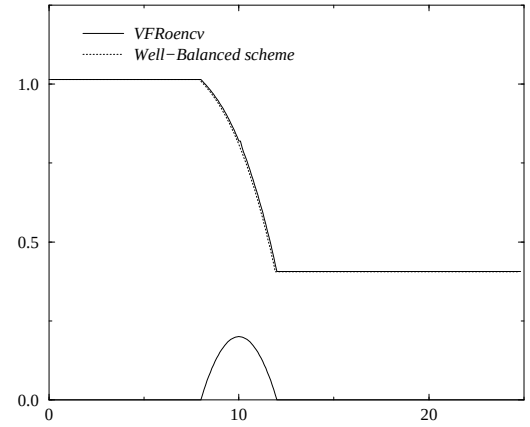

Figure 3.24: Transcritical flow: water height

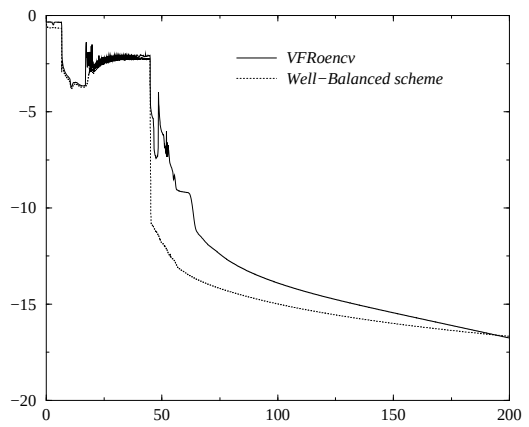

Figure 3.25: Transcritical flow: normalised time variation in L^2-norm

boundary conditions are $Q_{in} = 1,53\,m^2/s$ and $h_{out} = 0,66\,m$. The initial conditions are $Q(t = 0, x) = 0\,m^2/s$ and $h(t = 0, x) = h_{out}\,m$. Both profiles plotted on figure 3.24 provide a good

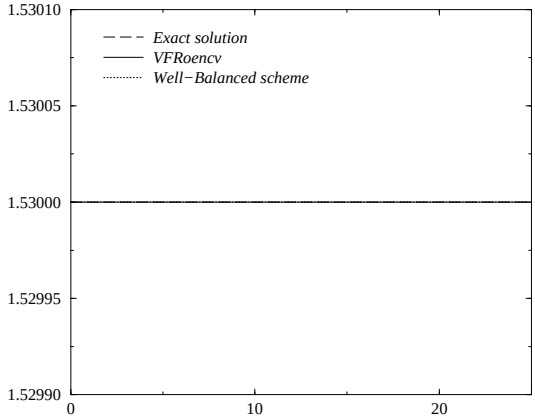

Figure 3.26: Transcritical flow: discharge

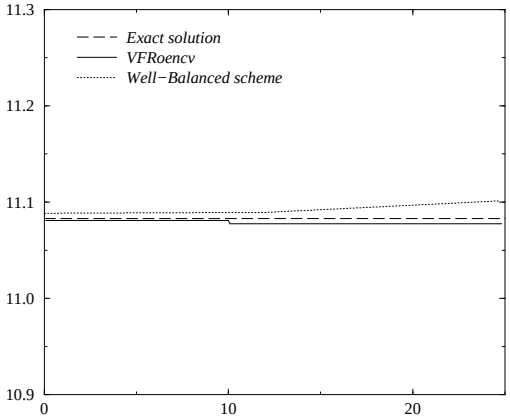

Figure 3.27: Transcritical flow: ψ

approximation of the expected steady solution. Moreover, figure 3.25 shows that the two schemes compute almost stationary solutions at $t = T_{MAX}$. Figure 3.26 shows that variable Q is accurately computed by both methods. Moreover, figure 3.27, which represents variable ψ, denotes a slight difference between the two methods, as it has already been noticed in the previous test case.

This appendix confirms the good behaviour of the VFRoe-ncv $(Z_f, 2c, u)$ scheme. Indeed, results provided by this method with the higher order extension are very close to those provided by the Well-Balanced scheme for the two presented test cases. Moreover, the CPU time required by the VFRoe-ncv scheme (with a second order Runge-Kutta time integration and the higher order extension) is between 10 and 100 times lower than the CPU time required by the "first" order Well-Balanced scheme (no accurate CPU measurement might be done, because different computers and different languages have been used to program the methods ; no optimization has been searched for the Well-Balanced scheme ; the accuracy and the CPU time of the Well-Balanced scheme deeply depend on the convergence of iterative methods in the exact interface Riemann solver).

3.B Comparison with the VFRoe (Z_f, h, Q) scheme

We present here a numerical test performed with the VFRoe (Z_f, h, Q) scheme, with the higher order extension previously presented and a second order Runge-Kutta time approximation. The test case performed is the subcritical flow over a bump (see test 3.6.2). Let us recall the configuration of this test. The topography is:

$$Z_f(x) = \begin{cases} 0,2 - 0,05(x-10)^2 & \text{if } 8\,m < x < 12\,m, \\ 0 & \text{else.} \end{cases}$$

The boundary conditions are $Q_{in} = 4,42\,m^2/s$ and $h_{out} = 2\,m$. The initial conditions are $Q(t = 0, x) = 0\,m^2/s$ and $h(t = 0, x) = 2\,m$. The mesh contains 300 cells and the CFL number is $0,4$. Both methods provide profiles of water height which are very close to each other in figure 3.28.

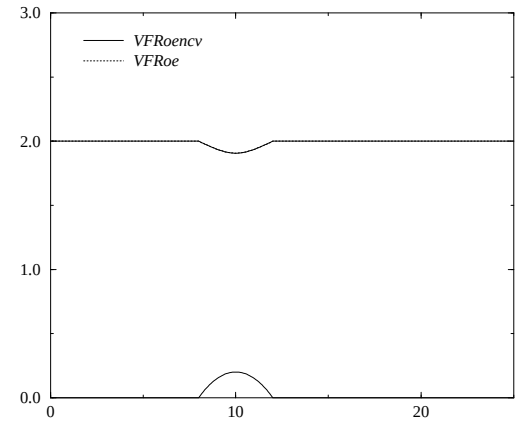

Figure 3.28: Subcritical flow: water height

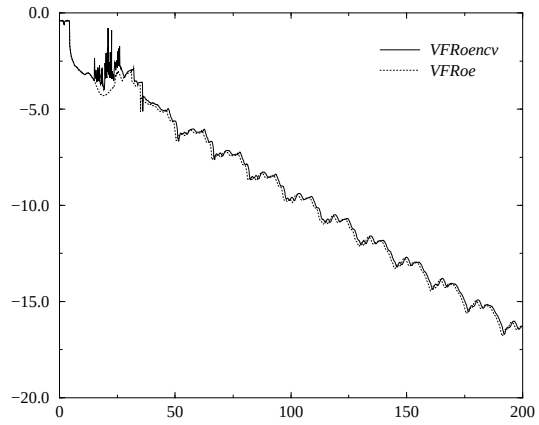

Figure 3.29: Subcritical flow: normalised time variation in L^2-norm

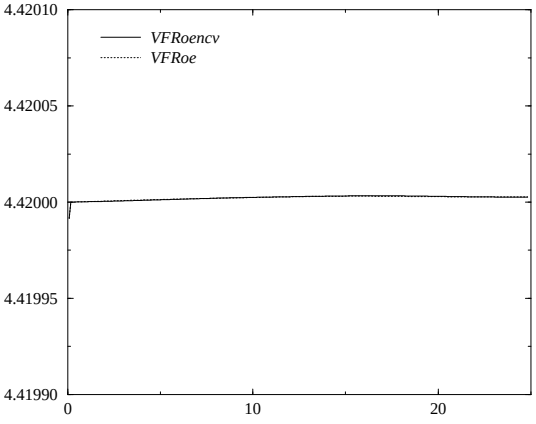

Figure 3.30: Subcritical flow: discharge

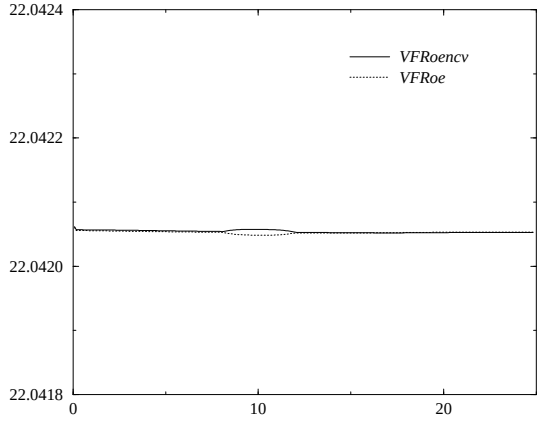

Figure 3.31: Subcritical flow: ψ

Moreover, the time variation decreases with the same slope on figure 3.29. Figures 3.30 and 3.31 show that the VFRoe scheme and the VFRoe-ncv scheme both compute almost constant values of Q and ψ, in agreement with the analytic solution (the relative error in L^∞-norm is around 10^{-5}). Thus, the VFRoe scheme also provides accurate results on this test case. As the high-resolution Godunov method proposed by R.J. LeVeque in [LeV98], the VFRoe scheme (but not the VFRoe-ncv scheme) fails to deal with occurence of transcritical flow by an inlet condition (see test 3.6.3), even with the higher order extension.

Bibliography

[BGH98a] T. Buffard, T. Gallouët, and J.M. Hérard. A naive Godunov scheme to compute a non-conservative hyperbolic system. *Int. Series Num. Math.*, 1998, vol. 129, pp. 129–138.

[BGH98b] T. Buffard, T. Gallouët, and J.M. Hérard. A naive Godunov scheme to solve shallow-water equations. *C. R. Acad. Sci. Paris*, 1998, vol. I-326, pp. 885–890.

[BGH00] T. Buffard, T. Gallouët, and J.M. Hérard. A sequel to a rough Godunov scheme. Application to real gas flows. *Computers and Fluids*, 2000, vol. 29-7, pp. 813–847.

[Bon97] C. Bon, *Modélisation et simulations numériques d'écoulements hydrauliques et de ruissellement en topographie quelconque*, Ph.D. thesis, Université Bordeaux I, France, 1997.

[BPV02] R. Botchorishvili, B. Perthame, and A. Vasseur, *Equilibrium schemes for scalar conservation laws with stiff sources*, 2002.

[CL99] A. Chinnayya and A.Y. LeRoux, *A new general Riemann solver for the shallow-water equations with friction and topography*, 1999. Available in the conservation law preprint server http://www.math.ntnu.no/conservation/.

[Col92] J.F. Colombeau, *Multiplication of distributions*, Springer Verlag, 1992.

[DLM95] G. Dal Maso, P.G. LeFloch, and F. Murat. Definition and weak stability of non conservative products. *J. Math. Pures Appl.*, 1995, vol. 74, pp. 483–548.

[EGH00] R. Eymard, T. Gallouët, and R. Herbin, Finite Volume Methods, In *Handbook of Numerical Analysis* (Vol. VII), editors : P.G. Ciarlet and J.L. Lions, North-Holland, pp. 729–1020, 2000.

[GHS00] T. Gallouët, J.M. Hérard, and N. Seguin, *Some recent Finite Volume schemes to compute Euler equations using real gas EOS*, LATP Report 00-021, Université de Provence, France, *accepted for publication in* Int. J. Num. Meth. Fluids, 2000.

[GHS02] T. Gallouët, J.M. Hérard, and N. Seguin. On the use of some symetrizing variables to deal with vacuum. submitted for publication, 2002.

[GL96a] L. Gosse and A.Y. LeRoux. A well balanced scheme designed for inhomogeneous scalar conservation laws. *C. R. Acad. Sci. Paris*, 1996, vol. I-323, pp. 543–546.

[GL96b] J.M. Greenberg and A.Y. LeRoux. A well balanced scheme for the numerical processing of source terms in hyperbolic equation. *SIAM J. Numer. Anal.*, 1996, vol. 33-1, pp. 1–16.

[GLBN97] J.M. Greenberg, A.Y. LeRoux, R. Baraille, and A. Noussair. Analysis and approximation of conservation laws with source terms. *SIAM J. Numer. Anal.*, 1997, vol. 34-5, pp. 1980–2007.

[GM97] N. Goutal and F. Maurel, *Proceedings of the 2nd workshop on dam-break wave simulation*, EDF-DER Report HE-43/97/016/B, 1997.

[GNVC00] P. Garcia-Navarro and M.E. Vazquez-Cendon. On numerical treatment of the source terms in the shallow water equations. *Computers and Fluids*, 2000, vol. 29-8, pp. 951–979.

[God59] S.K. Godunov. A difference method for numerical calculation of discontinuous equations of hydrodynamics. *Mat. Sb.*, 1959, pp. 271–300. In Russian.

[GR96] E. Godlewski and P.A. Raviart, *Numerical approximation of hyperbolic systems of conservation laws*, Springer Verlag, 1996.

[LeR98] A.Y. LeRoux, Discrétisation des termes sources raides dans les problèmes hyperboliques, In *Systèmes hyperboliques : nouveaux schémas et nouvelles applications*. Écoles CEA-EDF-INRIA "problèmes non linéaires appliqués", INRIA Rocquencourt (France), March 1998. Available on
http://www-gm3.univ-mrs.fr/∼leroux/publications/ay.le_roux.html, In French.

[LeV90] R.J. LeVeque, *Numerical Methods for Conservation Laws*, Birkhäuser-Verlag, Basel, 1990.

[LeV98] R.J. LeVeque. Balancing source terms and flux gradients in high-resolution Godunov methods. *J. Comp. Phys.*, 1998, vol. 146, pp. 346–365.

[LM79] P.L. Lions and B. Mercier. Splitting algorithms for the sum of two nonlinear operators. *SIAM J. Numer. Anal.*, 1979, vol. 16-6, pp. 964–979.

[MFG99] J.M. Masella, I. Faille, and T. Gallouët. On an approximate Godunov scheme. *Int. J. of Comp. Fluid Dyn.*, 1999, vol. 12, pp. 133–149.

[Roe81] P.L. Roe. Approximate Riemann solvers, parameter vectors and difference schemes. *J. Comp. Phys.*, 1981, vol. 43, pp. 357–372.

[Seg99] N. Seguin, *Génération et validation de Rozavel, un code équilibre en hydraulique 2D.* Mémoire de D.E.A., Université de Bordeaux I, 1999.
Available on http://www-gm3.univ-mrs.fr/∼leroux/publications/n.seguin.html.

[SV03] N. Seguin and J. Vovelle. Analysis and approximation of a scalar conservation law with a flux function with discontinuous coefficients. *M^3AS*, 2003, vol. 5-13.

[Tor97] E.F. Toro, *Riemann solvers and numerical methods for fluid dynamics*, Springer Verlag, 1997.

[Van79] B. VanLeer. Toward the ultimate conservative difference scheme V. A second order sequel to Godunov's method. *J. Comp. Phys.*, 1979, vol. 32, pp. 101–136.

[Yan68] N.N. Yanenko, *Méthode à pas fractionnaires. Résolution de problèmes polydimensionnels de physique mathématique*, Librairie Armand Colin, 1968. Traduit du russe par P.A. Nepomiastchy.

Chapitre 4

Modélisation numérique des écoulements diphasiques eau-vapeur par une approche bifluide à deux pressions

Ce chapitre traite de la simulation des écoulements diphasiques eau-vapeur en utilisant l'approche bifluide à deux phases compressibles. Celle-ci se distingue du cadre du chapitre 1 par le fait que les équations aux dérivées partielles sont obtenues grâce à des opérateurs de moyenne (en temps, en espace ou statistiques) appliqués aux équations de Navier-Stokes dans les domaines occupés par chacun des fluides, par opposition aux variables associées au mélange eau-vapeur. Une littérature très riche existe à propos des modèles supposant les deux fluides (l'eau et la vapeur) à vitesses distinctes et à pressions égales. Cette classe de modèles a deux inconvénients majeurs : le système convectif associé est conditionnellement hyperbolique et il est non conservatif. Le premier signifie que dans certaines configurations d'écoulements, certaines vitesses de propagation d'onde peuvent devenir complexes (on n'est plus alors assuré d'être en présence d'un problème de Cauchy bien posé). Le second pose le problème de la définition des solutions discontinues ainsi que de la mise en œuvre d'algorithmes convergeant vers la « bonne » solution. De plus, le calcul de la fraction volumique se fait par l'inversion d'une relation algébrique pouvant être fortement non linéaire et le principe du maximum sur cette variable peut être violé (voir l'annexe B).

Le modèle proposé ici se base sur l'approche bifluide avec deux vitesses et deux pressions distinctes. Une équation de transport sur la fraction volumique apparaît, incluant un terme de relaxation sur l'écart des pressions. Le système convectif est alors inconditionnellement hyperbolique. Néanmoins, certaines valeurs propres peuvent s'identifier, ce qui peut entraîner que la matrice associée aux termes différentiels d'ordre un n'est plus diagonalisable, comme pour les modèles étudiés dans les chapitres 2 et 3. Le principe du maximum sur la fraction volumique et la positivité des fractions massiques sont assurés pour les solutions régulières du modèle. Le système convectif est là aussi non conservatif et le problème de la définition des solutions discontinues se pose donc. Si on se réfère à

la littérature existant sur les modèles à deux pressions, on peut voir qu'il n'existe aucun consensus sur la fermeture de la vitesse interfaciale et de la pression interfaciale. On propose alors de définir ces deux variables de manière à fermer le système non seulement du point de vue algébrique, mais aussi du point de vue des produits non conservatifs. Tout d'abord, on peut montrer que la définition de la vitesse interfaciale est étroitement liée à la nature du champ associé à l'onde transportant le taux de vide. On isole alors trois définitions de la vitesse interfaciale telles que ce champ soit linéairement dégénéré, c'est-à-dire que l'interface associée au taux de vide soit infiniment mince pour toute condition initiale de type Riemann. On en déduit que le principe du maximum sur la fraction volumique est alors assuré à travers toutes les ondes du système. Ensuite, deux manières de définir la pression interfaciale sont présentées, toutes deux permettant une fermeture naturelle des produits non conservatifs. La première consiste à définir la pression interfaciale de manière à associer au système initial une inégalité d'entropie conservative. Après une étude champ par champ, on peut noter que la définition de la pression interfaciale conduisant à cette inégalité d'entropie assure *a posteriori* la positivité des fractions massiques et des énergies internes à la traversée de toutes les ondes du système convectif. Ainsi, la solution du problème de Riemann associé est bien admissible. Malheureusement, la résolution complète du problème de Riemann semble hors d'atteinte, les sept ondes n'étant pas ordonnées et pouvant même se superposer. La seconde manière de fermer les produits non conservatifs du système est de définir la pression interfaciale comme fonction des invariants de Riemann connus associés à l'onde de taux de vide. Bien que cette seconde voie semble elle aussi prometteuse, elle n'a pas été étudiée dans le cadre de cette thèse.

Concernant l'approximation numérique, on se base sur une technique de splitting d'opérateur, découplant les effets convectifs des différents termes sources (termes de relaxation, gravité, termes d'échange à l'interface, ...). Cette méthode d'approximation s'avère en effet très robuste et d'une précision tout à fait acceptable (voir les différents tests au chapitre 3). De plus, sa mise en œuvre est simple relativement à celle de méthodes couplant convection et termes source. La partie convection est approchée à l'aide de méthodes Volumes Finis adaptées au cadre non conservatif (elles s'étendent naturellement au cadre multidimensionnel et aux maillages non structurés). La première est basée sur le schéma de Rusanov. Elle assure de manière discrète le principe du maximum sur la fraction volumique et la positivité des fractions massiques. La seconde méthode est une extension du schéma de Godunov approché VFRoe-ncv (voir chapitre 1 et annexe A). On note que, pour les lois thermodynamiques admissibles par les opérateurs de moyenne classiques (voir l'annexe 4.A de ce chapitre), ces deux méthodes permettent de maintenir des écoulements à vitesse et pression constantes. La prise en compte des termes de relaxation en vitesse et en pression assure le principe du maximum sur la fraction volumique et la positivité des fractions massiques et des pressions phasiques du point de vue discret.

On présente ensuite plusieurs cas tests. Les premiers concernent des expériences de type problème de Riemann, et ne font intervenir aucun effet de relaxation. Une seconde partie concerne les cas tests avec prise en compte des effets de trainée statique et de relaxation en pression.

Bien sûr, diverses améliorations des schémas présentés ici sont possibles, notamment par rapport aux remarques soulevées dans le préambule du chapitre 1. Un des points essentiels concerne la condition CFL. En effet, celle-ci est basée sur la vitesse des ondes dites « de pression » associées à la phase liquide, qui est extrêmement rapide par rapport à la vitesse d'écoulement du mélange. De ce fait, le « nombre CFL » est loin d'être optimal pour le calcul du taux de présence de la phase vapeur. Ainsi, des méthodes de préconditionnement pourraient être mises en œuvre pour ajuster

le pas de temps sur les ondes lentes. Concernant les termes de relaxation en pression et en vitesse, il pourrait être nécessaire de les prendre en compte de manière couplée avec les termes convectifs, comme cela est fait dans le cadre du chapitre 3.

Numerical modeling of two phase flows using the two fluid two pressure approach

Co-authored with Thierry Gallouët and Jean-Marc Hérard.

Abstract

The present paper is devoted to the computation of two-phase flows using the two-fluid approach. The overall model is hyperbolic and has no conservative form. No instantaneous local equilibrium between phases is assumed, which results in a two-velocity two-pressure model. Original closure laws for interfacial velocity and interfacial pressure are proposed. These closures allow to deal with discontinuous solutions such as shock waves and contact discontinuities without ambiguity for the definition of Rankine-Hugoniot jump relations. Each field of the convective system is investigated, providing that the maximum principle for the void fraction and the positivity of densities and internal energies are ensured when focusing on the Riemann problem. After, two finite volume methods are presented, based on the Rusanov scheme and on an approximate Godunov scheme. Relaxation terms are taken into account using a fractional step method. At the end, numerical tests illustrate the ability of both method to compute two-phase flows.

4.1 Introduction

Computation of two-phase flows has been generally based on the homogeneous approach in order to compute either gas-solid flows or gas-liquid flows, see *e.g.* [FHBT00], [GF96], [Tou00]. When focusing on the two-fluid approach, the problem becomes tricky, due to the fact that two-fluid models with an equilibrium pressure assumption have some well-known drawbacks. One of them is that these systems contain non conservative terms (which is an annoying point [Col92], [DLM95], [Sai96]). Furthermore, such models do not necessarily remain hyperbolic in all situations, which means that the initial value problem may be "ill-posed" for a large class of initial conditions. Last but not least, it clearly appears that the maximum principle for the void fraction does not necessarily hold in general even for smooth solutions, except perhaps in some situations corresponding to the modeling of gas particle flows including granular pressure effects (see for instance [CH99], [Gid93], [GSG96], [Sim95]).

Some recent ideas have been proposed to cope with this kind of system. Roughly speaking, one way to deal with these is based on the use of developments written related to a some small parameter (for

En préparation.

instance the relative velocity [Tou00], [TKP99], the void fraction [Sai95] or the density ratio). Other ways to deal with these are based on use of an extension of the notion of upwinding [GKL96] or of the use of fractional step techniques [CEG$^+$97], [CH99], [HMS99]. Though numerical results are rather encouraging, one may still wonder whether the lack of hyperbolicity has not been enforced by some failure in closure assumptions. Some time ago, V.H. Ransom and D.L. Hicks [RH84] suggested to use a two-pressure model based on a eight-equation model. More recently, M.R. Baer and J.W. Nunziato suggested in [BN86] to adopt a similar approach. Their model has been studied and extended by A.K. Kapila *et al.* [KSB$^+$97] and S. Gavrilyuk and R. Saurel [GS02]. Other two-pressure models have been proposed by J. Glimm and co-workers [GSS96], [GSS99] and by K.A. Gonthier and J.M. Powers [GP00]. Here, the system is composed by seven partial differential equations: one transport equation for the void fraction, two for the mass of each fluid, two for the momentum of each fluid and two for the energy of each fluid. Several definitions of the interfacial velocity and of the interfacial pressure have been proposed in references mentionned above. The present paper adopts an original approach, based on the analysis of the one-dimensional Riemann problem and on the definition of discontinuous solutions in order to deal with non conservative products and to ensure the maximum principle for the void fraction, as presented in [CGHS02]. We restrict herein on the one-dimensional framework.

The present paper is organized as follows. The first section presents the model devoted to the computation of two-phase flows, using the two-fluid approach. No assumption towards equilibrium pressure is required here and the overall model is unconditionally hyperbolic and non conservative. Properties of smooth solutions are investigated. Several closures for the interfacial velocity and the interfacial pressure are then proposed. Assuming that the interface between two mixtures of fluids remains infinitely thin when restricting to convective effects, three different forms of interfacial velocity are exhibited. In other words, these closures for the interfacial velocity permit to obtain a linearly degenerate field associated to the wave which initially separates two mixtures. The definition of the interfacial pressure is strongly related to the closure of the non conservative terms. A first definition enables to complement the system with a natural entropy inequality and a field by field study of the solution of the one-dimensional Riemann problem is provided. Another way of closure for the interfacial pressure is proposed, but is not investigated here. We discuss afterwards about the approximation of solutions of the system. The approximation of convective terms and source terms is cast into two different steps using a splitting method. The convective part is computed using finite volume schemes adapted to the non conservative frame. Two methods, based on the Rusanov scheme [Rus61] and on the VFRoe-ncv scheme [BGH00], are tested here. Pertaining to relaxation terms (drag force and pressure relaxation), we propose an approximation in agreement with the properties fulfilled by smooth solutions. At the end, several numerical tests are performed to compare the robustness and the accuracy of both methods when computing shock tube test cases as well as the water faucet problem.

4.2 The two-fluid two-pressure model

We present here the global two-fluid system. We focus our analysis on the convective part of the system. The different properties of this system are investigated for smooth solutions as studying the associated Riemann problem.

4.2.1 Governing equations

The governing set of equations contains convective terms, source terms and diffusive terms. It takes the form for $t > 0$, $x \in \mathbb{R}$:

$$(Id + D(W))\frac{\partial W}{\partial t} + \frac{\partial F(W)}{\partial x} + C(W)\frac{\partial W}{\partial x} = S(W) + \frac{\partial}{\partial x}\left(E(W)\frac{\partial (W)}{\partial x}\right), \tag{4.1}$$

where $W = W(t,x)$ is the unknown function from $\mathbb{R}_+ \times \mathbb{R}$ to Ω (with Ω a subset of $\mathbb{R}^7$), F, and S are functions from Ω to $\mathbb{R}^7$, while C, D and E are functions from Ω to $\mathbb{R}^{7\times 7}$ and Id is the identity matrix of $\mathbb{R}^{7\times 7}$. Of course, the extension of (4.1) to a multidimensional framework is classical. The so called conservative variable W is

$$W = \begin{pmatrix} \alpha_1 \\ \alpha_1\rho_1 \\ \alpha_1\rho_1 U_1 \\ \alpha_1 E_1 \\ \alpha_2\rho_2 \\ \alpha_2\rho_2 U_2 \\ \alpha_2 E_2 \end{pmatrix},$$

where α_k is the void fraction of phase k, ρ_k, U_k and E_k are respectively the density, the velocity and the total energy of phase k, $k = 1, 2$. We define too the mass fraction $m_k = \alpha_k\rho_k$ and the pressure P_k of phase k. Let $\Omega = \{W \in \mathbb{R}^7; \alpha_1 \in (0,1), m_k > 0, E_k/\rho_k - (U_k)^2/2 > 0, k = 1, 2\}$ be the set of admissible states. The convective part (*i.e.* the left handside) of system (4.1) is defined by

$$D(W)\frac{\partial W}{\partial t} = \begin{pmatrix} 0 \\ 0 \\ 0 \\ P_i(W)\partial_t\alpha_1 \\ 0 \\ 0 \\ P_i(W)\partial_t\alpha_2 \end{pmatrix}, \; F(W) = \begin{pmatrix} 0 \\ \alpha_1\rho_1 U_1 \\ \alpha_1(\rho_1 U_1^2 + P_1) \\ \alpha_1 U_1(E_1 + P_1) \\ \alpha_2\rho_2 U_2 \\ \alpha_2(\rho_2 U_2^2 + P_2) \\ \alpha_2 U_2(E_2 + P_2) \end{pmatrix}, \; C(W)\frac{\partial W}{\partial x} = \begin{pmatrix} V_i(W)\partial_x\alpha_1 \\ 0 \\ -P_i(W)\partial_x\alpha_1 \\ 0 \\ 0 \\ +P_i(W)\partial_x\alpha_1 \\ 0 \end{pmatrix},$$

where $V_i(W)$ and $P_i(W)$ are the interfacial velocity and the interfacial pressure. Source terms S may be written as in [SA99a]:

$$\begin{aligned} S(W) = {}^t\big(& K_P(W)(P_1 - P_2), \\ & \dot{m}(W), -K_U(W)(U_1 - U_2) + \dot{m}(W)V_i(W), -K_U(W)V_i(W)(U_1 - U_2) + \dot{m}(W)E_i(W), \\ & -\dot{m}(W), +K_U(W)(U_1 - U_2) - \dot{m}(W)V_i(W), +K_U(W)V_i(W)(U_1 - U_2) - \dot{m}(W)E_i(W)\big) \end{aligned}$$

where we note K_U and K_P the positive functions of velocity and pressure relaxation, $\dot{m}$ the mass transfer and E_i the interfacial energy. Note that terms $K_U(W)(U_1 - U_2)$ correspond to drag force

effects. Viscous terms are accounted for through contribution pertaining to $E(W)$:

$$E(W)\frac{\partial(W)}{\partial x} = \begin{pmatrix} 0, \\ 0, \\ \partial_x(\mu_1 \Gamma(U_1)) \\ \partial_x(\mu_1 \Gamma(U_1)U_1) + \partial_x(\kappa_1 \partial_x T_1) \\ 0, \\ \partial_x(\mu_2 \Gamma(U_2)) \\ \partial_x(\mu_2 \Gamma(U_2)U_2) + \partial_x(\kappa_2 \partial_x T_2) \end{pmatrix}, \quad \text{with} \quad \Gamma(U_k) = \frac{4}{3}\partial_x U_k, \tag{4.2}$$

where T is the temperature $T = P/\rho$, and μ_k and κ_k refer to the laminar viscosity and the conductivity coefficient of phase k, $k = 1, 2$. Coefficient $4/3$ in the definition of the viscous stress tensor Γ is provided from the 3D framework.

The system (4.1) is associated with an initial data $W_0 \in \Omega$:

$$W(t = 0, x) = W_0(x), \quad x \in \mathbb{R}, \tag{4.3}$$

and must be complemented with some closure laws. The void fractions must comply with

$$\alpha_1 + \alpha_2 = 1.$$

Moreover, total energies E_k follow

$$E_k = \rho_k e_k + \rho_k (U_k)^2/2, \quad k = 1, 2,$$

where internal energies e_k verify the equations of state

$$e_k = \varepsilon_k(P_k, \rho_k), \quad k = 1, 2.$$

Remark 4.1. System (4.1) is obtained after an averaging process (see more details in [Ish75]) and variables considered here are mean values. Initially, phases are separated one from another, and a thermodynamics law is available in each phase. Usually, laws which link thermodynamical variables after the averaging process may differ from initial laws. However, basic laws, such as the perfect gas equation of state or the Tammann equation of state, which verify

$$\rho_k \varepsilon_k(P_k, \rho_k) = g_k P_k + b_k \rho_k + c_k \tag{4.4}$$

(where $g_k > 0$, b_k and c_k are real constants) remain unchanged after the averaging process unlike in more complex thermodynamical laws such as Van der Waals equation of state (see appendix 4.A for more details).

One still needs to detail both interfacial pressure P_i and interfacial velocity V_i. We assume that V_i follows

$$V_i(W) = \beta(W)U_1 + (1 - \beta(W))U_2 \tag{4.5}$$

Scalar dimensionless function β is non negative and bounded by 1. Definition (4.5) enables to account for kinematic equilibrium since $U_2 = U_1$ implies $V_i = U_1 = U_2$. Pertaining to P_i, one may expect that the relation

$$U_1 = U_2 \text{ and } P_1 = P_2 \implies P_i = P_1 = P_2 \tag{4.6}$$

holds. Of course, equation (4.5) and relation (4.6) are too general to deduce at this stage explicit forms of V_i and P_i. Nonetheless, several properties for the convective part of system (4.1) are available.

4.2.2 Some properties of the convective system

Though system (4.1) is not completely closed (V_i and P_i have not been explicited), some properties are exposed below to determine whether this system is relevant to describe two-phase flows. Hyperbolicity, maximum principle, positivity requirement are investigated. The isentropic framework is briefly dealt too. We emphasize that all the following results are independent from the closure of interfacial pressure P_i and interfacial velocity V_i.

The homogeneous problem associated to (4.1) may be written under the form, for $t > 0$ and $x \in \mathbb{R}$:

$$\partial_t(\alpha_1) + V_i(W)\,\partial_x\alpha_1 = 0, \tag{4.7a}$$
$$\partial_t(\alpha_1\rho_1) + \partial_x\left(\alpha_1\rho_1U_1\right) = 0, \tag{4.7b}$$
$$\partial_t(\alpha_2\rho_2) + \partial_x\left(\alpha_2\rho_2U_2\right) = 0, \tag{4.7c}$$
$$\partial_t(\alpha_1\rho_1U_1) + \partial_x\left(\alpha_1\rho_1U_1^2 + \alpha_1P_1\right) - P_i(W)\,\partial_x\alpha_1 = 0, \tag{4.7d}$$
$$\partial_t(\alpha_2\rho_2U_2) + \partial_x\left(\alpha_2\rho_2U_2^2 + \alpha_2P_2\right) + P_i(W)\,\partial_x\alpha_1 = 0, \tag{4.7e}$$
$$\partial_t(\alpha_1E_1) + \partial_x\left(\alpha_1U_1(E_1 + P_1)\right) - V_i(W)P_i(W)\,\partial_x\alpha_1 = 0, \tag{4.7f}$$
$$\partial_t(\alpha_2E_2) + \partial_x\left(\alpha_2U_2(E_2 + P_2)\right) + V_i(W)P_i(W)\,\partial_x\alpha_1 = 0. \tag{4.7g}$$

We define the celerity c_k and the coefficient $\hat{\gamma}_k$ of phase k by

$$\rho_k(c_k)^2 = \left(\frac{P_k}{\rho_k} - \rho_k\frac{\partial\varepsilon_k}{\partial\rho_k}\right)\left(\frac{\partial\varepsilon_k}{\partial P_k}\right)^{-1},$$
$$\rho_k(c_k)^2 = \hat{\gamma}_kP_k,$$

and the partial specific entropy s_k of phase k, $k = 1, 2$, by $s_k = \varsigma_k(P_k, \rho_k)$, where ς_k complies with

$$\hat{\gamma}_kP_k\frac{\partial\varsigma_k}{\partial P_k} + \rho_k\frac{\partial\varsigma_k}{\partial\rho_k} = 0.$$

The following proposition holds:

Proposition 4.1. *The homogeneous problem* (4.7) *is non strictly hyperbolic on* Ω*, in the sense that it admits real eigenvalues and the right eigenvectors span the whole space* $\mathbb{R}^7$*, except when some eigenvalues identify. Eigenvalues are simply:*

$$\lambda_1 = V_i,$$
$$\lambda_2 = U_1 - c_1, \quad \lambda_3 = U_1, \quad \lambda_4 = U_1 + c_1,$$
$$\lambda_5 = U_2 - c_2, \quad \lambda_6 = U_2, \quad \lambda_7 = U_2 + c_2.$$

Moreover, fields associated to waves λ_2*,* λ_4*,* λ_5 *and* λ_7 *are* genuinely non linear *and fields associated to waves* λ_3 *and* λ_6 *are* linearly degenerate*.*

Refer to [GR96] or [Smo83] for the definition of genuinely non linear or linearly degenerate fields.

Proof. Let us define $Y = {}^t(\alpha_1, s_1, U_1, P_1, s_2, U_2, P_2)$. The study of the hyperbolicity of system (4.7) does not depend on the use of W or Y. System (4.7) may be written with respect to Y,

which gives for regular solutions in Ω

$$\frac{\partial Y}{\partial t} + B(Y)\frac{\partial Y}{\partial x} = 0,$$

where

$$B(Y) = \begin{pmatrix} V_i & 0 & 0 & 0 & 0 & 0 & 0 \\ \beta_2(Y) & U_1 & 0 & 0 & 0 & 0 & 0 \\ \beta_3(Y) & 0 & U_1 & \tau_1 & 0 & 0 & 0 \\ \beta_4(Y) & 0 & \hat{\gamma}_1 P_1 & U_1 & 0 & 0 & 0 \\ \beta_5(Y) & 0 & 0 & 0 & U_2 & 0 & 0 \\ \beta_6(Y) & 0 & 0 & 0 & 0 & U_2 & \tau_2 \\ \beta_7(Y) & 0 & 0 & 0 & 0 & \hat{\gamma}_2 P_2 & U_2 \end{pmatrix}. \tag{4.8}$$

Coefficients β_p, $p = 2, ..., 7$ write

$$\begin{aligned} \beta_2(Y) &= \frac{-(U_1 - V_i)(P_1 - P_i)}{\alpha_1\rho_1}\left(\frac{\partial \varepsilon_1}{\partial P_1}\right)^{-1}\frac{\partial \varsigma_1}{\partial P_1}, & \beta_5(Y) &= \frac{(U_2 - V_i)(P_2 - P_i)}{\alpha_2\rho_2}\left(\frac{\partial \varepsilon_2}{\partial P_2}\right)^{-1}\frac{\partial \varsigma_2}{\partial P_2}, \\ \beta_3(Y) &= \frac{P_1 - P_i}{\alpha_1\rho_1}, & \beta_6(Y) &= -\frac{P_2 - P_i}{\alpha_2\rho_2}, \\ \beta_4(Y) &= \frac{U_1 - V_i}{\alpha_1\rho_1}\left(P_i - \frac{\partial \varepsilon_1}{\partial \rho_1}\right)\left(\frac{\partial \varepsilon_1}{\partial P_1}\right)^{-1}, & \beta_7(Y) &= -\frac{U_2 - V_i}{\alpha_2\rho_2}\left(P_i - \frac{\partial \varepsilon_2}{\partial \rho_2}\right)\left(\frac{\partial \varepsilon_2}{\partial P_2}\right)^{-1}. \end{aligned}$$

and we note $\tau_k = 1/\rho_k$, $k = 1, 2$. The hyperbolicity of system (4.7) is then proved by a classical analysis of matrix B. We focus now on right eigenvectors of B. The matrix R of right eigenvectors writes

$$R(Y) = \begin{pmatrix} r_1^{(1)}(Y) & 0 & 0 & 0 & 0 & 0 & 0 \\ r_1^{(2)}(Y) & 1 & 0 & 0 & 0 & 0 & 0 \\ r_1^{(3)}(Y) & 0 & \tau_1 & \tau_1 & 0 & 0 & 0 \\ r_1^{(4)}(Y) & 0 & -c_1 & c_1 & 0 & 0 & 0 \\ r_1^{(5)}(Y) & 0 & 0 & 0 & 1 & 0 & 0 \\ r_1^{(6)}(Y) & 0 & 0 & 0 & 0 & \tau_2 & \tau_2 \\ r_1^{(7)}(Y) & 0 & 0 & 0 & 0 & -c_2 & c_2 \end{pmatrix} \tag{4.9}$$

where $r_1^{(p)}$ is the p^{th} component of the first right eigenvector of matrix B, that is

$$\begin{aligned} {}^t r_1(Y) = \Bigg(1, &\frac{-\beta_2}{U_1 - V_i}, \frac{\tau_1\beta_4 - (U_1 - V_i)\beta_3}{(U_1 - V_i)^2 - c_1^2}, \frac{c_1^2\beta_3 - \tau_1(U_1 - V_i)\beta_4}{\tau_1((U_1 - V_i)^2 - c_1^2)}, \\ &\frac{-\beta_5}{U_2 - V_i}, \frac{\tau_2\beta_7 - (U_2 - V_i)\beta_6}{(U_2 - V_i)^2 - c_2^2}, \frac{c_2^2\beta_6 - \tau_2(U_2 - V_i)\beta_7}{\tau_2((U_2 - V_i)^2 - c_2^2)}\Bigg). \end{aligned}$$

For a sake of completeness, we provide the matrix of left eigenvectors:

$$R(Y)^{-1} = \begin{pmatrix} l_1^{(1)}(Y) & 0 & 0 & 0 & 0 & 0 & 0 \\ l_2^{(1)}(Y) & 1 & 0 & 0 & 0 & 0 & 0 \\ l_3^{(1)}(Y) & 0 & \frac{1}{2\tau_1} & \frac{-1}{2c_1} & 0 & 0 & 0 \\ l_4^{(1)}(Y) & 0 & \frac{1}{2\tau_1} & \frac{1}{2c_1} & 0 & 0 & 0 \\ l_5^{(1)}(Y) & 0 & 0 & 0 & 1 & 0 & 0 \\ l_6^{(1)}(Y) & 0 & 0 & 0 & 0 & \frac{1}{2\tau_2} & \frac{-1}{2c_2} \\ l_7^{(1)}(Y) & 0 & 0 & 0 & 0 & \frac{1}{2\tau_2} & \frac{1}{2c_2} \end{pmatrix} \tag{4.10}$$

with

$$\begin{pmatrix} l_1^{(1)} \\ l_2^{(1)} \\ l_3^{(1)} \\ l_4^{(1)} \\ l_5^{(1)} \\ l_6^{(1)} \\ l_7^{(1)} \end{pmatrix} = \begin{pmatrix} 1 \\ -r_1^{(2)} \\ \frac{\tau_1 r_1^{(4)} - c_1 r_1^{(3)}}{2\tau_1 c_1} \\ -\frac{\tau_1 r_1^{(4)} + c_1 r_1^{(3)}}{2\tau_1 c_1} \\ -r_1^{(5)} \\ \frac{\tau_2 r_1^{(7)} - c_2 r_1^{(6)}}{2\tau_2 c_2} \\ -\frac{\tau_2 r_1^{(7)} + c_2 r_1^{(6)}}{2\tau_2 c_2} \end{pmatrix}.$$

Then, we can provide the conditions ensuring that right eigenvectors of B span $\mathbb{R}^7$, that are

$$\lambda_1 \neq \lambda_p, \quad p = 2, 4, 5, 7. \tag{4.11}$$

If these conditions (4.11) are fulfilled, right eigenvectors of $B(Y)$ are linearly independent one to the other. Focusing on the nature of fields associated to waves λ_p, $p = 2, ..., 7$, see [Smo83]. □

Let us emphasize that the result on the hyperbolicity of system (4.7) is very important when dealing with two-fluid models. Indeed, no condition is required here on the initial data (4.3) to obtain real eigenvalues, contrary to the classical two-fluid one-pressure framework. This property is merely due to the partial differential equation for the void fraction α_1 which allows to replace non conservative terms $P_i \partial_t \alpha_k$ by $-P_i V_i \partial_x \alpha_k$ for $k = 1, 2$. Note that the hyperbolicity is non strict, which means that some eigenvalues may identify. In this case, a resonant behaviour may occur (see [CL99], [SM98], [SV03]).

Pertaining to the structure of matrix B and matrix R, one may see that phases 1 and 2 are only coupled by the first column, corresponding to $\partial_x \alpha_1$ in B and related to the wave $\lambda_1 = V_i$. This largely reduces the complexity of the study of the convective system (4.7) since phases evolve independently on each side of the 1-wave. Nevertheless, the nature of the field associated to λ_1 remains unknown, since V_i is not still defined.

We focus now on the maximum principle on the void fraction α_1 and on the positivity constraints on partial masses m_k, $k = 1, 2$. The study which follows is restricted to smooth solutions of system (4.7). Unfortunately, no similar property exists for pressures P_k (or internal energies e_k), $k = 1, 2$. In section 4.2.3, the Riemann problem is presented and maximum principle and positivity

requirements through elementary waves are investigated in order to extend these properties to discontinuous solutions.

First, let us consider the maximum principle on the void fraction α_1. The partial differential equation associated to α_1 is written with a general relaxation term in pressure:

$$\frac{\partial \alpha_1}{\partial t} + V_i(W)\frac{\partial \alpha_1}{\partial x} = \frac{\alpha_1\alpha_2}{\theta(W)}\frac{P_1 - P_2}{P_1 + P_2}, \quad t \in [0,T], x \in [0,L], \tag{4.12}$$

where θ is a positive real function of W, which may become small. Note that the right handside of (4.12) provides a exponentially decreasing relaxation (see section 4.3.2). The result for the maximum principle is stated by the following proposition:

Proposition 4.2. *Let L and T be two positive real constants. Assume that V_i, $\partial_x V_i$ and $(\alpha_1 - \alpha_2)/\theta$ belong to $L^\infty([0,T]\times[0,L])$. Then, equation (4.12) on the void fraction α_1 associated with admissible inlet boundary conditions, that is $\alpha_1(t, x = 0)$ and $\alpha_1(t, x = L)$ in $(0,1)$ for all t in $[0,T]$, leads to*

$$0 \leq \alpha_1(t,x) \leq 1, \quad \forall (t,x) \in [0,T]\times[0,L], \tag{4.13}$$

when restricting to regular solutions and assuming that $P_k > 0$, $k = 1,2$.

Of course, the maximum principle on α_2 is verified too, from (4.13) and the closure relation $\alpha_1 + \alpha_2 = 1$. Moreover, the same result obviously holds if the relaxation term is null as in equation (4.7a).

Proof. Let ν be the function defined as $\nu = \alpha_1\alpha_2$. Clearly, condition (4.13) is fulfilled iff $\nu > 0$. Equation (4.12) gives

$$\frac{\partial \nu}{\partial t} + V_i\frac{\partial \nu}{\partial x} = \nu\frac{(\alpha_2 - \alpha_1)}{\theta}\frac{P_1 - P_2}{P_1 + P_2}.$$

Lemma 4.6 ensures the positivity of ν, which concludes this proof. □

A property of positivity for $m_k = \alpha_k\rho_k$, $k = 1,2$, may be proved too for smooth solutions. The related partial differential equations write

$$\frac{\partial m_k}{\partial t} + U_k\frac{\partial m_k}{\partial x} + m_k\frac{\partial U_k}{\partial x} = 0 \tag{4.14}$$

when restricting to smooth solutions. We may state the following proposition:

Proposition 4.3. *Let L and T be positive real constants. Assume that U_k and $\partial_x U_k$ belong to $L^\infty([0,T]\times[0,L])$, $k = 1,2$. Then, for $k = 1,2$, equation (4.14) on the partial mass m_k associated with admissible inlet boundary conditions, that is $m_k(t, x = 0)$ and $m_k(t, x = L)$ positive for all t in $[0,T]$, leads to*

$$m_k(t,x) \geq 0, \quad \forall (t,x) \in [0,T]\times[0,L], \tag{4.15}$$

when restricting to regular solutions.

Once more, the *proof* of this proposition is directly given by Lemma 4.6.

We recall now the partial differential equation associated to pressure P_k, $k = 1, 2$:

$$\frac{\partial P_k}{\partial t} + U_k \frac{\partial P_k}{\partial x} + \hat{\gamma}_k P_k \frac{\partial U_k}{\partial x} + \frac{(U_k - V_i)}{\alpha_k} \left(\frac{P_i}{\rho_k} - \rho_k \frac{\partial \varepsilon_k}{\partial \rho_k} \right) \left(\frac{\partial \varepsilon_k}{\partial P_k} \right)^{-1} \frac{\partial \alpha_k}{\partial x} = 0. \tag{4.16}$$

Since V_i and P_i are not still defined, the behaviour of the coefficient of $\partial_x \alpha_k$ remains unknown. Hence, the positivity of pressures P_1 and P_2 is not ensured, even restricting to smooth solutions.

We provide herein a result concerning the isentropic framework. The following proposition holds:

Proposition 4.4. *We restrict once more to smooth solutions of system* (4.7)*. For each phase k, $k = 1, 2$, assume that function P_k may be written under the form $\varphi_k(\rho_k)$ where φ_k is a monotone increasing function. Therefore, P_k is solution of* (4.16) *if and only if*

$$\rho_k \varphi_k'(\rho_k) = \hat{\gamma}_k P_k \tag{4.17}$$

$$\text{and} \quad P_k = P_i, \tag{4.18}$$

assuming that, for $k = 1, 2$, product $(U_k - V_i)\partial_x \alpha_k$ is non null.

Proof. Using equations of pressure P_k and density ρ_k, some easy calculations lead to relations (4.17) and (4.18). Relation (4.17) is the counterpart of the relation when dealing with classical Euler system and (4.18) is derived from terms in $\partial_x \alpha_k$, appearing in equations of pressure and density. □

Remark 4.2. *a* — Assume first that $\beta(1 - \beta) \neq 0$ in (4.5). Then, if there exists a function $P_1 = \varphi_1(\rho_1)$ which is an integral solution of (4.16) with $k = 1$, then no solution of (4.16) with $k = 2$ of the form $P_2 = \varphi_2(\rho_2)$ may be found (except under pressure equilibrium $P_1 = P_2 = P_i$). This means that an isentropic form of system (4.7) for *both* phases does not exist far from the thermodynamical equilibrium, when using classical isentropic curves.
b — Assume now that $\beta = 1$ (respectively $\beta = 0$), that is $V_i = U_1$ (resp. $V_i = U_2$), then one may find $P_k = \varphi_k(\rho_k)$, $k = 1, 2$, solutions of (4.16) if and only if $P_i = P_2$ (resp. $P_i = P_1$). Note that these closures for V_i and P_i have been proposed in [BN86] for instance (see comments at the end of section 4.2.3).

4.2.3 Field by field study and closure relations for the interfacial pressure and for the interfacial velocity

We turn now to closure laws on P_i and V_i. Additionnal properties of the convective system, in particular when focusing on the Riemann problem and the parametrisation through the wave V_i, strongly depend on the definition of P_i and V_i. Let us recall that a Riemann problem corresponds to a Cauchy problem for system (4.7) with an initial condition of the form:

$$W(t = 0, x) = \begin{cases} W_L, & \text{if } x < 0, \\ W_R, & \text{if } x > 0, \end{cases} \tag{4.19}$$

where W_L and W_R belong to Ω. We restrict our study to self-similar solutions composed by constant states separated by elementary waves. Moreover, we assume that initial condition (4.19) does not provide a non diagonalizable convective matrix (see conditions (4.11)). At this stage, though P_i and V_i remain unknown, some informations are available on p-waves, $p = 2, ..., 7$. Actually, since α_1 is constant on each side of the 1-wave, system (4.7) locally reduces to two conservative Euler systems. Hence, related Riemann invariants and Rankine-Hugoniot jump relations are locally well defined for all p-waves, $p = 2, ..., 7$, and their parametrisation is classical (refer for instance to [Smo83] for a complete description). First, noting $I^p(W)$ the vector of p-Riemann invariants, we have:

$$
\begin{aligned}
I^2(W) &= {}^t(\tau_2, u_2, p_2, \alpha_1, s_1, u_1 + f_1(s_1, \rho_1)), & I^5(W) &= {}^t(\tau_1, u_1, p_1, \alpha_1, s_2, u_2 + f_2(s_2, \rho_2)),\\
I^3(W) &= {}^t(\tau_2, u_2, p_2, \alpha_1, p_1, u_1), & I^6(W) &= {}^t(\tau_1, u_1, p_1, \alpha_1, p_2, u_2),\\
I^4(W) &= {}^t(\tau_2, u_2, p_2, \alpha_1, s_1, u_1 - f_1(s_1, \rho_1)), & I^7(W) &= {}^t(\tau_1, u_1, p_1, \alpha_1, s_2, u_2 - f_2(s_2, \rho_2)),
\end{aligned}
$$

where f_1 and f_2 are defined by $\partial f_k/\partial \rho_k = c_k/\rho_k$, $k = 1, 2$. Since the system is locally conservative, p-Riemann invariants and jump relations for linearly degenerate p-fields, *i.e.* for $p = 3, 6$, identify. Pertaining to genuinely non linear fields, Rankine-Hugoniot jump relations through a discontinuity of speed σ write:

$$
\begin{aligned}
&[\alpha_k] = 0\,,\\
&[m_k(u_k - \sigma)] = 0\,,\\
&[m_k u_k(u_k - \sigma) + \alpha_k p_k] = 0\,,\\
&[\alpha_k E_k(u_k - \sigma) + \alpha_k p_k u_k] = 0\,,\\
&[\tau_{k'}] = 0\,, \quad [u_{k'}] = 0\,, \quad [p_{k'}] = 0\,,
\end{aligned}
$$

where for $p = 2, 4$, we have $k = 1$ and $k' = 2$, and for $p = 5, 7$, we have $k = 2$ and $k' = 1$. Moreover, brackets [.] denote the difference between the state at the right of the discontinuity and the state at the left of the discontinuity. Noting W_l (respectively W_r) the constant state just on the left side (resp. the right side) of the 1-wave, previous Riemann invariants and Rankine-Hugoniot jump relations allow to link W_L to W_l and W_R to W_r. A first result holds:

Proposition 4.5. *The Riemann problem* (4.7)-(4.19) *has a unique entropy consistent solution involving constant states separated by shocks, rarefaction waves and contact discontinuities, provided the initial data* (4.3) *is in agreement with*

$$
|(U_k)_R - (U_k)_L| < \frac{2}{\gamma_k - 1}((c_k)_L + (c_k)_R), \tag{4.20}
$$

$k = 1, 2$, *under the condition* $(\alpha_1)_L = (\alpha_1)_R$.

Proof. Since $(\alpha_1)_L = (\alpha_1)_R$, phases evolve independently ($W_l = W_r$). Therefore, this proof reduces to the classical theorem of existence and uniqueness for the solution of the Riemann problem associated to the Euler frame (see for instance [GR96] or [Smo83]). □

We turn now to the connection between W_l and W_r through the 1-wave. Since the interfacial velocity V_i and the interfacial pressure P_i are still undefined, this connection cannot be performed. Let us recall that we restrict our study to interfacial velocity of the form (4.5) and interfacial pressure such that (4.6) is verified.

Interfacial velocity

As stated in Proposition 4.1, the type of the field corresponding to the wave V_i is unknown. Two distinct cases immediately appear. In the first one, the function β in (4.5) is such that the 1-field is genuinely non linear. However, such a choice should give for a class of initial conditions a rarefaction wave for the 1-field. Therefore, a mixture zone would appear inside this rarefaction wave. To avoid this phenomenon, we assume that the 1-field is linearly degenerate, which means that the function β must be such that for all W in Ω we have

$$\nabla_W V_i(W).r_1(W) = 0,$$

where $r_1(W)$ stands for the right eigenvector associated with the first eigenvalue, namely V_i. Such an assumption ensures that the wave associated to this field remains infinitely thin, whatever initial condition (4.19) is. We have actually the following result:

Proposition 4.6. *The field associated to the eigenvalue V_i is linearly degenerate if*

$$\begin{aligned} \beta(W) &= \frac{\alpha_1\rho_1}{\alpha_1\rho_1 + \alpha_2\rho_2} \\ \text{or} \quad \beta(W) = 1 \quad &\text{or} \quad \beta(W) = 0, \end{aligned} \tag{4.21}$$

for all W in Ω in definition (4.5).

Proof. This result is obtained after some tedious calculations, which are not exposed here. These calculations are greatly simplified supposing that the interface velocity coefficient takes the form

$$\beta(W) = \beta\left(\alpha_1, \frac{\rho_1}{\rho_2}, \frac{P_1}{P_2}\right). \tag{4.22}$$

This assumption fulfills classical requirements such as galilean invariance and objectivity. Even more, under this assumption, the sufficient condition (4.21) becomes necessary. Nevertheless, one may note that the relative velocity $|U_1 - U_2|$ has not been accounted for in (4.22). Indeed, it seems unfeasable to obtain explicit definitions of β when adding this argument to (4.22). □

At this stage, the non conservative product $V_i\partial_x\alpha_1$ is well defined, from a local point of view. Indeed, by definition, V_i is a 1-Riemann invariant. Moreover, α_1 remains unchanged through p-waves ($p = 2, 3, ..., 7$). Therefore, when one of two factors of the non conservative product admits a discontinuity, the other one is constant. Therefore, using closure (4.21), one may try to connect state W_l with state W_r. In order to have a parametrisation for the 1-wave, one must find six 1-Riemann invariants $(I_p^1)_{p=1,...,6}$ such that their gradient $(\nabla I_p^1)_{p=1,...,6}$ are linearly independent. Since P_i is not defined, only five 1-Riemann invariants can be provided explicitely:

$$I_1^1(W) = V_i, \tag{4.23}$$

$$I_2^1(W) = \frac{m_1 m_2}{m_1 + m_2}(U_1 - U_2), \tag{4.24}$$

$$I_3^1(W) = \alpha_1 P_1 + \alpha_2 P_2 + I_2^1(W)(U_1 - U_2), \tag{4.25}$$

$$I_5^1(W) = \varepsilon_1 + \frac{P_1}{\rho_1} + \frac{1}{2(m_1)^2}(I_2^1(W))^2, \tag{4.26}$$

$$I_6^1(W) = \varepsilon_2 + \frac{P_2}{\rho_2} + \frac{1}{2(m_2)^2}(I_2^1(W))^2. \tag{4.27}$$

Now we propose two definition of the interfacial pressure P_i and derive the last 1-Riemann invariant I_4^1.

Interfacial pressure

The closure for the interfacial pressure P_i must allow to define the non conservative product $P_i\partial_x\alpha_1$ and to determine the last 1-Riemann invariant I_4^1. Here, two ways are investigated. The first one is based on an additionnal conservation law. This partial differential equation concerns the total entropy and a form of P_i is exhibited in order to ensure the divergence form of this equation. The 1-Riemann invariant I_4^1 is directly derived, which implicitely closes the product $P_i\partial_x\alpha_1$. The related parametrisation is discussed in appendix 4.D. The second way of closure presented here is directly based on the definition of the product $P_i\partial_x\alpha_1$. Following the behaviour of the product $V_i\partial_x\alpha_1$, if P_i corresponds to a function which only depends on the 1-Riemann invariants $(I_p^1)_{p=1,\dots,6}$, the product $P_i\partial_x\alpha_1$ is locally well defined. Furthermore, the definition of the 1-Riemann invariant I_4^1 immediately follows. Indeed, replacing $P_i\partial_x\alpha_1$ by $\partial_x(P_i\alpha_1)$ in the equations of partial momentum (4.7d) and (4.7e) provides two conservative equations and thus, an additionnal 1-Riemann invariant (the second conservation law corresponds to the 1-Riemann invariant I_3^1).

We must emphasize that, though the convective system is non conservative, 1-Riemann invariants and Rankine-Hugoniot jump relations identify for the linearly degenerate field associated to V_i, in the sense that they provide the same parametrisation, as stated in appendix 4.C. Therefore, no ambiguity holds for the definition of jump relations and non conservative products, contrary to the frame studied in [Sai96] for instance, where the knowledge of the matrix of diffusion is required.

A conservative equation for the total entropy We restrict here to interfacial pressures P_i of the form

$$P_i(W) = \mu(W)P_1 + (1-\mu(W))P_2, \tag{4.28}$$

where the dimensionless function μ is non negative and bounded by 1. Obviously, definition (4.28) ensures that relation (4.6) is verified. Let a_k be the function

$$a_k = \frac{1}{\varsigma_k}\left(\frac{\partial\varsigma_k}{\partial P_k}\right)\left(\frac{\partial\varepsilon_k}{\partial P_k}\right)^{-1}, \quad k=1,2. \tag{4.29}$$

Let us define $\eta_k = \mathrm{Log}(s_k)+\psi_k(\alpha_k)$ for $k=1,2$, with $\psi_1(\alpha_1)=\psi_2(1-\alpha_1)$. One may now provide the following result pertaining to the entropy inequality:

Proposition 4.7. *If the interfacial pressure P_i is defined by equation* (4.28) *with* (4.29) *in*

$$\mu = \frac{a_1(1-\beta)}{a_1(1-\beta)+a_2\beta}, \tag{4.30}$$

then the following entropy inequality holds for smooth solutions of system (4.7) *with diffusive terms:*

$$\frac{\partial\eta}{\partial t}+\frac{\partial F_\eta}{\partial x}\leq 0 \tag{4.31}$$

while setting $\eta = -\big(\alpha_1\rho_1\eta_1+\alpha_2\rho_2\eta_2\big)$ and $F_\eta = -\big(\alpha_1\rho_1\eta_1U_1+\alpha_2\rho_2\eta_2U_2\big)$.

Proof. Starting from system (4.7) with diffusive terms, non conservative entropy inequalities may be derived by classical calculations in each phase $k = 1, 2$:

$$\frac{\partial s_k}{\partial t} + U_k \frac{\partial s_k}{\partial x} + \frac{(V_i - U_k)(P_k - P_i)}{\alpha_k \rho_k} \left(\frac{\partial \varsigma_k}{\partial P_k} \right) \left(\frac{\partial \varepsilon_k}{\partial P_k} \right)^{-1} \frac{\partial \alpha_k}{\partial x} \geq 0.$$

Multiplying by $\alpha_k \rho_k / s_k$ these inequalities and using (4.14) gives for $k = 1, 2$:

$$\frac{\partial}{\partial t}\big(\alpha_k \rho_k Log(s_k)\big) + \frac{\partial}{\partial x}\big(\alpha_k \rho_k Log(s_k) U_k\big) + \mathcal{C}_k \frac{\partial \alpha_k}{\partial x} \geq 0 \tag{4.32}$$

with

$$\mathcal{C}_k = \frac{(V_i - U_k)(P_k - P_i)}{s_k} \left(\frac{\partial \varsigma_k}{\partial P_k} \right) \left(\frac{\partial \varepsilon_k}{\partial P_k} \right)^{-1}.$$

Summing for $k = 1, 2$, it follows

$$-\left(\frac{\partial \eta}{\partial t} + \frac{\partial F_\eta}{\partial x} + \mathcal{C}_1 \frac{\partial \alpha_1}{\partial x} + \mathcal{C}_2 \frac{\partial \alpha_2}{\partial x} \right) \geq 0. \tag{4.33}$$

If the interfacial pressure P_i is defined by (4.28-4.30), the non conservative term in (4.33) vanishes

$$\sum_{k=1,2} \mathcal{C}_k \frac{\partial \alpha_k}{\partial x} = 0,$$

and entropy inequality (4.31) holds. □

This result permits to define the interfacial pressure P_i in function of the interfacial velocity V_i. An advantage of this closure is that entropy inequality (4.31) obviously degenerates to give the expected – single phase – entropy inequality on each side of the 1-contact discontinuity. Herein, system (4.7) is completely closed. Using results of appendix 4.C, equation (4.31) leads to the Rankine-Hugoniot jump relation

$$V_i\big(\eta(W_r) - \eta(W_l)\big) = F_\eta(W_r) - F_\eta(W_l)$$

for the field associated to V_i and alternatively to the last 1-Riemann invariant

$$I_4^1(W) = \frac{\varsigma_1}{\varsigma_2}. \tag{4.34}$$

Now, the parametrisation through the 1-wave given by 1-Riemann invariants $(I_p^1)_{p=1,\dots,6}$ may be explicitely given (recall that this parametrisation is identical to the parametrisation given by Rankine-Hugoniot jump relations for this linearly degenerate field). This is done is appendix 4.D. The main result in this appendix is that the connection between W_l and W_r through the 1-wave is in agreement with the maximum principle on the void fraction and positivity requirements on densities and internal energies. This leads to the following result:

Proposition 4.8. *Assume now $(\alpha_1)_L \neq (\alpha_1)_R$. The connection of constant states through elementary waves in the solution of the Riemann problem* (4.7)-(4.19) *ensures that all states are in agreement with positivity requirements for void fraction, mass fractions and partial pressures assuming perfect gas state law within each phase.*

We insist that though the result seems obvious from a physical view point, it may actually not be clear whether solutions of the Riemann problem (4.7)-(4.19) should agree with positivity requirement. The choice of the above closures *a posteriori* ensures that physical positivity requirements hold. Unfortunately, the great complexity of the system (4.7) seems to prohibit the exact resolution of the Riemann problem. Indeed, eigenvalues are not arranged in order, which leads to an important number of different cases to investigate. Moreover, the connection through the 1-wave is not totally clear since, for a given state W_l, zero, one or two states W_r may be selected by the parametrisation. Hence, a deeper analysis of the 1-wave may be required, as done in [CL99] or [SV03] for rather simple models.

The interfacial pressure as a function of 1-Riemann invariants Here, the non conservative product $P_i\partial_x\alpha_1$ is directly closed using a definition of the interfacial pressure such that P_i remains unchanged when α_1 admits a discontinuity. In other words, recalling that the void fraction α_1 only jumps through the 1-wave, P_i remains constant though this wave if it is a function of the 1-Riemann invariants $(I_p^1)_{p=1,2,...,6}$

$$P_i(W) = \mathcal{F}\big(I_1^1(W), I_2^1(W), ..., I_6^1(W)\big).$$

Note that $\mathcal{F}$ must ensure condition (4.6). Of course, one must provide an explicit form of $\mathcal{F}$ to obtain an explicit form of I_4^1. Nevertheless, $\mathcal{F}$ and I_4^1 may be linked by

$$I_4^1(W) = \frac{P_1 - P_2}{2} + \Big(\frac{P_1 + P_2}{2} - P_i\Big)(\alpha_1 - \alpha_2) + (U_1 + U_2)I_2^1(W).$$

Remark that 1-Riemann invariants I_1^1 and I_4^1 do not fulfill the objectivity requirement (whatever function $\mathcal{F}$ is); furthermore, a dimensionless condition may be invoked, leading to the following list of arguments:

$$P_i(W) = \mathcal{G}\big(I_3^1(W), I_2^1(W)\big(I_5^1(W)\big)^{1/2}, I_6^1(W)\big(I_6^1(W)\big)^{1/2}\big).$$

Owing to condition (4.6), function $\mathcal{G}$ must verify $\mathcal{G}(a, 0, 0) = a$. Numerous functions $\mathcal{G}$ fulfill all these requirements. Among these, a simple choice could be

$$\mathcal{G}(a, b, c) = a + C_1(C_2|b| + (1 - C_2)|c|), \tag{4.35}$$

with C_1 and C_2 two real constants such that $C_1 > 0$ and $0 \leq C_2 \leq 1$. In addition to the dimensionless condition, the objectivity requirement and condition (4.6), this choice provides the positivity of the interfacial pressure P_i. Note that the particular choice $\mathcal{G}(a, b, c) = a$ corresponds to the closure retained in [SL01].

This deserves a few comments about closure laws available in the literature. We note first that proposals by Glimm and co-workers [GSS96], [GSS99] are quite different. Actually, coefficients occuring in their closure play a symmetric role in the interface velocity and interface pressure. Even more, they assume that the interface velocity tends towards the velocity of the vanishing phase $V_i = U_1$ when one phase is no longer present ($\alpha_1 = 0$). Their proposal looks like $P_i = \alpha_2 P_1 + \alpha_1 P_2$ and $V_i = \alpha_2 U_1 + \alpha_1 U_2$. Note that the closure for V_i implies that the 1-wave corresponds to a genuinely non linear field. Turning now to the work of Saurel and Abgrall [SA99a], we note

that the usual choice of interface velocity is (4.21). Nonetheless, their closure for the interface pressure is completely different from ours and takes the form: $P_i = \alpha_1 P_1 + \alpha_2 P_2$. Here again, when some phase (phase labelled 1 for instance, which means that $\alpha_1 = 0$) disappears, the couple of interface variables (V_i, P_i) identifies with the velocity-pressure couple in the remaining phase, namely (U_2, P_2). Furthermore, in [SL01], closures are (4.21) and $\mathcal{G}(a, b, c) = a$ in (4.35), but no information is provided about the Riemann problem. In [BN86], [KSB$^+$97] and [GS02], closures correspond to $P_i = P_1$ (dropping some terms in [GS02]) and $V_i = U_2$, where subscript 1 refers to the gas phase. As mentionned above, this set of closure fulfills Propositions 4.6 and 4.7. Moreover, this choice provides a conservative entropy inequality on each phase (non conservative term vanish in (4.32)).

4.3 Numerical methods

This section is devoted to the presentation of different finite volume methods computed here to approximate the solution of the Cauchy problem (4.1)-(4.3) (note that explicit definitions of interfacial pressure P_i and interfacial velocity V_i are not required to present both following methods). Though the current presentation is in one dimension, the extension to the multidimensional frame is straightforward. In the following of this paper, diffusion terms are omitted. Convective terms, source terms (relaxation terms) are taken into account by a fractional step approach. It is well known the latter is not optimal in terms of accuracy (see [GHS03] for instance), but it nonetheless leads to very stable algorithms. Each step aims at approximate the different terms. First, we note δt the time step and δx the length of a cell $(x_{j-1/2}; x_{j+1/2})$ of the regular mesh. Let W^n be the finite volume approximation at time $t^n = n\delta t$, $n \in \mathbb{N}$. The approximated solution W^{n+1} (*i.e.* at time $t^{n+1} = (n+1)\delta t$) of the Cauchy problem

$$\begin{cases} (Id + D(W))\dfrac{\partial W}{\partial t} + \dfrac{\partial F(W)}{\partial x} + C(W)\dfrac{\partial W}{\partial x} = S(W), \quad t \in (t^n, t^{n+1}), x \in \mathbb{R}, \\ W(t^n, x) = W^n(x), \quad x \in \mathbb{R}, \end{cases}$$

is approximated by splitting the complete problem in two steps. The first one corresponds to the convective part:

$$\begin{cases} (Id + D(W))\dfrac{\partial W}{\partial t} + \dfrac{\partial F(W)}{\partial x} + C(W)\dfrac{\partial W}{\partial x} = 0, \quad t \in (t^n, t^{n+1}), x \in \mathbb{R}, \\ W(t^n, x) = W^n(x), \quad x \in \mathbb{R}, \end{cases} \tag{4.36}$$

which provides $W^{n,1}$ (the approximation of $W(t^{n+1}, .)$, the solution of (4.36) at time t^{n+1}). The second one corresponds to the relaxation process:

$$\begin{cases} (Id + D(W))\dfrac{\partial W}{\partial t} = S(W), \quad t \in (t^n, t^{n+1}), x \in \mathbb{R}, \\ W(t^n, x) = W^{n,1}(x), \quad x \in \mathbb{R}, \end{cases} \tag{4.37}$$

which finally gives W^{n+1} (the approximation of $W(t^{n+1}, .)$, the solution of (4.37) at time t^{n+1}).

4.3.1 Computing hyperbolic systems under non conservative form

Two finite volume schemes are presented here. The first one is based on the Rusanov scheme [Rus61] and the second is an extension of an approximate Godunov scheme, namely the VFRoencv scheme. As usual, the notation

$$W_j^n = \frac{1}{\delta x}\int_{x_{j-1/2}}^{x_{j+1/2}} W(t^n,x)dx, \quad n \geq 0,\, j \in \mathbb{R},$$

is adopted in the following. Of course, finite volume schemes are merely dedicated to hyperbolic systems of conservation laws. Here, the set of partial differential equations (4.36) cannot be written under conservative form. An adaptation is thus required to take into account non conservative terms in the method. Several techniques have been proposed but numerical difficulties have been pointed out in [HL94] and in [DeV94] for instance. Nevertheless, the frame investigated in these references concerns non conservative products for genuinely non linear fields. Here, non conservative products only arise for linearly degenerate fields and are locally well defined (see Appendix 4.C). Therefore, one may expect that both finite volume schemes presented below are "consistent" with (4.36), since no additionnal information to the convective system is required to close non conservative products.

The Rusanov scheme

We detail herein the Rusanov scheme for the two-fluid two-pressure model (4.7). The equation on the void fraction α_1 (4.7a) is approximated by

$$\delta x\big((\alpha_1)_j^{n,1} - (\alpha_1)_j^n\big) + \delta t (V_i)_j^n\big((\overline{\alpha_1})_{j+1/2}^n - (\overline{\alpha_1})_{j-1/2}^n\big) - \frac{\delta t}{2}\Big(r_{j+1/2}\big((\alpha_1)_{j+1}^n - (\alpha_1)_j^n\big)\Big) + \frac{\delta t}{2}\Big(r_{j-1/2}\big((\alpha_1)_j^n - (\alpha_1)_{j-1}^n\big)\Big) = 0.$$

Equations (4.7b-4.7g) become for $k = 1, 2$:

$$\delta x\big((Z_k)_j^{n,1} - (Z_k)_j^n\big) + \delta t\big((H_k)_{j+1/2}^n - (H_k)_{j-1/2}^n\big) - \delta t (P_i)_j^n (\varphi_k)_j = 0.$$

where

$$Z_k = \begin{pmatrix} m_k \\ m_k U_k \\ \alpha_k E_k \end{pmatrix},\ H_k = \begin{pmatrix} m_k U_k \\ m_k (U_k)^2 + \alpha_k p_k \\ \alpha_k U_k (E_k + p_k) \end{pmatrix},\ (\varphi_k)_j^n = \begin{pmatrix} 0 \\ (\overline{\alpha_k})_{j+1/2}^n - (\overline{\alpha_k})_{j-1/2}^n \\ (V_i)_j^n\big((\overline{\alpha_k})_{j+1/2}^n - (\overline{\alpha_k})_{j-1/2}^n\big) \end{pmatrix}$$

and

$$\begin{aligned} r_j &= \max(|(V_i)_j^n|, |(U_1)_j^n| + (c_1)_j^n, |(U_2)_j^n| + (c_2)_j^n), \\ r_{j+1/2} &= \max(r_j, r_{j+1}), \\ 2(H_k)_{j+1/2}^n &= (H_k)_j^n + (H_k)_{j+1}^n - r_{j+1/2}((Z_k)_{j+1}^n - (Z_k)_j^n), \\ 2(\overline{\alpha_k})_{j+1/2}^n &= (\alpha_k)_j^n + (\alpha_k)_{j+1}^n. \end{aligned}$$

One may easily proove that the Rusanov scheme may preserve the maximum principle for the void fraction and the positivity of partial masses

$$0 < (\alpha_1)_j^{n,1} < 1 \quad \text{and} \quad (m_k)_j^{n,1} > 0,\ k = 1, 2$$

if W^n in (4.36) belongs to Ω and under the classical C.F.L. condition

$$\frac{\delta t}{\delta x}|\lambda_{MAX}| \leq 1,$$

where λ_{MAX} is the maximal speed of wave, computed on each cell of the mesh. These properties can be extended to the multidimensional framework.

The VFRoe-ncv scheme

The VFRoe-ncv scheme [BGH00] is an approximate Godunov scheme. This means that it may be written in a similar form to the Godunov scheme [God59], but the solution at each interface of the mesh is approximated. This approximation is provided by a linearisation of the convective system written with respect to a non conservative variable (which explains the name of the scheme). Numerous numerical tests in [GHS03] show that the VFRoe-ncv scheme provides accurate results, even when focusing on resonant systems [SV03]. Eventually, results obtained by the VFRoe-ncv scheme are very close to results provided by the Godunov scheme, when dealing with convergence in space (that is when the mesh is refined) as well as with convergence in time (*i.e.* convergence towards steady states when $t \to +\infty$).

Here again, the system which is computed corresponds to system (4.7) instead system of (4.36). Note that these two systems are equivalent, even when focusing on discontinuous solutions. The associated VFRoe-ncv scheme may be written on the cell $j \in \mathbb{Z}$ as

$$\begin{aligned}\delta x\big(W_j^{n,1} - W_j^n\big) + \delta t\big(F(W_{j+1/2}^*) - F(W_{j-1/2}^*)\big) \\ + \frac{\delta t}{2}\big(G(W_{j-1/2}^*) + G(W_{j+1/2}^*)\big)\big((\alpha_1)_{j+1/2}^* - (\alpha_1)_{j-1/2}^*\big) = 0.\end{aligned} \tag{4.38}$$

where vector G writes

$$G(W) = {}^t\big(V_i(W), 0, -P_i(W), -P_i(W)V_i(W), 0, P_i(W), V_i(W)P_i(W)\big).$$

The core of the method is the computation of values indexed by $(.)_{j+1/2}^*$, j in $\mathbb{Z}$. These values are computed from local Riemann problems at each interface of the mesh $x_{j+1/2}$, $j \in \mathbb{Z}$, as done with the Godunov scheme. Whereas the exact solution of these local Riemann problems is used for the Godunov scheme, the VFRoe-ncv scheme only approximates the solution, allowing a great reduction of the complexity of the solver when dealing with non linear systems. Moreover, we mentionned above that the complete computation of the exact solution of the Riemann problem (4.7)-(4.19) seems out of reach; nonetheless, the approximate solution of the VFRoe-ncv scheme is obtained by straightforward calculations. Let us provide the main guidelines to compute values $(.)_{j+1/2}^*$, $j \in \mathbb{Z}$. We focus on the local Riemann problem associated with interface $x_{j+1/2}$ at time t^n. It is composed by the set of partial differential equations (4.7) and by the initial condition

$$W(t = 0, x) = \begin{cases} W_i^n & \text{if } x < x_{j+1/2}, \\ W_{i+1}^n & \text{if } x > x_{j+1/2}. \end{cases} \tag{4.39}$$

Let Ψ be a regular function from $\mathbb{R}^7$ to $\mathbb{R}^7$ and define $Y = \Psi(W)$. Here, we choose the variable $Y = {}^t(\alpha_1, s_1, U_1, P_1, s_2, U_2, P_2)$. System (4.7) may be written for smooth solutions as

$$\frac{\partial Y}{\partial t} + B(Y)\frac{\partial Y}{\partial x} = 0$$

where $B(\Psi(W)) = \Psi'(W)(Id + D(W))^{-1}(F'(W) + C(W))(\Psi'(W))^{-1}$ and is given by (4.8). This system is linearised, giving the following local Riemann problem:

$$\begin{cases} \dfrac{\partial Y}{\partial t} + B(\hat{Y})\dfrac{\partial Y}{\partial x} = 0, \\ Y(t = t^n, x) = \begin{cases} \Psi(W_i^n) & \text{if } x < x_{j+1/2} \\ \Psi(W_{i+1}^n) & \text{if } x > x_{j+1/2} \end{cases}, \end{cases} \tag{4.40}$$

noting $\hat{Y} = (\Psi(W_i^n) + \Psi(W_{i+1}^n))/2$. The resolution of this system is obvious and its solution yields for all $t > t^n$ and x in $\mathbb{R}$

$$Y(t,x) = \Psi(W_i^n) + \sum_{\widetilde{\lambda_p} < (x - x_{j+1/2})/(t-t^n)} \big({}^t\widetilde{l_p}.(\Psi(W_{i+1}^n) - \Psi(W_i^n))\big)\widetilde{r_p} \tag{4.41a}$$

$$= \Psi(W_{i+1}^n) - \sum_{\widetilde{\lambda_p} > (x - x_{j+1/2})/(t-t^n)} \big({}^t\widetilde{l_p}.(\Psi(W_{i+1}^n) - \Psi(W_i^n))\big)\widetilde{r_p} \tag{4.41b}$$

where $(\widetilde{l_p})_{p=1,\dots,7}$, $(\widetilde{r_p})_{p=1,\dots,7}$ and $(\widetilde{\lambda_p})_{p=1,\dots,7}$ are respectively left and right eigenvectors and eigenvalues of matrix $B(\hat{Y})$ (see (4.9) and (4.10)). Therefore, since problem (4.40) provides a self-similar solution, we may set

$$W_{j+1/2}^* = \Psi^{-1}(Y(t > t^n, x = x_{j+1/2}))$$

which completes the construction of the VFRoe-ncv scheme. Of course, properties of this scheme depend on the choice of Y (in general, the function Ψ is non linear). So, the behaviour of the VFRoe-ncv scheme is closely related to the definition of Y. Here, $Y = {}^t(\alpha_1, s_1, U_1, P_1, s_2, U_2, P_2)$ has been selected in agreement with the analysis of the Riemann problem (4.7)-(4.19) and with numerical tests in [GHS02b].

We emphasize that both the Rusanov scheme and the VFRoe-ncv scheme may preserve some well-known solutions. Assume first that the equation of state of both phases writes

$$\rho_k \varepsilon_k(P_k, \rho_k) = g_k(P_k) + b_k \rho_k + c_k, \tag{4.42}$$

$k = 1, 2$, with b_k and c_k are real constant and g_k is an invertible function. If, for all cell $j \in \mathbb{Z}$, the approximated initial condition agrees with

$$(U_1)_j^0 = (U_2)_j^0 = U_0 \quad \text{and} \quad (P_1)_j^0 = (P_2)_j^0 = P_0,$$

then the approximation of the solution computed by both schemes agrees, at each time step $n \in \mathbb{N}$ and on each cell $j \in \mathbb{Z}$, with

$$(U_1)_j^n = (U_2)_j^n = U_0 \quad \text{and} \quad (P_1)_j^n = (P_2)_j^n = P_0.$$

Proofs are given in appendix 4.E.

4.3.2 Numerical treatment of source terms

Source terms of (4.1) are computed using a fractional step method, separating velocity relaxation, pressure relaxation and other contributions. Since $\partial_t \alpha_1$ may be given by the first equation of system (4.1), we have

$$\frac{\partial W}{\partial t} = S_U(W) + S_P(W) + S_O(W)$$

with

$$\begin{aligned}
S_U(W) = {}^t\big(&0,\, 0,\, -K_U(W)(U_1-U_2),\, -K_U(W)V_i(U_1-U_2),\\
&0,\, +K_U(W)(U_1-U_2),\, +K_U(W)V_i(U_1-U_2)\big),\\
S_P(W) = {}^t\big(&K_P(W)(P_1-P_2),\, 0,\, 0,\, -K_P(W)P_i(P_1-P_2),\, 0,\, 0,\, +K_P(W)P_i(P_1-P_2)\big),\\
S_O(W) = {}^t\big(&0,\, \dot m,\, +\dot m V_i,\, +\dot m E_i,\, -\dot m,\, -\dot m V_i,\, -\dot m E_i\big),
\end{aligned}$$

which is split in the three systems (steps 1, 2, 3):

$$\partial_t W = S_U(W)\,, \quad \partial_t W = S_P(W) \quad \text{and} \quad \partial_t W = S_O(W)\,.$$

According to this decomposition, we introduce some notations. $W^{n,U}$, $W^{n,P}$ and $W^{n,O}$ are the approximations of the solution after respectively: the velocity relaxation by S_U with $W^{n,1}$ as initial condition; the pressure relaxation S_P with $W^{n,U}$ as initial condition; and remaining phenomena S_O with $W^{n,P}$ as initial condition (the initial time corresponds to t^n). We examine below whether α_k, m_k and P_k and their approximations remain positive through these steps assuming that $W^{n,1}$ does lie in Ω and relaxation processes are time continuous.

step 1: velocity relaxation

Continuous frame The initial condition for this step is $W^{n,1}$ which is supposed to lie in Ω. Note that void fractions α_k and partial masses m_k remain unchanged during this step. Only velocities U_k and energies E_k may vary, giving the following system

$$\frac{\partial \alpha_k}{\partial t} = \frac{\partial m_k}{\partial t} = 0, \tag{4.43}$$

$$m_k \frac{\partial U_k}{\partial t} = (-1)^k K_U(W)(U_1-U_2), \tag{4.44}$$

$$m_k \frac{\partial}{\partial t}\big(e_k + (U_k)^2/2\big) = (-1)^k K_U(W) V_i (U_1-U_2), \tag{4.45}$$

$k = 1, 2$. We assume of course that $(U_1)^{n,1} \neq (U_2)^{n,1}$. The second ordinary differential equation may be easily replaced by equation on pressures P_k, $k = 1, 2$:

$$m_k \frac{\partial \varepsilon_k}{\partial P_k}\frac{\partial P_k}{\partial t} = (-1)^k K_U(W)(U_1-U_2)(V_i-U_k). \tag{4.46}$$

This equation provides the following result:

Lemma 4.1. *If $\partial \varepsilon_k / \partial P_k > 0$, then for all $t \geq t^n$ we have $P_k(t) > 0$ with $k = 1, 2$.*

In fact, using the general definition of V_i (4.5), equation (4.46) becomes

$$m_k \frac{\partial \varepsilon_k}{\partial P_k} \frac{\partial P_k}{\partial t} = \beta_{k'}(W) K_U(W)(U_1 - U_2)^2, \tag{4.47}$$

with $k' = 3 - k$, $\beta_1 = \beta$ and $\beta_2 = 1 - \beta$. Recalling that $0 \leq \beta \leq 1$ (which holds true when using $\beta(W) = m_1/(m_1 + m_2)$), pressures P_1 and P_2 remain positive (since $\partial_t P_k$ is positive for $k = 1, 2$) when focusing on simple thermodynamical laws, such as Tammann equation of state or perfect gas equation of state, *i.e.* equation of state following (4.4). In that case, we simply have $m_k \partial \varepsilon_k / \partial P_k = \alpha_k g_k > 0$.

Let us focus now on the variation of $U_1 - U_2$ during the velocity relaxation step. From equation (4.44), one may deduce the ordinary differential equation

$$\frac{\partial}{\partial t}(U_1 - U_2) = -\frac{m_1 + m_2}{m_1 m_2} K_U(W)(U_1 - U_2).$$

This provides for $t \geq t^n$

$$(U_1 - U_2)(t) = (U_1 - U_2)(t^n) \exp\left(- \int_{t^n}^{t} K_U(W(\tau)) \Big(\frac{m_1 + m_2}{m_1 m_2} \Big)(\tau) \, d\tau \right).$$

It results the lemma:

Lemma 4.2. *The velocity relaxation governed by system (4.43-4.45) follows*

$$\begin{aligned} & (U_1 - U_2)(t) \,.\, (U_1 - U_2)(t^n) > 0, \quad \textit{for all } t \geq t^n, \\ & \textit{the function } |U_1 - U_2| \textit{ is monotone decreasing over } [t^n; +\infty) \\ \textit{and} \quad & \lim_{t \to +\infty} (U_1 - U_2)(t) = 0. \end{aligned}$$

Numerical approximation We turn now to the numerical approximation of the system (4.43-4.45). Since $\partial_t \alpha_1 = \partial_t m_k = 0$, $k = 1, 2$, it simply results

$$(\alpha_1)^{n,U} = (\alpha_1)^{n,1} \quad \text{and} \quad (m_k)^{n,U} = (m_k)^{n,1}, k = 1, 2 \,.$$

Velocities U_k, governed by the ordinary differential equation (4.44), are approximated by:

$$\begin{pmatrix} (m_1)^{n,1} + K_U(W^{n,1})\delta t & -K_U(W^{n,1})\delta t \\ -K_U(W^{n,1})\delta t & (m_2)^{n,1} + K_U(W^{n,1})\delta t \end{pmatrix} \begin{pmatrix} (U_1)^{n,U} \\ (U_2)^{n,U} \end{pmatrix} = \begin{pmatrix} (m_1)^{n,1}(U_1)^{n,1} \\ (m_2)^{n,1}(U_2)^{n,1} \end{pmatrix},$$

dropping spatial indices (since this scheme is local on each cell). We now approximate the solution of equation (4.47) by:

$$(P_k)^{n,U} - (P_k)^{n,1} = \frac{\delta t \beta_{k'}(W^{n,U}) K_U(W^{n,U})}{(\alpha_k)^{n,U} g_k} \Big((U_1)^{n,U} - (U_2)^{n,U} \Big)^2,$$

assuming that the equation of state takes the form (4.4). Finally, using the equation of state and other relations, we obtain $W^{n,U}$. Note that, like in the "continuous" frame, new pressures $(P_k)^{n,U}$ are positive if $W^{n,1}$ belongs to Ω.

step 2: pressure relaxation

Continuous frame We study now the following system of ordinary differential equations:

$$\frac{\partial \alpha_1}{\partial t} = K_P(W)(P_1 - P_2), \tag{4.48}$$

$$\frac{\partial m_k}{\partial t} = \frac{\partial m_k U_k}{\partial t} = 0, \tag{4.49}$$

$$m_k \frac{\partial e_k}{\partial t} = (-1)^k K_P(W) P_i (P_1 - P_2), \tag{4.50}$$

for $k = 1, 2$. The initial condition associated with this system is $W^{n,U}$ (which belongs to Ω). As above, we assume that $(P_1)^{n,U} \neq (P_2)^{n,U}$. This system simply leads to equation

$$\alpha_k \frac{\partial P_k}{\partial t} + \left(\hat{\gamma}_k + (P_i - P_k) \Big(\rho_k P_k \frac{\partial \varepsilon_k}{\partial P_k} \Big)^{-1} \right) P_k \frac{\partial \alpha_k}{\partial t} = 0. \tag{4.51}$$

Subtracting the equation (4.51) with $k = k$ to the equation (4.51) with $k = k'$ gives

$$\frac{\partial (P_k - P_{k'})}{\partial t} + K_P(W) \left(\frac{\hat{\gamma}_{i1} P_1}{\alpha_1} + \frac{\hat{\gamma}_{i2} P_2}{\alpha_2} \right) (P_k - P_{k'}) = 0$$

where $k' = 3 - k$ and $\hat{\gamma}_{ik}$ is

$$\hat{\gamma}_{ik} = \hat{\gamma}_k + (P_i - P_k) \Big(\rho_k P_k \frac{\partial \varepsilon_k}{\partial P_k} \Big)^{-1}.$$

Therefore, for $t \geq t^n$, we have

$$(P_k - P_{k'})(t) = (P_k - P_{k'})(t^n) \exp \left(- \int_{t^n}^{t} K_P(W(\tau)) \left(\frac{\hat{\gamma}_{i1} P_1}{\alpha_1} + \frac{\hat{\gamma}_{i2} P_2}{\alpha_2} \right) (\tau) \, d\tau \right). \tag{4.52}$$

This provides the following result, which is the counterpart of Lemma 4.2:

Lemma 4.3. *If $\alpha_2 \hat{\gamma}_{i1} P_1 + \alpha_1 \hat{\gamma}_{i2} P_2 > 0$, then system (4.48-4.50) yields*

$$\begin{aligned} & (P_k - P_{k'})(t) \, (P_k - P_{k'})(t^n) > 0, \quad \textit{for all } t \geq t^n, \\ & \textit{the function } |P_k - P_{k'}| \textit{ is monotone decreasing over } [t^n; +\infty) \\ \textit{and} \quad & \lim_{t \to +\infty} (P_k - P_{k'})(t) = 0. \end{aligned}$$

Now, we divide equation (4.51) by $\alpha_k P_k$:

$$\frac{\partial}{\partial t}(\operatorname{Log} P_k) + \hat{\gamma}_{ik} \frac{\partial}{\partial t}(\operatorname{Log} \alpha_k) = 0$$

and add it for $k = 1$ and 2

$$\frac{\partial}{\partial t} \Big(\operatorname{Log}(P_1 P_2) \Big) + \hat{\gamma}_{i1} \frac{\partial}{\partial t}(\operatorname{Log} \alpha_1) + \hat{\gamma}_{i2} \frac{\partial}{\partial t}(\operatorname{Log} \alpha_2) = 0, \tag{4.53}$$

which becomes for $t \geq t^n$

$$(P_1P_2)(t) = (P_1P_2)(t^n) \exp\left(- \int_{t^n}^{t} \Big(\hat{\gamma}_{i1} \frac{\partial}{\partial t} (\mathrm{Log}\, \alpha_1) \Big)(\tau) + \Big(\hat{\gamma}_{i2} \frac{\partial}{\partial t} (\mathrm{Log}\, \alpha_2) \Big)(\tau)\, d\tau \right).$$

Therefore, we have

Lemma 4.4. *For all $t \geq t^n$, $P_k(t) > 0$ holds with $k = 1, 2$.*

We focus now on the preservation of the maximum principle for the void fraction during this relaxation step. We introduce equation (4.52) in (4.48), which provides

$$\frac{\partial \alpha_1}{\partial t} = K_P(W)(P_1 - P_2)(t^n) \exp\left(- \int_{t^n}^{t} K_P(W(\tau)) \left(\frac{\hat{\gamma}_{i1} P_1}{\alpha_1} + \frac{\hat{\gamma}_{i2} P_2}{\alpha_2} \right)(\tau)\, d\tau \right).$$

Furthermore, multiplying by $(1/\alpha_1 + 1/\alpha_2)$ the latter equation, there holds

$$\frac{\partial}{\partial t} \Big(\mathrm{Log}\, \frac{\alpha_1}{\alpha_2} \Big) = \frac{K_P(W)}{\alpha_1 \alpha_2} (P_1 - P_2)(t^n) \exp\left(- \int_{t^n}^{t} K_P(W(\tau)) \left(\frac{\hat{\gamma}_{i1} P_1}{\alpha_1} + \frac{\hat{\gamma}_{i2} P_2}{\alpha_2} \right)(\tau)\, d\tau \right).$$

So, it follows for $t \geq t^n$

$$\begin{aligned} \Big(\frac{\alpha_1}{\alpha_2} \Big)(t) = \Big(\frac{\alpha_1}{\alpha_2} \Big)(t^n) \exp\Bigg(& \int_{t^n}^{t} \frac{K_P(W(\tau))}{(\alpha_1\alpha_2)(\tau)} (P_1 - P_2)(t^n) \\ & \exp\left(- \int_{t^n}^{\tau} K_P(W(s)) \left(\frac{\hat{\gamma}_{i1} P_1}{\alpha_1} + \frac{\hat{\gamma}_{i2} P_2}{\alpha_2} \right)(s)\, ds \right) d\tau \Bigg) \end{aligned} \tag{4.54}$$

and gives the lemma:

Lemma 4.5. *For all $t \geq t^n$, $0 < \alpha_1(t) < 1$ holds.*

Numerical approximation Of course, according to (4.49), we have

$$(m_k)^{n,P} = (m_k)^{n,U} \quad \text{and} \quad (U_k)^{n,P} = (U_k)^{n,U}. \tag{4.55}$$

In the following, we use a more explicit form of K_P (see equation (4.12)), that is

$$K_P = \frac{1}{\theta} \frac{\alpha_1(1 - \alpha_1)}{P_1 + P_2}$$

where θ is assumed to be constant. Therefore, multiplying by $(1/\alpha_1 + 1/\alpha_2)$ equation (4.48), we have for $t \geq t^n$

$$\Big(\frac{\alpha_1}{1 - \alpha_1} \Big)(t) = \Big(\frac{\alpha_1}{1 - \alpha_1} \Big)(t^n) \exp\left(\frac{1}{\theta} \int_{t^n}^{t} \left(\frac{P_1 - P_2}{P_1 + P_2} \right)(\tau)\, d\tau \right).$$

Therefore, we compute $(\alpha_1)^{n,P}$ using

$$\Big(\frac{\alpha_1}{1 - \alpha_1} \Big)^{n,P} = \Big(\frac{\alpha_1}{1 - \alpha_1} \Big)^{n,U} \exp\left(\frac{1}{\theta} \int_{t^n}^{t^{n+1}} \left(\frac{P_1 - P_2}{P_1 + P_2} \right)(\tau)\, d\tau \right). \tag{4.56}$$

This equation has one and only one solution in $(0;1)$, in agreement with Lemma 4.5, whatever the approximation of the integral in (4.56) is. In practise, the integral is approximated by $A(t^n)\delta t$ where $A(\tau)$ is the function inside the integral.

The scheme for the computation of pressures is based on a discrete form of equations (4.52) and (4.53). It writes

$$(P_k - P_{k'})^{n,P} = (P_k - P_{k'})^{n,U} \exp\left(-\frac{1}{\theta} \int_{t^n}^{t^{n+1}} \left(\frac{\alpha_2 \hat{\gamma}_{i1} P_1 + \alpha_1 \hat{\gamma}_{i2} P_2}{P_1 + P_2} \right)(\tau)\, d\tau \right), \tag{4.57}$$

$$(P_1 P_2)^{n,P} = (P_1 P_2)^{n,U} \left(\frac{(\alpha_1)^{n,P}}{(\alpha_1)^{n,U}} \right)^{-\hat{\gamma}_{i1}(W^{n,U})} \left(\frac{(\alpha_2)^{n,P}}{(\alpha_2)^{n,U}} \right)^{-\hat{\gamma}_{i2}(W^{n,U})}. \tag{4.58}$$

As above, integrals in (4.57) and (4.58) are approximated using the value of functions at time t^n. Equations (4.57-4.58) provide two couples (P_1, P_2) of solutions. One consists of both negative pressures and the other of two positive pressures. Of course, the latter is retained, which agrees with Lemma 4.4. One may easily check that this couple verifies the discrete counterpart of Lemma 4.3.

Remark 4.3. To increase the accuracy of the scheme (4.55-4.58), the time step δt may be divided in several local time steps, in particular if θ is much smaller than δt. In such a case, the local time step may be set to θ.

step 3: other source terms

Other source terms such as the gravity field are accounted for using a centered approximation. No details are given here.

4.3.3 Boundary conditions

Until now, we have assumed that $x \in \mathbb{R}$. Let us focus here on the boundary conditions for the system (4.7) and their numerical approximation. Since the numerical methods we consider here are finite volume schemes, we only need the value of the numerical flux at the bound to account for the boundary condition. Two kinds of boundary condition are distinguished here.

The rigid wall boundary condition

This kind of boundary condition corresponds to a rigid wall aligned with the boundary interfaces. It is modeled at the bound by $U_k = 0$ in one space dimension and $U_k.n = 0$, $k = 1, 2$, in several dimensions (n is a vector normal to the bound). Let us place the boundary condition in $x = 0$ and suppose that the domain of computation of (4.7) is $\mathbb{R}_+$. Let us note W_0^n the approximation of the solution W at time t^n over the first cell $(0; \delta x)$. Therefore, to compute the numerical flux of a three-point scheme at the boundary $x = 0$, we use the virtual state

$$W_{-1}^n = {}^t\big((\alpha_1)_0^n, (\alpha_1\rho_1)_0^n, -(\alpha_1\rho_1 U_1)_0^n, (\alpha_1 E_1)_0^n, (\alpha_2\rho_2)_0^n, -(\alpha_2\rho_2 U_2)_0^n, (\alpha_2 E_2)_0^n\big)$$

and W_0^n. This technique is called the "mirror state" technique (see [GR96] for instance). It is clear that the exact solution of the associated local Riemann problem may be exhibited since the system (4.7) reduces to two Euler systems (non conservative terms of (4.7) vanish). The problem finally results in a rigid wall boundary condition for both fluids, each of which is governed by Euler equations. This technique in the classical frame of gas dynamics is widely discussed in [GR96] and [BGH00]. One may use W_{-1}^n and W_0^n to compute exactly or approximately the numerical flux at the bound $x = 0$. Furthermore, due to the properties of the Rusanov scheme (see section 4.3.1) and the VFRoe-ncv scheme with variable $Y = {}^t(\alpha_1, s_1, U_1, P_1, s_2, U_2, P_2)$ (see [GHS02b]) when dealing with low densities, the same scheme in the interior of the domain and at the bound may be used.

Inlet and outlet boundary conditions

For the sake of simplicity, the domain of computation is set to $x \in \mathbb{R}^+$ and, thus, the bound is located at $x = 0$. The inlet and outlet boundary conditions may be separated in three classes. The *first class* is defined by the addition of:

i. the system (4.7) over $\mathbb{R}_+ \times \mathbb{R}_+$,

ii. the initial data $W(t = 0, x) = W_0(x)$ with $x > 0$,

iii. the boundary condition $W(t, x < 0) = \overline{W}(t)$ for all $t > 0$, where $\overline{W}(t)$ is a given state in Ω.

Let us emphasize that this boundary condition is not imposed at the interface. Actually, this boundary condition must be rewritten as an admissibility condition at $x = 0$, as done by F. Dubois and P.G. LeFloch in [DL88]. The *second class* corresponds to problems which may be written under the following form:

i. the system (4.7) over $\mathbb{R}_+ \times \mathbb{R}_+$,

ii. the initial data $W(t = 0, x) = W_0(x)$ with $x > 0$,

iii'. the boundary condition $W(t, x = 0) \in \mathcal{V}(t)$ for all $t > 0$, $\mathcal{V}(t)$ a subset of Ω defined by

$$\mathcal{V}(t) = \{W \in \Omega; \Phi_l(t; W) = 0, 1 \leq l \leq n_b(t)\}$$

where $n_b(t)$ is the number of imposed boundary scalar data at time t, included between 0 (supersonic outflow) and 7 (supersonic inflow), and $\Phi_l(t; .)$ are functions from Ω to $\mathbb{R}$ for all $t > 0$.

It is clear that such problems may be ill-posed. We will describe in the following several ways to complete them. The *third class* is composed by items i, ii and a combination of items iii and iii', that is some components of W are imposed at $(t, x < 0)$ and other constraints must be fulfilled at the interface $(t, 0)$, in the same way as item iii'. This class is not dealt here.

We believe that for inlet and outlet boundary conditions the numerical treatment must be as accurate as possible, this is why we try, if possible, to base their computation on an exact approach,

using the solution of the Riemann problem. We have seen before that the solution of the Riemann problem (4.7)-(4.19) may not be exhibited for all initial condition (W_L, W_R) in $\Omega \times \Omega$. Nevertheless, if this initial condition verifies some properties such as $(\alpha_1)_L = (\alpha_1)_R$ or $(U_1)_L = (U_2)_L = (U_1)_R = (U_2)_R$ and $(P_1)_L = (P_2)_L = (P_1)_R = (P_2)_R$, the solution of the Riemann problem is known and may be exactly computed.

Let us first focus on the numerical treatment of the first class. In order to deal with this kind of boundary condition, we use a "virtual" outer cell that is $(-\delta x; 0)$, where the value is set to $\overline{W}(t^n)$ at the n-th time step (say between t^n and t^{n+1}). If the Riemann problem provided by $\overline{W}(t^n)$ and the first cell inside the domain of computation W_0^n may be exactly solved, the numerical flux is then constructed with the exact solution at the interface $x = 0$. If the exact solution of this local Riemann problem is not available, the system is approximated, following for instance the linearisation of the VFRoe-ncv scheme (4.40). Therefore, the approximate solution is used to construct the numerical flux. An other way to deal with the initial-boundary value problem i-ii-iii when the solution of the Riemann problem is not explicitely known can be the use of an iterative method to approximate the numerical flux at the bound. More precisely, one can use a naive scheme (such as the Lax-Friedrichs scheme) on a local grid refinement of $(t^n; t^{n+1}) \times (-\delta x; \delta x)$ to approximate the system (4.7), using $\overline{W}(t^n)$ for $x \in (-\delta x; 0)$ and W_0^n for $x \in (0; \delta x)$ as the local initial condition. Then, the numerical flux at the bound is constructed using the approximate solution.

Pertaining to the second class, one must solve at each time step the local problem composed by system (4.7) over $(t^n; t^{n+1}) \times (0; \delta x)$, the initial condition $W(t = t^n, x) = W_0^n$ for $x \in (0; \delta x)$ and $W(t, 0) \in \mathcal{V}(t^n)$ for all $t \in (t^n; t^{n+1})$. Such a problem may be ill-posed, in particular if $n_b(t^n) < 7$. Indeed, in some cases, an infinite number of states W_L may be found such that the solution at $x = 0$ of the Riemann problem with data (W_L, W_0^n) belongs to $\mathcal{V}(t^n)$. The main contribution about the approximation of this kind of boundary conditions has been provided by F. Dubois in [Dub87], in the frame of Euler equations. It is based on the notion of partial Riemann problems at the n-th time step, which means that the boundary condition $W(t, x = 0) \in \mathcal{V}(t^n)$ of each local problem becomes the boundary condition $W(t, x = 0^-) = \overline{W}_-^n$, $t \in (t^n; t^{n+1})$ where $\overline{W}_-^n$ belongs to $\mathcal{V}(t^n)$ and is a data. Of course, here, $7 - n_b(t^n)$ components of $\overline{W}_-^n$ are unknown (we assume that the functions $\Phi_l(t^n; .)$ are independent) and, without additional assumptions, the state $\overline{W}_-^n$ is not uniquely defined in general. Basically, the model of F. Dubois assumes that the solution of the partial Riemann problem is composed by $n_b(t^n) + 1$ constant states separated by $n_b(t^n)$ elementary waves. Under this assumption and some additional hypothesis on the form of functions $\Phi_l(t^n; .)$, $1 \leq l \leq n_b(t^n)$, one may proove the existence and the uniqueness of the solution of the local problem, when focusing on classical Euler equations, for which the solution of the Riemann problem is known. Therefore, the unknown components of $\overline{W}_-^n$ are uniquely defined (see also [DL88]). For system (4.7), this technique may be applied when the solution of the local partial Riemann problem is known, that is when the functions $\Phi_l(t^n; .)$ and W_0^n verify some properties similar to the ones on W_L and W_R which allow the resolution of the Riemann problem (4.7)-(4.19) (see the right boundary condition for the water faucet problem in section 4.4.5). If this local Riemann problem cannot be solved with this technique, the resolution becomes tricky. Indeed, the use of a linearised solver can lead to an ill-posed problem, since the number of positive eigenvalues corresponding to linearised waves may be different of $n_b(t^n)$. Therefore, some "numerical" boundary conditions must be adapted (say added or dropped). For instance, one may add some constraints on $\overline{W}_-^n$ such that defining a function Φ' from Ω to $\mathbb{R}$ and imposing

$\Phi'(\overline{W}_-^n) = 0$ or $\Phi'(\overline{W}_-^n) = \Phi'(W_0^n)$. Of course, the additional boundary condition imposed by the use of Φ' must be independent of the boundary conditions issued from the $\Phi_l(t^n;.)$, $1 \leq l \leq n_b(t^n)$. See in particular the left boundary condition for the water faucet problem in section 4.4.5 and the reference [Rov02].

It is clear that this list of boundary conditions is not exhaustive. Many other kinds of boundary conditions exist and proposing relevant numerical approximations still remains difficult, especially in the frame of two-phase flows. For instance, a very interesting problem which occurs in the petroleum industry is the treatment of a boundary limit where one imposes that one of the two fluids cannot cross this bound.

4.4 Numerical results

In the following, we assume that the equations of state within each phase agrees with

$$\varepsilon_1(P_1, \rho_1) = \frac{P_1}{(\gamma_1 - 1)\rho_1} \quad \text{and} \quad \varepsilon_2(P_2, \rho_2) = \frac{P_2}{(\gamma_2 - 1)\rho_2}. \tag{4.59}$$

The C.F.L. number N_{CFL} fulfills stability condition:

$$\max(|U_k| + c_k)\delta t < N_{CFL}\delta x. \tag{4.60}$$

In the following, N_{CFL} is set to 0.45. Note that for the Rusanov scheme, the maximum is computed using cell values whereas for the VFRoe-ncv scheme, the maximum is computed using interface values.

4.4.1 Moving contact discontinuity

The length of the domain is $1000\,m$. Initial data for the first Riemann problem are given by :

$$(\alpha_1)_L = 0.9,\ (\tau_1)_L = 1,\ (U_1)_L = 100,\ (P_1)_L = 10^5,\ (\tau_2)_L = 1,\ (U_2)_L = 100,\ (P_2)_L = 10^5,$$
$$(\alpha_1)_R = 0.5,\ (\tau_1)_R = 8,\ (U_1)_R = 100,\ (P_1)_R = 10^5,\ (\tau_2)_R = 8,\ (U_2)_R = 100,\ (P_2)_R = 10^5.$$

We also set $\gamma_1 = \gamma_2 = 1.4$. The resulting flow is rather simple, since $P_1(x,t) = P_2(x,t) = 10^5\,Pa$ and $U_1(x,t) = U_2(x,t) = 100\,m/s$. Thus the mass fractions and the void fraction are governed by the mass balance equations and the solution is

$$\alpha_1(t,x) = \alpha_1(0, x - 100\,t) \quad \text{and} \quad \alpha_k\rho_k(t,x) = \alpha_k\rho_k(0, x - 100\,t),\ k = 1, 2.$$

Results displayed below have been obtained using 1000 nodes. The final time is $T_{MAX} = 3\,s$.

One may check on figure 4.1 that both schemes exactly preserve constant velocities and pressures, in agreement with Appendix 4.E. Figures 4.1.a to 4.1.c show that the numerical diffusion of the VFRoe-ncv scheme is less important than the numerical diffusion associated with the Rusanov scheme.

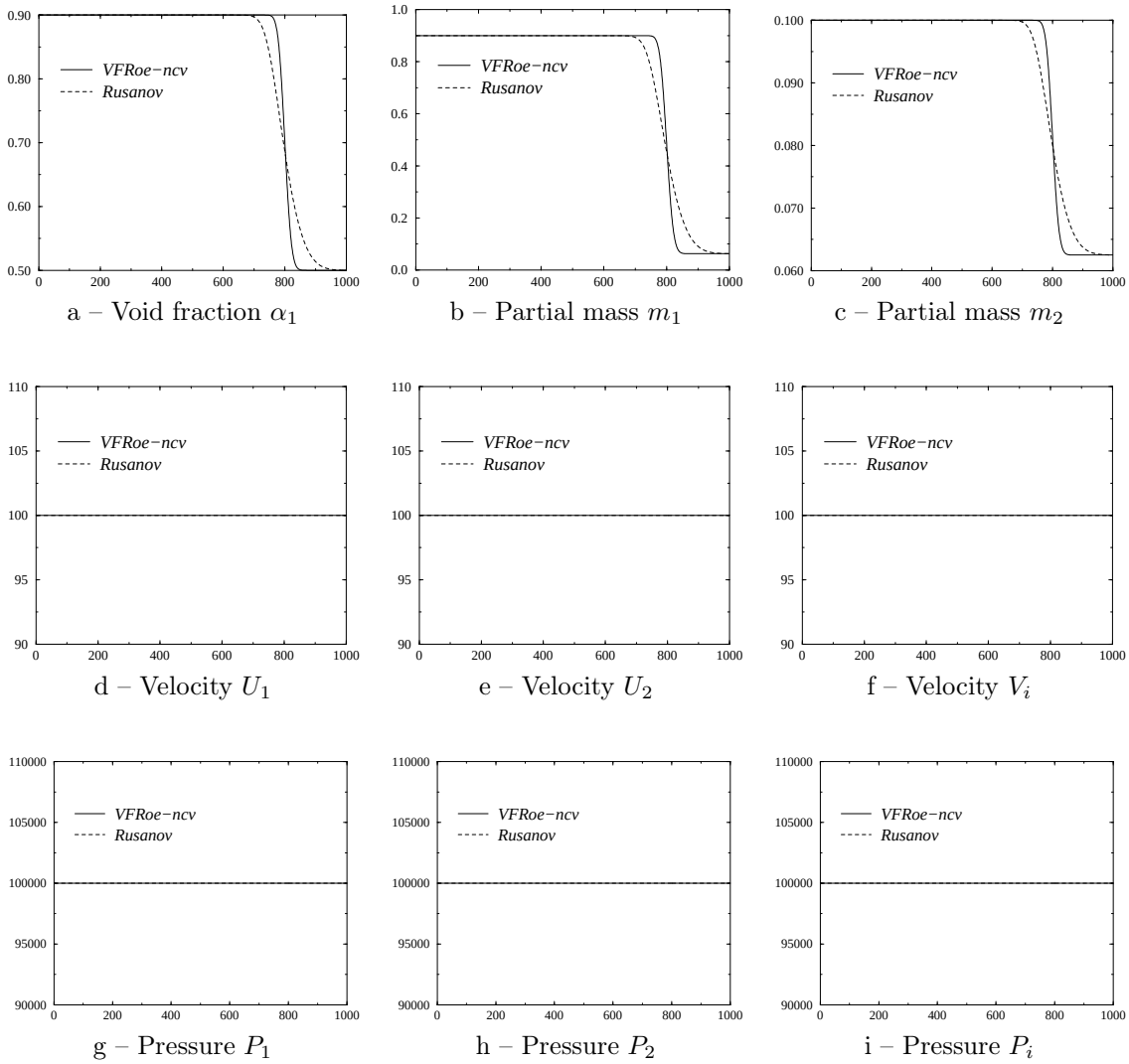

a – Void fraction α_1 b – Partial mass m_1 c – Partial mass m_2

d – Velocity U_1 e – Velocity U_2 f – Velocity V_i

g – Pressure P_1 h – Pressure P_2 i – Pressure P_i

Fig. 4.1: Moving contact discontinuity

4.4.2 Shock tube test

In the second test case, we assume a strong desequilibrium between both phases in terms of pressure fields. Initial conditions are

$$(\alpha_1)_L = 0.9,\ \ (\tau_1)_L = 1,\ \ (U_1)_L = 0,\ \ (P_1)_L = 10^5,\ \ (\tau_2)_L = 0.1,\ \ (U_2)_L = 0,\ \ (P_2)_L = 10^4,$$
$$(\alpha_1)_R = 0.5,\ \ (\tau_1)_R = 8,\ \ (U_1)_R = 0,\ \ (P_1)_R = 10^4,\ \ (\tau_2)_R = 0.8,\ \ (U_2)_R = 0,\ \ (P_2)_R = 10^3.$$

Due to the number of different waves, this test has been performed on a very fine mesh (it contains 50000 nodes) in order to obtain good approximation of intermediate states. All figures are plotted with $T_{MAX} = 0.7\,s$. Figures 4.2.a to 4.2.c permit to locate different waves. It is worth noting on figure 4.2.c that the 7-wave (that is the wave associated with the eigenvalue $U_2 + c_2$) is resonant with the 1-wave. Indeed, the 7-wave is composed by a rarefaction wave followed by a constant state and a shock wave. The jump of m_2 at the end of the rarefaction wave corresponds to the 1-contact discontinuity. Figures 4.2.d to 4.2.i represent the six 1-Riemann invariants defined in equations (4.23-4.27) and (4.34), zoomed around the position of the 1-wave. Bold lines correspond to the numerical location of the 1-contact discontinuity expanded due to the numerical diffusion of schemes. Let us emphasize that the scale of the y-axis on figures 4.2.d to 4.2.i is very small with regard to the amplitude of variations of each 1-Riemann invariants (the scale of the y-axis represents around 2% and 10% of the difference between the maximal value and the minimal value of the k-Riemann invariant which is plotted).

4.4.3 Wall boundary: shock waves

In the third test case, we compute strong symetrical shock waves. Initial data are

$$(\alpha_1)_L = 0.9,\ \ (\tau_1)_L = 1,\ \ (U_1)_L = 100,\ \ \ (P_1)_L = 10^5,\ \ (\tau_2)_L = 0.1,\ \ (U_2)_L = 50,\ \ \ (P_2)_L = 10^4,$$
$$(\alpha_1)_R = 0.9,\ \ (\tau_1)_R = 1,\ \ (U_1)_R = -100,\ \ (P_1)_R = 10^5,\ \ (\tau_2)_R = 0.1,\ \ (U_2)_R = -50,\ \ (P_2)_R = 10^4.$$

The void fraction remains constant with respect to time and space. This enables to model the behaviour of the two-phase flow close to a wall boundary when applying for the mirror technique, when the flow is impinging the wall. The mesh contains one thousand cells and $T_{MAX} = 0.5\,s$. Results provided by both methods on figures 4.3.a to 4.3.i are very close to each other.

4.4.4 Wall boundary: rarefaction waves

We compute symetrical rarefaction waves. Initial data is now

$$(\alpha_1)_L = 0.9,\ \ (\tau_1)_L = 1,\ \ (U_1)_L = -100,\ \ (P_1)_L = 10^5,\ \ (\tau_2)_L = 0.1,\ \ (U_2)_L = -50,\ \ (P_2)_L = 10^4,$$
$$(\alpha_1)_R = 0.9,\ \ (\tau_1)_R = 1,\ \ (U_1)_R = 100,\ \ \ (P_1)_R = 10^5,\ \ (\tau_2)_R = 0.1,\ \ (U_2)_R = 50,\ \ \ (P_2)_R = 10^4.$$

Once again, the void fraction profile is uniform. The flow corresponds to the one behind some bluff body. It is emphasized that Rusanov scheme performs very well in this case, even when using fully unstructured meshes. This means that cell values of partial masses and void fraction remain

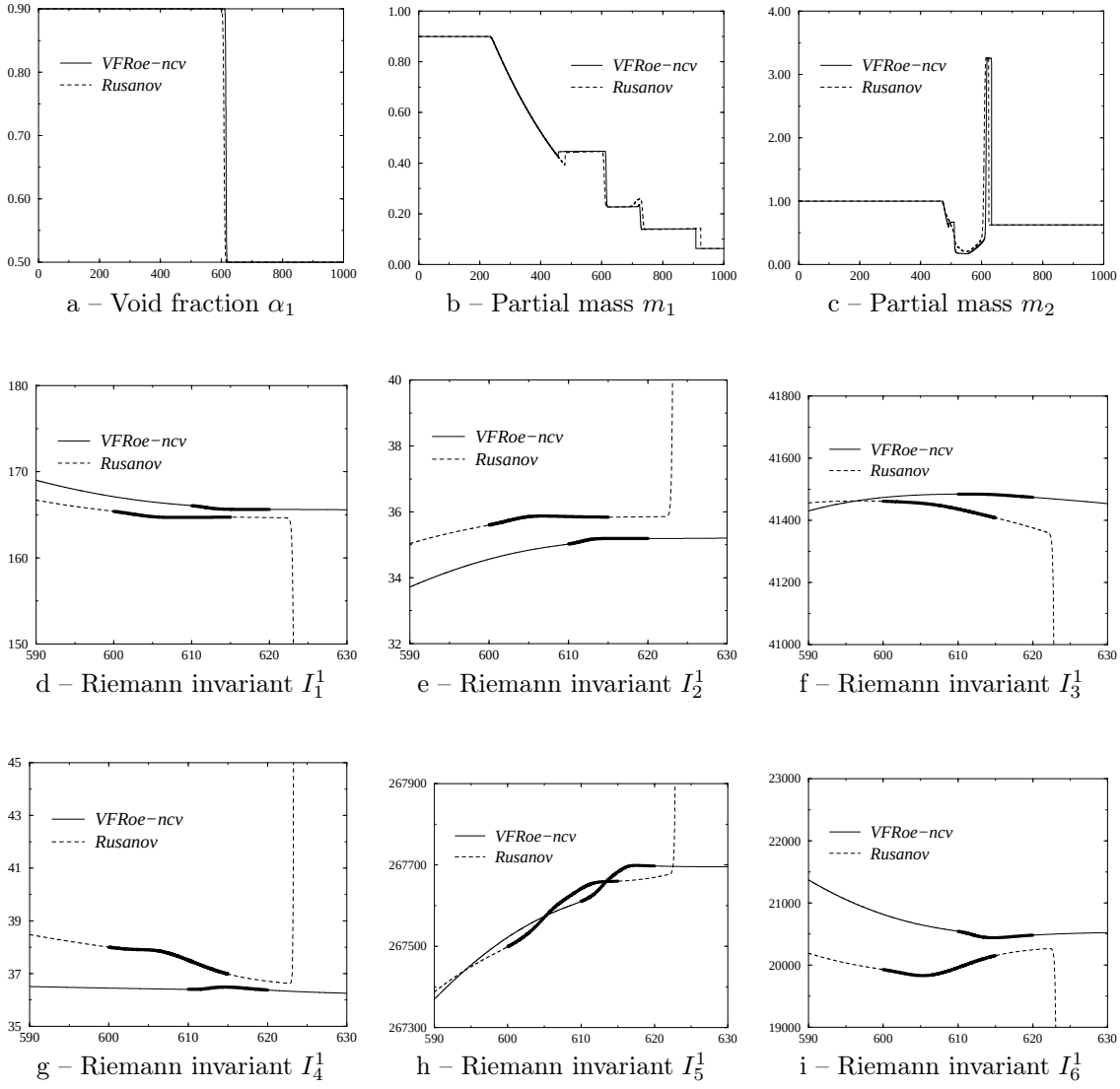

a – Void fraction α_1 b – Partial mass m_1 c – Partial mass m_2

d – Riemann invariant I_1^1 e – Riemann invariant I_2^1 f – Riemann invariant I_3^1

g – Riemann invariant I_4^1 h – Riemann invariant I_5^1 i – Riemann invariant I_6^1

Fig. 4.2: Shock tube test case with resonance

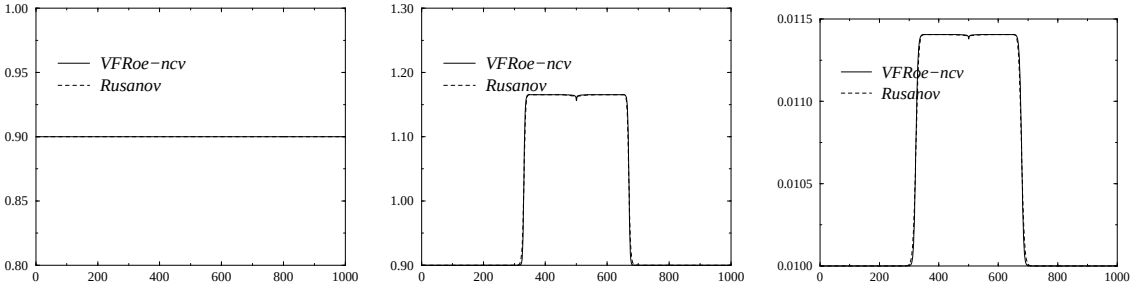

a – Void fraction α_1 b – Partial mass m_1 c – Partial mass m_2

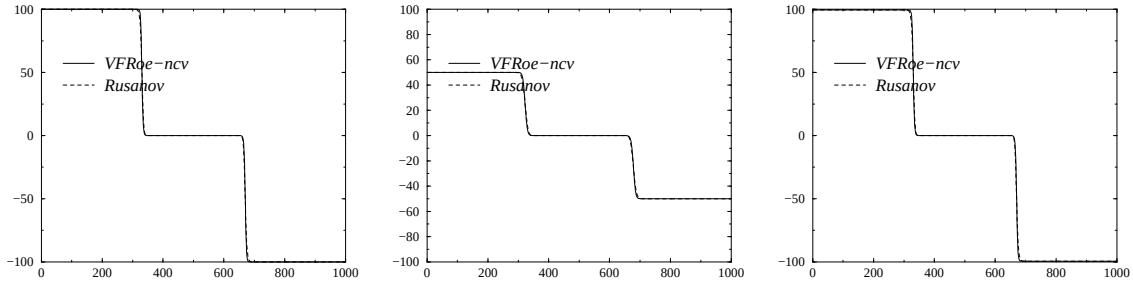

d – Velocity U_1 e – Velocity U_2 f – Velocity V_i

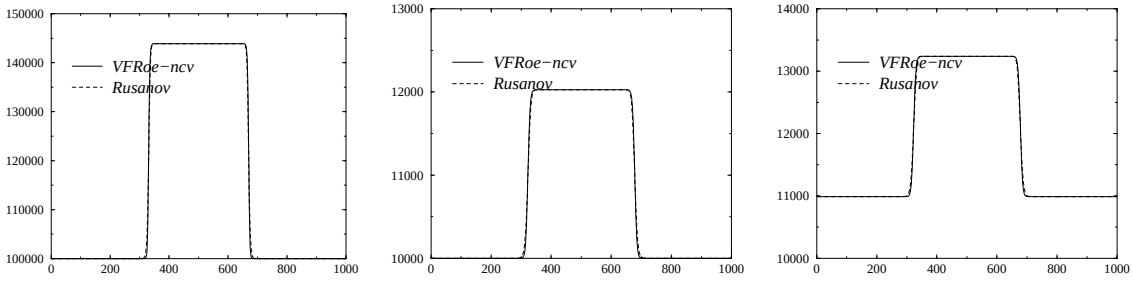

g – Pressure P_1 h – Pressure P_2 i – Pressure P_i

Fig. 4.3: Wall boundary condition: shock waves

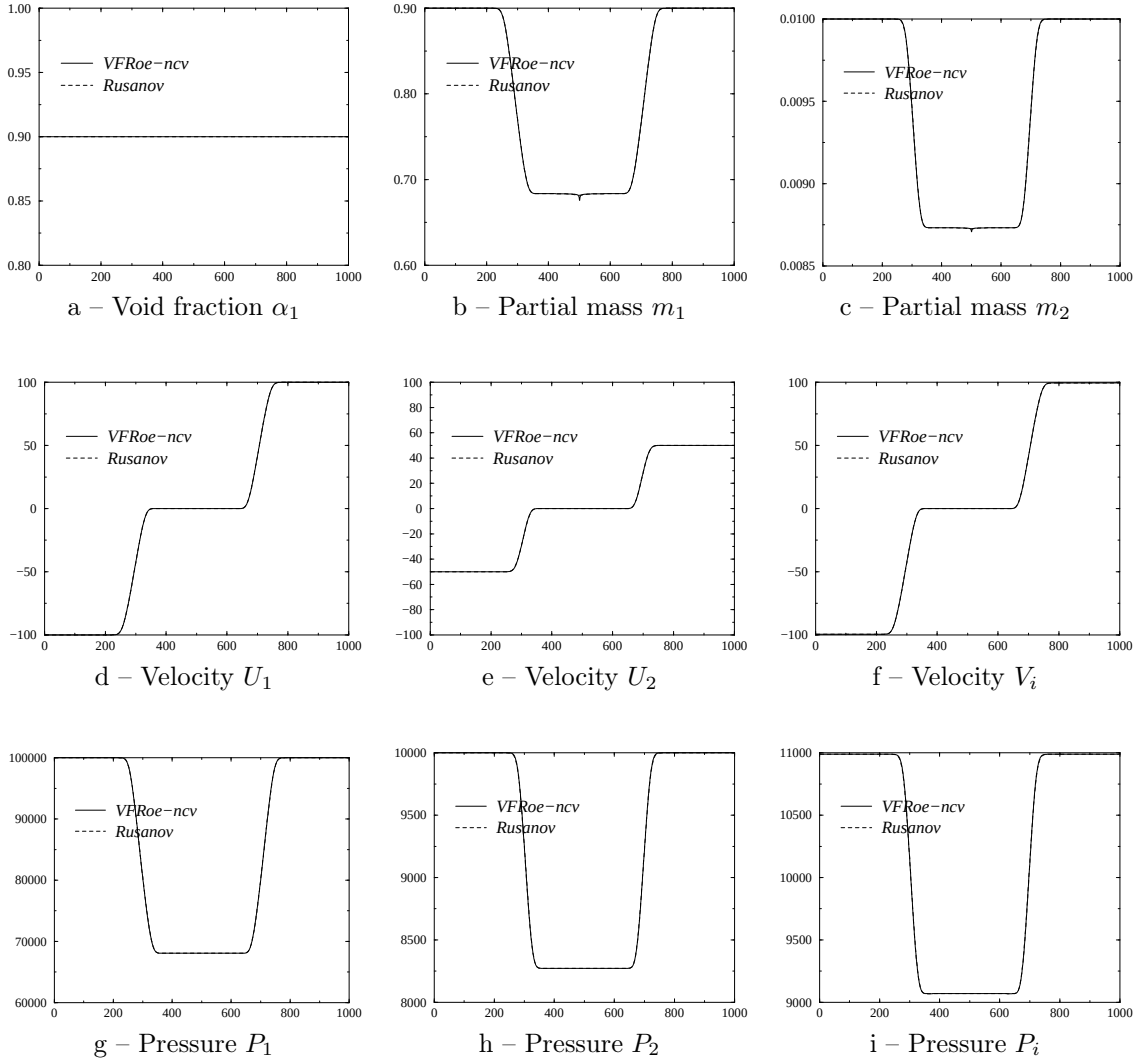

a – Void fraction α_1 b – Partial mass m_1 c – Partial mass m_2

d – Velocity U_1 e – Velocity U_2 f – Velocity V_i

g – Pressure P_1 h – Pressure P_2 i – Pressure P_i

Fig. 4.4: Wall boundary condition: rarefaction waves

positive for given C.F.L. number smaller than one (here, N_{CFL} has been set to 0.45). Note that initial data ensures that no vacuum may occur. As above, the mesh contains one thousand cells and $T_{MAX} = 0.5\,s$. Results provided by the VFRoe-ncv scheme and by the Rusanov scheme are very similar.

4.4.5 The water faucet problem

This test case is a classical benchmark test in the frame of the numerical simulation of two-phase flow [Ran87]. This is a one-dimensional configuration, corresponding to a $L = 12\,m$ long vertical tube. The initial condition is a uniform column of water (indexed by 1) in the air (indexed by 2), with a void fraction of the water α_1 equal to $0,8$ over the domain. Note that we set $\gamma_1 = 1,0005$ and $\gamma_2 = 1,4$ in (4.59). The velocity of the water U_1 is 10 and the velocity of the air U_2 is null. All pressures are set to 10^5. The initial densities are $\rho_1(t = 0,.) = 1000$ and $\rho_2(t = 0,.) = 1$. This initial data may be interpreted as a flow of water without gravity.

The simulation consists in introducing the gravity field for $t > 0$. The flow is thus driven by the boundary conditions: $\alpha_1(t,0) = 0,8$, $U_1(t,0) = 10$, $U_2(t,0) = 0$, $P_1(t,L) = P_2(t,L) = 10^5$, and by the governing equations (4.7) complemented with gravity terms $g = 9.8$ in $(0;L)$. Moreover, the drag force is not included and the time scale is $\theta = 5.10^{-4}\,s$ in the pressure relaxation term (4.12). An analytical solution of this test is available for a very simple model, which is actually too simple since the present model (4.7) cannot degenerate to it unless assuming unrealistic hypotheses [Hal98]. The left boundary condition at $x = 0$ corresponds to the problem i-ii-iii' in section 4.3.3 with $n_b = 3$. After some time steps, the void fraction $(\alpha_1)_0^n$ becomes different from $0,8$ and the solution of the associated partial Riemann problem (in the sense of F. Dubois [Dub87]) cannot be solved exactly. Therefore, the previous boundary condition has been changed to $\alpha_1(t,x<0) = 0,8$, $\rho_1(t,x<0) = 1000$, $\rho_2(t,x<0) = 1$, $U_1(t,x<0) = 10$, $U_2(t,x<0) = 0$ and $P_1(t,x<0) = P_2(t,x<0) = 10^5$. This results in a boundary condition following item iii in section 4.3.3 and is solved using the linearisation of the VFRoe-ncv scheme. Pertaining to the boundary condition at $x = L$, we may reasonably assume that $V_i > 0$ since the velocities U_1 and U_2 are positive all along the simulation. In such a case, the void fraction $\alpha_1(t,L^-)$, $t > t^n$, is equal to $(\alpha_1)_N^n$ (where N is the index of the last cell of the domain) and the partial Riemann problem may be exactly solved by the technique proposed by F. Dubois. The first results presented here correspond to the profiles plotted at $T_{MAX} = 0.5\,s$. Only the VFRoe-ncv scheme has been tested here for the convective part (4.36). Several meshes have been used. A usual problem of the two-fluid one-pressure approach is that, for this test, some complex speeds of waves arise and if the cell number is too large (more than 1000 cells), the void fraction of the air α_2 becomes negative. Here, computations have been performed over 20000 cells (and may probably be extended to smaller space steps δx). This is due to the unconditional hyperbolicity of the model. Note that, for the finest mesh presented here, the approximate solution of α_2 on figure 4.5 seems smoothed. This is a consequence of the pressure relaxation which is not instantaneous. Furthermore, profiles of velocity U_1 on figure 4.6 are in agreement with classical results obtained when focusing on two-fluid one-pressure models, since no pressure relaxation term appears in the governing equations of velocities U_1 and U_2. We now focus on the convergence of the scheme when $t \to \infty$. In order to evaluate the convergence of the VFRoe-ncv scheme, the normalised time variations in the L^2-norm associated to α_1 and U_1, that

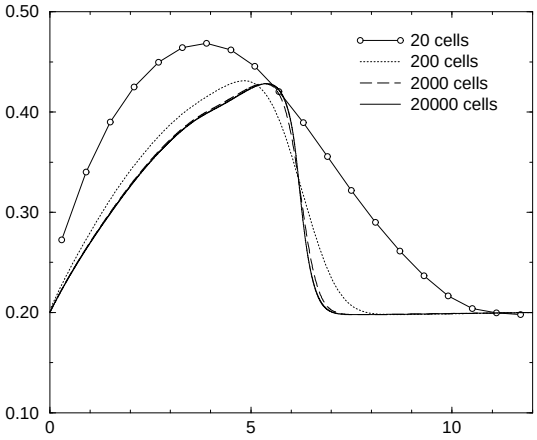

Fig. 4.5: Water faucet
Void fraction α_2

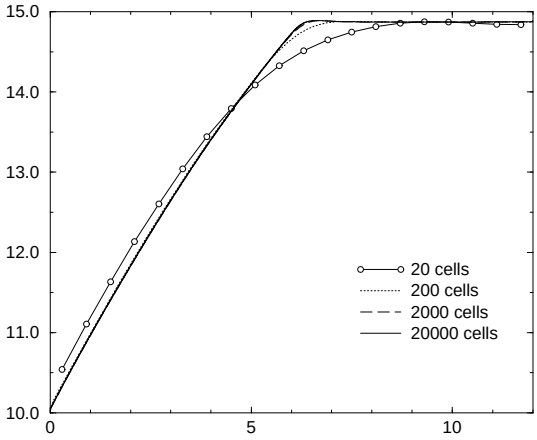

Fig. 4.6: Water faucet
Water velocity U_1

are

$$\ln \frac{\Big(\sum_i \big((\alpha_1)_i^{n+1} - (\alpha_1)_i^n\big)^2\Big)^{1/2}}{\max\limits_{\{n;t^n \le T_{MAX}\}} \Big(\sum_i \big((\alpha_1)_i^{n+1} - (\alpha_1)_i^n\big)^2\Big)^{1/2}}$$

and

$$\ln \frac{\Big(\sum_i \big((U_1)_i^{n+1} - (U_1)_i^n\big)^2\Big)^{1/2}}{\max\limits_{\{n;t^n \le T_{MAX}\}} \Big(\sum_i \big((U_1)_i^{n+1} - (U_1)_i^n\big)^2\Big)^{1/2}}$$

are plotted on figures 4.7-4.8.

4.4.6 The sedimentation test case

This test case corresponds to a very simple configuration, which is a classical benchmark test for the simulation of two-phase flows [AST02], [CEG+97]. A uniform mixture of gas and liquid, $\alpha_1(0,x) = 0,5,\ x \in [0;7,5]$, lies in a vertical tube (the subscript 1 corresponds to the water and the subscript 2 corresponds to the air). The initial densities are set to $\rho_1(0,x) = 10^3$ and $\rho_2(0,x) = 1$, both pressures are $P_1(0,x) = P_2(0,x) = 10^5$ and velocities $U_1(0,x)$ and $U_2(0,x)$ are null, $x \in [0;7,5]$. The domain is closed, which means that rigid wall boundary conditions are imposed at $x = 0$ and $x = 7,5$. The equations of state are the same as for the previous test case and $\theta = 5.10^{-4}\,s$ in the pressure relaxation term (4.12) (here again, the drag force is not taken into account). The gravity field provides a separation of the phases for $t > 0$ and the solution at $t = +\infty$ is composed by a distribution at rest of pure air for $x \in [0;3,25]$ and by a distribution of

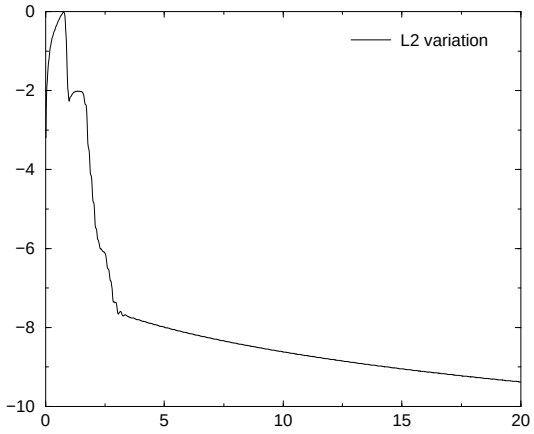

Fig. 4.7: Water faucet
Variation of void fraction α_2

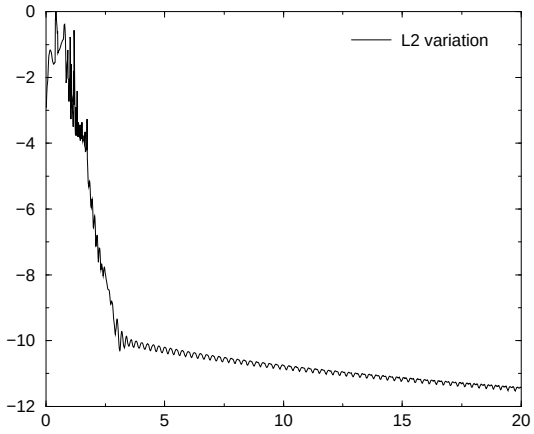

Fig. 4.8: Water faucet
Variation of water velocity U_2

pure water for $x \in [3,25; 7,5]$. The figure 4.9 corresponds to the results obtained by the VFRoe-ncv scheme over 200 cells.

4.5 Conclusion

Some new results concerning modeling of two-phase flows with help of the two-fluid approach have been presented herein. The main difference with the models issued from the classical literature about the simulation of two-phase flows is that the phase pressures are assumed to be distinct. The system requires giving adequate closures for the interface velocity and the interface pressure, in addition with standard closure laws for drag terms, viscous terms and mass transfer terms. The interfacial velocity has been chosen such that the 1-wave (which corresponds to the transport of the void fraction) is a contact discontinuity. This implies that this interface remains infinitely thin whatever the initial condition is. Pertaining to the interfacial pressure, several ways of closure are proposed. The first way of closure aims at defining products of distributions occuring in non conservative terms. This may be done choosing the interfacial pressure as a function of the 1-Riemann invariants. The other way of closure permits to obtain a meaningful entropy inequality. It enables to check that intermediate states occuring in the solution of the one dimensional Riemann problem are physically releavant, which means that expected positive constraints on some quantities are preserved throughout the connection of states through waves. The system obtained with these closures thus seems adequate to compute two-phase flows. The property of hyperbolicity ensures that for all initial data in Ω the speeds of waves are real. Furthermore, for a class of closure laws for the interfacial pressure and the interfacial velocity, the connection through these waves is in agreement with the maximum principle for the void fraction and with the positivity requirements for partial masses and pressures. Note that these important properties are maintained through the relaxation processes. Actually, our study has been led following the theory associated to Riemann problems, such as the one presented in [Smo83] in the frame of gas dynamics for instance. Nonetheless,

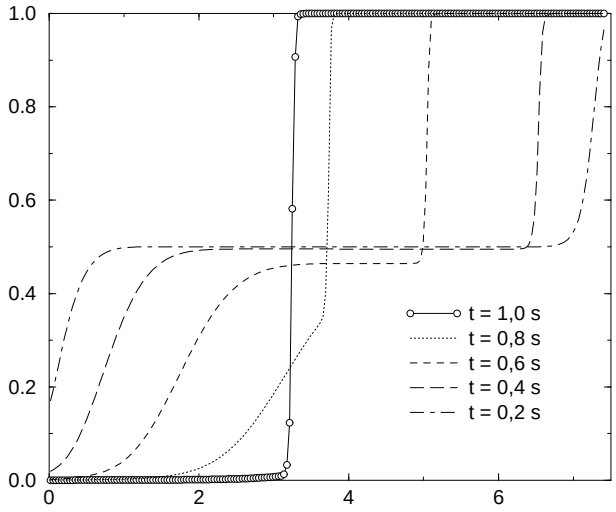

Fig. 4.9: Variation of α_1 for the sedimentation test case (distance *vs* α_1)

another way of investigation should be proposed. Indeed, the model presented here may be seen as an extension by a relaxation process of the well-known six equations model [CEG$^+$97], which supposes the pressure equilibrium. Then, one might try to follow the analysis of T.P. Liu [Liu88] and G.Q. Chen, C.D. Levermore and T.P. Liu [CLL94] about hyperbolic systems with relaxation.

Two different finite volume methods to compute the convective set have been described, which are based on a non conservative form of Rusanov scheme and a modified form of VFRoe scheme with non conservative variables. Source terms have been accounted using a splitting method. Several properties of both methods have been described and emphasized by numerical tests. Evenmore, some computational results enable deeper understanding of the solution of the whole set of partial differential equations, in particular for the resonance phenomenon. A classical benchmark for the simulation of two-phase flows, namely the water faucet problem, has been tested. Very encouraging results have been obtained, since the computations may be performed over very fine meshes without a loss of stability and physical releavance, due to the unconditional hyperbolicity of the model.

Acknowledgments: The third author has been supported by Electricité de France (EDF) grant under contract C02770/AEE2704. Computational facilities were provided by EDF-Division Recherche et Développement. Part of the work has benefited from discussions with Frédéric Coquel.

4.A Equations of state remaining unchanged by averaging process for the two-fluid two-pressure model

The two-fluid two-pressure model (4.1) is classically obtained after an averaging process. Initially, phases are separated one to the other by an interface (namely the local instant formulation), but most of configurations of flow prohibit the computation of the geometry of this interface and physical phenomena occuring at the interface are very complex. Hence, initial equations are averaged, leading to a system of partial differential equations in terms of means values, see [Ish75] for more details. First, let us note a statistical average by $< . >$ and the function for phase k by χ_k. Focusing on the density for instance, the phase average is given by

$$\overline{\overline{\rho_k}} = \frac{< \chi_k \rho_k >}{< \chi_k >}.$$

The mass weighted mean value (for the velocity for instance) is defined by

$$\overline{U_k} = \frac{< \chi_k \rho_k U_k >}{< \chi_k \rho_k >} = \frac{\overline{\overline{\rho_k U_k}}}{\overline{\overline{\rho_k}}}.$$

The phase average is dedicated to *extensive* variables (pressure, density, momentum, ...) while velocity, internal energy, ... correspond to mass weighted mean values. Assume that equation of state on phase k follows

$$\rho_k e_k = \mathcal{F}_k(\rho_k, P_k).$$

Now, we aim at write the equation which links mean values $\overline{\overline{P_k}}$, $\overline{\overline{\rho_k}}$ and $\overline{e_k}$. Of course, function $\mathcal{F}_k$ must be more explicit. Actually, if $\mathcal{F}_k$ takes the form

$$\mathcal{F}_k(\rho_k, P_k) = g_k P_k + b_k \rho_k + c_k$$

where g_k, b_k, c_k are real constant, we have

$$\begin{aligned} \overline{\overline{\rho_k e_k}} &= \overline{\overline{\mathcal{F}_k(\rho_k, P_k)}}, \\ \overline{\overline{\rho_k}}\,\overline{e_k} &= \overline{\overline{g_k P_k + b_k \rho_k + c_k}}, \\ &= g_k \overline{\overline{P_k}} + b_k \overline{\overline{\rho_k}} + c_k, \end{aligned}$$

and finally the equation for mean values in phase k

$$\overline{\overline{\rho_k}}\,\overline{e_k} = \mathcal{F}_k(\overline{\overline{\rho_k}}, \overline{\overline{P_k}})$$

holds, which is the exact counterpart of local instant equation of state. Note that perfect gas equation of state or Tammann equation of state belongs to this class, contrary to Van der Waals equation of state. Nonlinearities of the latter one prohibit such a property.

4.B Positivity for smooth solutions

Let L and T two positive real constants. We focus in this appendix on the positivity of a function φ from $[0,T]\times[0,L]$ to $\mathbb{R}$ which verifies an equation of the form

$$\frac{\partial \varphi}{\partial t} + u\frac{\partial \varphi}{\partial x} + \varphi\frac{\partial u}{\partial x} = \varphi m, \tag{4.61}$$

where u and m are two smooth functions from $[0,T]\times[0,L]$ to $\mathbb{R}$.

Lemma 4.6. *Assume that u, $\partial_x u$ and m belong to $L^\infty([0,T]\times[0,L])$. Then, equation (4.61) on φ associated with positive inlet boundary conditions, that is $\varphi(t,x=0)$ and $\varphi(t,x=L)$ positive for all t in $[0,T]$, and admissible initial condition, that is $\varphi(t=0,x)$ for all x in $[0,L]$, leads to*

$$\varphi(t,x) \geq 0, \quad \forall (t,x)\in[0,T]\times[0,L] \tag{4.62}$$

when restricting to smooth functions.

Proof. Let introduce the decomposition $\varphi = \varphi^+ - \varphi^-$, with $\varphi^+ \geq 0$, $\varphi^- \geq 0$ and $\varphi^+\varphi^- = 0$. Multiplying (4.61) by $-\varphi^-$ yields

$$-\varphi^-\frac{\partial}{\partial t}(\varphi^+ - \varphi^-) - u\varphi^-\frac{\partial}{\partial x}(\varphi^+ - \varphi^-) - \varphi^-(\varphi^+ - \varphi^-)\frac{\partial u}{\partial x} = -\varphi^-(\varphi^+ - \varphi^-)m.$$

Defining the norm $\|.\| = \left(\int_0^L |.|^2\, dx\right)^{1/2}$, one may obtain by integration over $[0,L]$

$$\frac{\partial}{\partial t}(\|\varphi^-\|^2) + \int_0^L u\frac{\partial}{\partial x}(\varphi^-)^2\, dx + 2\int_0^L (\varphi^-)^2\frac{\partial u}{\partial x}\, dx = -2\int_0^L (\varphi^-)^2 m\, dx.$$

Integrating by part the second term of the left handside gives

$$\frac{\partial}{\partial t}(\|\varphi^-\|^2) + [u(\varphi^-)^2]_0^L + \int_0^L (\varphi^-)^2\frac{\partial u}{\partial x}\, dx = -2\int_0^L (\varphi^-)^2 m\, dx.$$

Thanks to assumptions of inlet boundary conditions, it follows

$$\frac{\partial}{\partial t}(\|\varphi^-\|^2) \leq -\int_0^L (\varphi^-)^2\left(\frac{\partial u}{\partial x} + 2m\right)\, dx.$$

Since the initial data on φ is positive, the Gronwall's lemma gives for any time t in $[0,T]$

$$\|\varphi^-\|(t) = 0.$$

Therefore, φ^- is null and φ remains positive on the whole domain $[0,T]\times[0,L]$. □

4.C Rankine-Hugoniot jump relations for a linearly degenerate field of a non conservative system

Let us study the following system:

$$\frac{\partial}{\partial t}W + A(W)\frac{\partial}{\partial x}W = 0, \tag{4.63}$$

with W a function from $\mathbb{R}_+ \times \mathbb{R}$ to Ω (Ω an open subset of $\mathbb{R}^p$). We suppose that this system is non conservative and hyperbolic. We focus on the k^{th} field ($1 \leq k \leq p$), which is assumed to be *linearly degenerate*, which means that

$$\nabla\lambda_k(W).r_k(W) = 0, \quad W \in \Omega, \tag{4.64}$$

where $\lambda_k(W)$ is the k^{th} eigenvalue of $A(W)$ and $r_k(W)$ the k^{th} right eigenvector of $A(W)$. Let $(I_l^k)_{l=1,\dots,p-1}$ be a family of k-Riemann invariants, *i.e.* smooth functions from Ω to $\mathbb{R}$ verifying

$$\nabla I_l^k(W).r_k(W) = 0, \quad W \in \Omega. \tag{4.65}$$

Assume now that the gradients of the k-Riemann invariants $(I_l^k)_{l=1,\dots,p-1}$ are linearly independent (such a family of k-Riemann invariants exists, see Proposition 17.2 of [Smo83]). Using this set of k-Riemann invariants, one may define the curve $\mathcal{C}_k(W_L)$, W_L in Ω, by

$$\mathcal{C}_k(W_L) = \left\{W \in \Omega; I_l^k(W) = I_l^k(W_L), 1 \leq l \leq p-1\right\}. \tag{4.66}$$

We suppose that there exists a parametrisation $\Phi_k(W_L, \varepsilon)$ of $\mathcal{C}_k(W_L)$, from $\Omega \times \mathbb{R}$ to Ω, such that $\Phi_k(W_L, 0) = W_L$. One may easily check that

$$\frac{\partial}{\partial \varepsilon} I_l^k(\Phi_k(W_L, \varepsilon)) = 0, \quad \forall 1 \leq l \leq p-1. \tag{4.67}$$

We have the following result:

Proposition 4.9. *The curve $\mathcal{C}_k(W_L)$ is the integral curve of the vector field r_k passing through the point W_L.*

Proof. Let us define the function V by $V(\varepsilon) = \Phi_k(W_L, \varepsilon)$. Obviously, $V(0) = W_L$ holds. We now aim at verify that vectors $V'(\varepsilon)$ and $r_k(V(\varepsilon))$ are collinear in $\mathbb{R}^p$. Equation (4.67) becomes

$$\nabla I_l^k(V).V'(\varepsilon) = 0, \quad \forall 1 \leq l \leq p-1. \tag{4.68}$$

Therefore, recalling that the right eigenvector r_k verifies equation (4.65), this proof reduces to check that the family $(\nabla I_l^k(V))_{l=1,\dots,p-1}$ is free, which holds. □

Let us introduce now two smooth functions u and f from Ω to $\mathbb{R}$ such that

$$u'(W)A(W) = f'(W), \quad W \in \Omega, \tag{4.69}$$

or equivalently such that

$$\frac{\partial}{\partial t}u(W(t,x)) + \frac{\partial}{\partial x}f(W(t,x)) = 0, \quad W \in \Omega. \tag{4.70}$$

Note that the partial differential equation (4.70) is a conservation law which is, in general, only available for smooth solutions W of system (4.63). However, focusing on the k^{th} field, the following Rankine-Hugoniot jump relation holds:

Theorem 4.1. *Let us note $\sigma(W) = \lambda_k(W)$. Then we have*

$$\sigma(W)\big(u(W) - u(W_L)\big) = f(W) - f(W_L), \quad \forall W \in \mathcal{C}_k(W_L). \tag{4.71}$$

Proof. As above, we define the function V by $V(\varepsilon) = \Phi_k(W_L, \varepsilon)$. Moreover, we set

$$E(\varepsilon) = -\sigma(V(\varepsilon))\big(u(V(\varepsilon)) - u(W_L)\big) + \big(f(V(\varepsilon)) - f(W_L)\big). \tag{4.72}$$

Clearly, $E(0) = 0$. Note that by definition $\lambda_k(W)$ is a k-Riemann invariant, which provides $\sigma(W) = \lambda_k(W_L)$ for all W in $\mathcal{C}_k(W_L)$. Derivating equation (4.72) with respect to ε gives

$$\begin{aligned} E'(\varepsilon) &= -\sigma(V(0))u'(V(\varepsilon)).V'(\varepsilon) + f'(V(\varepsilon)).V'(\varepsilon) \\ &= -\sigma(V(0))u'(V(\varepsilon)).V'(\varepsilon) + u'(V(\varepsilon))A(V(\varepsilon)).V'(\varepsilon). \end{aligned}$$

Using Proposition 4.9, it follows

$$\begin{aligned} E'(\varepsilon) &= -\sigma(V(0))u'(V(\varepsilon)).r_k(V(\varepsilon)) + u'(V(\varepsilon))A(V(\varepsilon)).r_k(V(\varepsilon)) \\ &= u'(V(\varepsilon)).\big(A(V(\varepsilon))r_k(V(\varepsilon)) - \lambda_k(V(\varepsilon))r_k(V(\varepsilon))\big) \\ &= 0. \end{aligned}$$

Hence, $E(\varepsilon) = 0$ for all ε in $\mathbb{R}$. □

As done before for $\mathcal{C}_k(W_L)$ with k-Riemann invariants, we define the curve $\mathcal{S}_k(W_L)$ from Rankine-Hugoniot jump relations of the form (4.71) associated with system (4.63). A straightforward consequence is that curves $\mathcal{C}_k(W_L)$ and $\mathcal{S}_k(W_L)$ identify. So, the k-contact discontinuity propagates at speed $\sigma = \lambda_k$ (which is constant through the discontinuity) and is defined by the curve $\mathcal{S}_k(W_L)$ (or equivalently by $\mathcal{C}_k(W_L)$). Finally, the non conservative frame is identical to the conservative frame focusing on linearly degenerate fields (note that this result has already been stated in [BCG$^+$02]).

4.D Connection through the 1-wave

The system studied here corresponds to the set of partial differential equations (4.7) with the interfacial velocity V_i defined by (4.5)-(4.21) and the interfacial pressure P_i given by (4.28-4.30), associated with the Riemann initial data (4.19). Both equations of state follow $P_k = (\gamma_k - 1)\rho_k e_k$, $\gamma_k > 1$, $k = 1, 2$. We focus here on the parametrisation through the 1-contact discontinuity between

W_l and W_r (see notations in the body of the text). Recall that 1-Riemann invariants and Rankine-Hugoniot jump relations lead to the same parametrisation, since this field is linearly degenerate. Therefore, through the 1-wave, equality

$$I_p^1(W_l) = I_p^1(W_r) \tag{4.73}$$

holds for all $1 \leq p \leq 6$, where 1-Riemann invariants $(I_p^1)_{p=1,\dots,6}$ are given in equations (4.23-4.27)-(4.34). Combining I_2^1, I_3^1, I_5^1 and I_6^1 may lead to

$$I_3^1(W) = (I_2^1(W))^2 \left(\frac{\gamma_1+1}{2\gamma_1}\frac{1}{m_1} + \frac{\gamma_2+1}{2\gamma_2}\frac{1}{m_2} \right) + I_5^1(W)\frac{\gamma_1-1}{\gamma_1}m_1 + I_6^1(W)\frac{\gamma_2-1}{\gamma_2}m_2. \tag{4.74}$$

Using jump relations (4.73) in (4.74) gives

$$\begin{aligned} I_3^1(W_l) = (I_2^1(W_l))^2 \left(\frac{\gamma_1+1}{2\gamma_1}\frac{1}{(m_1)_r} + \frac{\gamma_2+1}{2\gamma_2}\frac{1}{(m_2)_r} \right) \\ + I_5^1(W_l)\frac{\gamma_1-1}{\gamma_1}(m_1)_r + I_6^1(W_l)\frac{\gamma_2-1}{\gamma_2}(m_2)_r, \end{aligned} \tag{4.75}$$

where only $(m_1)_r$ and $(m_2)_r$ are unknown.

We turn now to the jump relation (4.73) with $p = 4$. Since we are dealing with a perfect gas state law within each phase, specific entropies are defined by $s_k = P_k \rho_k^{-\gamma_k}$, $k = 1, 2$. One can easily obtain

$$s_k = \frac{\alpha_k^{-\gamma_k+1}}{m_k^{\gamma_k}} \left(\frac{\gamma_k - 1}{\gamma_k} \right) \left(I_{k+4}^1(W) m_k - \frac{(I_2^1(W))^2}{2m_k} \right). \tag{4.76}$$

So, Rankine-Hugoniot jump relations (4.73) and equation (4.76) yield

$$\begin{aligned} \frac{(1-(\alpha_1)_r)^{-\gamma_2+1}}{(m_2)_r^{\gamma_2}} \left(\frac{\gamma_2-1}{\gamma_2} \right) \left(I_6^1(W_l)(m_2)_r - \frac{(I_2^1(W_l))^2}{2(m_2)_r} \right) \\ = \frac{(s_2)_l}{(s_1)_l} \frac{(\alpha_1)_r^{-\gamma_1+1}}{(m_1)_r^{\gamma_1}} \left(\frac{\gamma_1-1}{\gamma_1} \right) \left(I_5^1(W_l)(m_1)_r - \frac{(I_2^1(W_l))^2}{2(m_1)_r} \right). \end{aligned} \tag{4.77}$$

As mentionned above, focusing on the complete Riemann problem, we have $(\alpha_1)_r = (\alpha_1)_R$, where $(\alpha_1)_R$ denotes $\alpha_1(t = 0, x > 0)$, which means that $(\alpha_1)_r$ is not an unknown. Hence, equations (4.75) and (4.77) compose a non linear system of two equations with two unknowns $(m_1)_r$ and $(m_2)_r$. Let us describe the solution of this system. First, equation (4.77) is rewritten to provide $(m_2)_r$ as a function of $(m_1)_r$. After, $(m_2)_r$ is replaced in (4.75) by the expression, in order to obtain an equation of the form

$$\mathcal{H}((m_1)_r) = I_3^1(W_l) \tag{4.78}$$

where $\mathcal{H}$ is the suitable function defined from (4.75) and (4.77). Hence, the resolution of the 2×2 system is reduced to the inversion of the function $\mathcal{H}$. The behaviour of $\mathcal{H}$ may be describe by the

following table:

m	0		m_0		$+\infty$
$\mathcal{H}'(m)$	$-\infty$	$-$	0	$+$	$+\infty$
$\mathcal{H}(m)$	$+\infty$	↘	$\mathcal{H}(m_0)$	↗	$+\infty$

where

$$m_0 = \left(\frac{(\gamma_1 + 1)(I_2^1(W_l))^2}{2(\gamma_1 - 1) I_5^1(W_l)} \right)^{\frac{1}{2}}.$$

Some constraints on the solution $(m_1)_r$ must be added, in order to ensure that W_r is an admissible state, that is $W_r \in \Omega$. Of course, $(\alpha_1)_r$ belongs to $]0,1[$ since $(\alpha_1)_r = (\alpha_1)_R$. Furthermore, assuming that $(m_1)_r > 0$, positivity of partial mass $(m_2)_r$ is directly ensured by equation (4.75). The internal energy of phase 1 noted $(e_1)_r$ is positive if

$$(m_1)_r^2 > \mu_0 \quad \text{where} \quad \mu_0 = \frac{(I_2^1(W_l))^2}{2 I_5^1(W_l)}. \tag{4.79}$$

Finally, the internal energy $(e_2)_r$ is positive using the equality $I_4^1(W_l) = I_4^1(W_r)$. Therefore, if a solution $(m_1)_r$ of equation (4.78) verifies inequality (4.79), the whole state W_r calculated from $(m_1)_r$ and jump relations (4.73) is admissible. This allows to state proposition 4.8.

We discuss now the existence of solutions of equation (4.78) (see Figure 4.10 for an illustration). A first condition comes from the value of $I_3^1(W_l)$. If $I_3^1(W_l) < \mathcal{H}(m_0)$, then equation (4.78) admits no solution (see Remark 4.4 for more details). If $I_3^1(W_l) \geq \mathcal{H}(m_0)$, two solutions of equations (4.78) can be constructed (which identify if the inequality is an equality), refered as $(m_1)_r^-$ and $(m_1)_r^+$ on Figure 4.10. We turn now to inequality (4.79). Note that, since $\gamma_1 > 1$, we have $m_0 > \mu_0$. Hence, $(m_1)_r^+$ always verifies (4.79), which means that if $(m_1)_r^+$ exists, this is always an admissible solution of (4.78). Moreover, the root $(m_1)_r^-$ is admissible iff $(m_1)_r^- > \mu_0$, which provides two distinct solutions of equation (4.78) (it corresponds to Figure 4.10).

Remark 4.4. As mentionned above, if $I_3^1(W_l) < \mathcal{H}(m_0)$, equation (4.78) admits no solution. It means that no state W_r can be connected to W_l by the 1-contact discontinuity. Therefore, a wave must appear between W_l and the wave V_i to solve the Riemann problem. The same phenomenon occurs when focusing on systems with source terms [LeR98], [CL99] or systems with a flux function involving discontinuous coefficients [SV03].

4.E Numerical preservation of some basic solutions

We note first that the Cauchy problem composed by the homogeneous non conservative hyperbolic convective system (4.7) and by a initial condition (4.3) which verifies:

$$P_1(x,0) = P_2(x,0) = P_0,$$
$$U_1(x,0) = U_2(x,0) = U_0,$$

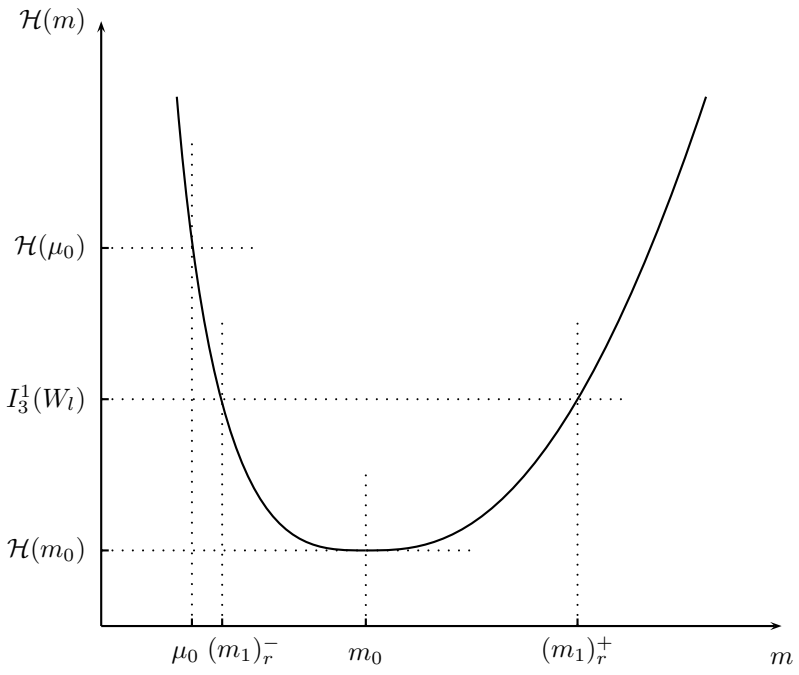

Fig. 4.10: Resolution of equation (4.78)

$U_0 \in \mathbb{R}$, $P_0 \in \mathbb{R}_+^*$, $x \in \mathbb{R}$, has a solution which agrees with

$$\begin{aligned} P_1(x,t) = P_2(x,t) = P_0, \\ U_1(x,t) = U_2(x,t) = U_0, \end{aligned}$$

$x \in \mathbb{R}$ and $t > 0$.

We may thus wonder whether the non conservative version of Rusanov scheme (section 4.3.1) and of the VFRoe-ncv scheme (section 4.3.1) preserve this solution. We assume here that the equation of state of each phase $k = 1, 2$ satisfies:

$$\rho_k \varepsilon_k(P_k, \rho_k) = g_k(P_k) + b_k \rho_k + c_k \tag{4.80}$$

where b_k and c_k are real constants, and g_k an invertible function (for instance perfect gas equation of state, Tammann equation of state, ...). Note that this class of equations of state is larger than the one defined by (4.42).

4.E.1 The Rusanov scheme

Let us first recall the Rusanov scheme. The non conservative equation on the void fraction α_1 is approximated by

$$\begin{aligned} (\alpha_1)_j^{n+1} - (\alpha_1)_j^n + \frac{\delta t}{\delta x}(V_i)_j^n \big((\overline{\alpha_1})_{j+1/2}^n - (\overline{\alpha_1})_{j-1/2}^n\big) - \frac{\delta t}{2\delta x}\Big(r_{j+1/2}\big((\alpha_1)_{j+1}^n - (\alpha_1)_j^n\big)\Big) \\ + \frac{\delta t}{2\delta x}\Big(r_{j-1/2}\big((\alpha_1)_j^n - (\alpha_1)_{j-1}^n\big)\Big) = 0. \end{aligned} \tag{4.81}$$

The Rusanov scheme applied to the remaining of the system writes, $k = 1, 2$:

$$(Z_k)_j^{n+1} - (Z_k)_j^n + \frac{\delta t}{\delta x}\big((H_k)_{j+1/2}^n - (H_k)_{j-1/2}^n\big) - \frac{\delta t}{\delta x}(P_i)_j^n\big((\varphi_k)_j\big) = 0. \tag{4.82}$$

where

$$Z_k = \begin{pmatrix} m_k \\ m_k U_k \\ \alpha_k E_k \end{pmatrix}, \quad H_k = \begin{pmatrix} m_k U_k \\ m_k (U_k)^2 + \alpha_k p_k \\ \alpha_k U_k (E_k + p_k) \end{pmatrix}, \quad (\varphi_k)_j = \begin{pmatrix} 0 \\ (\overline{\alpha_k})_{j+1/2}^n - (\overline{\alpha_k})_{j-1/2}^n \\ (V_i)_j^n ((\overline{\alpha_k})_{j+1/2}^n - (\overline{\alpha_k})_{j-1/2}^n) \end{pmatrix}$$

and

$$\begin{aligned} r_j &= \max(|(V_i)_j^n|, |(U_1)_j^n| + (c_1)_j^n, |(U_2)_j^n| + (c_2)_j^n), \\ r_{j+1/2} &= \max(r_j, r_{j+1}), \\ 2(H_k)_{j+1/2}^n &= (H_k)_j^n + (H_k)_{j+1}^n - r_{j+1/2}((Z_k)_{j+1}^n - (Z_k)_j^n), \\ 2(\overline{\alpha_k})_{j+1/2}^n &= (\alpha_k)_j^n + (\alpha_k)_{j+1}^n. \end{aligned}$$

The Rusanov scheme verifies the following proposition:

Proposition 4.10. *Suppose that, for all cell $j \in \mathbb{Z}$, the approximated initial condition agrees with*

$$(U_1)_j^0 = (U_2)_j^0 = U_0 \quad \textit{and} \quad (P_1)_j^0 = (P_2)_j^0 = P_0.$$

Then, the approximation of the solution computed by the Rusanov scheme (4.81)-(4.82) *agrees, at each time step $n \in \mathbb{N}$ and on each cell $j \in \mathbb{Z}$, with*

$$(U_1)_j^n = (U_2)_j^n = U_0 \quad \textit{and} \quad (P_1)_j^n = (P_2)_j^n = P_0, \tag{4.83}$$

if equation of state of both phases satisfy (4.80).

Proof. We use a proof by recurrence. Property (4.83) is clearly verified for $n = 0$. Assume now that (4.83) is verified at the n^{th} time step.
Mass conservation within phase k provides

$$(m_k)_j^{n+1} - (m_k)_j^n + \frac{\delta t}{\delta x} U_0\big((\overline{m_k})_{j+1/2}^n - (\overline{m_k})_{j-1/2}^n\big) - \frac{\delta t}{\delta x} r_{j+1/2}\big((m_k)_{j+1}^n - (m_k)_j^n\big) + \frac{\delta t}{\delta x} r_{j-1/2}\big((m_k)_j^n - (m_k)_{j-1}^n\big)\big) = 0.$$

Besides, discrete momentum equation within phase k yields:

$$(m_k U_k)_j^{n+1} - (m_k U_k)_j^n + \frac{\delta t}{\delta x}(U_0)^2\big((\overline{m_k})_{j+1/2}^n - (\overline{m_k})_{j-1/2}^n\big) - \frac{\delta t}{\delta x} U_0 r_{j+1/2}\big((m_k)_{j+1}^n - (m_k)_j^n\big) + \frac{\delta t}{\delta x} U_0 r_{j-1/2}\big((m_k)_j^n - (m_k)_{j-1}^n\big) = 0.$$

Thus, combining the latter two equations, and using hypothesis $(U_k)_j^n = U_0$, for all $j \in \mathbb{Z}$, $k = 1, 2$, gives successively:

$$(m_k U_k)_j^{n+1} - (m_k U_k)_j^n - U_0((m_k)_j^{n+1} - (m_k)_j^n) = 0$$

and then $(U_k)_j^{n+1} = U_0$, for all $j \in \mathbb{Z}$, $k = 1, 2$. Turning then to the discrete governing equation for total energy within phase k, the following holds:

$$(\alpha_k E_k)_j^{n+1} - (\alpha_k E_k)_j^n + \frac{\delta t}{\delta x} U_0\big((\overline{\alpha_k E_k})_{j+1/2}^n - (\overline{\alpha_k E_k})_{j-1/2}^n\big) - \frac{\delta t}{\delta x} r_{j+1/2}\big((\alpha_k E_k)_{j+1}^n - (\alpha_k E_k)_j^n\big) + \frac{\delta t}{\delta x} r_{j-1/2}\big((\alpha_k E_k)_j^n - (\alpha_k E_k)_{j-1}^n\big) = 0.$$

Hence, using the fact that in addition $(U_k)_j^{n+1} = U_0$, $\forall j \in \mathbb{Z}$, we have

$$(m_k \varepsilon_k)_j^{n+1} - (m_k \varepsilon_k)_j^n + \frac{\delta t}{\delta x} U_0\big((\overline{m_k \varepsilon_k})_{j+1/2}^n - (\overline{m_k \varepsilon_k})_{j-1/2}^n\big) - \frac{\delta t}{\delta x} r_{j+1/2}\big((m_k \varepsilon_k)_{j+1}^n - (m_k \varepsilon_k)_j^n\big) + \frac{\delta t}{\delta x} r_{j-1/2}\big((m_k \varepsilon_k)_j^n - (m_k \varepsilon_k)_{j-1}^n\big) = 0.$$

This result is valid for any kind of equation of state. We from now assume that the equation of state takes the form (4.80). Thus, it follows

$$m_k \varepsilon_k(P_k, \rho_k) = \alpha_k(g_k(P_k) + c_k) + b_k m_k.$$

Combining previous equation with mass conservation equation in phase k, and using the fact that $(g_k(P_k)+c_k)_j^n = g_k(P_0)+c_k$, $k=1,2$, it gives:

$$(\alpha_k)_j^{n+1} - (\alpha_k)_j^n + \frac{\delta t}{\delta x} U_0\big((\overline{\alpha_k})_{j+1/2} - (\overline{\alpha_k})_{j-1/2}\big) \\ - \frac{\delta t}{\delta x} r_{j+1/2}\big((\alpha_k)_{j+1} - (\alpha_k)_j\big) + \frac{\delta t}{\delta x} r_{j-1/2}\big((\alpha_k)_j - (\alpha_k)_{j-1}\big) = 0,$$

which precisely represents the governing discrete equation for the void fraction, if and only if: $(P_k)_j^{n+1} = P_0$, for all $j \in \mathbb{Z}$, $k=1,2$. This ends the proof by recurrence. □

4.E.2 The VFRoe-ncv scheme

We turn now to the VFRoe-ncv scheme, using variable $Y = {}^t(\alpha_1, s_1, U_1, P_1, s_2, U_2, P_2)$, described in section 4.3.1. Let us recall briefly the general form of the VFRoe-ncv scheme:

$$\delta x\Big((\alpha_1)_j^{n+1} - (\alpha_1)_j^n\Big) + \delta t \hat{V}_i\Big((\alpha_1)_{j+1/2}^* - (\alpha_1)_{j-1/2}^*\Big) = 0, \tag{4.84}$$

$$\delta x\Big((\alpha_k\rho_k)_j^{n+1} - (\alpha_k\rho_k)_j^n\Big) + \delta t\Big((\alpha_k\rho_k U_k)_{j+1/2}^* - (\alpha_k\rho_k U_k)_{j-1/2}^*\Big) = 0, \tag{4.85}$$

$$\delta x\Big((\alpha_k\rho_k U_k)_j^{n+1} - (\alpha_k\rho_k U_k)_i^n\Big) + \delta t\Big((\alpha_k\rho_k (U_k)^2 + \alpha_k P_k)_{j+1/2}^* - (\alpha_k\rho_k (U_k)^2 + \alpha_k P_k)_{j-1/2}^*\Big) \\ -\delta t \hat{P}_i\Big((\alpha_1)_{j+1/2}^* - (\alpha_1)_{j-1/2}^*\Big) = 0, \tag{4.86}$$

$$\delta x\Big((\alpha_k E_k)_j^{n+1} - (\alpha_k E_k)_j^n\Big) + \delta t\Big((\alpha_k U_k (E_k+P_k))_{j+1/2}^* - (\alpha_k U_k (E_k+P_k))_{j-1/2}^*\Big) \\ -\delta t \hat{P}_i \hat{V}_i\Big((\alpha_1)_{j+1/2}^* - (\alpha_1)_{j-1/2}^*\Big) = 0, \tag{4.87}$$

$k=1,2$, with

$$\hat{P}_i = \frac{(P_i)_{j-1/2}^* + (P_i)_{j+1/2}^*}{2} \quad \text{and} \quad \hat{V}_i = \frac{(V_i)_{j-1/2}^* + (V_i)_{j+1/2}^*}{2}. \tag{4.88}$$

Values noted by $(.)_{j+1/2}^*$ correspond to the exact solution of the linearised Riemann problem associated with the convective system (written related to $Y = {}^t(\alpha_1, s_1, U_1, P_1, s_2, U_2, P_2)$).

Once again, the following proposition holds:

Proposition 4.11. *Suppose that, for all cell $j \in \mathbb{Z}$, the approximated initial condition agrees with*

$$(U_1)_j^0 = (U_2)_j^0 = U_0 \quad \textit{and} \quad (P_1)_j^0 = (P_2)_j^0 = P_0.$$

Then, the approximation of the solution computed by the VFRoe-ncv scheme when using the variable $Y = {}^t(\alpha_1, s_1, U_1, P_1, s_2, U_2, P_2)$ (see section 4.3.1) agrees, at each time step $n \in \mathbb{N}$ and on each cell $j \in \mathbb{Z}$, with

$$(U_1)_j^n = (U_2)_j^n = U_0 \quad \textit{and} \quad (P_1)_j^n = (P_2)_j^n = P_0. \tag{4.89}$$

if the equation of state of both phases satisfy (4.80).

Proof. As above, a proof by recurrence is used. Of course, (4.89) is verified at the first time step $n = 0$. Now, let us assume that (4.89) holds at the n^{th} time step.
One can check that, if two neighbor cells j and $j+1$ comply with

$$\begin{aligned}(U_1)_j^n = (U_2)_j^n = (U_1)_{j+1}^n = (U_2)_{j+1}^n = U_0,\\ (P_1)_j^n = (P_2)_j^n = (P_1)_{j+1}^n = (P_2)_{j+1}^n = P_0,\end{aligned} \tag{4.90}$$

then the state $Y_{j+1/2}^*$ computed by the VFRoe-ncv scheme with $Y = {}^t(\alpha_1, s_1, U_1, P_1, s_2, U_2, P_2)$ also complies with

$$\begin{aligned}(U_1)_{j+1/2}^* = (U_2)_{j+1/2}^* = (V_i)_{j+1/2}^* = U_0,\\ (P_1)_{j+1/2}^* = (P_2)_{j+1/2}^* = (P_i)_{j+1/2}^* = P_0.\end{aligned} \tag{4.91}$$

Using (4.91) in equations (4.85), (4.86) and (4.88), one may deduce that $(U_k)_j^{n+1} = U_0$, for all $j \in \mathbb{Z}$, $k = 1, 2$. By the same way, noting that each equation of state verifies (4.80), we introduce (4.91) in energy equations (4.87). After, using mass conservation equations (4.85) and the equation on the void fraction (4.84), one may deduce that for all $j \in \mathbb{Z}$, $(P_k)_j^{n+1} = P_0$, $k = 1, 2$. This concludes the proof. □

Remark 4.5. The non conservative variable $Y = {}^t(\alpha_1, s_1, U_1, P_1, s_2, U_2, P_2)$ has been chosen here to define the VFRoe-ncv scheme. Thanks to this variable, equations (4.90) imply equations (4.91). If another variable had been chosen (such as ρ_k, $1/\rho_k$, ...) instead of s_k, the same property would have been fulfilled. In fact, within each phase, only the choice of the velocity U_k and the pressure P_k is important to verify (4.91). The third variable have only to be independent from U_k and P_k.

Propositions 4.10 and 4.11 emphasize that the Rusanov scheme and the VFRoe-ncv scheme are suitable to preserve above mentionned solutions. This requires however some adequate closure law between pressure and internal energy within each phase (4.80). This is in some sense the counterpart of the well known problem of the travelling contact discontinuity for Euler set of equations. The reader is refered to [BGH00], [GHS02a], [SA99b] for instance for such a discussion.

Bibliography

[AST02] European Project ASTAR, *Publication DM2S: "ASTAR: Delivrable D2" Contract FIKS–CT–2000–00050*, CEA Report SFME/LTMF/PU/02-039/A, unpublished, 2002.

[BCG+02] P. Bagnerini, F. Coquel, E. Godlewski, C. Marmignon, and S. Rouy. A void fraction relaxation principle for averaged two phase flow models. in preparation, 2002.

[BGH00] T. Buffard, T. Gallouët, and J.M. Hérard. A sequel to a rough Godunov scheme. Application to real gas flows. *Computers and Fluids*, 2000, vol. 29-7, pp. 813–847.

[BN86] M.R. Baer and J.W. Nunziato. A two phase mixture theory for the deflagration to detonation (DDT) transition in reactive granular materials. *Int. J. Multiphase Flow*, 1986, vol. 12-6, pp. 861–889.

[CEG+97] F. Coquel, K. El Amine, E. Godlewski, B. Perthame, and P. Rascle. A numerical method using upwind schemes for the resolution of two-phase flows. *J. Comp. Phys.*, 1997, vol. 136, pp. 272–288.

[CGHS02] F. Coquel, T. Gallouët, J.M. Hérard, and N. Seguin. Closure laws for a two-fluid two-pressure model. *C. R. Acad. Sci. Paris*, 2002, vol. I-334, pp. 927–932.

[CH99] L. Combe and J.M. Hérard. Finite volume algorithm to compute dense compressible gas-solid flows. *AIAA journal*, 1999, vol. 37, pp. 337–345.

[CL99] A. Chinnayya and A.Y. LeRoux, *A new general Riemann solver for the shallow-water equations with friction and topography*, 1999. Available in the conservation law preprint server http://www.math.ntnu.no/conservation/.

[CLL94] G.Q. Chen, C.D. Levermore, and T.P. Liu. Hyperbolic conservation laws with stiff relaxation terms and entropy. *Comm. Pure and Appl. Math.*, 1994, vol. 7, pp. 787–830.

[Col92] J.F. Colombeau, *Multiplication of distributions*, Springer Verlag, 1992.

[DeV94] F. DeVuyst, *Schémas non conservatifs et schémas cinétiques pour la simulation numérique d'écoulements hypersoniques non visqueux en déséquilibre thermochimique*, Ph.D. thesis, Université Paris VI, France, December 1994.

[DL88] F. Dubois and P.G. LeFloch. Boudary conditions for nonlinear hyperbolic systems of conservation laws. *J. Diff. Equations*, 1988, vol. 71, pp. 93–122.

[DLM95] G. Dal Maso, P.G. LeFloch, and F. Murat. Definition and weak stability of non conservative products. *J. Math. Pures Appl.*, 1995, vol. 74, pp. 483–548.

[Dub87] F. Dubois, *Boundary conditions and the Osher scheme for Euler equations of gas dynamics*, CMAP Report, 1987. In French.

[FHBT00] E. Faucher, J.M. Hérard, M. Barret, and C. Toulemonde. Computation of flashing flows in variable cross section ducts. *Int. J. of Comp. Fluid Dyn.*, 2000, vol. 13-3.

[GF96] S. Gavrilyuk and J. Fabre. Lagrangien coordinates for a drift flux model of a gas-liquid mixture. *Int. J. of Multiphase Flow*, 1996, vol. 22, pp. 453–460.

[GHS02a] T. Gallouët, J.M. Hérard, and N. Seguin. A hybrid scheme to compute contact discontinuities in one-dimensional euler systems. accepted for publication in M^2AN, 2002.

[GHS02b] T. Gallouët, J.M. Hérard, and N. Seguin. On the use of some symetrizing variables to deal with vacuum. submitted for publication, 2002.

[GHS03] T. Gallouët, J.M. Hérard, and N. Seguin. Some approximate godunov schemes to compute shallow-water equations with topography. *Computers and Fluids*, 2003, vol. 32-4, pp. 479–513.

[Gid93] D. Gidaspow, *Multiphase flow and fluidization*, Academic Press, 1993.

[GKL96] J.M. Ghidaglia, A. Kumbaro, and G. LeCoq. Une approche volume fini à flux caractéristiques pour la résolution numérique des systèmes hyperboliques de lois de conservation. *C. R. Acad. Sci. Paris*, 1996, vol. I-322, pp. 981–988.

[God59] S.K. Godunov. A difference method for numerical calculation of discontinuous equations of hydrodynamics. *Mat. Sb.*, 1959, pp. 271–300. In Russian.

[GP00] K. A. Gonthier and J. M. Powers. A high-resolution method for a two-phase model of deflagration-to-detonation transition. *J. Comp. Phys.*, 2000, vol. 163, pp. 376–433.

[GR96] E. Godlewski and P.A. Raviart, *Numerical approximation of hyperbolic systems of conservation laws*, Springer Verlag, 1996.

[GS02] S. Gavrilyuk and R. Saurel. Mathematical and numerical modelling of two phase compressible flows with inertia. *J. Comp. Phys.*, 2002, vol. 175-1, pp. 326–360.

[GSG96] A. Goldstein, M. Shapiro, and C. Gutfinger. Mechanics of collisional motion of granular materials. Part 3. self similar shock wave propagation. *Journal of Fluid Mechanics*, 1996, vol. 316, pp. 29–51. In Russian.

[GSS96] J. Glimm, D. Saltz, and D.H. Sharp. Renormalization group solution of two phase flow equations for Rayleigh-Taylor mixing. *Phys. Lett. A*, 1996, vol. 222, pp. 171–176.

[GSS99] J. Glimm, D. Saltz, and D.H. Sharp. Two phase flow modelling of a fluid mixing layer. *Journal of Fluid Mechanics*, 1999, vol. 378, pp. 119–143.

[Hal98] K. Halaoua, *Quelques solveurs pour les opérateurs de convection et leur application à la mécanique des fluides diphasiques*, Ph.D. thesis, École Normale Supérieure de Cachan, France, June 1998.

[HL94] X. Hou and P. G. LeFLoch. Why non conservative schemes converge to wrong solutions: error analysis. *Mathematics of computation*, 1994, vol. 62-206, pp. 497–530.

[HMS99] J.M. Hérard, P. Mogavéro, and O. Simonin. Computation of shock waves entering a dense granular material. *AIAA paper 99-3332*, 1999.

[Ish75] M. Ishii, *Thermo-fluid dynamic theory of two-phase flows*, Collection de la Direction des Etudes et Recherches d'Électicité de France, 1975.

[KSB+97] A.K. Kapila, S.F. Son, J.B. Bdzil, R. Menikoff, and D.S. Stewart. Two-phase modeling of DDT: Structure of the velocity-relaxation zone. *Phys. Fluids*, 1997, vol. 9-12.

[LeR98] A.Y. LeRoux, Discrétisation des termes sources raides dans les problèmes hyperboliques, In *Systèmes hyperboliques : nouveaux schémas et nouvelles applications*. Écoles CEA-EDF-INRIA "problèmes non linéaires appliqués", INRIA Rocquencourt (France), March 1998. Available on
http://www-gm3.univ-mrs.fr/∼leroux/publications/ay.le_roux.html, In French.

[Liu88] T.P. Liu. Hyperbolic conservation laws with relaxation. *Comm. Math. Phys.*, 1988, vol. 108, pp. 153–175.

[Ran87] V.H. Ransom, *Numerical benchmark tests, Multiphase Science and Technology*, Hemisphere publishing corporation, 1987, G.F. Hewitt, J.M. Delhaye & N. Zuber edition.

[RH84] V.H. Ransom and D.L. Hicks. Hyperbolic two-pressure models for two-phase flow. *J. Comp. Phys.*, 1984, vol. 53-1, pp. 124–151.

[Rov02] J.M. Rovarch, *in preparation*, Ph.D. thesis, École Normale Supérieure de Cachan, France, 2002.

[Rus61] V.V. Rusanov. Calculation of interaction of non-steady shock waves with obstacles. *J. Comp. Math. Phys. USSR*, 1961, vol. 1, pp. 267–279.

[SA99a] R. Saurel and R. Abgrall. A multiphase Godunov method for compressible multifluid and multiphase flows. *J. Comp. Phys.*, 1999, vol. 150, pp. 425–467.

[SA99b] R. Saurel and R. Abgrall. A simple method for compressible multifluid flows. *SIAM J. Sci. Comp.*, 1999, vol. 21-3, pp. 1115–1145.

[Sai95] L. Sainsaulieu. Finite volume approximations of two phase-fluid flows based on approximate Roe-type Riemann solver. *J. Comp. Phys.*, 1995, vol. 121, pp. 1–28.

[Sai96] L. Sainsaulieu. Traveling-wave solutions of convection-diffusion systems in nonconservative form. *SIAM J. Math. Anal.*, 1996, vol. 27-5, pp. 1286–1310.

[Sim95] O. Simonin. Modélisation numérique des écoulements turbulents diphasiques à inclusions dispersées. *École de printemps de mécanique des fluides numérique*, 1995.

[SL01] R. Saurel and O. LeMetayer. A multiphase model for compressible flows with interfaces, shocks, detonation waves and cavitation. *J. Fluid Mech.*, 2001, vol. 431, pp. 239–271.

[SM98] A.J. De Souza and D. Marchesin. Resonances for contact wave in systems of conservation laws. *Comp. Appl. Math.*, 1998, vol. 17-3, pp. 317–341.

[Smo83] J. Smoller, *Shock waves and reaction diffusion equations*, Springer Verlag, 1983.

[SV03] N. Seguin and J. Vovelle. Analysis and approximation of a scalar conservation law with a flux function with discontinuous coefficients. *M^3AS*, 2003, vol. 5-13.

[TKP99] I. Toumi, A. Kumbaro, and H. Paillère. Approximate Riemann solvers and flux vector splitting schemes for two-phase flow. *Von Karmann Institute Lecture Series 99*, 1999.

[Tou00] I. Toumi, *Contribution à la modélisation numérique des écoulements diphasiques eau-vapeur*, Thèse d'habilitation, Université Paris Sud, France, 2000.

Conclusion et perspectives

On a étudié au cours de cette thèse l'analyse et l'approximation des écoulements diphasiques eau-vapeur par des méthodes Volumes Finis. Le travail a été axé autour d'un modèle bifluide avec chaque phase compressible et ne supposant pas l'équilibre des pressions. Ce modèle est hyperbolique et non conservatif. On a pu voir que la structure de ce système est relativement simple, étant donné que, pour une condition initiale de type Riemann (c'est-à-dire deux états constants séparés par une interface), le couplage entre les deux fluides ne se fait qu'à travers l'onde évoluant à la vitesse interfaciale V_i. Plus précisément, la fraction volumique est constante de part et d'autre de cette onde et le système se réduit localement aux équations d'Euler pour chaque fluide. Indépendamment de cela, ce modèle nécessite de fournir des lois de fermetures pour la vitesse interfaciale et la pression interfaciale. On a proposé de définir la vitesse interfaciale de manière à obtenir un champ linéairement dégénéré associé à l'onde de vitesse V_i, ce qui implique que l'onde pour les fractions volumiques reste infiniment mince pour une condition initiale discontinue. Cette hypothèse permet d'obtenir trois formes distinctes pour la vitesse interfaciale. Pour définir la pression interfaciale, on adjoint au système un bilan d'entropie conservatif, ce qui permet non seulement de relier la pression interfaciale aux pressions de chaque phase et aux vitesses phasiques, mais surtout de fermer le système au sens des relations algébriques et au sens des relations de saut. Ainsi, le problème des relations de saut est localement résolu pour toutes les ondes. Une étude *a posteriori* de la paramétrisation de chaque onde assure que la solution du problème de Riemann est en accord avec le principe du maximum sur la fraction volumique et les principes de positivité de masses partielles et des énergies internes de chaque phase. Ce résultat est à associer à plusieurs propriétés de positivité pour les solutions régulières et est très important dans le contexte diphasique (voir l'annexe B pour une comparaison – partielle – avec d'autres modèles diphasiques issus de la littérature). Néanmoins, plusieurs problèmes demeurent. La difficulté majeure concernant l'analyse du système est qu'on ne peut pas paramétriser explicitement l'onde de vitesse V_i, c'est-à-dire que pour un état donné, on ne peut déterminer explicitement l'ensemble des états admissibles à travers cette onde. La résolution complète du problème de Riemann unidimensionnel semble alors impossible. De plus, ce système inclut le phénomène de résonnance, comme la loi de conservation étudiée au chapitre 2 et le système du chapitre 3. Il serait alors intéressant d'étudier précisément la superposition d'ondes grâce à l'approche décrite au chapitre 2, qui avait été initialement proposée par A.Y. LeRoux *et al.* [LeR98] pour le système du chapitre 3.

Par ailleurs, diverses perspectives concernant le modèle diphasique peuvent être proposées. Tout d'abord, une voie alternative de fermeture de la pression interfaciale a été décrite qu'il serait intéressant d'étudier plus en détail. De plus, il semble nécessaire d'envisager une extension de ce

modèle au cadre des écoulements turbulents, puisque ce type de phénomènes entre bien souvent en jeu dans les applications indutrielles diphasiques. L'extension ne pose pas de problème particulier lorsque l'on se focalise sur les modèles à une équation de transport d'énergie cinétique turbulente par phase. Cela signifie en fait qu'on peut étendre les fermetures de vitesse d'interface et de pression d'interface obtenues à ce cadre, en conservant la même structure d'ondes. Par contre, et cela est normal, on ne peut fermer totalement le problème des relations de saut (pour les champs vraiment non linéaires), celles-ci n'étant pas fermées dans le cadre monophasique.

Du point de vue de l'approximation numérique, la méthode Volumes Finis utilisée pour la simulation des écoulements diphasiques dans le chapitre 4 se base largement sur les études effectuées dans les chapitres 1 et 3 et dans l'annexe A. Le splitting d'opérateur utilisé pour séparer la partie convective homogène et les termes source a été comparé à une technique de décentrement proposée par A.Y. LeRoux *et al.* dans le chapitre 3. Deux schémas explicites ont été proposés pour l'approximation de la partie convective homogène du système bifluide. Le premier se base sur le schéma de Rusanov et le second est un schéma de Godunov approché appelé VFRoe-ncv. Ils ont tous deux été retenus pour leur bon comportement lors de la simulation des équations d'Euler en présence de zones à densité faible (voir les tests dans le chapitre 1 et l'annexe A). De plus, ils préservent les écoulements à vitesse et pression constantes aussi bien pour les équations d'Euler que pour le système du chapitre 4, pour des lois thermodynamiques simples (une modification du schéma VFRoe-ncv est proposé dans l'annexe C pour maintenir ces états dans le cadre Euler pour une large classe de lois thermodynamiques).

On rappelle que les termes de relaxation en vitesse et en pression ont été pris en compte en utilisant une technique de splitting d'opérateur qui, d'un point de vue numérique, n'est certes pas optimale mais qui s'avère très stable en général (voir les tests de comparaison du chapitre 3). On renvoie de plus au travail d'A. Forestier [For02] sur la pertinence de la forme lois de fermeture de la vitesse interfaciale et de la pression interfaciale. Comme cela a été évoqué dans la conclusion du chapitre 4, il serait utile d'étudier le système convectif avec relaxation en suivant le formalisme à T.P. Liu [Liu88] et à G.Q. Chen, D. Levermore et T.P. Liu [CLL94]. Cela permettrait en outre d'envisager l'utilisation des schémas de relaxation de S. Jin et Z.P. Xin [JX95].

La prise en compte des effets de diffusion dans le cadre de maillages triangulaires non structurés sera *a priori* effectuée en utilisant les schémas convergents issus de [EGH00], [EGH02] et [Her95]. L'utilisation de macro-éléments pourrait s'avérer utile dans le cadre tridimensionnel [Per01]. De plus, comme cela a été mis en avant dans le chapitre 1 et l'annexe C, la faible vitesse de convergence en maillage associée à la discontinuité de contact pour les équations d'Euler (ou de manière équivalente pour les systèmes HEM et HRM) introduit localement une erreur importante des schémas numériques pour l'approximation de cette onde. Pour rémédier à cela, une méthode de raffinement local de maillage est actuellement en cours de développement [Jul03].

Bibliographie

[CLL94] G.Q. Chen, C.D. Levermore, and T.P. Liu. Hyperbolic conservation laws with stiff relaxation terms and entropy. *Comm. Pure and Appl. Math.*, 1994, vol. 7, pp. 787–830.

[EGH00] R. Eymard, T. Gallouët, and R. Herbin, Finite Volume Methods, In *Handbook of Numerical Analysis* (Vol. VII), editors : P.G. Ciarlet and J.L. Lions, North-Holland, pp. 729–1020, 2000.

[EGH02] R. Eymard, T. Gallouët, and R. Herbin. Finite volume approximation of elliptic problems and convergence of an approximate gradient. *Appl. Num. Math.*, 2002, vol. 37-1-2, pp. 31–53.

[For02] A. Forestier. Pressure relaxation process for multiphase compressible flows. *preprint*, 2002.

[Her95] R. Herbin. An error estimate for a four point finite volume scheme for the convection-diffusion equation on a triangular mesh. *Numer. Meth. P.D.E.*, 1995, pp. 165–173.

[Jul03] N. Jullian, *in preparation*, Ph.D. thesis, Université de Provence, France, 2003.

[JX95] S. Jin and Z.P. Xin. The relaxation schemes for systems of conservation laws in arbitrary space dimensions. *Comm. Pure and Appl. Math.*, 1995, vol. 48-3, pp. 235–276.

[LeR98] A.Y. LeRoux, Discrétisation des termes sources raides dans les problèmes hyperboliques, In *Systèmes hyperboliques : nouveaux schémas et nouvelles applications*. Écoles CEA-EDF-INRIA "problèmes non linéaires appliqués", INRIA Rocquencourt (France), March 1998. Available on
http://www-gm3.univ-mrs.fr/∼leroux/publications/ay.le_roux.html, In French.

[Liu88] T.P. Liu. Hyperbolic conservation laws with relaxation. *Comm. Math. Phys.*, 1988, vol. 108, pp. 153–175.

[Per01] S. Perron, *Résolution numérique d'écoulements 3D avec une nouvelle méthode de Volumes Finis pour maillages non structurés*, Ph.D. thesis, Université de Chicoutimi, Québec, Canada, November 2001.

Annexe A

On the use of some symmetrizing variables to deal with vacuum

Ce travail a initialement fait l'objet d'une présentation orale au congrès intitulé « *15th AIAA CFD Conference* » qui a eu lieu à Anaheim, Californie, du 11 au 14 juin 2001, qui est référencée sous le numéro *AIAA 2001-2670*. Cette annexe correspond à une version longue qui est actuellement soumise à publication.

On the use of some symmetrizing variables to deal with vacuum

Thierry Gallouët[1] , Jean-Marc Hérard[1,2] , Nicolas Seguin[1]

[1] Université de Provence, Centre de Mathématiques et d'Informatique,
Laboratoire d'Analyse, Topologie et Probabilités - UMR CNRS 6632,
39 rue Joliot Curie, 13453 Marseille cedex 13, FRANCE
gallouet@cmi.univ-mrs.fr Tel: 04-91 11 35 42

[2] Électricité de France, Division Recherche et Développement,
Département Mécanique des Fluides et Transferts Thermiques,
6 quai Watier, 78401 Chatou cedex, FRANCE
herard@cmi.univ-mrs.fr - herard@chi80bk.der.edf.fr
seguin@chi80bk.der.edf.fr Tel: 1- 30 87 70 37

Abstract

The paper is devoted to the computation of shallow-water equations (or Euler equations) when using some approximate Godunov scheme called VFRoe, when the flow may include dry areas (or very low density regions). This is achieved with help of some symmetrizing variables. The whole enables to insure the discrete preservation of positive variables on interfaces, and meanwhile to compute vacuum occurence or propagation of shock waves over near-vacuum. A short section is also dedicated to the non conservative hyperbolic equations arising within the frame of one-equation or two-equation turbulent compressible models. Many numerical tests confirm the capabilities of the scheme, and measure of L^1 error norm in some particular cases enables to detail the actual rate of convergence.

Keywords: finite volume scheme, approximate Godunov scheme, Riemann problem, positive variables, symmetrizing variables.

An abridged version of the paper has been presented during the 15th AIAA CFD Conference (AIAA paper 2001-2670)

1 Introduction

The paper examines the suitability of some approximate Godunov schemes to deal with computation of either shallow water equations or Euler equations (including turbulence model or not) when vacuum occurs in the solution. This may happen in the latter frame when strong double rarefaction waves propagate, or when some shock wave expands over a dry area. In the former frame, it is well known that the use of the exact Godunov scheme [1], or other approximate Riemann solvers hardly provides satisfactory results when bluff bodies are present in the computational domain [2, 3, 4, 5, 6], or when computing flows in safety valves for instance. Thus, we propose herein an alternative *numerical* way to deal with vacuum in each case, based on the use of an approximate Godunov scheme combined with a particular choice of symetrizing variables. The method aims at providing suitable interface values of states, and we emphasize that it does not imply that cell values of states are physically admissible due to the averaging procedure, which is not a projection method (unlike when using the exact Godunov scheme).

Vacuum may of course occur rigorously when focusing on shallow water equations, since the water height may either become null when flow is leaving some area, which is usually connected with presence of variations in topography, or may be a relevant initial condition, for instance when simulating some dam breakdown. We emphasize that the suitability of the Euler equations to provide correct description of the flow including low density regions (or near vacuum) is not a silly assumption, and that it can hardly be replaced by simulation of Boltzmann equations, in many circomstances, unless the main part of the physics investigated is disregarded. Thus current problems should not be confused with those where the rarefied gas approach should be prefered (in that case, some schemes such as the DSMC method may of course be privileged, and the reader is referred to reviews pertaining to that field [7], [8]). The problem of the coupling of Euler equations with Boltzmann equations, which seems indeed a promising way for improvment of local prediction of flows, is also beyond the scope of the present work, and cannot be imposed in many industial situations, since vacuum only arises in some specific cases, at a certain time in the simulation, in the close vicinity of particular regions. The problem of the capability of current computer facilities to cope with any range of -high- Knudsen number must also be accounted for, and the accuracy of the model should not be confused with the accuracy of numerical methods involved in computations. We also eventually underline that the problem of vacuum becomes even more crucial when trying to compute some particular unsteady cases arising in the frame of two phase flows, especially when focusing on fluid flows in nuclear power plants. For instance, the problem of predicting flashing flows in safety valves (which may require to use Euler equations with complex EOS or alternatively the Homogeneous Relaxation Model) filled with pressurised water is a good challenge for people working in the numerical community, since both high density and low density regions are present in the field.

A first section is dedicated to the general presentation of the approximate Godunov scheme nicknamed VFRoe [9, 10, 11] when applying for non conservative variables. It requires solving a linearised Riemann problem at each interface in order to evaluate an approximate interface state; the numerical flux is then defined by computing the exact flux function for given approximate interface state. This formalism should not be confused with Godunov-type schemes, which have been introduced in [12] and require consistency with the integral form of the conservation law and consistency with the entropy inequality. A first version of the former scheme has been used to investigate a rather wide variety of industrial applications computing Euler equations with help of variable $(1/\rho, u, p)$. The main idea in this paper concerns the use of some symmetrizing variables to determine an approximate interface state by linearizing the symmetric form of the system. We

recall that the symmetrised form of first order set of PDE is as follows:

$$M(Y)\frac{\partial Y}{\partial t} + B(Y)\frac{\partial Y}{\partial x} = 0 \tag{1}$$

where Y is the symmetrizing variable, and $M(Y)$ (and $B(Y)$) respectively stands for some symmetric positive definite matrix (respectively symmetric matrix). We also recall that using the latter variables enables to prove theoretical existence of a linearisation in the sense of Roe [13], which is strongly linked with the existence of an entropy function for hyperbolic systems under conservative form. Nevertheless, they are seldomly used in numerical methods in practice except perhaps when building Petrov-Galerkine weak formulations using the Finite Element Method (see for instance [14]). We emphasize that the technique presented here is devoted to Finite Volume approximations, and the suitability of the choice of symetrizing variables will be discussed.

Afterwards, the framework of shallow water equations is briefly examined when restricting to symmetrizing variables [10] $(u, 2c)$. It will be shown that numerical vacuum appears at the interface exactly when real vacuum occurs in the continuous solution. The specific case [15, 16] where bottom slopes should be accounted for (which results in the fact that the whole system is no longer under conservative form) is discussed in detail in a companion paper [17]. The third section is devoted to the Euler equations with arbitrary equation of state, though practical numerical examples focus on perfect gas Equation of State (EOS). More emphasis is given on this section, and focus is given on variable (s, u, p). It will be seen that a condition -which is slightly more restrictive than the one dedicated to exact vacuum occurence- enables to insure positivity of interface values of density and pressure. A short section completes the paper by focusing on the convective part of a four equation model arising when computing compressible K-epsilon models. In this case too, numerical vacuum may occur in the solution at the interface before it occurs in the exact solution of the Riemann problem, but a scalar condition - which is not much constraining- enables to insure positive values of mean density, mean pressure and turbulent kinetic energy at the interface.

Actually, there is a great similarity in all "Euler-type" systems discussed herein. The three of them require that one scalar condition on initial data holds ((14) for Euler equations for instance), otherwise vacuum occurs in the exact solution. Considering then the problem of approximating solutions of the latter, it clearly appears that all approximate Riemann solvers usually involve intermediate states which :
(i) do not satisfy preservation of Riemann invariants through the contact discontinuity -if any-,
(ii) require that k_0 distinct scalar conditions should be fulfilled in order to insure that k_0 (expected) positive components are non-negative.
The proposed strategy aims at providing some remedy to that failure.

This approach also concerns workers in the field of statistical description of turbulence, using full Reynolds stress closures and Favre averaging process.

2 Basic principle of VFRoe schemes

We briefly recall herein the basis of VFRoe scheme with non conservative variables. We restrict for the sake of simplicity to regular meshes of size Δx such that: $\Delta x = x_{i+\frac{1}{2}} - x_{i-\frac{1}{2}}$, $i \in \mathbb{Z}$, and denote as usual Δt the time step, where $\Delta t = t^{n+1} - t^n$, $n \in \mathbb{N}$.
We define $W \in \mathbb{R}^p$ the exact solution of the non degenerated hyperbolic system:

$$\left\{ \begin{array}{l} \dfrac{\partial W}{\partial t} + \dfrac{\partial F(W)}{\partial x} = 0 \\ W(x,0) = W_0(x) \end{array} \right.$$

with $F(W)$ in $\mathbb{R}^p$. Let W_i^n be the approximate value of $\frac{1}{\Delta x}\int_{x_{i-\frac{1}{2}}}^{x_{i+\frac{1}{2}}} W(x,t^n)dx$. Integrating over $[x_{i-\frac{1}{2}};x_{i+\frac{1}{2}}]\times[t^n;t^{n+1}]$ provides:

$$W_i^{n+1} = W_i^n - \frac{\Delta t}{\Delta x}\left(\phi_{i+\frac{1}{2}}^n - \phi_{i-\frac{1}{2}}^n\right)$$

where $\phi_{i+\frac{1}{2}}^n$ stands for the numerical flux through the interface $\{x_{i+\frac{1}{2}}\}\times[t^n;t^{n+1}]$. The time step is in agreement with some CFL condition in order to gain stability. Thus $\phi_{i+\frac{1}{2}}^n$ only depends on W_i^n and W_{i+1}^n when restricting to first order schemes. Whatever the scheme is, the numerical flux complies with consistent condition (see [4]):

$$\phi(V,V) = F(V)$$

We present now approximate Godunov fluxes $\phi(W_L,W_R)$ associated with the 1D Riemann problem:

$$\left\{\begin{array}{l} \dfrac{\partial W}{\partial t} + \dfrac{\partial F(W)}{\partial x} = 0 \\ W(x,0) = \left\{\begin{array}{ll} W_L & \text{if } x<0 \\ W_R & \text{otherwise}\end{array}\right. \end{array}\right. \tag{2}$$

and initial condition: $W_L = W_i$ and $W_R = W_{i+1}$, $i\in\mathbb{Z}$.

VFRoe scheme is an approximate Godunov scheme where the approximate value at the interface between two cells is computed as detailed below. Let us consider some change of variable $Y = Y(W)$ in such a way that $W_{,Y}(Y)$ is invertible. The counterpart of above system for regular solutions is:

$$\frac{\partial Y}{\partial t} + B(Y)\frac{\partial Y}{\partial x} = 0$$

where $B(Y) = (W_{,Y}(Y))^{-1}A(W(Y))\,W_{,Y}(Y)$ ($A(W)$ stands for the Jacobian matrix of flux $F(W)$).

Now, the numerical flux $\phi(W_L,W_R)$ is obtained by solving the linearized hyperbolic system:

$$\left\{\begin{array}{l} \dfrac{\partial Y}{\partial t} + B(\tilde{Y})\dfrac{\partial Y}{\partial x} = 0 \\ Y(x,0) = \left\{\begin{array}{ll} Y_L = Y(W_L) & \text{if } x<0 \\ Y_R = Y(W_R) & \text{otherwise}\end{array}\right. \end{array}\right. \tag{3}$$

where $\tilde{Y}$ agrees with the condition: $\tilde{Y}(Y_L,Y_L) = Y_L$, and also $\tilde{Y}(Y_L,Y_R) = \tilde{Y}(Y_R,Y_L)$.

Once the exact solution $Y^*(\frac{x}{t};Y_L,Y_R)$ of this approximate problem is obtained, the numerical flux is defined as:

$$\phi(W_L,W_R) = F(W(Y^*(0;Y_L,Y_R)))$$

Let us set $\widetilde{l_k}$, $\widetilde{\lambda_k}$ and $\widetilde{r_k}$, $k=1,...,p$, left eigenvectors, eigenvalues and right eigenvectors of matrix $B(\overline{Y})$ respectively. The solution $Y^*(\frac{x}{t};Y_L,Y_R)$ of the linear Riemann problem is defined everywhere (except along $\frac{x}{t}=\widetilde{\lambda_k}$):

$$\begin{aligned} Y^*\left(\frac{x}{t};Y_L,Y_R\right) &= Y_L + \sum_{\frac{x}{t}>\widetilde{\lambda_k}} ({}^t\widetilde{l_k}.(Y_R-Y_L))\widetilde{r_k} \\ &= Y_R - \sum_{\frac{x}{t}<\widetilde{\lambda_k}} ({}^t\widetilde{l_k}.(Y_R-Y_L))\widetilde{r_k} \end{aligned}$$

Combining the last equalities enables to write the latter in a slightly different form:

$$Y_R - Y_L = \sum_{k=1,p} ({}^t\widetilde{l_k}.(Y_R - Y_L))\widetilde{r_k} = \sum_{k=1,p} \tilde{\alpha}_k \widetilde{r_k} \tag{4}$$

setting: $\tilde{\alpha}_k = {}^t\widetilde{l_k}.(Y_R - Y_L)$.

Before going on, we recall that the Basic VFRoe scheme was first proposed in [18], and was based on the choice $Y(W) = W$ and thus $B(\overline{Y}) = A(\overline{W})$. (we recall that $A(W)$ is the Jacobian matrix of $F(W)$, and we note throughout the paper: $\overline{\phi}_{LR} = (\phi_L + \phi_R)/2$ whatever ϕ is). Other choices for Euler equations have already been examined [9],[19].

Hence, the explicit form of the Finite Volume method called VFRoe will be:

$$W_i^{n+1} - W_i^n + \frac{\Delta t}{\Delta x}\left(F(W(Y^*(0; Y_i^n, Y_{i+1}^n))) - F(W(Y^*(0; Y_{i-1}^n, Y_i^n)))\right) = 0$$

Despite from its name, it is emphasised that VFRoe scheme should not be confused with the approximate riemann solver proposed by P.L. Roe. We now examine specific schemes obtained when dealing with symmetrizing variables.

3 Shallow-water equations

3.1 Governing equations

In a one dimensional framework, shallow-water equations may be written in conservative form, using conservative variable $W = {}^t(h, hu)$, noting h the water height, u and $Q = hu$ the velocity and the momentum (or discharge) respectively, and g the gravity constant:

$$h_{,t} + (hu)_{,x} = 0 \tag{5a}$$

$$(hu)_{,t} + \left(hu^2 + g\frac{h^2}{2}\right)_{,x} = 0 \tag{5b}$$

Vacuum will occur when both momentum and water height vanish: $h = hu = 0$. Note that in this case u is undefined. Otherwise the solution of the associated Riemann problem is composed of three distinct states separated by two Genuinely Non Linear fields. The speed of the two waves are $u - c$ and $u + c$ respectively, noting as usual $c = \sqrt{gh}$. The intermediate state is indexed by subscript 1. Noting $h_1 = \frac{(c_1)^2}{g}$, and $Q_1 = h_1 u_1$, the standard solution of the 1D Riemann problem consists in three distinct states with subscripts L, 1 and R separated by rarefaction waves or shock waves as recalled by the following figure 1.

The one dimensional Riemann problem has a unique entropy consistent solution with no vacuum occurence provided that initial data satisfies the following condition:

$$u_R - u_L < 2(\sqrt{gh_R} + \sqrt{gh_L}) \tag{6}$$

3.2 Symmetrizing variables

This system may be written in terms of non conservative variable $Y(W) = {}^t(2c, u)$ in a symmetrized form setting in (1):

$$B(Y) = \begin{pmatrix} u & c \\ c & u \end{pmatrix} \quad \text{and} \quad M(Y) = \begin{pmatrix} 1 & 0 \\ 0 & 1 \end{pmatrix}$$

Matrix $B(Y)$ is clearly symmetric and $M(Y)$ is the identity matrix which of course is symmetric positive definite.

3.3 Approximate Godunov scheme VFRoe using symmetrizing variable

We turn now to the associated linearised problem, and set for any quantity ψ: $(\Delta\psi)_{LR} = \psi_R - \psi_L$. The computation of the intermediate state in the linearised solver at each interface between two cells labelled L, R is straightforward (we set here: $\hat{Y} = \overline{Y}$):

$$u_1 = \overline{u}_{LR} - (\Delta c)_{LR} \quad \text{and} \quad c_1 = \overline{c}_{LR} - \frac{(\Delta u)_{LR}}{4}$$

Note that the linearization has been made around the state $(2\overline{c},\overline{u})$. The numerical flux thus writes:

$$Q_1 = \frac{(c_1)^2 U_1}{g} \quad \text{and} \quad \left(hU^2 + g\frac{h^2}{2}\right)_1 = (c_1)^2 \frac{2(U_1)^2 + (c_1)^2}{2g}$$

3.4 Some properties

Property 1: Vacuum arises in the intermediate state of linearized Godunov solver if and only if initial data makes vacuum occur in the exact solution of the Riemann problem associated with the non linear set of equations:

$$u_R - u_L < 2(c_L + c_R) \tag{7}$$

Proof: Actually, when focusing on the solution of the exact Riemann problem, vacuum may only occur when initial data is such that two rarefaction waves develop. Riemann invariants are preserved in that case, hence $u + 2c$ (respectively $u - 2c$) is constant in the 1-rarefaction wave (respectively the 2-rarefaction wave) ; if subscript 1 refers to the intermediate state in the *exact* solution of the Riemann problem, then:

$$u_R - 2c_R = u_1 - 2c_1$$
$$u_L + 2c_L = u_1 + 2c_1$$

where subscripts L and R refer to values of initial data in the Riemann problem. Using some algebra enables to rewrite the latter as:

$$u_1 = \frac{u_R + u_L}{2} - (\Delta c)_{LR} \quad \text{and} \quad c_1 = \frac{c_L + c_R}{2} - \frac{(\Delta u)_{LR}}{4}.$$

One may here check that physically releavant states (with positive values of c_1) imply that the former condition (6) is fulfilled. More over, it can be easily seen that this couple (u_1, c_1) exactly represents the intermediate state provided by the linearised approximate Godunov scheme we

focus on. This completes the proof of property 1. Thus, the present linearized solver is well suited to handle double rarefaction waves in the solution of the exact Riemann problem, at least when predicting interface values. Due to the averaging procedure, it doesn't mean anyway that cell values of water height remain positive, since the first order scheme does not construct the projection of the approximate solution. Appendix $7a$ however shows that close to a wall boundary, the cell value of water height remains positive when a very strong rarefaction wave develops (eg when $U.n \leq 0$, where n denotes the unit outward normal vector at the wall boundary), assuming standard CFL condition $CFL = 0.5$.

3.5 Numerical results

The computational results described below correspond to a Riemann problem with the following initial data:

$$h_L = h_R = 10 \quad \text{and} \quad u_L = -u_R = -15.$$

Constant g is set to 2. The CFL number is 0.49, and the regular mesh contains 5000 nodes. Figures 2 show the approximation of water height, discharge and local velocity which have been obtained using the basic first order scheme.

Recall that the basic advantage of the symmetrical case is that it provides some good idea of the behaviour of the scheme close to wall boundary conditions when applying for the mirror technique. Though the scheme is stable, we note anyway that approximate values of velocity in the near vacuum zone (eg the end of the 1-rarefaction wave or the beginning of the 2-rarefaction wave) are poorly accurate.

We give below on figures 3 some measure of the L^1 norm of the error, which is plotted for two cases including the shock tube case and symmetrical double rarefaction wave discussed above, and includes comparison with results obtained using the basic Godunov scheme [1]. The measured rate of convergence is close to 0.85 in both cases, which is slightly smaller than expected 1, but is in agreement with measurements provided in [9] in the frame work of Euler equations when focusing on perfect gas EOS.

The present solver has also been used successfully when computing shallow-water equations with topography [17]. The main problem in that case is that one needs in addition to account for so-called source terms associated with mean gradient of bottom elevation. This means in particular that one has to provide some discrete approximation in such a way that steady states are perfectly preserved on any mesh size. The method relies on the so-called well-balanced scheme, as first introduced by A. Y. Leroux and co authors [15], [16] previously, and takes advantage of the potentialities of the present approximate Godunov scheme. We only provide below some results associated with a rather difficult test case, which consists in emptying a reservoir containing some bump under the initial free surface, and initially at rest. The left boundary condition corresponds to some wall condition, and the right boundary condition enables to empty the computational domain. The regular mesh contains 1000 nodes, and the discretised bump profile contains 200 cells. The CFL number here was set to 0.45. The initial condition is: $h(x, t = 0) = 0.5$, and $Q(x, t = 0) = 0$. The flow around the steady state is such that no water passes over the bump.

4 Euler equations

4.1 Governing equations

Governing Euler equations may first be written in conservative form in terms of the mean density ρ, the mean pressure p, the mean velocity u and the total energy E as follows:

$$\frac{\partial W}{\partial t} + \frac{\partial F(W)}{\partial x} = 0 \tag{8}$$

setting:

$$W = \begin{pmatrix} \rho \\ \rho u \\ E \end{pmatrix} \quad \text{and} \quad F(W) = \begin{pmatrix} \rho u \\ \rho u^2 + p \\ u(E+p) \end{pmatrix}$$

where $E = \rho(\frac{1}{2}u^2 + \varepsilon)$. If ε denotes the internal energy, then some law is required to close the whole system:

$$p = p(\rho, \varepsilon) \tag{9}$$

such that the Jacobian matrix may be diagonalized in $\mathbb{R}$ for $W \in \Omega$, Ω the set of admissible states, so that $\hat{\gamma}(p,\rho)p > 0$, $\rho > 0$, where:

$$\rho c^2(p,\rho) = \hat{\gamma}(p,\rho)p = \left(\frac{\partial \varepsilon}{\partial p}_{|\rho}\right)^{-1} \left(\frac{p}{\rho} - \rho \frac{\partial \varepsilon}{\partial \rho}_{|p}\right)$$

We also need to introduce entropy $s = s(p,\rho)$ which must comply with:

$$\hat{\gamma} p \frac{\partial s}{\partial p}_{|\rho} + \rho \frac{\partial s}{\partial \rho}_{|p} = 0 \tag{10}$$

Herein, c stands for the speed of density waves.
The Jacobian matrix $A(W) = \dfrac{\partial F(W)}{\partial W}$ may be written:

$$A(W) = \begin{pmatrix} 0 & 1 & 0 \\ K - u^2 & u(2-k) & k \\ (K-H)u & H - ku^2 & u(1+k) \end{pmatrix}$$

setting $H = \frac{E+p}{\rho}$, $k = \frac{1}{\rho}\dfrac{\partial p}{\partial \varepsilon}_{|\rho}$, $K = c^2 + k(u^2 - H)$. Eigenvalues of the Jacobian matrix $A(W)$ read:

$$\lambda_1 = u - c,\ \lambda_2 = u,\ \lambda_3 = u + c$$

Recall that the 1-wave and the 3-wave are Genuinely Non Linear fields and that the 2-wave is Linearly Degenerated [20]. A sketch of the solution of the 1D Riemann problem is recalled below (see figure 5, which consists in four states labeled L, 1, 2 and R separated by rarefaction waves, shocks and contact discontinuity, depending on the initial condition. In an alternative way, Euler equations may be written in a non conservative form, when restricting to smooth solutions.

4.2 Symmetrizing variables

Another way to rewrite Euler equations is to use symmetrizing variables:

$$Y(W) = {}^t(s, u, p)$$

defining matrices $B(Y)$ and $M(Y)$:

$$B(Y) = \begin{pmatrix} u & 0 & 0 \\ 0 & u\hat{\gamma}p\rho & \hat{\gamma}p \\ 0 & \hat{\gamma}p & u \end{pmatrix} \quad \text{and} \quad M(Y) = \begin{pmatrix} 1 & 0 & 0 \\ 0 & \hat{\gamma}p\rho & 0 \\ 0 & 0 & 1 \end{pmatrix}.$$

Obviously $B(Y)$ is symmetric and $M(Y)$ is symmetric positive definite, provided both density and pressure remain positive. Right eigenvectors of $(M)^{-1}(Y)B(Y)$ are:

$$r_1(Y) = \begin{pmatrix} 0 \\ \frac{1}{\rho} \\ -c \end{pmatrix}, \; r_2(Y) = \begin{pmatrix} 1 \\ 0 \\ 0 \end{pmatrix}, \; r_3(Y) = \begin{pmatrix} 0 \\ \frac{1}{\rho} \\ c \end{pmatrix}.$$

4.3 Approximate Godunov scheme VFRoe using symmetrizing variable

Turning now to the linearised problem, it may be easily checked that eigenvalues of $(M)^{-1}(\overline{Y})B(\overline{Y})$ are: $\tilde{\lambda}_1 = \overline{u} - \tilde{c}$, $\tilde{\lambda}_2 = \overline{u}$, $\tilde{\lambda}_3 = \overline{u} + \tilde{c}$, setting ; $\overline{p}(\tilde{c})^2 = \overline{\gamma p}$. The decomposition of $Y_R - Y_L$ on the basis of right eigenvectors of $(M)^{-1}(\overline{Y})B(\overline{Y})$ provides intermediate states occuring in the linearised Riemann problem. While setting for any quantity ψ: $(\Delta\psi)_{LR} = \psi_R - \psi_L$, where subscripts L, R refer to the left and right side of the initial discontinuity, coefficients $\tilde{\alpha}_1$ and $\tilde{\alpha}_3$ as introduced in the previous section are now:

$$\tilde{\alpha}_1 = \frac{1}{2\tilde{c}}(\overline{\rho}\tilde{c}(\Delta u)_{LR} - (\Delta p)_{LR}) \quad \text{and} \quad \tilde{\alpha}_3 = \frac{1}{2\tilde{c}}(\overline{\rho}\tilde{c}(\Delta u)_{LR} + (\Delta p)_{LR}).$$

The linearization has been made around the state ($\overline{\rho}$,$\overline{u}$,$\overline{p}$). Hence, the two intermediate states Y_1, Y_2 occuring in the solution of the *linearised* Riemann problem are the following:

$$Y_1 = \begin{pmatrix} s_L \\ u_L + \tilde{\alpha}_1 \frac{1}{\overline{\rho}} \\ p_L - \tilde{\alpha}_1 \tilde{c} \end{pmatrix} \quad \text{and} \quad Y_2 = \begin{pmatrix} s_R \\ u_R - \tilde{\alpha}_3 \frac{1}{\overline{\rho}} \\ p_R - \tilde{\alpha}_3 \tilde{c} \end{pmatrix}.$$

$$u_2 = u_1 = \overline{u} - \frac{1}{2\overline{\rho}\tilde{c}}(\Delta p)_{LR} \tag{11}$$

$$p_2 = p_1 = \overline{p} - \frac{\overline{\rho}\tilde{c}}{2}(\Delta u)_{LR} \tag{12}$$

Values $u_1 = u_2$ and $p_1 = p_2$ identify with intermediate values computed by any VFRoe scheme with variable $Y = {}^t(., u, p)$ (see [9] when focusing on $Y = {}^t(1/\rho, u, p)$). Intermediate values $s_1 = s_L$ and $s_2 = s_R$ are obviously physically releavant. The intermediate pressure (together with velocity and density) is set to its minimal value if p_1 is below the admissible range. This minimum is 0 for perfect gas EOS (or a mixture of perfect gases), or alternatively $-p_\infty$ for Tamman EOS ($\varepsilon = \frac{p+\gamma p_\infty}{(\gamma-1)\rho}$). This should not be confused with the standard clipping approximation which violates (with respect to time) the conservative form of discrete equations.

4.4 Some properties

Property 2: a- Intermediate value of pressure $p_1 = p_2$ remains positive provided that the initial conditions of the Riemann problem agree with condition:

$$(\Delta u)_{LR} < \frac{2\overline{p}}{\overline{\rho}\widetilde{c}} \tag{13}$$

b- Intermediate values of density ρ_1 and ρ_2 remain positive provided the latter condition is insured.

Proof: a- The proof is obvious since p_1 in (12) is positive if and only if (13) holds.
b- Intermediate states of density agree with:

$$\rho_1 = \rho(s_1, p_1) = \rho(s_L, p_1) \quad \text{and} \quad \rho_2 = \rho(s_2, p_2) = \rho(s_R, p_2)$$

Thus, the admissibility of $p_1 = p_2$ insures the admissibility of both ρ_1 and ρ_2.

This condition should be compared with the condition of existence and uniqueness of the solution of the Riemann problem for Euler equations with any EOS (and no vacuum occurence) which is [20],[5]:

$$(\Delta u)_{LR} < X_L + X_R \quad \text{where} \quad X_i = \int_0^{\rho_i} \frac{c(\rho, s_i)}{\rho} d\rho. \tag{14}$$

We here first restrict to perfect gas EOS ($p = (\gamma - 1)\rho\epsilon$, $1 < \gamma < 3$). Focusing on initial condition such that a double symmetrical rarefaction wave develops (that is : $Y_L =^t (s, u, p)$ and $Y_R =^t (s, -u, p)$ with $u < 0$), the condition (13) is more restrictive than its counterpart (14), unlike when dealing with shallow water equations. More precisely, numerical vacuum (in terms of pressure) occurs at the interface using VFRoe scheme as soon as $u/c > 1/\gamma$, whereas numerical vacuum (in terms of pressure or density) occurs at the interface with Roe scheme [3] as soon as $u^2/c^2 > 2/(\gamma(3-\gamma))$ and vacuum really arises when $u/c > 2/(\gamma - 1)$. Nonetheless, when plotting the ratio $p_{interface}/p$ as a function of $|u|/c$, it clearly appears that both curves associated with Godunov scheme and VFRoe scheme are monotone decreasing, whereas the one connected with Roe scheme is decreasing for $0 < |u|/c < 1/2$ and then increasing. Thus, though the constraint provided by Roe scheme to obtain releavant interface values of pressure and density is less restrictive than the one given by VFRoe scheme, the general behaviour of $p_{interface}/p$ vs $|u|/c$ is in better agreement with the exact Riemann solution [9] when applying VFRoe scheme. As a result, computations of safety valves with supersonic behaviour around the exit may blow up when using Roe scheme at the wall boundary instead of Godunov scheme (or VFRoe scheme), using the mirror technique in all cases. Anyway, even when condition (13) is fulfilled, there is no theoritical proof that cell values of pressure p_i^n remain positive, when using the VFRoe scheme (or the Roe scheme). Nonetheless, appendix 7*b* shows the important fact that close to a wall boundary (where near-vacuum almost always appears in practice), the cell value of pressure will remain positive when a very strong rarefaction wave develops (that is to say when $U.n \leq 0$, where n denotes the unit outward normal vector at the boundary), assuming standard CFL condition $CFL = 0.5$.

If we turn now to Tamman's EOS: $\varepsilon = \frac{p+\gamma p_\infty}{(\gamma-1)\rho}$ (and thus $s = (p + p_\infty)(\rho)^{-\gamma}$) , we emphasize that equation (12) may be read as $p_2 + p_\infty = p_1 + p_\infty = \overline{p + p_\infty} - \frac{\overline{\rho}\widetilde{c}}{2}(\Delta u)_{LR}$. Hence vacuum patterns (which turns to be $p + p_\infty = 0$ when focusing on this EOS) are similar than in the perfect gas framework. Results on discussion above thus hold true.

The scheme also benefits from the following properties, shared by all VFRoe schemes using variable $Y = {}^t(., u, p)$:

Property 3: Approximate values of intermediate states occuring in the linearized Riemann problem preserve invariance of (u, p) variables through the numerical contact discontinuity.

The proof is trivial since inserting $u_L = u_R$ together with $p_L = p_R$ in equations $(11 - 12)$ results in: $u_1 = u_2 = u_L = u_R$ and also $p_1 = p_2 = p_L = p_R$.

Property 4: Assuming the state law takes the form:

$$\rho\varepsilon = f(p) + a\rho + b$$

where a and b are real constants, then cell values apart from a moving contact discontinuity preserve invariance of both velocity and pressure variables.

The proof may be found in appendix 8. Note that the latter family of internal energies includes not only perfect gas EOS, but also Tamman EOS and Tait EOS ($\varepsilon = \frac{p}{(\gamma-1)\rho} + A(\frac{1}{\rho} - \frac{1}{(\rho)_0})$). The reader is also referred to recent work by Saurel and Abgrall [21] for an alternative way to handle contact discontinuity when restricting to stiffened gas EOS, or to [22], [23] for more complex EOS.

4.5 Numerical results

A perfect gas state law has been used together with: $\gamma = \frac{7}{5}$. We first provide some results obtained using initial data in shock tube experiments, which generate vacuum. Hence, we use:

	ρ	p	u
Left	1	10^5	-4000
Right	1	10^5	4000

This results in a rather wide zone of vacuum. Actually, the limit Mach number in a symmetrical double rarefaction wave is $\frac{2}{\gamma-1}$ (which is thus equal to 5 here), whereas in the present case, the initial Mach number is approximately 11.7. The computational results were obtained using the following CFL number: $CFL = 0.45$, and a fine regular mesh with 12800 nodes (figures 6) respectively. Velocity profiles have been plotted though they are *meaningless* in the vacuum area. It must be emphasized that no clipping approximation is used here. Minimum values of density or pressure in the vacuum area are approximately 10^{-14} and 10^{-11} respectively.

The second series of results (figures 7) corresponds to the computation of a strong shock wave propagating over (near) vacuum. In this case, the initial data of the Riemann problem reads:

	ρ	p	u
Left	1	10^5	0
Right	$1,25.10^{-7}$	10^{-2}	0

The sonic point in the 1-rarefaction wave requires introducing an entropy correction. The CFL number is the same as in previous cases. The mesh contains 3200 nodes here. These initial conditions typically result in a blow up of the code when using standard variable $Y = {}^t(\tau, u, p)$ (where $\tau = \frac{1}{\rho}$) as usually done [9] instead of the current symmetrizing variable.

The last series of results (figures 8) corresponds to the computation of a strong double shock wave, which shows again how the scheme behaves when computing impinging jets on wall boundaries. In this case, the initial data of the Riemann problem reads:

	ρ	p	u
Left	1	10^5	100
Right	1	10^5	-100

The regular mesh still contains 3200 nodes.

To conclude this part, we again provide below the true rate of convergence obtained when computing the standard Sod shock tube case, a double rarefaction wave and eventually a double shock wave, using first order (respectively second order) version of the scheme. We recall initial condition , which respectively are:

	ρ_L	ρ_R	p_L	p_R	u_L	u_R
Sod shock tube	1	0.125	10^5	10^4	0	0
Double rarefaction wave	1	1	10^5	10^5	-1200	1200
Double shock wave	1	1	10^5	10^5	300	-300

The second-order scheme is based on second-order Runge-Kutta time integration combined with standard MUSCL-type reconstruction of variables ρ, u, p inside each cell. Plotting of L^1 error corresponds to density -squares-, velocity -triangles- and pressure -circles-. Straight lines correspond to the first-order scheme, and the dashed line refers to the second-order scheme. Results (see figures 9) are indeed very close to those provided in a previous work [9] when using variable $Y = {}^t(\tau, u, p)$, where $\tau = \frac{1}{\rho}$. An important point to emphasize is that the mean density converges slower than both pressure and velocity variables, unless the case is symmetric (figures 9 right top and bottom). This is due to the smearing of the contact discontinuity associated with eigen value $\lambda = u$, through which the density varies, whereas both pressure and velocity do not -or at least should not, since the latter are Riemann invariants through this wave-. The rate is close to 1 when restricting to u, P, when using the so-called second-order scheme, and is a bit lower for the density, especially when focusing on the Sod shock tube problem.

5 The K model

5.1 Governing equations

Governing equations of the convective part of the K model may only be written in non conservative form. These usually appear written in terms of the mean density ρ, the mean momentum ρu, the mean total energy E and the turbulent kinetic energy K as follows, when focusing on perfect gas EOS:

$$\frac{\partial W}{\partial t} + \frac{\partial F(W)}{\partial x} + C(W)\frac{\partial W}{\partial x} = 0$$

setting:

$$W = \begin{pmatrix} \rho \\ \rho u \\ E \\ K \end{pmatrix} \quad \text{and} \quad F(W) = \begin{pmatrix} \rho u \\ \rho u^2 + p + 2\frac{K}{3} \\ u(E + p + 2\frac{K}{3}) \\ uK \end{pmatrix}$$

with $C(W)\frac{\partial W}{\partial x} = {}^t\left(0,0,0,2\frac{K}{3}\frac{\partial u}{\partial x}\right)$, and noting $E = \rho\frac{1}{2}u^2 + \rho\varepsilon + K$. Herein, ε denotes the mean internal energy. The EOS for turbulent perfect gases is:

$$p = p(\rho,\varepsilon) = (\gamma-1)\rho\varepsilon$$

The speed of mean density waves is modified by the presence of turbulence:

$$c^2(p,\rho,K) = \gamma\frac{p}{\rho} + 10\frac{K}{9\rho}$$

Introducing :

$$\mu = \frac{K}{(\rho)^{\frac{5}{3}}} \quad \text{and} \quad s = \frac{p}{(\rho)^{\gamma}}.$$

it is an easy matter to check that this system is a non strictly hyperbolic system. Real eigenvalues are:

$$\lambda_1 = u - c,\ \lambda_2 = \lambda_3 = u,\ \lambda_4 = u + c.$$

and associated right eigenvectors span IR^4. Both the 1-wave and the 4-wave are Genuinely Non Linear, whereas the 3-4-wave is Linearly Degenerated. Riemann invariants through the contact discontinuity are $\pi = p + 2K/3$ and u. Riemann invariants through the 1-wave are: $s = p\rho^{-\gamma}$, $\mu = K\rho^{-5/3}$,$u + Z$, and s, μ,$u - Z$ through the 4-wave, while setting:

$$Z_i = \int_0^{\rho_i} \frac{c(\rho, s_i, \mu_i)}{\rho} d\rho$$

Moreover, assuming that the following jump conditions hold through shocks (σ denotes the speed of the discontinuity separating states with subscripts L and R):

$$\begin{gathered}
-\sigma[\rho]_{LR} + [\rho u]_{LR} = 0 \\
-\sigma[\rho u]_{LR} + [\rho u^2 + p + \tfrac{2K}{3}]_{LR} = 0 \\
-\sigma[E]_{LR} + [u(E + p + \tfrac{2K}{3})]_{LR} = 0 \\
-\sigma[K]_{LR} + [uK]_{LR} + \tfrac{2\overline{K}_{LR}}{3}[u]_{LR} = 0
\end{gathered}$$

we recall [24] that the 1-dimensional Riemann problem associated with the latter problem and given initial data admits a unique solution with no vacuum occurence provided that the following condition holds:

$$u_R - u_L < Z_L + Z_R \tag{15}$$

5.2 Symmetrizing variables

Another way to write the latter equations is to use some symmetrisation variables. We focus here on $Y(W) = {}^t(u,\pi,\mu,s)$. Thus comes:

$$M(Y)\frac{\partial Y}{\partial t} + B(Y)\frac{\partial Y}{\partial x} = 0$$

with:

$$B(Y) = \begin{pmatrix} \rho^2 c^2 u & \rho c^2 & 0 & 0 \\ \rho c^2 & u & 0 & 0 \\ 0 & 0 & u & 0 \\ 0 & 0 & 0 & u \end{pmatrix} \quad \text{and} \quad M(Y) = \begin{pmatrix} \rho^2 c^2 & 0 & 0 & 0 \\ 0 & 1 & 0 & 0 \\ 0 & 0 & 1 & 0 \\ 0 & 0 & 0 & 1 \end{pmatrix},$$

$B(Y)$ is symmetric and $M(Y)$ is symmetric positive definite, provided that mean density, mean turbulent kinetic energy and mean pressure remain positive. Right eigenvectors of $(M)^{-1}(Y)B(Y)$ are:

$$r_1(Y) = \begin{pmatrix} \frac{1}{\rho} \\ -c \\ 0 \\ 0 \end{pmatrix}, r_2(Y) = \begin{pmatrix} 0 \\ 0 \\ 1 \\ 0 \end{pmatrix}, r_3(Y) = \begin{pmatrix} 0 \\ 0 \\ 0 \\ 1 \end{pmatrix}, r_4(Y) = \begin{pmatrix} \frac{1}{\rho} \\ c \\ 0 \\ 0 \end{pmatrix}.$$

5.3 Approximate Godunov scheme VFRoe using symmetrizing variable

We only provide here the main ingredients to construct the scheme.

$$\tilde{\alpha}_1 = \frac{1}{2\widetilde{c}}(\overline{\rho}\widetilde{c}(\Delta u)_{LR} - (\Delta\pi)_{LR}) \quad \text{and} \quad \tilde{\alpha}_4 = \frac{1}{2\widetilde{c}}(\overline{\rho}\widetilde{c}(\Delta u)_{LR} + (\Delta\pi)_{LR}).$$

The linearization is made around the state $(\overline{\rho}, \overline{u}, \overline{p}, \overline{K})$. Hence, the two intermediate states Y_1, Y_2 occuring in the solution of the *linearised* Riemann problem are the following:

$$Y_1 = \begin{pmatrix} u_L + \tilde{\alpha}_1 \frac{1}{\overline{\rho}} \\ \pi_L - \tilde{\alpha}_1 \widetilde{c} \\ \mu_L \\ s_L \end{pmatrix} \quad \text{and} \quad Y_2 = \begin{pmatrix} u_R - \tilde{\alpha}_4 \frac{1}{\overline{\rho}} \\ \pi_R - \tilde{\alpha}_4 \widetilde{c} \\ \mu_R \\ s_R \end{pmatrix}.$$

$$u_2 = u_1 = \overline{u} - \frac{1}{2\overline{\rho}\widetilde{c}}(\Delta\pi)_{LR} \tag{16}$$

$$\pi_2 = \pi_1 = \overline{\pi} - \frac{\overline{\rho}\widetilde{c}}{2}(\Delta u)_{LR} \tag{17}$$

5.4 Some properties

The Godunov scheme would naturally insure that K_1, K_2, ρ_1, ρ_2 and also $\pi_1 = \pi_2$ remain positive, assuming the scalar condition (15) holds true. Now we note that :

Property 5: a- Intermediate value of total pressure $\pi_1 = \pi_2$ remains positive provided that the initial conditions of the Riemann problem agree with:

$$(\Delta u)_{LR} < \frac{2\overline{\pi}}{\overline{\rho}\widetilde{c}} \tag{18}$$

b- Intermediate values of density ρ_1, K_1, p_1 and ρ_2, K_2, p_2 remain positive provided the latter condition is insured.

Proof: a- This clearly follows from equation (17).
b- Introducing $K_1 = \mu_L \rho_1^{5/3}$ and $p_1 = s_L \rho_1^{\gamma}$ in equation $\pi_1 > 0$ (due to condition (18)) enables to check that positive solution of $g(\rho_1) := \frac{2}{3}\mu_L \rho_1^{5/3} + s_L \rho_1^{\gamma} - \pi_1 = 0$ exists and is unique, since g is a monotone increasing function from $[0, \infty]$ to $[-\pi_1, +\infty]$. Hence follows positivity of K_1, p_1. A similar result holds for ρ_2, K_2, p_2 on the other side of the contact discontinuity.

Once again, condition (18) is more restrictive than its continuous counterpart (15); this may be easily checked having a glance at the Riemann problem with a double symetric rarefaction wave. VFRoe scheme with $Y(W) = {}^t(u, \pi, \mu, s)$ also enables to preserve invariance of invariants π and u through the numerical contact discontinuity when computing the interface states.

Property 6: Assume that initial data in the Riemann problem agrees with:

$$u_R - u_L = 0$$
$$\pi_R - \pi_L = 0$$

Then intermediate states provided by VFRoencv scheme agree with the continuous condition since:

$$u_2 = u_1 = u_L = u_R$$
$$\pi_2 = \pi_1 = \pi_L = \pi_R$$

The proof is obvious owing to insertion of $\Delta u_{LR} = 0$ and $\Delta \pi_{LR} = 0$ in $(16 - 17)$. Now :

Property 7: Assuming the state law takes the form:

$$\rho\varepsilon = f(p) + a\rho + b$$

where a and b are real constants, then cell values apart from a moving contact discontinuity preserve invariance of both u and π.

The proof is very similar to the proof of property 4 and thus is not detailed here. This means that the contact discontinuity is perfectly preserved when restricting to turbulent perfect gas EOS. *When focusing on turbulent real gas EOS, this property no longer holds.*

Though not discussed here, it is worth mentionning that use of other symetrizing variables such as (U, P, K, s) does not enable to insure positive values of density, mean pressure and turbulent kinetic energy at the interface, unless one requires very hard constraints on initial conditions.

5.5 Numerical results

In figures 10 are plotted results on a mesh with 200 cells, setting $\gamma = 1,4$, with the following initial conditions:

	ρ	p	u	K
Left	1	10^5	0	100
Right	0.125	10^4	0	1000

6 Conclusion

The use of symmetrizing variables thus allows computation of rather difficult flow configurations. It is emphasized that all schemes discussed herein rely on the Finite Volume techniques, and apply

for very simple approximate Riemann solvers at each interface between two neighbouring cells. The method has been successfully applied for shallow water equations, Euler equations, turbulent compressible closures based on one or two-equation models [24], [25] (for second-order Reynolds stress closures, see reference[26]). The method has been proved to be as accurate as previous approximate Godunov schemes investigated [9], and meanwhile is more robust than similar approximate Godunov schemes in some specific cases including either real vacuum (when focusing on shallow water equations), or near-vacuum (when dealing with Euler equations for compressible gas dynamics). Measure of the L^1 error norm in some specific cases confirms that this solver is as accurate as Godunov scheme (shallow water equations) and of course much cheaper. Similar comments hold when turning to Euler equations. Though one might think that this kind of approach is much more in favour of the treatment of rarefaction waves, it nonetheless permits dealing with Riemann problems including strong double shock waves. The reason why the scheme converges towards the right weak solutions, despite from the fact that it uses so called non conservative variable, is due to the fact that it is written under conservative form.

These approximate Riemann solvers indeed seem promising to compute approximations of complex sets of equations such as those arising in two phase flow modelling [27], [21], [28],[29], [30]. In this frame, the counterpart of real vacuum may occur (when one phase disappears), as well as the near vacuum when strong rarefaction waves develop. These models indeed represent a hard challenge since they also involve many different time scales.

Acknowledgments:
The third author has benefitted from financial support under EDF-CNRS contract CO2770/AEE2704.

References

[1] S.K. GODUNOV, A difference method for numerical calculation of discontinuous equations of hydrodynamics, *Mat. Sb.*, 1959, pp. 271–300. In Russian.

[2] E.F. TORO, *Riemann solvers and numerical methods for fluid dynamics*, Springer Verlag, 1997.

[3] B. EINFELDT, C.D. MUNZ, P.L. ROE AND B. SJÖGREEN, On Godunov-type methods near low densities, *J. Comp. Phys.*, 1991, vol. 92-2, pp. 273–295.

[4] R.J. LEVEQUE, *Numerical Methods for Conservation Laws*, Birkhäuser-Verlag, Basel, 1990.

[5] E. GODLEWSKI AND P.A. RAVIART, *Numerical approximation of hyperbolic systems of conservation laws*, Springer Verlag, 1996.

[6] P.L. ROE, Approximate Riemann solvers, parameter vectors and difference schemes, *J. Comp. Phys.*, 1981, vol. 43, pp. 357–372.

[7] G.A. BIRD, *Molecular gas dynamics and the direct simulation of gas flows*, Clarendon, Oxford UK, 1994.

[8] E.S ORAN, C.K. OH AND B.Z. CYBYK, Direct Simulation Monte-Carlo: recent advances and applications, *Ann. Rev. of Fluid Mech.*, 1998, vol. 30, pp. 403–441.

[9] T. BUFFARD, T. GALLOUËT AND J.M. HÉRARD, A sequel to a rough Godunov scheme. Application to real gas flows, *Computers and Fluids*, 2000, vol. 29-7, pp. 813–847.

[10] T. BUFFARD, T. GALLOUËT AND J.M. HÉRARD, A naive Godunov scheme to compute a non-conservative hyperbolic system, *Int. Series Num. Math.*, 1998, vol. 129, pp. 129–138.

[11] T. GALLOUËT, J.M. HÉRARD AND N. SEGUIN, *Some recent Finite Volume schemes to compute Euler equations using real gas EOS*, LATP Report 00-021, Université de Provence, France. *to appear in Int. J. for Num. Meth. in Fluids*, 2000.

[12] A. HARTEN, P.D. LAX AND B. VAN LEER, On upstream differencing and Godunov-type schemes for hyperbolic conservation laws, *SIAM Review*, 1983, vol. 25, pp. 35–61.

[13] A. HARTEN, On the symmetric form of systems of conservation laws with entropy, *J. Comp. Phys.*, 1983, vol. 49, pp. 151–164.

[14] K. JANSEN, Z. JOHANN AND T.J.R. HUGHES, Implementation of a one equation turbulence model within a stabilized finite element formulation of a symmetric advective-diffusive system, *Comput. Methods Appl. Mech. Engrg.*, 1993, vol. 105, pp. 405–433.

[15] J.M. GREENBERG AND A.Y. LE ROUX, A well balanced scheme for the numerical processing of source terms in hyperbolic equation, *SIAM J. Numer. Anal.*, 1996, vol. 33-1, pp. 1–16.

[16] A.Y. LE ROUX, Discrétisation des termes sources raides dans les problèmes hyperboliques, In *Systèmes hyperboliques : Nouveaux schémas et nouvelles applications.* Écoles CEA-EDF-INRIA "problèmes non linéaires appliqués", INRIA Rocquencourt (France), March 1998. Available on http://www-gm3.univ-mrs.fr/~leroux/publications/ay.le_roux.html, In French.

[17] T. GALLOUËT, J.M. HÉRARD AND N. SEGUIN, *Some approximate Godunov schemes to compute shallow-water equations with topography*, EDF-DRD Report HI-81/01/05/A, *to appear in Computers and Fluids*, 2001.

[18] T. GALLOUËT AND J.M. MASELLA, A rough Godunov scheme, *C. R. Acad. Sci. Paris*, 1996, vol. I-323, pp. 77–84.

[19] T. BUFFARD, T. GALLOUËT AND J.M. HÉRARD, An approximate Godunov scheme to compute turbulent real gas flow models, *AIAA paper 99-3349*, 1999.

[20] J. SMOLLER, *Shock waves and reaction diffusion equations*, Springer Verlag, 1983.

[21] R. SAUREL AND R. ABGRALL, A simple method for compressible multifluid flows, *SIAM J. Sci. Comp.*, 1999, vol. 21-3, pp. 1115–1145.

[22] K.M. SHYUE, A fluid mixture type algorithm for compressible multicomponent flow with Van der Waals equation of state, *J. Comp. Phys.*, 1999, vol. 156, pp. 43–88.

[23] T. GALLOUËT, J.M. HÉRARD AND N. SEGUIN, *An hybrid scheme to compute contact discontinuities in Euler systems*, EDF-DRD Report HI-81/01/011/A, *Submitted for publication*, 2001.

[24] A. FORESTIER, J.M. HÉRARD AND X. LOUIS, A Godunov type solver to compute turbulent compressible flows, *C. R. Acad. Sci. Paris*, 1997, vol. I-324, pp. 919–926.

[25] J.M. HÉRARD, A. FORESTIER AND X. LOUIS, *A non strictly hyperbolic system to describe compressible turbulence*, EDF-DER Report HE-41/94/011/A, 1994.

[26] C. BERTHON, F. COQUEL, J.M. HÉRARD AND M. UHLMANN, An approximate solution of the Riemann problem for a realizable second moment turbulent closure, *Shock Waves*, 2002, vol. 11, pp. 245–269.

[27] T. GALLOUËT, J.M. HÉRARD AND N. SEGUIN, An alternative way to deal with two fluid models, *AIAA paper 01-2653*, 2001.

[28] J. GLIMM, D. SALTZ AND D.H. SHARP, Two phase flow modelling of a fluid mixing layer, *Journal of Fluid Mechanics*, 1999, vol. 378, pp. 119–143.

[29] V. RANSOM AND D.L. HICKS, Hyperbolic two-pressure models for two-phase flow, *J. Comp. Phys.*, 1984, vol. 53-1, pp. 124–151.

[30] M.R. BAER AND J.W. NUNZIATO, A two phase mixture theory for the deflagration to detonation (DDT) transition in reactive granular materials, *Int. J. Multiphase Flow*, 1986, vol. 12-6, pp. 861–889.

7 Behaviour of cell values near wall boundaries

We introduce initial conditions of a Riemann problem which generate symmetrical double rarafaction waves, thus mimicking the exact behaviour of the approximate Godunov scheme, and wonder whether expected positive values (that is: water height (for shallow water equations); density and pressure (for Euler equations)) remain positive, *under classical CFL-like condition* :

$$CFL = V_{max}\lambda = 0.5 \tag{19}$$

while setting $\lambda = \frac{\Delta t}{h}$, and V_{max} the maximum speed of waves.

7.1 Shallow water equations

We apply the classical mirror state technique, and assume that the initial condition in cell w neighbouring the wall boundary is $(h_w^n = h, U_w^n = -U)$, and thus that mirror state in the fictitious cell on the right side of the wall boundary is :$(h_m^n = h, U_m^n = U)$, assuming that $U > 0$. Recall that vacuum occurs at the wall boundary if $2\sqrt{gh} = 2c \leq U$, otherwise not. Applying for the approximate Godunov scheme results in the following value h_w^{n+1} at the end of the time step:

$$h_w^{n+1} - h + \lambda(hU) = 0$$

and thus h_w^{n+1} identifies with prediction of Godunov scheme. Noting that CFL restriction necessarily implies that $\lambda U < 1$ insures that h_w^{n+1} is positive.

7.2 Euler equations with perfect gas EOS

The EOS is assumed to be perfect gas EOS, hence : $P = (\gamma - 1)(E - 1/2\rho U^2)$, with $1 < \gamma < 3$. We still use the mirror state technique, and thus initial condition : $(\rho_w^n = \rho, U_w^n = -U, P_w^n = P)$ in the fluid cells on the left side of the wall, and (ρ, U, P) in the mirror cell on the right side of the wall, assuming that $U > 0$. This may be in agreement with $(\gamma - 1)U < 2\sqrt{\gamma P/\rho}$ -in that case no vacuum occurs at the wall boundary-, or not. This initial data corresponds to the case called WBC in the main part of the paper, and also to the framework of analysis conducted in reference [3]. Setting $M = U/c$, and using the approximate Godunov scheme VFRoe with variable $Y^t = (s, U, P)$, the predicted value at the wall interface is simply :

$$s^* = s(\rho, P),\ U^* = 0,\ P^* = P(1 - \gamma M)$$

if $\gamma M < 1$, and otherwise:

$$s^* = s(\rho, P),\ U^* = 0,\ P^* = 0$$

Hence the updated cell value of density ρ_w^{n+1} agrees with :

$$\rho_w^{n+1} - \rho + \lambda(\rho U) = 0$$

and thus still equals its counterpart obtained with the exact Godunov scheme. A similar result holds for total energy, since :

$$E_w^{n+1} - E + \lambda(U(E + P)) = 0$$

Nonetheless, predicted value of momentum on cell close to the wall

$$(\rho U)_w^{n+1} - (\rho U) + \lambda((\rho U^2) + P^* - P) = 0$$

differs from the one obtained with exact Godunov scheme, since values of pressure on the wall boundary are distinct : $P^* < P^*_{Godunov}$.
The above CFL-like condition may be rewritten as: $2\lambda c(1+M) = 1$.

If $0 < \gamma M < 1$, straightforward calculations show that :

$$\rho_w^{n+1} P_w^{n+1} = \frac{\rho P}{2(1+M)^2} g(M)$$

where :

$$g(M) = 8 + 4(3-\gamma)M + M^2(4 - 5\gamma + 3(\gamma)^2) + 2\gamma(\gamma-1)M^3$$

which is obviously positive when $M > 0$, since all four coefficients in the polynomial expression are positive when $1 < \gamma < 3$.

If $\gamma M > 1$, a similar result may be obtained, since :

$$\rho_w^{n+1} P_w^{n+1} = \rho P h(M)$$

where $h(M) = (1 - \frac{M - \sqrt{(\gamma-1)/(2\gamma)}}{2(1+M)})(1 - \frac{M + \sqrt{(\gamma-1)/(2\gamma)}}{2(1+M)})$.

8 Numerical preservation of velocity and pressure through the contact discontinuity in Euler equations

We focus here on initial conditions of a Riemann problem, with uniform velocity and uniform pressure. Schemes investigated here can be derived from the formalism of VFRoe ncv scheme, with variable :

$$Y = {}^t(\varphi, u, p)$$

where $\varphi = \varphi(\rho, s)$ (s denotes the specific entropy) must be independant of pressure p (for instance $\varphi = s, \rho, \tau, ...$). Euler equations are rewritten in terms of $Y = {}^t(\varphi, u, p)$ as:

$$Y_{,t} + A(Y)Y_{,x} = 0$$

where :

$$A = \begin{pmatrix} u & \rho\varphi_{,\rho} & 0 \\ 0 & u & \rho^{-1} \\ 0 & \hat{\gamma}p & u \end{pmatrix}$$

The eigenvalues are (c stands for the sound speed) :

$$\lambda_1 = u - c,\ \lambda_2 = u,\ \lambda_3 = u + c$$

and the associated right eigenvectors are :

$$r_1(Y) = \begin{pmatrix} -\frac{1}{c}\varphi_{,\rho} \\ \frac{1}{\rho} \\ -c \end{pmatrix},\ r_2(Y) = \begin{pmatrix} 1 \\ 0 \\ 0 \end{pmatrix},\ r_3(Y) = \begin{pmatrix} \frac{1}{c}\varphi_{,\rho} \\ \frac{1}{\rho} \\ c \end{pmatrix}$$

We recall that (see section 4.3) Y_1 and Y_2 read :

$$\begin{aligned} Y_1 &= Y_L + \widetilde{\alpha_1}\tilde{r_1} \\ Y_2 &= Y_R - \widetilde{\alpha_3}\tilde{r_3} \end{aligned}$$

where :

$$\begin{aligned} \widetilde{\alpha_1} &= -\frac{1}{2\tilde{c}}\Delta u + \frac{1}{2\tilde{\rho}\tilde{c}^2}\Delta p \\ \widetilde{\alpha_3} &= \frac{1}{2\tilde{c}}\Delta u + \frac{1}{2\tilde{\rho}\tilde{c}^2}\Delta p \end{aligned}$$

noting $\Delta(.) = (.)_R - (.)_L$. Y_1 and Y_2 do not depend on the choice of φ. Initial conditions generate an unsteady contact discontinuity:

$$\begin{aligned} \Delta u = \Delta p = 0 \quad &\Rightarrow \quad \widetilde{\alpha_1} = \widetilde{\alpha_3} = 0 \\ &\Rightarrow \quad Y_1 = Y_L \text{ and } Y_2 = Y_R \end{aligned}$$

These equalities are satisfied at each interface of the mesh. Hence, if we denote $\rho_{i+1/2}$ the numerical density of the linearised Riemann problem at the interface $i + 1/2$, u_0 and p_0 initial velocity and pressure, the Finite Volume scheme applied to the mass conservation equation gives :

$$\begin{aligned} \rho_i^{n+1} &= \rho_i^n - \frac{\Delta t}{\Delta x}((\rho u)_{i+1/2} - (\rho u)_{i-1/2}) \\ &= \rho_i^n - \frac{\Delta t}{\Delta x}u_0(\rho_{i+1/2} - \rho_{i-1/2}) \end{aligned}$$

Now, if we apply the Finite Volume scheme to the momentum conservation equation, we get :

$$\begin{aligned}
(\rho u)_i^{n+1} &= (\rho u)_i^n - \frac{\Delta t}{\Delta x}((\rho u^2 + p)_{i+1/2} - (\rho u^2 + p)_{i-1/2}) \\
&= (\rho u)_i^n - \frac{\Delta t}{\Delta x}((\rho_{i+1/2} u_0^2 + p_0) - (\rho_{i-1/2} u_0^2 + p_0)) \\
&= (\rho u)_i^n - \frac{\Delta t}{\Delta x} u_0^2 (\rho_{i+1/2} - \rho_{i-1/2}) \\
&= u_0 \left(\rho_i^n - \frac{\Delta t}{\Delta x} u_0 (\rho_{i+1/2} - \rho_{i-1/2}) \right) \\
&= u_0 \rho_i^{n+1}
\end{aligned}$$

Thus, $u_i^{n+1} = u_0$, $\forall i \in \mathbb{Z}$.
To study the discrete preservation of pressure, let us write the Finite Volume scheme applied to energy conservation equation :

$$\begin{aligned}
E_i^{n+1} &= E_i^n - \frac{\Delta t}{\Delta x}((u(E+p))_{i+1/2} - (u(E+p))_{i-1/2}) \\
&= E_i^n - \frac{\Delta t}{\Delta x} u_0 (E_{i+1/2} - E_{i-1/2})
\end{aligned}$$

Energy is defined by $E = \rho\varepsilon + \frac{1}{2}\rho u^2$. Thus:

$$(\rho\varepsilon)_i^{n+1} = (\rho\varepsilon)_i^n - \frac{\Delta t}{\Delta x} u_0 ((\rho\varepsilon)_{i+1/2} - (\rho\varepsilon)_{i-1/2})$$

Let us assume that the equation of state can be written under the form :

$$\rho\varepsilon = f(p) + b\rho + c \tag{20}$$

where b and c are real constants, and f a inversible function (for instance perfect gas EOS, Tammann EOS, ...). If we introduce this equation of state in the previous equation, it gives :

$$\begin{aligned}
(f(p) + b\rho + c)_i^{n+1} &= (f(p) + b\rho + c)_i^n \\
&\quad - \frac{\Delta t}{\Delta x} u_0 ((f(p) + b\rho + c)_{i+1/2} - (f(p) + b\rho + c)_{i-1/2}) \\
f(p_i^{n+1}) + b\rho_i^{n+1} + c &= f(p_0) + b\rho_i^n + c \\
&\quad - \frac{\Delta t}{\Delta x} u_0 ((f(p_0) - f(p_0)) + b(\rho_{i+1/2} - \rho_{i-1/2}) + (c - c)) \\
f(p_i^{n+1}) &= f(p_0)
\end{aligned}$$

Thus, $p_i^{n+1} = p_0$.

Hence,provided that a state law can be written under the form (20), then a VFRoe ncv scheme, with variable (φ, u, p), maintains uniform velocity and pressure profiles.

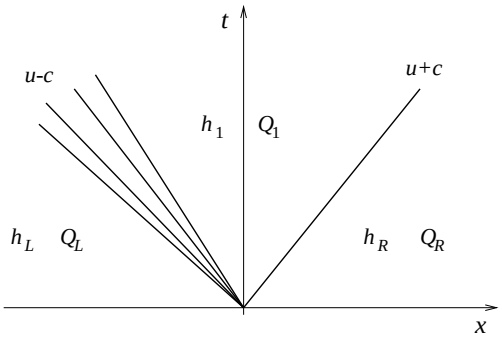

Figure 1: Solution of the 1D Riemann problem of SW equations

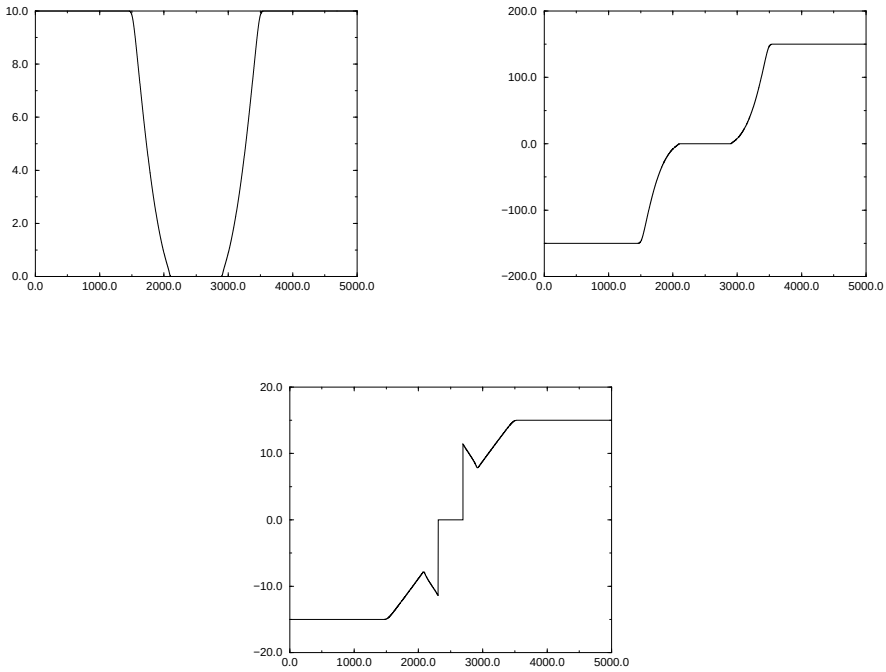

Figure 2: Dry area: water height (left top), momentum (right top), velocity (bottom), as functions of x

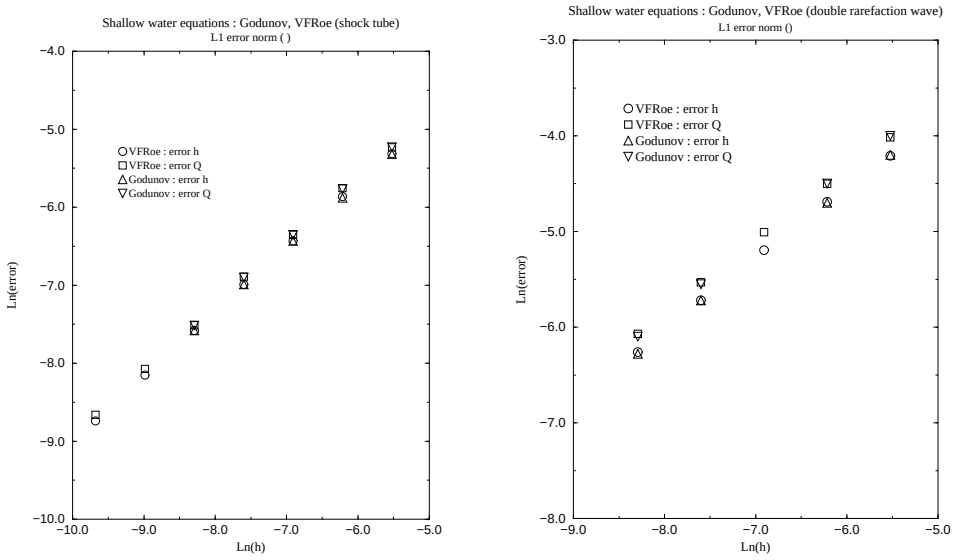

Figure 3: L^1 norm of the error

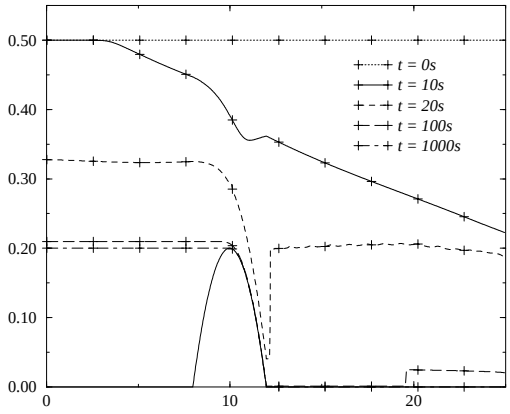

Figure 4: Dry area occuring when emptying a reservoir (water height as a function of x)

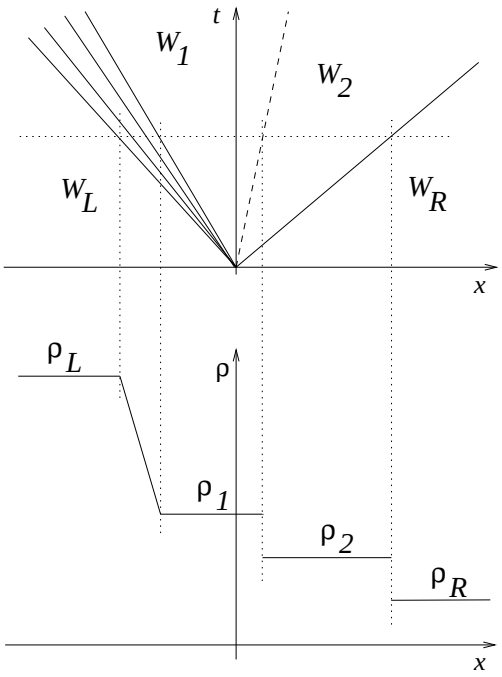

Figure 5: Solution of the 1D Riemann problem for Euler equations

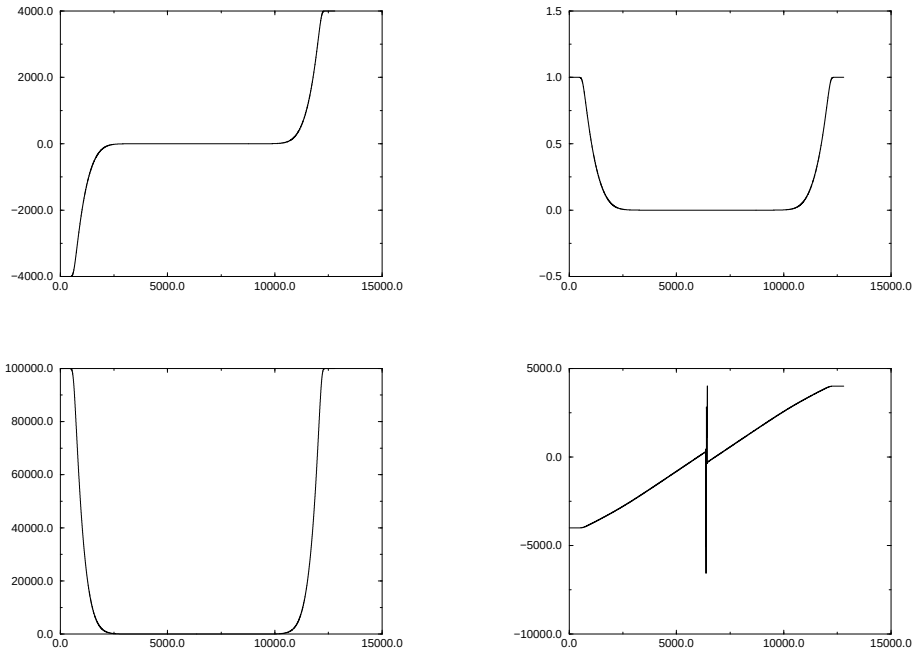

Figure 6: Vacuum occurence: momemtum (left top), density (right top), pressure (left bottom), velocity (right bottom), as functions of x

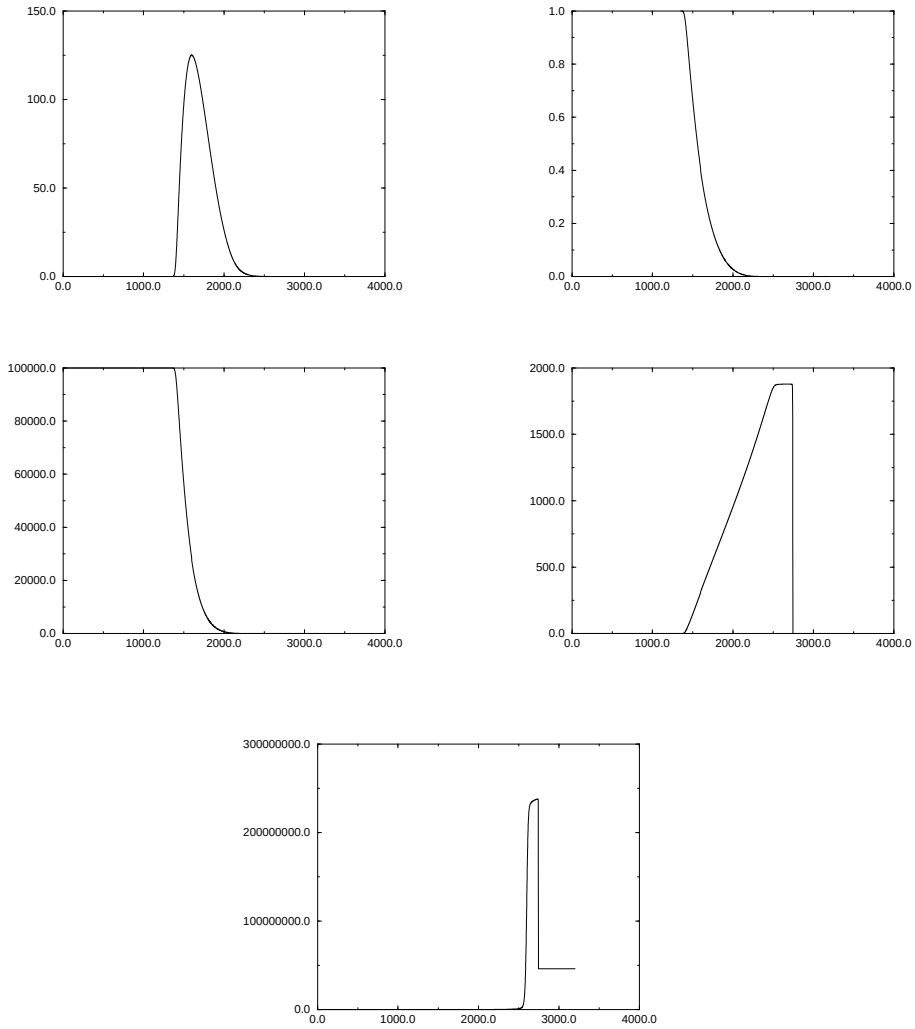

Figure 7: Shock wave over vacuum: momentum (left top), density (right top), pressure (left middle), velocity (right middle), specific entropy (bottom), as functions of x

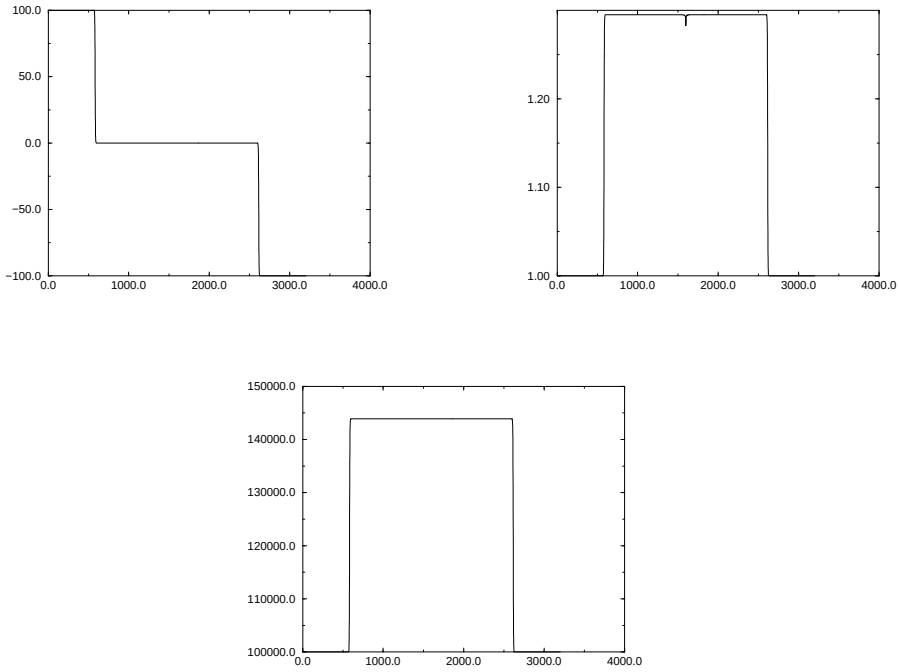

Figure 8: Double shock wave: momentum (left top), density (right top), pressure (bottom), as functions of x

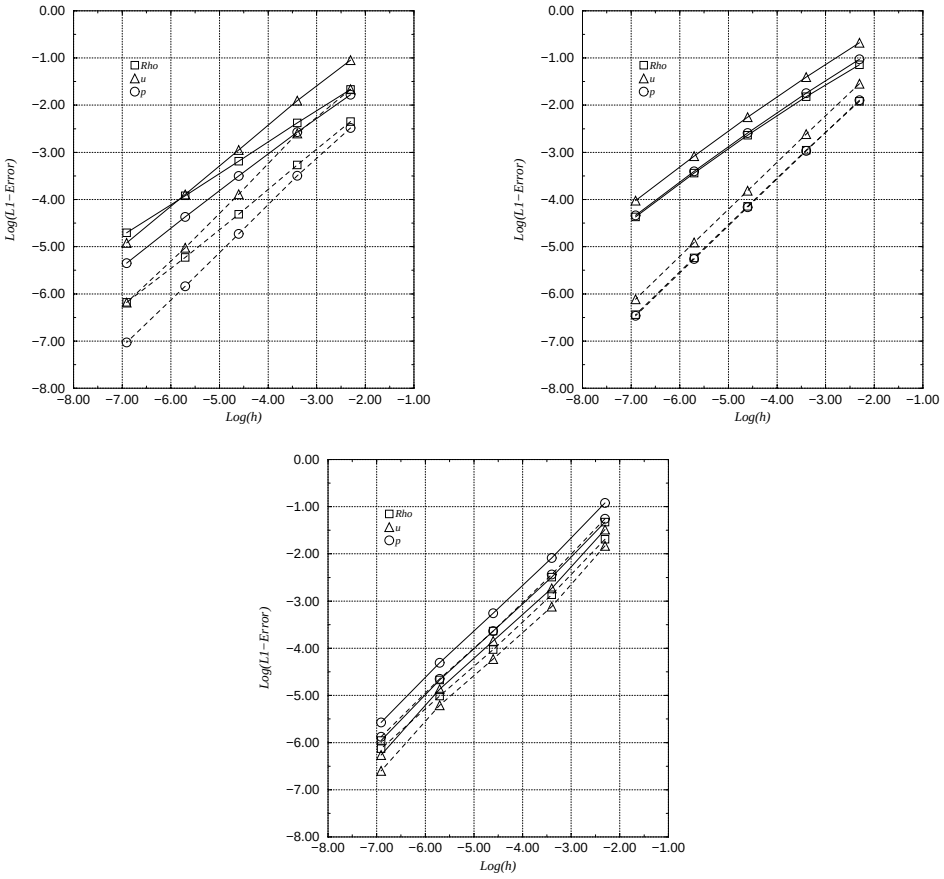

Figure 9: L^1 error norm - Sod shock tube (left top), double rarefaction wave (right top), double shock wave (bottom)

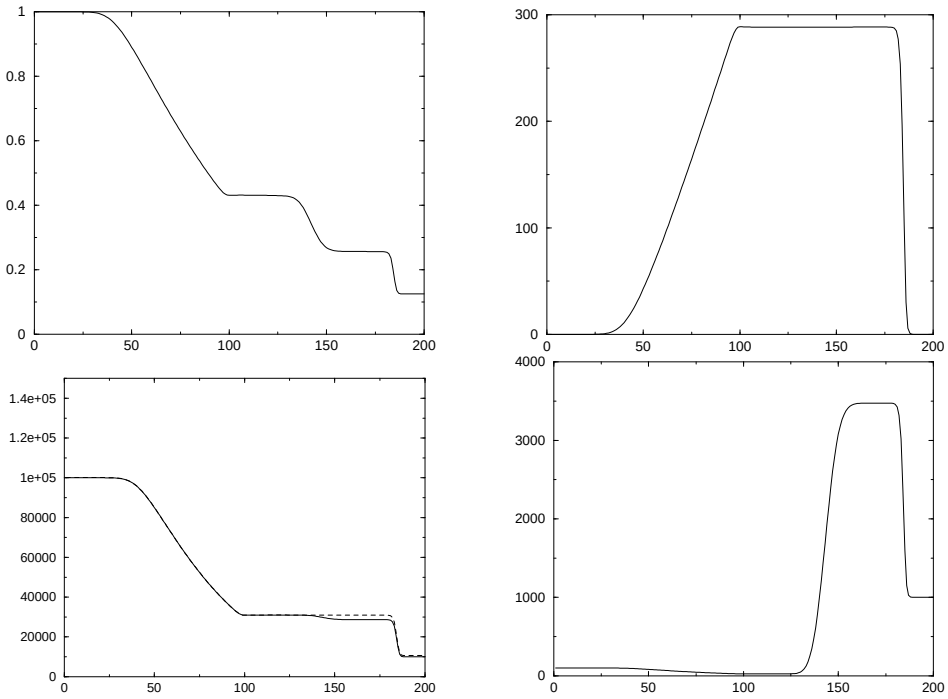

Figure 10: Turbulent Sod shock tube: density (left top), velocity (right top), p (—) and $p+2K/3$ (- -) (left bottom), K (right bottom), as functions of x

Annexe B

Partial review of positivity constraints in some two phase flow models

L'article suivant correspond au papier *2002-3185* accepté pour le congrès intitulé « *32nd AIAA Fluid Dynamics Conference* » à Saint-Louis, Missouri, du 24 au 27 juin 2002.

AIAA-2002-3185

PARTIAL REVIEW OF POSITIVITY CONSTRAINTS IN SOME TWO PHASE FLOW MODELS

Sebastien Clerc[1,*], Thierry Gallouët[2,†], Jean-Marc Hérard[2,3,‡], Nicolas Seguin[2,§]

[1] CEA/DEN/SFME/LETR, Centre d'etudes de Saclay
91191, Gif sur Yvette, FRANCE

[2] Université de Provence, Centre de Mathématiques et d'Informatique, L.A.T.P. - UMR CNRS 6632,
39 rue Joliot Curie, 13453 Marseille cedex 13, FRANCE
Thierry.Gallouet@cmi.univ-mrs.fr, Herard@cmi.univ-mrs.fr

[3] Électricité de France, Division Recherche et Développement, Département MFTT
6 quai Watier, 78401 Chatou cedex, FRANCE

ABSTRACT

The present paper adresses the problem of the preservation of positivity constraints or realisability conditions when computing two phase flows. Starting with continuous models, several classes of models are first described, and a brief discussion is given in each case. Afterwards, we examine whether schemes enable reaching discrete realisability concept. Both the single fluid approach and the two fluid approach are considered, with special emphasis on the latter when retaining pressure equilibrium. We start with Homogeneous Equilibrium Model (HEM) and Homogeneous Relaxation Model (HRM) or their counterpart in the framework of gas solid flows, focusing on either dilute or dense flows. We then turn to two-fluid models using single pressure models. This requires to distinguish three distinct cases, depending whether:
(i) - both densities are constant,
(ii) - one phase si caracterized by constant density,
(iii) - EOS must be given within each phase $\rho_k = \rho_k(e_k, P_k)$. Technical proofs require to distinguish regular solutions, and solutions of the Riemann problem associated with the convective subset.

*Research Engineer
†Professor
‡Research Engineer in EDF, Associate Research Director at CNRS -UMR CNRS 6632-, AIAA member
§PhD student

INTRODUCTION

We discuss in this paper the suitability of some two phase models in terms of ability to fulfill some positivity constraints which are usually assumed to be satisfied. These are essentially ; positivity of physical variables such as mean density of the mixture or density within each phase ; mean pressure for the mixture or partial pressures within each phase or alternatively internal energy depending on EOS. But perhaps the most obvious and important point concerns the maximum principle for the void fraction α_{k_0} of phase k_0. We examine succesively the framework of single fluid models for gas solid or gas liquid flows, and then turn to two fluid models which use the pressure equilibrium assumption. Though it seems to be a much promising area of research, the problem of mathematical and numerical modelling of two fluid flows using the two-fluid two-pressure approach will not be discussed herein. The reader is refered to[51,33,34,38,55,31,13,28], among others for this new class of modelling. It seems worth emphasizing that closures should be revisited in that case. Moreover, though the whole problem is hyperbolic without any assumption on closures, the problem of resonance and the analysis of the associated one dimensional Riemann problem represents a great challenge for research. Introducing statistical turbulence in this kind of models is almost contained in the single phase approach, and

does not seem to introduce additional difficulties.

The basics of physical, mathematical and numerical modelling of two-phase flows using either the single-fluid approach or the two-fluid single pressure approach will not be recalled herein, since it is out of our concern. The reader is refered to the following works which of course are only sampling references ([18],[44],[32],[37],[4],[3],[56], ... and also[14],[11],[12],[59],[16], ...). It also seems worth mentionning that all two-fluid models involve non conservative convective terms , due to momentum interfacial transfer terms, but also due to exchange between total energies. We only mention here some of the main references available for mathematical and numerical modelling of systems of hyperbolic systems under conservative form[57],[58],[35],[52],[53],[36],[20],[15],[39],[49]. We also recall that recent works pertaining to mathematical or numerical investigation of hyperbolic systems under non conservative form should be carefully examined in order to evaluate the meaning of some models and computational results.

Obviously, the straightforward counterpart of this standard problem on positivity constraints in the framework of single phase turbulent flows is known as the realisability concept. It has been mainly investigated by J.L. Lumley, S. B. Pope and co-workers (see for instance the pioneering papers[45],[50]). This has also been examined by C.G. Speziale who also underlined the fact that some unclosed terms in "turbulent equations" should (or should not) comply with objectivity. Though sometimes disregarded, this latter point is crucial since it enables to get rid of a lot of meaningless closures. More recently, some work has been devoted to that topic, with special emphasis on the numerical modelling of turbulent single phase incompressible flows ([47] and[40],[41],....), or for compressible flows ([25],[7],[2],.....). The problem of introducing 'turbulence' in two phase problems will not be investigated herein, but this does not change the main issues already present in so called "laminar" closures.

The first part of the paper is devoted to continuous investigation of positivity requirement for *ad hoc* variables. The second part will deal with numerical techniques and only aims at listing some existing methods which preserve realisability. Work under progress in this area will not be adressed.

REALISABILITY CONDITIONS

Models based on Euler type systems ; HEM, HRM

These models are widespread in the nuclear industry, and rely on the conservation of the mixture of the vapour phase plus the liquid phase. Roughly speaking, and for instance starting from the governing unclosed set of equations of the two-fluid model, HEM may be obtained adding mass conservation equations within each phase, and a similar approach for both momentum and total energy equations. Hence one gets rid of problems pertaining to closure of interfacial transfer terms. In addition the common assumption of equal velocities (and equal pressures) in both phases is usually kept, which results in conservative systems involving first order PDE of the Euler type. The field of applications of these rather rough models is nonetheless wide, and permits computing flashing flows or other unsteady and inhomogeneous flows with rather good agreement with experimental results. Assuming reasonable closures for the EOS of the mixture, and neglecting relative velocities, yields hyperbolicity of the whole. We restrict below to such a kind of closures and focus on HRM, but we emphasize that non zero relative velocities may render the whole hyperbolic *under* condition.

Governing equations for HRM model

For given IC $W(x,0) = W_0(x)$, the governing set of equations takes the form :

$$\frac{\partial W}{\partial t} + \frac{\partial F(W)}{\partial x} = S(W)$$

with W, $F(W)$ and $S(W)^t = (0, \rho\Gamma, 0, 0)$ in $\mathbb{R}^4$. The conservative variable W and convective flux $F(W)$ read : $W = (\rho, \rho X, Q = \rho U, E)$ and $F(W) = (\rho U, \rho XU, \rho U^2 + P, U(E+P))$. The total energy E is written in terms of the kinetic energy plus the internal energy ρe which depends on density ρ and pressure P, but may also depend on vapour quality X.Thus :

$$E = \frac{\rho U^2}{2} + \rho e(P, \rho, X)$$

The closure for the mass transfer term Γ must be chosen in such a way that it will not yield violation of maximum principle for the vapour quality (see examples in[22],[1],[8]). A standard form reads:

$$\Gamma = -\frac{X - \overline{X}(\rho, P)}{\theta}$$

In a certain sense, the HRM model degenerates to HEM model when Γ is null, more precisely

when: $X = \overline{X}(\rho, P)$. For the sake of simplicity, we will discuss here both models without any distinction, but this is quite formal, since it is known that the (usually) high ratio between time scales pertaining to both convective effects and return to vapour quality equilibrium may lead to tough numerical problems, which require higher order methods than those discussed here or at least suitable unsplit schemes. The whole must be complemented with a physically relevant entropy inequality (which requires consistency of entropy-entropy flux pair with viscous fluxes) :

$$\frac{\partial \eta}{\partial t} + \frac{\partial F_\eta}{\partial x} \leq 0$$

The speed of acoustic waves c is:

$$\rho(c)^2 = (\frac{\partial e(P,\rho,X)}{\partial P})^{-1}(\frac{P}{\rho} - \rho\frac{\partial e(P,\rho,X)}{\partial \rho})$$

and it is assumed that $\gamma P = \rho(c)^2$ is strictly positive. Thus the system is hyperbolic, since it has real eigenvalues and the associated right eigenvectors span the whole space $\mathbb{R}^4$. Eigenvalues are : $\lambda_1 = U - c$, $\lambda_2 = \lambda_3 = U$, $\lambda_4 = U + c$. We also need to define specific entropy s as a function complying with :

$$\gamma P\frac{\partial s(P,\rho,X)}{\partial P} + \rho\frac{\partial s(P,\rho,X)}{\partial \rho} = 0$$

Recall that the couple $(\eta = -\rho Ln(s), F_\eta = -\rho Ln(s)U)$ is admissible. The 1-field and 4-field are Genuinely Non Linear[57], and the 2-field and the 3-field are Linearly Degenerated, since: $\nabla_W \lambda_2(W).r_2(W) = 0$ and $\nabla_W \lambda_3(W).r_3(W) = 0$ where $\lambda_k(W)$ and $r_k(W)$ respectively stand for k-th eigenvalue and associated k-th right eigenvector of the Jacobian matrix $\frac{\partial F(W)}{\partial W}$. Whatever the EOS is, both the pressure and the velocity are Riemann invariants in the two LD fields. Jump conditions simply write (σ stands for the speed of the discontinuity between states l, r):

$$\begin{cases} -\sigma[\rho] + [\rho U] = 0 \\ -\sigma[\rho X] + [\rho XU] = 0 \\ -\sigma[\rho U] + [\rho U^2 + P] = 0 \\ -\sigma[E] + [U(E+P)] = 0 \end{cases}$$

using standard notations $[\phi] = \phi_r - \phi_l$. Riemann invariants are given below in each wave :

$$I_1 = s, U + \int_0^\rho \frac{c(\rho,s,X)}{\rho} d\rho, X$$

$$I_4 = s, U - \int_0^\rho \frac{c(\rho,s,X)}{\rho} d\rho, X$$

$$I_{2,3} = P, U$$

Properties and discussion

We now restrict to the homogeneous convective part and distinguish two cases. The first one will require some assumptions and at least C^1 regularity. The second frame is dedicated to solutions of the one dimensional Riemann problem which is composed of constant waves separated by contact discontinuities (CD), shock waves (SW) and rarefaction waves (RW). The latter SW and CD involve zeroth order discontinuities, whereas RW involve first order discontinuities.

We focus first on the behaviour of the density and pressure variables for smooth solutions. The governing equation for the density and the pressure are simply:

$$\frac{\partial \rho}{\partial t} + U\frac{\partial \rho}{\partial x} + \rho\frac{\partial U}{\partial x} = 0$$

$$\frac{\partial P}{\partial t} + U\frac{\partial P}{\partial x} + \gamma P\frac{\partial U}{\partial x} = 0$$

Hence, for smooth enough solutions, straightforward application of lemma 1 (see appendix, or appendix in[1] or equivalently in[28]) ensures positive values of density and pressure, as soon as both the velocity field and the divergence of the velocity field remain bounded over $\Omega \times [0,T]$, and assuming of course suitable inlet (parts of the boundary where $U.n < 0$, where n stands for the unit outward normal vector) conditions and initial conditions. This is also true for the vapour quality X and also $A - X$ (for given value of constant A) since both follow the law :

$$\frac{\partial \phi}{\partial t} + U\frac{\partial \phi}{\partial x} = 0$$

Remark that we nonetheless need to check that the function γ remains bounded. We now restrict to Tamman EOS and stiffened gas EOS, which enables to check that P is not the adequate variable to be discussed. The EOS is :$(\gamma_c - 1)\rho e = P + \gamma_c P_\infty$, setting $P_\infty = 0$ in perfect gas EOS. Actually, we note that when restricting to Tamman EOS, regular solutions $\pi = P + P_\infty$ agree with:

$$\frac{\partial \pi}{\partial t} + U\frac{\partial \pi}{\partial x} + \gamma_c \pi\frac{\partial U}{\partial x} = 0$$

Previous remark still holds true when using a stiffened gas EOS : $(\gamma_c(\mu)-1)\rho\epsilon = P + \gamma_c(\mu)P_\infty(\mu)$, where the colour function μ is governed by :

$$\frac{\partial \mu}{\partial t} + U\frac{\partial \mu}{\partial x} = 0$$

The governing equation in that case for $\pi = P + P_\infty(\mu)$ is simply once more:

$$\frac{\partial \pi}{\partial t} + U\frac{\partial \pi}{\partial x} + \gamma_c(\mu)\pi\frac{\partial U}{\partial x} = 0$$

Hence, assuming similar conditions as before, we are ensured to preserve positivity of the adequate variables (see discussion below). Source terms and diffusive terms may be accounted for in this analysis.

We turn now to the behaviour of the solution of the one dimensional Riemann problem associated with the convective subset.

- When focusing on rarefaction waves first, a glance at formulas in I_1 and I_4 recalled above ensures that both the entropy and the vapour quality will remain constant. Since intermediate states $1-2$ are connected to states $L-R$ respectively, the maximum principle for the vapour quality obviously holds true, since $X_1 = X_L$ and $X_2 = X_R$. Physically releavant values of pressure (or internal energy) will follow. To clarify ideas, it is clear that focusing on perfect gas EOS or Tamman EOS , the entropy formula implies that : $P_1 + P_\infty = s_L(\rho_1)^{\gamma_c}$, which guarantees that both $P + P_\infty$ and ρ remain simultaneously positive in rarefaction waves. We recall that the vacuum state corresponds for these EOS to $P = -P_\infty$ and $\rho = 0$ (and $Q = \rho U = 0$). Thus standard solutions of the Riemann problem (i.e. with no vacuum occurence) will be guided by the necessary and sufficient condition on initial data:

$$u_R - u_L \leq \int_0^{\rho_L} \frac{c(\rho,s,X)}{\rho}d\rho + \int_0^{\rho_R} \frac{c(\rho,s,X)}{\rho}d\rho$$

- Turning then to shock waves, and using some algebra enables to rewrite shock relations between states l, r as :

$$\left\{ \begin{array}{l} v = U - \sigma \\ +[\rho v] = 0 \\ +[X] = 0 \\ \rho v[v] + [P] = 0 \\ 2[e] = -(P_l + P_r)[\tau] \end{array} \right.$$

for any EOS. Obviously the vapour quality has no jump through the 1-field and 4-field. Moreover, intermediate states of density ρ_1, ρ_2 remain positive since density agrees with $\rho_L \leq \rho_1$ (respectively $\rho_R \leq \rho_2$) in case of a 1 shock (respectively a 4 shock). Owing to the entropy inequality, which provides $[U] < 0$, one gets a unique representation of shock relations and thus one may check that intermediate states may not generate positivity problems in the case of shock occurence. This completes the discussion in the frame of solutions of the 1D Riemann problem. These results are classical (see[48],[57],[35]).

Homogeneous gas-solid flow models

These models are rather classical too. The main assumption is that velocities in both phases are equal. Hence, the sum of both momentum equations is used, which of course no longer requires the interfacial momentum transfer term. In addition, a polytropic state law is often used within each phase, so that one gets rid of total energy equations and associated closure problems.

Governing equations

These are based on the following conservative PDE, given IC $W(x,0) = W_0(x)$:

$$\frac{\partial W}{\partial t} + \frac{\partial F(W)}{\partial x} = 0$$

with W and $F(W)$ in $\mathbb{R}^3$:

$$W = (\rho_1(1-\alpha_2), \rho_2\alpha_2, \rho U = (\rho_1\alpha_1 + \rho_2\alpha_2)U)$$

$$F(W) = \left(\begin{array}{c} \rho_1(1-\alpha_2)U \\ \rho_2\alpha_2 U \\ \rho U^2 + P \end{array} \right)$$

This three-equation model with four unknowns requires some closure, and is usually complemented with $\rho_2 = (\rho_2)_0$ when focusing on gas-solid flows (label 2 refers to the solid phase), or gas-liquid flows (where label 2 refers to the bubble phase). The conservative variable may be taken as $(\alpha_1\rho_1, \alpha_2, \rho U)$, and an EOS must be prescribed: $P = P(\rho_1, \rho_2, \alpha_2) = P_1(\rho_1) + (\rho_2)_0 P_2(\alpha_2)$. The latter usually take forms which agree with $\frac{\partial P_1(\rho_1)}{\partial \rho_1} > 0$, and $\frac{\partial P_2(\alpha_2)}{\partial \alpha_2} > 0$. Nonetheless, there exists many different forms in the literature to account for P_2, among which one must at least list :

(a) $P_2(\alpha_2) = (P_2)_0(\alpha_2)^\beta$, with $\beta > 0$,

(b) $P_2(\alpha_2) = (P_2)_0(\alpha_2)^\eta(1 + G(\alpha_2))$,

where $G(\alpha_2)$ is a positive monotone increasing function of α_2 which is unbounded close to the asymptot $\alpha_2 = (\alpha_2)_{max} < 1$. This problem has been adressed in many references, including for instance[11] which discusses the problem of the maximum principle for the void fraction and the positivity of density ρ_1 by investigating the 1D Riemann problem associated with the latter set of PDE. One may summarize as follows :

(a)- The unique entropy-consistent solution is such that α_2 lies in $[0, 1]$;
(b)- The unique entropy-consistent solution is such that α_2 lies in $[0, (\alpha_2)_{max}[$.

The specific term P_2 is usually disregarded in gas-liquid flows (thus form (a) is applied), where $(\alpha_2)_{max} = 1$. On the opposite, the form (b) is almost always included in codes when users aim at predicting dense gas-solid flows.

Two-fluid models with single pressure

Many times, the equilibrium velocity assumption is disregarded when counter-current flows are obviously present in the flow field. One of the main drawbacks of this kind of closure which is well known from long and has motivated passionate debates over past years is that associated initial value problems are perhaps not well posed due to some physically admissible states which do not correspond to hyperbolic situations. In addition, it is clear that these models involve some first order non conservative terms which render rather tricky the problem of formulation of jump conditions in Genuinely Non Linear fields (see[10],[23],[24],[17],[54]). Before going further on , we insist that equations below valid in the 3D framework, simply replacing $\frac{\partial .}{\partial x}$ by divergence or gradient operators, and products of velocities by tensorial products. Even more, results discussed below still hold when accouting for viscous effects. For non conservative systems, we emphasize that some tempting manipulations, which are valid (for regular solutions) in a one space dimension -but not in higher dimension-, and which are some times used (for instance: $2u\frac{\partial u}{\partial x} = \frac{\partial u^2}{\partial x}$), and which in this particular case enable to rewrite the whole system in conservative form, will be disregarded.

Governing equations for 4-equation gas-solid models

When modeling gas-solid two-phase flows, two distinct frames may appear at least. The first one corresponds to applications where both densities may be assumed to be constant. The second one refers to compressible flows loaded with particles. We *on purpose* do not assume that the flow is dilute. In both cases, the standard governing set of equations takes the form :

$$\left\{ \begin{array}{l} \frac{\partial W}{\partial t} + \frac{\partial F(W)}{\partial x} + C(W)\frac{\partial G(W)}{\partial x} = S(W) \\ W(x,0) = W_0(x) \end{array} \right.$$

with W, $F(W)$ and $S(W)^t = (0, 0, I(W), -I(W))$ in $\mathbb{R}^4$. The interfacial momentum transfer term I accounts for drag effects. The so-called "conservative" variable W, convective flux $F(W)$ and first order non conservative terms read :

$$W = (\rho_1\alpha_1, \rho_2\alpha_2, \rho_1\alpha_1U_1, \rho_2\alpha_2U_2)$$

$$F(W) = \left(\begin{array}{c} \rho_1\alpha_1U_1 \\ \rho_2\alpha_2U_2 \\ \rho_1\alpha_1(U_1)^2 \\ \rho_2\alpha_2(U_2)^2 + \rho_2\alpha_2\theta(\alpha_2) \end{array} \right)$$

$$C(W)\frac{\partial G(W)}{\partial x} = (0, 0, \alpha_1\frac{\partial P}{\partial x}, \alpha_2\frac{\partial P}{\partial x})$$

since added mass effects are usually disregarded in this framework. In these equations α_k is the volumetric fraction of phase k, ρ_k is the density of phase k, and U_k is the mean velocity in phase k. The gas phase is labeled with subscript 1 and the solid phase with 2. The θ function is a monotone increasing function which enables to account for granular pressure effects (see[32], and also[37]). In most closures, the following criteria is valid: $lim_{\alpha->\alpha_{max}}\theta(\alpha) = +\infty$, where α_{max} stands for the maximum compactness rate.

Case 1. *We now first assume that both densities are constant:* $\rho_1 = (\rho_1)_0$, *and:* $\rho_2 = (\rho_2)_0$. Obviously, this yields that $U = \alpha_1U_1 + \alpha_2U_2$ is a divergent free velocity field. Owing to this, the time matrix is no longer invertible and one needs to reconsider the whole system as a mixed hyperbolic-elliptic problem (with respect to pressure field) in terms of "non conservative variable" (α_2, P, U, U_2),

that is to say :

$$\left\{\begin{array}{l}\frac{\partial U}{\partial x}=0\\ \frac{\partial \alpha_2}{\partial t}+\frac{\partial \alpha_2 U_2}{\partial x}=0\\ \frac{\partial U}{\partial t}+\frac{\partial \frac{U^2+\alpha_2(U_2)^2-2\alpha_2 U U_2}{1-\alpha_2}+\alpha_2\theta(\alpha_2)}{\partial x}+...\\ +(\frac{1-\alpha_2}{(\rho_1)_0}+\frac{\alpha_2}{(\rho_2)_0})\frac{\partial P}{\partial x}=I(\frac{1}{(\rho_1)_0}-\frac{1}{(\rho_2)_0})\\ \frac{\partial \alpha_2 U_2}{\partial t}+\frac{\partial \alpha_2(U_2)^2+\alpha_2\theta(\alpha_2)}{\partial x}+...\\ +\frac{\alpha_2}{(\rho_2)_0}\frac{\partial P}{\partial x}=-\frac{I}{(\rho_2)_0}\end{array}\right.$$

The only condition to be ensured here is : $0 \leq \alpha_2 \leq A \leq 1$, where $A = 1$ or $A = \alpha_{max}$. Using second equation in system above enables first to ensure positivity of void fraction α_2, provided bounded U_2 and $\frac{\partial U_2}{\partial x}$, and meaningful inlet boundary and initial conditions. Setting now $\phi = A - \alpha_2$, and using the first two equations enables to check that :

$$\frac{\partial \phi}{\partial t}+\frac{\partial \phi U_1}{\partial x}=(A-1)\frac{\partial U_1}{\partial x}$$

Assuming that U_1 and $\frac{\partial U_1}{\partial x}$ remain bounded, we are ensured when $A = 1$ that the upper bound for α_2 is preserved, and this is the only positivity condition to be considered. However, when computing dense granular clouds or clusters, constant A is usually assumed to be smaller than one, typically $A = \alpha_{max} = 0.64$ when computing smooth rigid spherical uniform particles. In that case, one needs to examine the coupling of mass and momentum. Assuming convergence of the fractional step method, we will prove that the maximum principle for the void fraction holds passing to the limit on a time discretization. The computation of the velocity-pressure field will require solving the sequence of two steps associated with continuous systems. For given initial condition and boundary condition:

$$\left\{\begin{array}{l}\text{Compute solution of step I:}\\ \frac{\partial \alpha_2}{\partial t}+\frac{\partial \alpha_2 U_2}{\partial x}=0\\ \frac{\partial U}{\partial t}+\frac{\partial \frac{U^2+\alpha_2(U_2)^2-2\alpha_2 U U_2}{1-\alpha_2}+\alpha_2\theta(\alpha_2)}{\partial x}..\\ =-(\frac{1-\alpha_2}{(\rho_1)_0}+\frac{\alpha_2}{(\rho_2)_0})\frac{\partial P}{\partial x}+I(\frac{1}{(\rho_1)_0}-\frac{1}{(\rho_2)_0})\\ \frac{\partial \alpha_2 U_2}{\partial t}+\frac{\partial \alpha_2(U_2)^2+\alpha_2\theta(\alpha_2)}{\partial x}...\\ =-\frac{\alpha_2}{(\rho_2)_0}\frac{\partial P}{\partial x}-\frac{I}{(\rho_2)_0}\end{array}\right.$$

$$\left\{\begin{array}{l}\text{Then, compute solution of step II:}\\ \frac{\partial U}{\partial x}=0\\ \frac{\partial \alpha_2}{\partial t}=0\\ \frac{\partial U}{\partial t}+(\frac{1-\alpha_2}{(\rho_1)_0}+\frac{\alpha_2}{(\rho_2)_0})\frac{\partial \psi}{\partial x}=0\\ \frac{\partial \alpha_2 U_2}{\partial t}+\frac{\alpha_2}{(\rho_2)_0}\frac{\partial \psi}{\partial x}=0\end{array}\right.$$

where ψ represents some pressure variable. A more "usual " version of the second step may be written as :

$$\left\{\begin{array}{l}\text{Then, compute solution of:}\\ \frac{\partial(\frac{1-\alpha_2}{(\rho_1)_0}+\frac{\alpha_2}{(\rho_2)_0})\frac{\partial \psi}{\partial x}}{\partial x}=0\\ \frac{\partial U}{\partial t}+(\frac{1-\alpha_2}{(\rho_1)_0}+\frac{\alpha_2}{(\rho_2)_0})\frac{\partial \psi}{\partial x}=0\\ \frac{\partial \alpha_2 U_2}{\partial t}+\frac{\alpha_2}{(\rho_2)_0}\frac{\partial \psi}{\partial x}=0\end{array}\right.$$

(with $\alpha_2(x,.) = \alpha_2(x,t_0)$) in order to ensure divergence free velocity for U. Step II of course preserves the maximum principle for α_2. The right hand side of system in first step is a conservative hyperbolic system. Eigenvalues are : $\lambda_1 = U_2 - c_2$, $\lambda_2 = 2\frac{(U-\alpha_2 U_2)}{1-\alpha_2}$, $\lambda_3 = U_2 + c_2$, noting : $(c_2)^2 = \frac{\partial \alpha_2\theta(\alpha_2)}{\partial \alpha_2}$ the celerity of void fraction waves in the step . The volumetric fraction is frozen in the second step. The reader has recognized an almost straightforward counterpart of numerical techniques dedicated to single phase incompressible flows. Obviously, the first and third equations in the first step couple with each other, and the resulting system of pure convection reduces to the isentropic Euler equations in conservative form, with a specific EOS. The solution of the associated Riemann problem may be exhibited, and it enables to prove that double shock waves involve values of α_2 which remain in the range $[0, \alpha_{max}[$. More precisely, a unique entropy-consistent solution with no particle vacuum (eg $\alpha_2 > 0$) and no violation of the maximum principle for α_2 exists if and only if :

$$(u_2)_R - (u_2)_L \leq X_L + X_R$$

where : $X_i = \int_0^{(\alpha_2)_i} \frac{c_2(\alpha_2)}{\alpha_2} d\alpha_2$. The situation which may violate the upper bound for the void fraction α_2 corresponds to a double shock wave. Owing to the specific form of granular pressure which guarantees that $lim_{\alpha_2 -> \alpha_{max}}\theta(\alpha_2) = +\infty$, the upper bound cannot be violated since any

amount of incoming kinetic energy may be transfered to -granular- pressure energy with bounded argument. The counterpart for the lower bound for α_2 corresponds to a double rarefaction wave. The two remaining configurations (1-rarefaction and 2-shock ; and reverse case) do not provide "dangerous" situations, in terms of positivity. Hence, no problem arises in both steps, and assuming that the fractional step method converges, the maximum principle will hold true.

Case 2. *We now assume that* $\rho_2 = (\rho_2)_0$, *but no longer neglect compressible effects within the gas phase.* It thus requires a closure law for the mean pressure as a function of ρ_1, assuming for instance isentropic behaviour within the gas phase, and hence :$P(\rho_1) = P_0(\frac{\rho_1}{(\rho_1)_0})^\gamma$. We also note $(c_1)^2 = \dfrac{\partial P(\rho_1)}{\partial \rho_1}$. The reader is refered in that case to[12] and references therein. The argument in this approach still relies on the use of Trotter formula (that is convergence of the fractional step method), and examines successively the two fractional steps:

$$\begin{cases} \text{Step I} \\ \dfrac{\partial \alpha_1\rho_1}{\partial t} = 0 \\ \dfrac{\partial \alpha_2}{\partial t} + \dfrac{\partial \alpha_2 U_2}{\partial x} = 0 \\ \dfrac{\partial \alpha_1\rho_1 U_1}{\partial t} + \dfrac{\partial \alpha_1\rho_1 (U_1)^2}{\partial x} = I \\ \dfrac{\partial \alpha_2 U_2}{\partial t} + \dfrac{\partial \alpha_2 (U_2)^2 + \alpha_2\theta(\alpha_2)}{\partial x} = -\dfrac{I}{(\rho_2)_0} \end{cases}$$

$$\begin{cases} \text{Step II} \\ \dfrac{\partial \alpha_1\rho_1}{\partial t} + \dfrac{\partial \alpha_1\rho_1 U_1}{\partial x} = 0 \\ \dfrac{\partial \alpha_2}{\partial t} = 0 \\ \dfrac{\partial \alpha_1\rho_1 U_1}{\partial t} + \alpha_1 \dfrac{\partial P}{\partial x} = 0 \\ \dfrac{\partial \alpha_2 U_2}{\partial t} + \dfrac{\alpha_2}{(\rho_2)_0} \dfrac{\partial P}{\partial x} = 0 \end{cases}$$

Smooth solutions.
Step I involves a conservative hyperbolic system and smooth solutions of step I are ensured to agree with: $0 \leq \alpha_1\rho_1$ and $0 \leq \alpha_2$. This however does not permit to conclude that the maximum principle holds true for α_2. Smooth solutions of step II agree with $0 \leq \alpha_2 \leq A$ and $0 \leq \alpha_1\rho_1$ provided that U_1 and $\dfrac{\partial U_1}{\partial x}$ remain bounded and with reasonable IC and inlet BC.

Solutions of the 1D Riemann problem.
Once more , investigation of step I shows that the maximum principle for the void fraction holds in the first step (as in previous case), and obviously through step II. The condition reads again:

$$(u_2)_R - (u_2)_L \leq Y_L + Y_R$$

with :$Y_i = \int_0^{(\alpha_2)_i} \frac{c_2(\alpha_2)}{\alpha_2} d\alpha_2$. Even more, the positivity of density ρ_1 holds owing to the second step which governs speed of gas density waves in medium loaded with particles (seen as obstacles), under condition on IC:

$$(\rho_1 u_1)_R - (\rho_1 u_1)_L \leq Z_L + Z_R$$

with : $Z_i = \int_0^{(\rho_1)_i} c_1(\rho_1) d\rho_1$. We underline that some approximation of jump conditions is necessary to get this last result owing to the non conservative form of momentum equation within each phase in step II. One has used here a jump condition associated with:

$$\frac{\partial \rho_1 U_1}{\partial t} + \frac{\partial P(\rho_1)}{\partial x} = 0$$

that is to say :

$$\begin{cases} -\sigma[\alpha_2] = 0 \\ -\sigma[\alpha_1\rho_1] + [\alpha_1\rho_1 U_1] = 0 \\ -\sigma[\rho_1 U_1] + [P(\rho_1)] = 0 \\ -\sigma[\rho_2 U_2] + [P(\rho_1)] = 0 \end{cases}$$

One may nonetheless conjecture that this result does not depend on the closure jump relation which should be consistent with Riemann invariants through the associated field.

Governing equations for six equation gas-liquid flow models

Case 3. *We deal now with gas-liquid two-phase flow models and assume pressure equiilibrium between phases but no longer neglect compressibility whatever the label phase is.* Thus, we need to give $P_k(\rho_k, e_k)$ for $k = 1, 2$ and equilibrium means that: $P = P_1(\rho_1, e_1) = P_2(\rho_2, e_2)$ at any time and everywhere. Noting $m_k = \alpha_k\rho_k$, we get the governing equations (using IC $W(x, 0) = W_0(x)$):

$$M(W)\frac{\partial W}{\partial t} + \frac{\partial F(W)}{\partial x} + C(W)\frac{\partial G(W)}{\partial x} = S(W)$$

where $M(W) = Id + D(W)$ and the three W, $F(W)$ and $S(W)^t = (\Gamma(W), -\Gamma(W), I(W), -I(W), \Pi_1(W), \Pi_2(W))$ lie in $\mathbb{R}^6$. We note here $E_k = \rho_k e_k(P, \rho_k) + \frac{\rho_k (U_k)^2}{2}$. The specific entropy $s_k(P, \rho_k)$ agrees with :

$$\gamma_k P \frac{\partial s_k(P, \rho_k)}{\partial P} + \rho_k \frac{\partial s_k(P, \rho_k)}{\partial \rho_k} = 0$$

ple for the void fraction and positive densities on any type of mesh, but the internal energy is not necessarily positive.

Homogeneous gas-solid flow models

The reader is refered to[11] which provides computational results obtained using the approximate Godunov scheme VFRoe-ncv on 2D unstructured meshes. Recall that this system is a conservative system and thus introduces no specific difficulty. The only scheme which ensures positivity of partial masses $\alpha_k \rho_k$ is the Godunov scheme or alternatively the Rusanov scheme. Anyway the latter does not ensure the upper bound for the void fraction.

Numerical modeling of two-fluid models

Four-equation gas-solid or gas-liquid models

Case 1 : Some preliminary results on unstructured meshes were described in[6], on the basis of the initial work[12] and[5]. This scheme enables to ensure positive values of the void fraction on any mesh owing to Rusanov scheme, but preservation of the upper bound may require a great decrease of the time step since no clipping approximation is allowed in the code. A possible remedy is to use Godunov scheme (in 1D framework).

Case 2: In the specific case of dilute regimes, schemes based on approximate forms of Roe scheme were proposed in[54]. The scheme is in that case dedicated to structured meshes. Some algorithms relying on the previous analysis have been developped in the past years. These aimed at providing meaningful results on any mesh size using unstructured meshes. The controle volumes were dual "INRIA" cells associated with some basic triangulation. Many upwinding techniques were implemented which were:
(i) - Rusanov scheme to compute convection of particles,
(ii) - an approximate form of Roe scheme to account for non conservative terms,
(iii) - a Godunov scheme (for dilute cases only).

The most difficult cases included computation of dense clouds entering a convergent-divergent nozzle, a computation of dense fluidised beds (up to maximum compactness,[12]), and compaction of powders ([42]). Though these methods provided rather spectacular results, we insist that there no proof of preservation of positivity for α_2, even in the one dimensional case, except when using scheme (i) or (iii) with standard CFL like condition (which nonetheless may constrain much the time step in cluster regions). Scheme (iii) is the only candidate which preserves the upper bound for α_2. Moreover, when turning to unstructured 2D meshes, scheme (i) is the only one which ensures positive values of α_2.

Six equation gas-liquid flow models

Case 3: A first proposal is provided in[14]. It assumes that a perfect gas EOS holds within each phase, $P_k = (\gamma_k - 1)\rho_k e_k$, and it relies on the fractional step method. The first step solves for given pressure equilibrium on each cell ($(P_1)_i^n = (P_2)_i^n$):

$$\frac{\partial W}{\partial t} + \frac{\partial H(W)}{\partial x} = -E(W)\frac{\partial G(W)}{\partial x}$$

$$H(W) = \begin{pmatrix} m_1 U_1 \\ m_2 U_2 \\ m_1 (U_1)^2 + \alpha_1 P_1 \\ m_2 (U_2)^2 + \alpha_2 P_2 \\ \alpha_1 U_1 (E_1 + P_1) \\ \alpha_2 U_2 (E_2 + P_2) \end{pmatrix}$$

$$E(W)\frac{\partial G(W)}{\partial x} = (0, 0, -P_i \frac{\partial \alpha_1}{\partial x}, -P_i \frac{\partial \alpha_2}{\partial x}, 0, 0)$$

The term on the RHS is viewed as a source term, and thus both phases decouple. The system in phase $k = 1, 2$ is a Euler system with perfect gas EOS , and m_k stands for the density of phase k. Thus either standard Godunov or kinetic schemes may be used to get approximations of solutions in the first step. The second step aims at computing the same pressure in each cell at the end of the time step, and meanwhile the void fraction. We provide below a continuous (wrt time) formulation which is clearly not valid since the time operator is "unknown" :

$$\frac{\partial W}{\partial t} = (0, 0, 0, 0, P\frac{\partial \alpha_1}{\partial t}, -P\frac{\partial \alpha_2}{\partial t})$$

This algorithm enables to preserve the positivity of both partial masses under standard CFL condition, due to the use of kinetic schemes within each phase. Nonetheless, a rather constraining point concerns the discrete realisability conditions pertaining to internal energies and void fraction. This is due to the presence of the so-called source term $P_i \frac{\partial \alpha_k}{\partial x}$ where the usual assumption $P_i = P + \beta(U_r)^2$ holds. A different interpretation of this scheme enables to weaken this second condition on time step. Other numerical methods based

ple for the void fraction and positive densities on any type of mesh, but the internal energy is not necessarily positive.

Homogeneous gas-solid flow models

The reader is refered to[11] which provides computational results obtained using the approximate Godunov scheme VFRoe-ncv on 2D unstructured meshes. Recall that this system is a conservative system and thus introduces no specific difficulty. The only scheme which ensures positivity of partial masses $\alpha_k \rho_k$ is the Godunov scheme or alternatively the Rusanov scheme. Anyway the latter does not ensure the upper bound for the void fraction.

Numerical modeling of two-fluid models

Four-equation gas-solid or gas-liquid models

Case 1 : Some preliminary results on unstructured meshes were described in[6], on the basis of the initial work[12] and[5]. This scheme enables to ensure positive values of the void fraction on any mesh owing to Rusanov scheme, but preservation of the upper bound may require a great decrease of the time step since no clipping approximation is allowed in the code. A possible remedy is to use Godunov scheme (in 1D framework).

Case 2: In the specific case of dilute regimes, schemes based on approximate forms of Roe scheme were proposed in[54]. The scheme is in that case dedicated to structured meshes. Some algorithms relying on the previous analysis have been developped in the past years. These aimed at providing meaningful results on any mesh size using unstructured meshes. The controle volumes were dual "INRIA" cells associated with some basic triangulation. Many upwinding techniques were implemented which were:
(i) - Rusanov scheme to compute convection of particles,
(ii) - an approximate form of Roe scheme to account for non conservative terms,
(iii) - a Godunov scheme (for dilute cases only).

The most difficult cases included computation of dense clouds entering a convergent-divergent nozzle, a computation of dense fluidised beds (up to maximum compactness,[12]), and compaction of powders ([42]). Though these methods provided rather spectacular results, we insist that there no proof of preservation of positivity for α_2, even in the one dimensional case, except when using scheme (i) or (iii) with standard CFL like condition (which nonetheless may constrain much the time step in cluster regions). Scheme (iii) is the only candidate which preserves the upper bound for α_2. Moreover, when turning to unstructured 2D meshes, scheme (i) is the only one which ensures positive values of α_2.

Six equation gas-liquid flow models

Case 3: A first proposal is provided in[14]. It assumes that a perfect gas EOS holds within each phase, $P_k = (\gamma_k - 1)\rho_k e_k$, and it relies on the fractional step method. The first step solves for given pressure equilibrium on each cell ($(P_1)_i^n = (P_2)_i^n$):

$$\frac{\partial W}{\partial t} + \frac{\partial H(W)}{\partial x} = -E(W)\frac{\partial G(W)}{\partial x}$$

$$H(W) = \begin{pmatrix} m_1 U_1 \\ m_2 U_2 \\ m_1 (U_1)^2 + \alpha_1 P_1 \\ m_2 (U_2)^2 + \alpha_2 P_2 \\ \alpha_1 U_1 (E_1 + P_1) \\ \alpha_2 U_2 (E_2 + P_2) \end{pmatrix}$$

$$E(W)\frac{\partial G(W)}{\partial x} = (0, 0, -P_i \frac{\partial \alpha_1}{\partial x}, -P_i \frac{\partial \alpha_2}{\partial x}, 0, 0)$$

The term on the RHS is viewed as a source term, and thus both phases decouple. The system in phase $k = 1, 2$ is a Euler system with perfect gas EOS , and m_k stands for the density of phase k. Thus either standard Godunov or kinetic schemes may be used to get approximations of solutions in the first step. The second step aims at computing the same pressure in each cell at the end of the time step, and meanwhile the void fraction. We provide below a continuous (wrt time) formulation which is clearly not valid since the time operator is "unknown" :

$$\frac{\partial W}{\partial t} = (0, 0, 0, 0, P\frac{\partial \alpha_1}{\partial t}, -P\frac{\partial \alpha_2}{\partial t})$$

This algorithm enables to preserve the positivity of both partial masses under standard CFL condition, due to the use of kinetic schemes within each phase. Nonetheless, a rather constraining point concerns the discrete realisability conditions pertaining to internal energies and void fraction. This is due to the presence of the so-called source term $P_i \frac{\partial \alpha_k}{\partial x}$ where the usual assumption $P_i = P + \beta(U_r)^2$ holds. A different interpretation of this scheme enables to weaken this second condition on time step. Other numerical methods based

on the use of approximate forms of Roe type Riemann solvers and developpemnt wrt some small parameter probably cannot handle any situation with reasonable constraint on time step. Several recent proposals ([59],[16]) have nonetheless been succesively used in industrial codes.

REFERENCES

[1] M. BARRET, E. FAUCHER AND J.M. HÉRARD, Some schemes to compute unsteady flashing flows, *AIAA Journal*, 2002, vol. 40-4.

[2] C. BERTHON, F. COQUEL, J.M. HÉRARD AND M. UHLMANN, An approximate solution of the Riemann problem for a realizable second moment turbulent closure, *Shock Waves*, 2002, vol. 11-4, pp. 245–269.

[3] S. BILICKI AND J. KESTIN, Physical aspects of the relaxation model in two phase flows, *Proc. of the Royal Soc. of London*, 1990, pp. 379–397.

[4] S. BILICKI, J. KESTIN AND M.M. PRATT, A reinterpretation of the results of the moby dick experiments in terms of the non equilibrium model, *J. of Fluid Eng.*, 1990, vol. 112, pp. 212–217.

[5] S. BOIVIN, F. CAYRE AND J.M. HERARD, A finite volume method to solve the navier stokes equations for incompressible flows on triangular meshes, *Int. Journal of Thermal Sciences*, 2000, vol. 39-8, pp. 806–825.

[6] ———, Un schéma volumes finis pour la simulation d'écoulements diphasiques gaz particules à deux phases incompressibles sur maillage triangulaire, *Revue Européenne des Eléments Finis*, 2001, vol. 10-5, pp. 539–574.

[7] G. BRUN, J.M. HÉRARD, D. JEANDEL AND M. UHLMANN, An approximate Roe-type Riemann solver for a class of realizable second order closures, *Int. J. of Comp. Fluid Dyn.*, 2000, vol. 13-3, pp. 233–249.

[8] S. CLERC, Accurate computation of contact discontinuities in flows with general equations of state, *Comp. Meth. Appl. Meth. and Eng.*, 1999, vol. 178, p. 245.

[9] ———, Numerical simulation of the homogeneous equilibrium model for two phase flows, *J. Comp. Phys.*, 2000, vol. 161-1, pp. 354–375.

[10] J.F. COLOMBEAU, *Multiplication of distributions*, Springer Verlag, 1992.

[11] L. COMBE AND J.M. HÉRARD, *Principe du maximum pour un modèle diphasique gaz-solide à trois équations*, EDF-DER Report HE-41/96/045/A, 1996. In French.

[12] ———, Finite volume algorithm to compute dense compressible gas-solid flows, *AIAA journal*, 1999, vol. 37, pp. 337–345.

[13] F. COQUEL, T. GALLOUËT, J.M. HÉRARD AND N. SEGUIN, Closure laws for two-fluid two-pressure models, *CRAS Paris*, 2002.

[14] F. COQUEL, K. EL AMINE, E. GODLEWSKI, B. PERTHAME *et al.*, A numerical method using upwind schemes for the resolution of two phase flows, *J. Comp. Phys.*, 1997, vol. 136, pp. 272–288.

[15] F. COQUEL AND B. PERTHAME, Relaxation of energy and approximate Riemann solvers for general pressure laws in fluid dynamics equations, *SIAM J. Numer. Anal.*, 1998, vol. 35-6, pp. 2223–2249. In Memory of Ami Harten.

[16] J. CORTES, A. DEBUSCHE AND I. TOUMI, A density perturbation method to study the eigenstructure of two phase flow systems, *J. Comp. Phys.*, 1998, vol. 147, pp. 463–484.

[17] G. DAL MASO, P. LE FLOCH AND F. MURAT, Definition and weak stability of non conservative products, *J. Math. Pures Appl.*, 1995, vol. 74, pp. 483–548.

[18] D.A. DREW, Mathematical modelling of two phase flows, *Annual Review of Fluid Mechanics*, 1983, vol. 15, pp. 261–291.

[19] B. DUBROCA, Solveur de roe positivement conservatif, *C. R. Acad. Sci. Paris*, 1999, vol. I-329.

[20] B. EINFELDT, C.D. MUNZ, P.L. ROE AND B. SJOGREEN, On Godunov type methods near low densities, *J. Comp. Phys.*, 1991, vol. 92, pp. 273–295.

[21] R. EYMARD, T. GALLOUËT AND R. HERBIN, Finite Volume Methods, In *Handbook of Numerical Analysis* (Vol. VII), editors : P.G. Ciarlet and J.L. Lions, North-Holland, 2000.

[22] E. FAUCHER, J.M. HÉRARD, M. BARRET AND C. TOULEMONDE, Computation of flashing flows in variable cross section ducts, *Int. J. of Comp. Fluid Dyn.*, 2000, vol. 13-3.

[23] P. LE FLOCH, Entropy weak solutions to non linear hyperbolic systems in non conservative form, *Comm. in Part. Diff. Equations*, 1988, vol. 13, pp. 669–727.

[24] P. LE FLOCH AND T. P. LIU, Existence theory for non linear hyperbolic systems in non conservative form, *C.M.A.P. report 254, also in Forum Mathematicum*, 1992.

[25] A. FORESTIER, J.M. HÉRARD AND X. LOUIS, A Godunov type solver to compute turbulent compressible flows, *C. R. Acad. Sci. Paris*, 1997, vol. I-324, pp. 919–926.

[26] G. GALLICE, Schemas de godunov entropiques et positifs preservant les discontinuites de contact, *C. R. Acad. Sci. Paris*, 2000, vol. I-331, pp. 149–152.

[27] T. GALLOUËT, J.M. HÉRARD AND N. SEGUIN, Hybrid schemes to compute euler equations using real gas eos, *submitted.*

[28] ———, Numerical modelling of two phase flows using the two-fluid two pressure approach, *EDF report HI-81/01/043/A*, 2002.

[29] ———, On the use of some symmetrizing variables to deal with vacuum, *submitted*, 2002.

[30] ———, Some recent Finite Volume schemes to compute Euler equations using real gas EOS, *Int. J. for Num. Meth. in Fluids*, 2002.

[31] S. GAVRILYUK AND R. SAUREL, Mathematical and numerical modelling of two phase compressible flows with inertia, *J. Comp. Phys.*, submitted.

[32] D. GIDASPOW, *Multiphase flow and fluidization*, Academic Press, 1993.

[33] J. GLIMM, D. SALTZ AND D.H. SHARP, Renormalization group solution of two phase flow equations for rayleigh-taylor mixing, *Phys. Lett. A*, 1996, vol. 222, pp. 171–176.

[34] ———, Two phase flow modelling of a fluid mixing layer, *Journal of Fluid Mechanics*, 1999, vol. 378, pp. 119–143.

[35] E. GODLEWSKI AND P.A. RAVIART, *Numerical analysis for hyperbolic systems of conservation laws*, Springer Verlag, 1996.

[36] S.K. GODUNOV, A difference method for numerical calculation of discontinous equations of hydrodynamics, *Sbornik*, 1959, pp. 271–300. In Russian.

[37] A. GOLDSTEIN, M. SHAPIRO AND C. GUTFINGER, Mechanics of collisional motion of granular materials. part 3 self similar shock wave propagation, *Journal of Fluid Mechanics*, 1996, vol. 316, pp. 29–51.

[38] K.A. GONTHIER AND J.M. POWERS, A high resolution numerical method for a two-phase model of deflagration to detonation transition, *J. Comp. Phys.*, 2000, vol. 163, pp. 376–433.

[39] A. HARTEN, P.D. LAX AND B. VAN LEER, On upstream differencing and godunov type schemes for hyperbolic conservation laws, *SIAM review*, 1983, vol. 25-1.

[40] J.M. HÉRARD, Basic analysis of some second moment closures: incompressible isothermal turbulent flows, *Theor. Comp. Fluid Dyn.*, 1994, vol. 6-4, pp. 213–233.

[41] ———, Modeles au second ordre réalisables non dégénérés pour les écoulements turbulents incompressibles, *C. R. Acad. Sci. Paris*, 1996, vol. IIb-322, pp. 371–377.

[42] J.M. HÉRARD, P. MOGAVÉRO AND O. SIMONIN, Computation of shock waves entering a dense granular material, *AIAA paper 99-3332*, 1999.

[43] X. HOU AND P. G. LE FLOCH, Why non conservative schemes converge to wrong solutions, *Mathematics of computation*, 1995.

[44] M. ISHII, *Thermo-fluid dynamic theory of two-phase flows*, Collection de la Direction des Etudes et Recherches d'Electicité de France, 1975.

[45] LUMLEY J.L., Turbulence modelling, *Advances in Applied Mechanics*, 1978, vol. 18, pp. 123–176.

[46] S. KARNI, Multicomponent flow calculations by a consistent primitive algorithm, *J. Comp. Phys.*, 1994, vol. 112, pp. 31–43.

[47] R. LEWANDOWSKI, Modèles de turbulence et équations paraboliques, *C. R. Acad. Sci. Paris*, 1993, vol. I-317, pp. 835–840.

[48] R. MENIKOFF AND B. PLOHR, The riemann problem for fluid flow of real materials, *Rev. Mod. Phys.*, 1989, vol. 61, p. 757.

[49] B. PERTHAME AND C. SHU, On positive preserving finite volume schemes for compressible euler equations, *Numer. Math.*, 1996, vol. 73, pp. 119–130.

[50] S.B. POPE, Pdf methods for turbulent reactive flows, *Progress Energy Combustion Sci.*, 1985, vol. 11, pp. 119–192.

[51] V. RANSOM AND D.L. HICKS, Hyperbolic two-pressure models for two-phase flow, *J. Comp. Phys.*, 1984, vol. 53, pp. 124–151.

[52] P.L. ROE, Approximate Riemann solvers, parameter vectors and difference schemes, *J. Comp. Phys.*, 1981, vol. 43, pp. 357–372.

[53] V.V. RUSANOV, Calculation of interaction of non-steady shock waves with obstacles, *J. Comp. Math. Phys. USSR*, 1961, vol. 1, pp. 267–279.

[54] L. SAINSAULIEU, *Contribution à la modélisation mathématique et numérique des écoulements diphasiques constitués d'un nuage de particules dans un écoulement de gaz*, Thèse d'habilitation, Université Paris VI, France, 1995.

[55] R. SAUREL AND R. ABGRALL, A multiphase godunov method for compressible multifluid and multiphase flows, *J. Comp. Phys.*, 1999, vol. 150, pp. 425–467.

[56] O. SIMONIN, Continuum modelling of dispersed turbulent two phase flows, *Von Karmann Institute Lecture Series 96*, 1996.

[57] J. SMOLLER, *Shock waves and reaction diffusion equations*, Springer Verlag, 1983.

[58] E.F. TORO, *Riemann solvers and numerical methods for fluid dynamics*, Springer Verlag, 1997.

[59] I. TOUMI AND A. KUMBARO, An approximate linearized Riemann solver of a two-fluid model, *J. Comp. Phys.*, 1996, vol. 124, pp. 286–300.

Annexe C

Hybrid schemes to compute contact discontinuities in Euler equations with any EOS

Cette annexe correspond à une note publiée dans les *Comptes Rendus Mécanique* 330 (2002), 445-450.

C. R. Mecanique 330 (2002) 445–450

Hybrid schemes to compute contact discontinuities in Euler equations with any EOS

Thierry Gallouët [a], Jean-Marc Hérard [a,b], Nicolas Seguin [a,b]

[a] L.A.T.P. (UMR 6632), C.M.I., Université de Provence, 39, rue Joliot Curie, 13453 Marseille cedex 13, France

[b] Département M.F.T.T., E.D.F. recherche et développement, 6, quai Watier, 78401 Chatou cedex, France

Received 26 September 2001; accepted after revision 6 May 2002

Note presented by Michel Combarnous.

Abstract We propose here some explicit hybrid schemes which enable accurate computation of Euler equations with arbitrary (analytic or tabulated) equation of state (EOS). The method is valid for the exact Godunov scheme and some approximate Godunov schemes. ***To cite this article: T. Gallouët et al., C. R. Mecanique 330 (2002) 445–450.*** © 2002 Académie des sciences/Éditions scientifiques et médicales Elsevier SAS

computational fluid mechanics / Euler equations / Godunov schemes

Schémas hybrides pour la simulation des discontinuités de contact des équations d'Euler avec une loi d'état quelconque

Résumé On propose un schéma explicite hybride permettant d'effectuer des simulations précises des équations d'Euler pour un choix de loi thermodynamique quelconque, analytique ou tabulée. La méthode est définie pour les schémas de Godunov exact ou approchés. ***Pour citer cet article : T. Gallouët et al., C. R. Mecanique 330 (2002) 445–450.*** © 2002 Académie des sciences/Éditions scientifiques et médicales Elsevier SAS

mécanique des fluides numérique / équations d'Euler / schémas de Godunov

Version française abrégée

La simulation des écoulements diphasiques de type eau-vapeur, ou de certains écoulements monophasiques compressibles nécessite l'utilisation de lois d'état assez complexes, qui peuvent parfois même n'être que tabulées. Il en est de même pour la simulation des écoulements multi-matériaux dans certaines configurations. La représentation de ces phénomènes se fait couramment à l'aide des équations d'Euler (ou de modèles de type Navier–Stokes pour prendre en compte les effets de viscosité), ou de modèles plus complexes dits à deux fluides, qui nécessitent clairement une excellente maîtrise du système précédent. Or, lorsque la thermodynamique s'écarte du comportement de la loi des gaz parfaits monoconstituants, les schémas conservatifs utilisant une stabilisation par décentrement (par exemple le schéma de Godunov [1]) se comportent de manière médiocre au voisinage des discontinuités de contact (sans inhiber la convergence). De fortes oscillations peuvent apparaître, et dans la meilleure configuration, la vitesse de convergence très lente [13] (de type $h^{1/2}$) interdit la prédiction précise de certains phénomènes physiques. Plusieurs auteurs ont proposé des méthodes permettant de contourner ces difficultés, en se focalisant essentiellement

E-mail addresses: Thierry.Gallouet@cmi.univ-mrs.fr (T. Gallouët); Herard@cmi.univ-mrs.fr, Jean-Marc.Herard@der.edf.fr (J.-M. Hérard); seguin@chi80bk.der.edf.fr (N. Seguin).

S1631-0721(02)01482-1/FLA

T. Gallouët et al. / C. R. Mecanique 330 (2002) 445–450

sur le mélange de gaz parfaits, ou de manière analogue sur la loi d'état « stiffened gas » [5–7]. Récemment, une contribution au débat concernant la loi d'état de Van der Waals a été proposée par Shyue [8]. Une approche distincte a été proposée dans [14]. On se propose ici de donner un cadre général permettant d'effectuer des simulations avec tout type de loi thermodynamique, en se focalisant sur le schéma de Godunov et sur une large classe de solveurs de Godunov approchés tels qu'introduits récemment [3,4], et utilisant la variable $Y^t = (U, P, g(\rho, s), C, \psi)$ (les notations sont introduites dans la partie anglaise). Pour cela, il est tout d'abord nécessaire de décomposer l'énergie interne $\rho e = E - \rho U^2/2$ en fonction des variables P, ρ, C, ψ (respectivement pression, densité, concentration et fonction couleur) sous la forme : $\rho e = \phi_1(P, \rho, C, \psi) + f_2(C, \psi)h_2(P) + g_2(C, \psi) + \phi_3(P, \rho, C, \psi)$. Les fonctions ϕ_1 sont de la forme : $\phi_1(P, \rho, C, \psi) = \rho(a_1(P) + b_1(P)C + c_1(P)\psi) + d_1(P)$. Pour traiter les situations où la loi d'état n'est pas dans T_1, on propose le schéma explicite modifié suivant (4) pour simuler le système conservatif hyperbolique non strict (1), où les grandeurs C et ψ sont « convectées » à la vitesse U (ce qui est crucial pour le traitement des lois dans T_2). Ce schéma nécessite seulement de définir la pression de maille p_i^{n+1} en fin de pas de temps comme la solution $\widetilde{P}_i^{n+1}$ de l'équation de maille (5). Il permet de représenter parfaitement sur maillage « grossier » les discontinuités de contact instationnaires au sens suivant : *si la condition initiale discrète est telle que* : $U_k^n = U_0$ *et* $p_k^n = P_0$ *pour* $k = i-1, i, i+1$, *le schéma doit fournir des valeurs de pression et de vitesse de maille au pas de temps suivant telles que* : $p_i^{n+1} = P_0$ *et* $U_i^{n+1} = U_0$. On retrouve naturellement la proposition d'Abgrall et Saurel pour la loi « stiffened gas » caractéristique de la classe T_2. Le schéma est basé sur la discrétisation des équations redondantes (6) en zone régulière. La validation de ce schéma nécessite un examen précis du comportement de la suite d'approximations en présence de chocs, lorsque le pas de maillage tend vers 0, à nombre de CFL constant. Dans le cas d'une thermodynamique dans T_2, il est intéressant de constater que la vitesse de convergence (Fig. 2) mesurée en norme L^1 est en tout point identique pour la variable densité à celle de la concentration [13]. De surcroît, la vitesse de convergence pour les variables U, P qui sont invariantes à travers le contact est de 1 (elle est de 1/2 dans le cas du schéma conservatif de base). Le schéma semble donc fournir une approximation convergeant vers la bonne solution, ce qui est cohérent avec la spécificité de la classe T_2 [13]. Le comportement du schéma modifié est encore très bon sur maillage grossier, lorsque la loi d'état comporte une contribution dans T_3 (Van der Waals, Chemkin, ...), mais la simulation numérique d'un « vrai » produit non conservatif perturbe la convergence sur maillage très fin (plus de 10^4 noeuds en dimension 1, voir Fig. 4, et également [9]). Ce résultat suggère ainsi d'utiliser le schéma modifié sur maillage grossier de préférence, et le dernier point est confirmé par une analyse de sensibilité à la décomposition thermodynamique [13].

La méthode se comporte bien pour les configurations thermodynamiques considérées, analytiques (loi « stiffened gas », loi de Van der Waals [10], Chemkin [11]) ou tabulées [12]. Pour les lois de type Chemkin ou les lois analytiques complexes, le coût calcul pour l'obtention de $\widetilde{P}_i^n$ solution de (5) est beaucoup plus faible en pratique que celui associé à P_i^n solution de $e(P_i^n, \rho_i^n, C_i^n, \psi_i^n) = e_i^n$ (méthode classique) ; l'algorithme modifié est dès lors plus performant en terme de précision et de coût, à maillage donné. On renvoie le lecteur à [13] pour plus de détails. Les extensions à l'ordre deux par des techniques de type MUSCL sont possibles.

1. Introduction

We focus here on the computation of Euler equations with arbitrary type of equation of state (EOS) with help of exact Godunov scheme [1,2], or some particular approximate Godunov schemes issuing from VFRoe-ncv formalism with help of $Y^t = (U, P, g(\rho, s), C, \psi)$ variables – see notations below –, [3,4]. The main objective here is to derive schemes which 'perfectly resolve unsteady contact discontinuities in Euler equations' in the following sense: *if the initial data is in agreement with*: $U_k^n = U_0$ *and* $p_k^n = P_0$ *with* $k = i-1, i, i+1$, *the scheme must provide updated cell pressures and cell velocities such that*: $p_i^{n+1} = P_0$, *and* $U_i^{n+1} = U_0$. Some ways to deal with simple analytic laws have been suggested recently by several

To cite this article: T. Gallouët et al., C. R. Mecanique 330 (2002) 445–450

authors (see [5–7] for stiffened gas EOS and mixture of perfect gases, [8] for Van der Waals EOS for instance). No general frame work clearly arises in order to deal with arbitrary state law. This is one objective of the present work, which also aims at clarifying the true rate of convergence achieved in some specific cases, and the achieved accuracy level on given mesh size. First, we introduce some classification of EOS based on three classes. Unsteady contact discontinuities are perfectly represented on coarse or fine meshes for EOS belonging to the first class. We then propose some generic way to account for any EOS using decomposition of the EOS on the three classes, and introducing some adequate scheme to deal with the whole. On the basis of several one dimensional Riemann problems, the L^1 error norm is plotted which confirms the behaviour is rather good though it is not a fully conservative scheme (see [9]). Exact analytic EOS such as stiffened gas EOS, mixture of perfect gases, Van der Waals EOS [10] those arising in Chemkin database [11], or tabulated laws [12] may be used with the present approach. Details can be found in [13].

2. Governing equations and classification of EOS

The one-dimensional governing set of Euler equations takes the form (x in $\mathbb{R}$):

$$\begin{cases} \dfrac{\partial W}{\partial t} + \dfrac{\partial F(W)}{\partial x} = 0, \\ W(x,0) = W_0(x) \end{cases} \tag{1}$$

with $W = (\rho, \rho C, \rho U, E, \rho\psi)$, $F(W) = (\rho U, \rho CU, \rho U^2 + P, U(E+P), \rho\psi U)$ and suitable boundary conditions. A physically relevant entropy inequality must be added to select admissible shocks, which requires defining the specific entropy $s(P, \rho, C, \psi)$. The total energy is written in terms of the kinetic energy plus the internal energy ρe which depends on density ρ and pressure P, but may also depend on concentration C and colour function ψ. Thus total energy is $E = \rho U^2/2 + \rho e$ where ρe is a function of (P, ρ, C, ψ) and U denotes the velocity. We then introduce classes T_1 and T_2 which contain EOS which respectively take the form:

$$\begin{cases} \rho e = \phi_1(P, \rho, C, \psi) = \rho(a_1(P) + b_1(P)C + c_1(P)\psi) + d_1(P) \\ \rho e = \phi_2(P, C, \psi) = f_2(C, \psi)h_2(P) + g_2(C, \psi) \end{cases} \tag{2}$$

We recall here that both C, ψ are regular solutions of the first equation of (6). Any EOS may be decomposed in terms of contribution in $T_1 \cup T_2$ and the remaining part if necessary: $\rho e = \phi_1(P, \rho, C, \psi) + f_2(C, \psi)h_2(P) + g_2(C, \psi) + \phi_3(P, \rho, C, \psi)$. For instance, the perfect gas EOS and the Tamman law belong to T_1, and the mixture of perfect gases and the stiffened gas EOS lie in T_2 exactly. If the EOS lies in T_1, standard conservative Godunov scheme (or conservative approximate Godunov scheme VFRoe-ncv with above mentionned variable Y) perfectly represents unsteady contact discontinuities on any mesh. This means that when using standard definition of the pressure on each cell $p_i^n = P_i^n$ solution of $e(P_i^n, \rho_i^n, C_i^n, \psi_i^n) = e_i^n$, and standard notations for the time step δt, the mesh size $h_i = x_{i+1/2} - x_{i-1/2}$, denoting $W(Y^*_{x_{i+1/2}})$ the interface value predicted by the exact or approximate Godunov scheme, the mean value of conservative variable W over cell i at time $k\delta t$, namely W_i^k, is obtained through:

$$h_i\big(W_i^{n+1} - W_i^n\big) + \delta t\big(F\big(W\big(Y^*_{x_{i+1/2}}\big)\big) - F\big(W\big(Y^*_{x_{i-1/2}}\big)\big)\big) = 0 \tag{3}$$

3. Modified form of approximate or exact Godunov schemes

We now present the modified version of the explicit scheme, setting $\gamma = \rho c^2/P$ for any EOS. *For any EOS which does not lie in* T_1, setting $g_0(C, \psi) = f_2(C, \psi)h_2(P_{\text{ref}}) + g_2(C, \psi)$, enables us to define the explicit first order version of the modified explicit scheme which is:

$$h_i\big(W_i^{n+1} - W_i^n\big) + \delta t\big(F\big(W\big(Y^*_{x_{i+1/2}}\big)\big) - F\big(W\big(Y^*_{x_{i-1/2}}\big)\big)\big) = 0 \tag{4a}$$

$$h_i\big((g_0)_i^{n+1} - (g_0)_i^n\big) + \delta t\widehat{U}_i\big((g_0)^*_{x_{i+1/2}} - (g_0)^*_{x_{i-1/2}}\big) = 0 \tag{4b}$$

T. Gallouët et al. / C. R. Mecanique 330 (2002) 445–450

$$h_i\big((\phi_3)_i^{n+1}-(\phi_3)_i^n\big)+\delta t\,\widehat{U}_i\big((\phi_3)^*_{x_{i+1/2}}-(\phi_3)^*_{x_{i-1/2}}\big)+\delta t\,\widehat{H}_i\big((U)^*_{x_{i+1/2}}-(U)^*_{x_{i-1/2}}\big)=0 \tag{4c}$$

$$2\widehat{U}_i=U^*_{x_{i+1/2}}+U^*_{x_{i-1/2}} \tag{4d}$$

$$2\widehat{H}_i=\left(\gamma P\frac{\partial\phi_3}{\partial P}+\rho\frac{\partial\phi_3}{\partial\rho}\right)^*_{x_{i-1/2}}+\left(\gamma P\frac{\partial\phi_3}{\partial P}+\rho\frac{\partial\phi_3}{\partial\rho}\right)^*_{x_{i+1/2}} \tag{4e}$$

Any quantity $m^*_{j+1/2}$ on interface $j+1/2$ stands for $m(Y^*_{j+1/2})$. The definition of the numerical flux is the following: $F(W(Y^*))=(\rho^*U^*,\rho^*U^*C^*,\rho^*U^*U^*+P^*,U^*(\rho^*U^*U^*/2+P^*+(\rho e)^*),\rho^*U^*\psi^*)$, where: $(\rho e)^*=\phi_1(P^*,\rho^*,C^*,\psi^*)+f_2(C^*,\psi^*)h_2(P^*)+g_2(C^*,\psi^*)+\phi_3(P^*,\rho^*,C^*,\psi^*)$. Both series $(f_2)_i^k$ and $(g_2)_i^k$ issue from computation of g_0 setting $h_2(P_{\text{ref}})=0$ and $h_2(P_{\text{ref}})=1$ successively. The cell pressure used to compute the local Riemann problems at the beginning of the next time step, namely $p_i^{n+1}=\widetilde{P}_i^{n+1}$, is obtained by computing the solution $\widetilde{P}_i^{n+1}$ of equation:

$$\rho_i^{n+1}e_i^{n+1}-\big((g_2)_i^{n+1}+(\phi_3)_i^{n+1}\big)=\phi_1\big(\widetilde{P}_i^{n+1},\rho_i^{n+1},C_i^{n+1},\psi_i^{n+1}\big)+(f_2)_i^{n+1}h_2\big(\widetilde{P}_i^{n+1}\big) \tag{5a}$$

$$\rho_i^{n+1}e_i^{n+1}=E_i^{n+1}-\frac{(Q_i^{n+1})^2}{2\rho_i^{n+1}} \tag{5b}$$

with given values E_i^{n+1}, Q_i^{n+1}, ρ_i^{n+1}, C_i^{n+1}, ψ_i^{n+1} provided by discrete conservative equations, and $(f_2)_i^{n+1}$, $(g_2)_i^{n+1}$, $(\phi_3)_i^{n+1}$ provided by discrete non-conservative equations. The resulting value of cell pressure is used to initialize Riemann problems at each cell interface at the beginning of the following time step. Discrete equations (4b)–(4e) are associated with governing equations:

$$\frac{\partial g_0}{\partial t}+U\frac{\partial g_0}{\partial x}=0\quad\text{and}\quad\frac{\partial\phi_3}{\partial t}+U\frac{\partial\phi_3}{\partial x}+\left(\gamma P\frac{\partial\phi_3}{\partial P}+\rho\frac{\partial\phi_3}{\partial\rho}\right)\frac{\partial U}{\partial x}=0 \tag{6}$$

The latter two provide *redundent* information for regular solutions. Note that, for Chemkin EOS or for some complex analytic laws, the CPU time required to compute $\widetilde{P}_i^n$ is lower than the CPU time for P_i^n. Unsteady contact discontinuities are now perfectly represented on any mesh size since we have (see [13]):

PROPERTY. – For any EOS in $T_1\cup T_2\cup T_3$, and for given initial data in agreement with: $U_k^n=U_0$ and $p_k^n=P_0$ with $k=i-1,i,i+1$, the modified Godunov scheme (4) ensures that $p_i^{n+1}=P_0$, and $U_i^{n+1}=U_0$. This is still true when using the above mentionned approximate Godunov scheme with $Y^t=(U,P,g(\rho,s),C,\psi)$.

4. Numerical results

We focus here on the behaviour of schemes when at least one shock wave occurs in the solution. Detailed investigation of rates of convergence of the basic approximate Godunov scheme is available in [4], when restricting to EOS in T_1 such as perfect gas state law or Tamman EOS. In addition the rate of convergence of variables supported by the contact discontinuity such as the mean concentration is clearly $1/2$ (see [4]). Numerical tests have been obtained using $Y^t=(U,P,\rho,C,\psi)$.

4.1. EOS in the second class

Results below are associated with the stiffened gas EOS or equivalently with a mixture of perfect gases (see [6,7] for instance). Decomposition gives: $\rho e=\phi_2(P,C,\psi)=f_2(C,\psi)P+g_2(C,\psi)$ with $f_2(C,\psi)=1/(\gamma(\psi)-1)$, and $g_2(C,\psi)=P_{\text{inf}}(\psi)/(\gamma(\psi)-1)$. Recall that $\phi_1(P,\rho,C,\psi)=0$, $\phi_3(P,\rho,C,\psi)=0$ here. Fig. 1 represents a shock tube, computed by the VFRoe-ncv (ρ,U,P,C) scheme and its hybrid modification. Fig. 2 refers to the measure of the L^1 norm of the error when computing a pure 3-shock wave followed by a moving contact discontinuity with the hybrid scheme (the rate of convergence is close to $1/2$ (respectively 1) for ρ (resp. U, P)) and with the basic VFRoe-ncv scheme (the rate of convergence is close to $1/2$ for ρ, U, P). Meshes contain from 100 to 160000 cells.

Pour citer cet article : T. Gallouët et al., C. R. Mecanique 330 (2002) 445–450

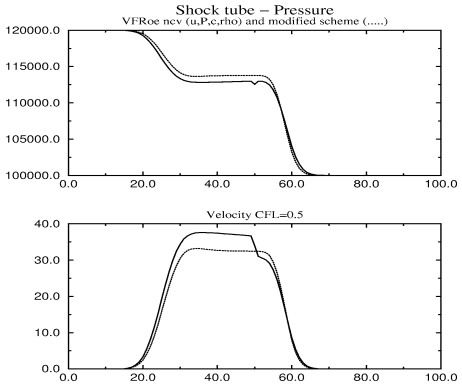

Figure 1. Shock tube – stiffened gas EOS – coarse mesh.

Figure 1. *Tube à choc – stiffened gas EOS – maillage grossier.*

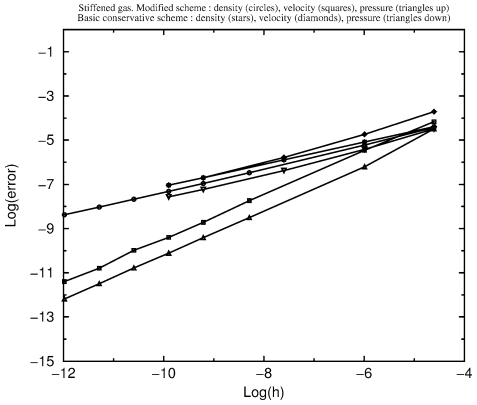

Figure 2. Pure unsteady 3-shock – stiffened gas EOS – L^1 error norm.

Figure 2. *3-choc pur instationnaire – stiffened gas EOS – erreur en norme L^1.*

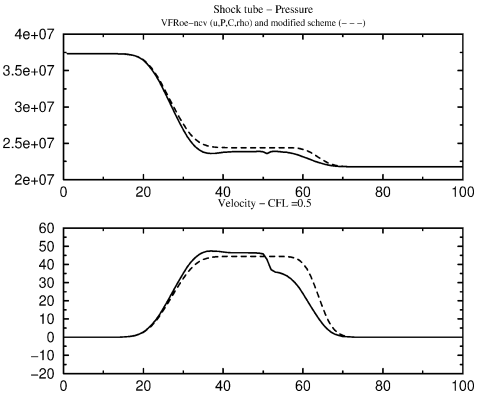

Figure 3. Shock tube – Van der Waals EOS – coarse mesh.

Figure 3. *Tube à choc – Van der Waals EOS – maillage grossier.*

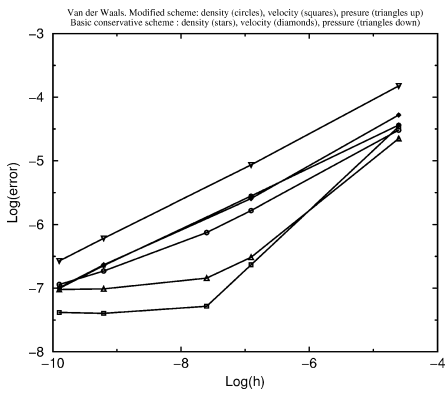

Figure 4. Pure unsteady 3-shock – Van der Waals EOS – L^1 error norm.

Figure 4. *3-choc pur instationnaire – Van der Waals EOS – erreur en norme L^1.*

4.2. EOS in the third class

We turn now to Van der Waals EOS (see [8]). Decomposition of EOS can be written: $\rho e = \phi_1(P,\rho,C,\psi) + \phi_3(P,\rho,C,\psi)$, $\phi_2(P,C,\psi) = 0$, where $b_1(P) = c_1(P) = 0$, $d_1(P) = P/(\gamma-1)$, $a_1(P) = -bP/(\gamma-1)$, $\phi_3(P,\rho,C,\psi) = a\rho^2(-b\rho+2-\gamma)(\gamma-1)^{-1}$. Fig. 3 provides computational results obtained with both schemes, when approximating shock tube apparatus. Fig. 4 refers to the L^1 error norm when computing a 3 shock wave with the hybrid scheme and the basic conservative scheme (for which the rate of convergence is still $1/2$ for ρ, U, P). Meshes contain from 100 to 20000 cells.

5. Conclusion

The hybrid method enables to increase accuracy of computations on coarse meshes, and also to get rid of some oscillations in some cases. It has been applied in a very wide class of numerical tests including double shock waves, double rarefaction waves, combination of contact discontinuity with ghost 1 wave and 3 shock wave, and many EOS including those discussed herein, Chemkin database and tabulated EOS. This has been achieved using meshes with 100 up to 160000 nodes. The influence of the decomposition is examined in [13] which shows that a 'correct' decomposition should be prefered to a 'wrong' decomposition (for instance by enforcing the perfect gas EOS in T_3 instead of T_1), as expected, and in relation to the work in [9]. This nonetheless appears when using fine meshes which are far beyond the reach of current computer facilities for industrial purposes (this would concern meshes with more than 10^{12} nodes in a three dimensional framework). The modified scheme is thus useful: for given – coarse – mesh size it is in practice less time consuming (at least when dealing with complex analytic EOS) and more accurate than the initial fully conservative scheme. Higher order schemes may be derived using standard MUSCL approach. A blend scheme also seems appealing for industrial purposes, in order to benefit from properties of modified and initial – fully conservative – schemes (see [13]).

References

[1] S.K. Godunov, A difference method for numerical calculation of discontinous equations of hydrodynamics, Sbornik (1959) 271–300 (in Russian).
[2] E. Godlewski, P.A. Raviart, Numerical Approximation of Hyperbolic Systems of Conservation Laws, Appl. Math. Series, Vol. 118, Springer-Verlag, 1996.
[3] T. Buffard, T. Gallouët, J.M. Hérard, A sequel to a rough Godunov scheme. Application to real gas flows, Comput. Fluids 29 (7) (2000) 813–847.
[4] T. Gallouët, J.M. Hérard, N. Seguin, Some recent Finite Volume schemes to compute Euler equations using real gas EOS, Preprint LATP 00-021, 2000, Int. J. Numer. Methods Fluids, to appear.
[5] S. Karni, Multicomponent flow calculations by a consistent primitive algorithm, J. Comput. Phys. 112 (1994) 31–43.
[6] R. Abgrall, How to prevent pressure oscillations in multicomponent flow calculations: a quasi conservative approach, J. Comput. Phys. 125 (1995) 150–160.
[7] R. Saurel, R. Abgrall, A simple method for compressible multifluid flows, SIAM J. Sci. Comput. 21 (3) (1999) 1115–1145.
[8] K.M. Shyue, A fluid mixture type algorithm for compressible multicomponent flow with Van der Waals equation of state, J. Comput. Phys. 156 (1999) 43–88.
[9] X. Hou, P.G. Le Floch, Why nonconservative schemes converge to wrong solutions, Math. Comput. 62 (1995) 497–530.
[10] A. Letellier, A. Forestier, Le problème de Riemann en fluide quelconque, CEA-DMT Report 93/451, 1993.
[11] R. Kee, J. Miller, T. Jefferson, Chemkin: a general purpose, problem independant transportable fortran chemical kinetics code package, SAND Report 80-8003, Sandia National Laboratories.
[12] P. Rascle, O. Morvant, Interface utilisateur de Thetis – THErmodynamique en Tables d'Interpolations, EDF-DER Report HT-13/95021B, 1995.
[13] T. Gallouët, J.M. Hérard, N. Seguin, Hybrid schemes to compute contact discontinuities in Euler systems, EDF report HI-81/01/011/A, 2001.
[14] G. Allaire, S. Clerc, S. Kokh, A five equation model for the numerical solution of interfaces in two phase flows, C. R. Acad. Sci. Paris, Série I 331 (2000) 1017–1022.

Modélisation et simulation numérique des écoulements diphasiques

Résumé : On s'intéresse dans ce travail à la simulation des écoulements diphasiques. Différents modèles, tous hyperboliques, sont considérés suivant les configurations étudiées. Dans un premier temps, plusieurs schémas Volumes Finis sont comparés pour l'approximation du modèle HEM (Homogeneous Equilibrium Model), notamment en présence de faibles densités. Ensuite on démontre l'existence et l'unicité de la solution faible entropique d'une loi de conservation scalaire gouvernant l'évolution de la saturation d'un écoulement diphasique dans un milieu poreux. On propose alors deux schémas Volumes Finis tenant compte du caractère résonnant de cette équation. La troisième partie concerne les écoulements en eaux peu profondes et l'approximation des termes sources raides. Une méthode permettant le maintien d'états au repos ainsi que le recouvrement et l'apparition de zones sèches, est présentée et comparée aux méthodes habituellement utilisées dans l'industrie. Enfin, une classe de modèles hyperboliques non conservatifs se basant sur l'approche bifluide à deux vitesses et deux pressions est proposée. Une étude des solutions discontinues du système convectif permet d'exhiber une classe de fermetures sur la vitesse interfaciale et sur la pression interfaciale, tout en permettant de définir de manière unique les produits non conservatifs. L'approximation se fait à l'aide d'une méthode de *splitting* d'opérateur. On utilise deux schémas Volumes Finis, le schéma de Rusanov et le schéma de Godunov approché VFRoe-ncv pour l'étape de convection. Plusieurs cas tests sont présentés et commentés : tubes à choc, conditions limites de paroi, robinet d'eau, sédimentation.

Mots-clés : écoulement diphasique, système hyperbolique, résonnance, Volumes Finis, schéma de Godunov approché.

Modeling and numerical simulation of two-phase flows

Abstract: The main topic of this work is the simulation of two-phase flows. Several hyperbolic models are considered here. In the first part, recent Finite Volume schemes are compared for the approximation of the Homogeneous Equilibrium Model, in particular when the simulation involves low densities. The existence and uniqueness of the weak entropy solution of a conservation law is proved afterwards. This scalar equation is a simplified model of a oil-liquid mixture flowing in a porous media. Two Finite Volume schemes are proposed and tested in agreement with the resonant behavior of this model. The third part deals with the numerical approximation of stiff source terms occuring in the shallow-water equations when the topography gradient is included. An original approximate Godunov scheme, which enables to simulate steady states and dry zones, is presented and compared with the methods used in the industrial context. The last part corresponds to the analysis of a class of non-conservative hyperbolic models of two-phase flows, based on the two velocity and two pressure two-fluid approach. Some closure laws for the interfacial velocity and for the interfacial pressure are proposed, allowing to define discontinuous solutions. The convective part is approximated by Finite Volume schemes and the relaxation terms are taken into account with the help of a splitting method. Several numerical experiments are investigated: shock tubes, wall boundary conditions, water faucet and sedimentation.

Key-words: two-phase flow, hyperbolic system, resonance, Finite Volume, approximate Godunov scheme.

Discipline : Mathématiques appliquées.

Laboratoire d'analyse, topologie et probabilités, Centre de mathématiques et d'informatique,
Université de Provence, Marseille.